Investigations on Multiwalled Carbon Nanotube Reinforced Copper

THESIS

Submitted in the partial fulfillment
of the requirements for the degree of

DOCTOR OF PHILOSOPHY

by

SACHIN ULHASRAO BELGAMWAR

Under the supervision of

PROF. NITI NIPUN SHARMA

BITS Pilani
Pilani | Dubai | Goa | Hyderabad

BIRLA INSTITUTE OF TECHNOLOGY & SCIENCE
PILANI – 333 031 (RAJASTHAN) INDIA

2014

Investigations on Multiwalled Carbon Nanotube Reinforced Copper

THESIS

Submitted in the partial fulfillment
of the requirements for the degree of

DOCTOR OF PHILOSOPHY

by

SACHIN ULHASRAO BELGAMWAR
(ID.No. 2007PHXF403P)

Under the supervision of

PROF. NITI NIPUN SHARMA

BITS Pilani
Pilani | Dubai | Goa | Hyderabad

BIRLA INSTITUTE OF TECHNOLOGY & SCIENCE
PILANI – 333 031 (RAJASTHAN) INDIA

2014

BIRLA INSTITUTE OF TECHNOLOGY & SCIENCE
PILANI – 333 031 (RAJASTHAN) INDIA

CERTIFICATE

This is to certify that the thesis entitled **"Investigations on Multiwalled Carbon Nanotube Reinforced Copper"** submitted by **Sachin Ulhasrao Belgamwar**, ID.No. **2007PHXF403P** for award of Ph.D. Degree of the institute embodies original work done by him under my supervision.

Signature: _____

Prof. NITI NIPUN SHARMA
Professor, Mechanical Engineering Department
BITS-Pilani, Pilani Campus

Date: _____

Dedicated

to

my parents

my wife & my son ‘Ansh’

ACKNOWLEDGEMENT

If there is one thing, Institute made me realize, it is the truth of the axiom that "no man is an island." All my life I consider my achievements, somehow personal rather than a result of a complex system of support from both permanent and transient people in my life. Realizing this has opened up the door for continuous appreciation of all the things in my life, good and bad.

No words can express my boundless gratitude towards my Aai (Mother) and Baba (father) for their many sacrifices that they made in their life to make sure that myself had the opportunities I have had. I am thankful for their unfaltering support, guidance, and enduring love.

I am extremely grateful to my Ph.D. supervisor Prof. Niti Nipun Sharma. He is an immensely kind and patient person and goes out of his way to help the people. I cannot find enough words to thank him for his help and support during my research work at BITS-Pilani, Pilani Campus. In addition, he is terrific researcher, great advisor, and wonderful teacher. He has a logical, rational, and holistic way of approaching any scientific issue and goes to the depth of every research problem. He was available at any time for discussing any research query and any other problem that I had. He has an expertise in presenting the scientific work, which helped me in my presentation. I am fortunate to work under such supervisor.

I am immensely thankful to Professor B.N. Jain, Vice-Chancellor, BITS - Pilani; Prof. G. Raghurama, Director, BITS-Pilani, Pilani Campus; Prof. R. K. Mittal, Director (Special Projects) BITS, Pilani for providing me the opportunity to teach in the Mechanical Engineering Department of BITS-Pilani, Pilani Campus and allowing me to pursue my doctoral thesis by providing necessary facilities and financial support. I express my gratitude to Prof. S. K. Verma (Dean, Academic Research Division); Prof. Hemant R Jadhao (Professor-in-Charge, Academic Research Division) BITS-Pilani, Pilani Campus for their constant official support and encouragement. I feel obliged to Prof. Ravi Prakash (former Dean, Research and Consultancy Division); Prof. Kuldeep S. Sangwan (former Head of the Department, Mechanical Engineering); Prof. Ajit Pratap Singh (Dean, Admission and Instruction

Division) and Prof. Srikanta Routroy (Associate Dean, Instruction Division) for their support.

My sincere thanks to Prof. Sai Jagan Mohan (Head of the Department, Mechanical Engineering) for his support and spur during completion of the research work. I am grateful to the entire faculty and staff of Mechanical Engineering Department and central workshop unit BITS - Pilani for their kind support and assistance.

I thank Prof. M.S. Dasgupta (Chief, Placement Unit); Prof. B.K. Rout (Associate Dean, Academic Registration & Counselling Division) and Prof. P Srinivasan (Associate Dean, Practice School) Doctoral Research Committee (DRC) and Doctoral Advisory Committee (DAC) members, Mechanical Engineering Department, who spared their precious time to provide valuable suggestions that immensely helped in improving the quality of my Ph.D. thesis.

I also express my gratitude to all my colleagues in BITS-Pilani, Pilani Campus in particular, Prof. R.N. Saha (Director, BITS-Pilani, Dubai Campus); Prof. Anshuman Dalvi, Prof. Subit K. Saha, Dr. Shrikant Charde, Prof. Suresh Gupta, Prof. Arvind Sharma, Prof. S. C. Sivasubramanian (Dean, Administration); Prof. Abhijeet K. Digalwar, Prof. Manojkumar S. Soni, and Prof. Subhashis Gangopadyay for their continuous support, motivation, guidance, and for providing unrestricted access to their experimental lab resources. I am thankful to Dr. Jamil Akhatar, Dr. G. Eranna, Dr. K. J. Rangara, Dr. Rahul Verma, Dr. Sanjeev Gupta, Mr. Prateek Kothari, Mr. Surojit Das all from CEERI Pilani for their support during characterization of samples. I am also thankful to Mr. Prashant Raut, Mr. Chandrashekhar, Mr. Bhupendra Mishra, Mr. Mukund Tantak, Mr. Emil Joseph, Mr. Mutthu, Mr. Vasant, Mr. Subodh k Azad, Ms Neha Gupta, Ms. Munesh for their support and help during experimentation.

I have been gifted with friends like Dr. Amol Marathe, Dr. Arun K Jalan, Dr. Dileep Kumar Gupta, Mr. Girish Kant, Dr. Jitendra Singh Rathore, Dr. Maheshwar Dwivedy, Dr. Murali Palla, Dr. Satish Kumar Dubey, Dr. Sharad Shrivastava, Dr. R. P. Mishra, Dr. T. C. Bera, Ms. Neha Arora, Ms. Paridhi Puri, Mr. Rahul Ramchandran, Ms. Shivani Nain, Ms. Tamalika Bhakat and Mr. Vijay Kumar, who have not only supported me in times thick and thin but have also made the journey of life extremely interesting, meaningful and fun.

I would like to thanks Mr. Santosh Kumar Saini (ARC Division) for his help in compilation of thesis. I also express my thanks to all other faculty and staff of ARC Division and CAHU, BITS-Pilani, Pilani Campus for their kind support and cooperation towards the completion of my thesis.

My special thanks to my lovable family. My sincere thanks to my loving sisters, brother, and in laws for making all my dreams come true and for their fathomless love, support, motivation and all help.

Lastly, I owe the deepest gratitude to my wife Kajal and my son Ansh for all the sacrifices they have gone through these years for the successful completion of my thesis.

SACHIN U BELGAMWAR

ABSTRACT

Since last decade, composite reinforced with nanoparticles are extensively researched to obtain good electrical, mechanical, and functional properties. Due to remarkable mechanical, thermal, and electrical properties, carbon nanotubes (CNT) are the potential reinforcement for the composites. However, due to ease in fabrication of CNT-reinforced polymer matrix more studies have been carried out on this topic. Nevertheless, considering the fact that most of the applications related to the structural material in present world are of metal. Hence, metal matrix composite reinforced with carbon nanotube can be considered for better mechanical, electrical, thermal, and lightweight application.

Towards realization of this newer material, in this thesis we focused on synthesis of CNT reinforced copper composite and characterization of CNT/Cu composite. The composite of interest is a few milestones away and this thesis is an attempt to cover a couple of miles in that direction. To achieve the objective of proposed research, the thesis is divided in to seven chapters. Some of the salient features of these chapters are as follows:

Chapter 1 introduces the problem statement and discusses about on the composite, composite reinforced with nanosize particles and need of composite. The aim of the present work is also discussed at the end of the chapter.

In Chapter 2, different techniques for the synthesis of CNT/Cu composite have been classified and discussed thoroughly for their merits and demerits with respect to CNT/Cu composites. With critical analysis of the different processes, a scope for further development is also discussed and the new method is conceptualized. Detail review of mechanical and electrical properties of the CNT/Cu composites is carried out and arranged chronologically to study the evolution of the composite. At the end the scope of the present work towards designing of newer method is discussed.

In Chapter 3, a newer modified method is developed by tweaking the existing method. In this attempt, we relooked at all existing methods, their relative advantages/disadvantage, Figure out one best method and try to improve that particular method. A thorough work out and combining two existing methods, we improved and form a modified method, which enables bulk production of CNT/Cu metal composite in powder form.

In Chapter 4, X-ray diffraction method, EDS, scanning electron microscopy, and transmission electron microscopy analysis was carried out for ensuring uniform dispersion and proper reinforcement of CNT in the copper matrix. The most critical issue of CNT dispersion in the metal matrix is addressed.

In Chapter 5, the bulk produced CNT/Cu composite synthesized by modified electro-co-deposition method is investigated for the mechanical properties. The mechanical properties determined experimentally are compared with the mechanical properties determined using micro models. A statistical analysis was carried out to determine the effect of synthesis parameters on the mechanical property.

In Chapter 6, on similar argument as in Chapter 5, investigation of the electrical properties of the composite is also quite essential, which is done and presented in this chapter. In this chapter we also statistically figure out the process parameters, which are significantly affecting the variation in the electrical properties of the product

In Chapter 7 discusses the overall conclusions and future scope of the present study.

CONTENTS **Page No.**

List of Figures

List of Tables

Chapter 1

Introduction

Mankind's quest for material with better electrical and mechanical properties had been axiomatic and asymptotic in the available historical time period. With advent of application of metals, formulation of alloys and invention of composite, the rise and fall of civilization witnessed Copper to Iron Age. Alloying of iron with carbon to produce steel led to industrial revolution in 1800's and there after sustaining adventures and comfort of humankind in last two centuries.

We today are set for another technology revolution because of onset of nanotechnology led product development. For example, a probable energy starvation in the near future owing to growing population and usage needs urgent attention and salvation probably by developing a material (composite) which reduces transmission and other losses. By an estimate total electrical transmission losses in India are about 25182 MW/year (assuming 20% loss[1]) which if saved then around 15000 MW/ year will be surplus in India (Power deficit in 2013-2014 is about 10000 MW/year as per Government of India Report [1]). Therefore, saving of losses during electrical transmission and during usage in electrical appliances can be a substantial contribution towards salvation of energy problem. This have led researchers to look for materials with improved electrical conductivity and that too without compromising with the mechanical properties of the newer material, to be used in electrical transmission and in electrical appliances.

Towards realization of this newer material, composites of copper with better conductivity by reinforcing the copper matrix with carbon nanotube is being widely considered, as a possibility to replace the existing material and this will have world changing potential on energy scenario[1]. The composite of interest is a few milestones away and this thesis is an attempt to cover a couple of miles in that direction. We start in next section with defining composite and then in this chapter, work is to understand and frame the problem statement investigated in this thesis.

[1] Available at http://cordis.europa.eu/projects/rcn/108893_en.html n.d

1.1 Composite

A composite, in general, is defined as a combination of two or more components differing in form or composition on a macro-scale like metals, ceramics, and polymers [2], with two or more distinct phases having recognizable interfaces between them [2,3].

The design goal of a composite is to achieve a combination of properties that is not displayed by any single material and to incorporate the best characteristics of each of the component materials. Different combinations of metals, ceramics, and polymers represent a large number of composite types. Furthermore, materials of biological origin are generally composites. For example, Bone, achieves its combination of lightness and strength by combining crystals of a compound of calcium with fiber of the protein collagen, whereas wood contains cellulose fibers surrounded by lignin and hemicelluloses. However, we are only going to consider the synthetic (or human-made) composites.

One of the most common and familiar synthetic composites is concrete, in which crushed rock aggregate are mixed with the cement to produce a composite structure, with reduced the cost and with improved compressive strength. Another technologically important synthetic composite is the carbon fiber-reinforced polymer (CFRP) composite in which carbon fibers (CFs) are embedded within a polymer. These materials are stiffer and stronger. Structural weight savings (while retaining the reliability and strength), are achieved for aerospace, rocket applications, automobile industry, sports goods etc. by the use of CFRP composite materials.

Composites are produced to optimize material properties namely mechanical (mainly strength), and chemical and/or physical properties. Since the early 1960s, there has been an increasing demand for materials that are stiffer and stronger, yet lighter in weight in aeronautics, energy sector, civil engineering and in various structural applications. Unfortunately, no *monolithic*[2] engineering material available is able to satisfy them. This need and demand necessitated the development of the concept of combining different materials in an integral composite structure.

[2] *Monolithic* means having a microstructure that is uniform and continuous and was formed from a single material; furthermore, more than one micro constituent may be present.

Composite consists of a reinforcing material embedded in a parent material matrix. The effective method to increase the strength and to improve overall properties is to incorporate uniformly dispersed reinforcing material into the matrix, which can be an engineering material such as ceramic, metal, or polymer. Hence, ceramic matrix composites, metal matrix composites (MMC) or polymer matrix composites (PMC) or ceramic/metal/polymer composites, carbon matrix composites (CMC) or even hybrid composites are obtained. In a composite, in general, matrices are of low modulus, while reinforcing elements are typically 50 times stronger and 20-150 times stiffer [2].

Polymer matrix composites (PMCs) consist of a polymer resin as the matrix and fibers as the reinforcement medium. These materials are used in the greatest diversity of composite applications, as well as in the largest quantities, in light of their room-temperature mechanical properties, ease of fabrication, and cost [4].

There are several limitations to this group of materials. In spite of having high strengths, they are not very stiff and do not display the rigidity that is necessary for engineering applications for example, as structural members for airplanes and bridges. Most fiberglass materials are limited to service temperatures below 200°C; at higher temperatures, most polymers begin to flow or start to deteriorate. Service temperatures may be extended to approximately 300°C by using high-purity fused silica for the fibers and using high temperature polymers such as the polyimide resins.

Ceramic matrix composite (CMC) materials are inherently resilient to oxidation and deterioration at elevated temperatures. These materials would be ideal candidates for use in high-temperature and severe-stress applications, specifically for components in automobile and aircraft gas turbine engines. The PMC are usually inadequate for such applications owing to their weak mechanical properties. Ceramic matrix composite lags behind PMC and MMC due to three main reasons. First, the processing methods for CMCs involve high temperatures and can only be embedded with fibers and whiskers of ceramics, which will not decompose or deteriorates at high temperature. A major attribute of monolithic[2] ceramics is that they maintain their properties at high temperatures and this characteristic is only retained in CMCs if the reinforcing materials also have stable properties at high temperature. Hence, there is only limited interest in toughening ceramics by incorporation of reinforcements of materials, which lose their strength and stiffness at intermediate temperatures. Secondly, almost

all ductile materials lose their strength and stiffness at intermediate temperature and therefore are ruled out as reinforcing material. This leaves only brittle material as a choice of reinforcing materials and therefore limits the objective of achieving a composite with desired properties. The third factor that has hindered the progress of CMCs is also concerned with the high temperatures. Differences in coefficients of thermal expansion, between the matrix and the reinforcement lead to thermal stresses on cooling from the processing temperature. However, the thermal stresses can generally be relieved in metal matrix composites by plastic deformation of the matrix, this is not possible for CMCs and cracking of the matrix can result. The nature of the cracking depends on the whether the reinforcement contracts more or less in comparison to the matrix on cooling. The rate of contraction during cooling determines the character (tensile or compressive) of the local thermal stresses and is termed as fracture toughness. The fracture toughness values for ceramic materials are low and typically lie between 5 to $20\,MPa\sqrt{m}$. The fracture toughness value of metal is much higher than the CMC, which lie in between 30 to $150\,MPa\sqrt{m}$ [2]. The metal matrix composite seemingly therefore, is better alternative composite when compared to the CMCs. As the name implies, for metal-matrix composites (MMCs) the matrix is a ductile metal. These materials may be used at higher service temperatures than their base metal counterparts; furthermore, the reinforcement may improve specific stiffness, specific strength, abrasion resistance, creep resistance, and dimensional stability. Some of the advantages of these materials over the polymer-matrix composites include higher operating temperatures, non-flammability, and greater resistance to degradation by organic fluids. Furthermore, since metals are more conductive (electrically and thermally), MMCs are also useful in heat dissipation in applications like electronic transmission applications.

Metal-matrix composites (MMCs) reinforced with ceramic offer the attractive combination of strength, stiffness, wear- and creep-resistant characteristics over monolithic alloys. The composites were initially developed for military and space applications. However, recent demand for materials with specified functional properties has led to their broad applications in ground transportation, automotive, chemical, electronic and recreational industries. In context to MMCs, continuous ceramic fiber-reinforced MMCs generally possess higher mechanical strength and stiffness, but the higher cost of fibers and complicated processing methods make

them uneconomical for most industrial applications. In this regard, particulate-reinforced MMCs have received increased attention recently because of their ease of fabrication, lower cost, and near-isotropic properties. Also lately, the size of the particulate reinforcement used is mostly in the dimension of nanometer. Many nanomaterials used for reinforcement allowed reaping benefits of extraordinary properties of nanomaterials. In next section, a brief introduction to few reinforcing nanomaterials and the importance of nanosize effect is presented.

1.2 Nanomaterial

Unlike other materials, nanomaterials are not distinguished on the basis of their chemistry but rather their size; the nano prefix denotes that the dimensions of these structural entities are on the order of a nanometer (10^{-9} m) as a rule, less than 100 nanometers (nm) (equivalent to approximately 500 atom diameters). Nanomaterials may be any one of the three basic types-metals, ceramics, and polymers. Nanomaterials are used in several areas of scientific studies and applications domains such as chemistry, electronics, sensors and biotechnology. Nanomaterials have received much attention because of their excellent and unique optical, electrical, magnetic, catalytic, or mechanical properties. Such properties originate from the finely tuned nano-architectures and nanostructures of these materials. However, the fabrication and analysis of nanomaterials remains challenging. Nanomaterials have brought about many great changes and new research opportunities in physics, chemistry, material science, and biology. Several important milestones have been marked in the field of development of nanomaterials. Generally, nanomaterials include colloidal crystals (nanocrystals), nanoparticles, nanorods, nanobelts, nonotubes, nanowires, superlattices, etc. [5] The properties of nanomaterials are influenced and modified by reduced dimensionality, proximity effects, and surface effects dominating over the bulk effects. Owing to the fact that the surface/volume ratio drastically increases in nanomaterials, hence, applications associated with reaping the benefits of the surface effect have appeared, for example, the development of catalysts. One of the nanomaterial which is very widely investigated and used in various engineering application is carbon nanotubes (CNTs).

The discovery and popularity of carbon nanotube is extensively credited to Sumio Ijima in 1991 [6], though prior to Iijima, also the CNTs were reported. Prior to Iijima [6], some of the most important work in this category are the investigation on 50 nm diameter hollow graphitic carbon fibers by Radushkevich and Lukyanovich [7] in 1952. In 1960, Bollmann and Spreadborough [8] discussed friction properties of carbon due to rolling sheets of graphene in nature. They had shown the electron microscopy image of multiwalled carbon nanotube (MWCNT), in 1976. Oberlin, Endo, and Koyama [9] reported Chemical Vapor Deposition (CVD) growth of nanometer-scale carbon fibers. Though CNTs had been synthesized earlier, the report of Sumio Ijima introduced the CNT to the world in a better way and his report acted as a catalyst for the research activity in the field of nanotechnology. Subsequently, Iijima and Ichihashi [10] and Bethune et al. [11] discovered single-walled carbon nanotubes (SWCNT) independently.

The carbon nanotubes are of interest because of strong carbon-carbon covalent bonds and their similar and aligned bonding along the axis of nanotubes. In comparison to most widely used engineering material mild steel, CNTs shows extraordinary better value of mechanical and electrical properties. Theoretically, therefore it is predicted that the nanotubes are exceedingly strong with Young's modulus of MWCNT lies between 1.7 TPa to 5.5 TPa [12–16] and tensile strength 13 to 63 GPa. In comparison to mild steel, these values are five times higher for Young's modulus and fifty times higher for tensile strength. Strain in CNTs is in range of 5 to 12% [17–19]. Among other mechanical properties, density of CNT is very less and falls in the range of 1.3 to 2.1 g/m^3 [20–23] as compared with density 7850×10^3 g/m^3 of mild steel. Theoretical calculations and experimental measurements showed that the thermal conductivity for a SWNT ropes and MWNTs at room temperature could be between 1800 and 6000 W/mK [24–31] compared to thermal conductivity of 401 W/mK of the good conductor like copper , this is 5 to 15 times higher.

These remarkable properties make the CNTs, an ideal reinforcing material for the composites, for possible improvement in physical properties both mechanical as well as electrical. In order to have advantage of their extraordinary properties at bulk level, scientists are investigating possibility of preparing composites, termed as CNT reinforced composites, which are detailed in next section.

1.3 Composite reinforced with nano size reinforcement

Among many nano sized particles/fibers/tubes, carbon nanotube have gained a repute of extremely used reinforcement material. Research groups have worked for synthesizing CNT/metal composite for different metals like Cu [32–47], Al [48–68], Mg [69–73], Ni [74–83], Ag [84–86], Au [87–91], and inter-metallic compound like Fe_3Al [92]. Among these attempts, most of research has been done with developing CNT/Ni composite by electro-co-deposition or by electroless method. CNT/Al and CNT/Cu composites are also fabricated for high thermal conductivity, lightweight and high strength material. Copper had been a metal of interest since ages because of its high thermal and electrical conductivity apart from its aesthetic usage. Higher value of electrical and thermal conductivity has made copper as a prominent material for use in almost all electrical appliances. About 64% [93] of metal used in electrical industry sector is copper. Keeping in view the importance of copper and its high usage in the human life, its ever-growing demand, scientists are looking forward and investigating a possibility of ultra-conductive copper[3]. The ultra-conductive copper is being developed with an objective of at least twice the conductivity of pure copper without compromising on its mechanical and thermal properties. In that direction CNT/Cu composite is being researched across the globe. For example, a consortium of 14 countries[3] have come together to develop the ultra-conductive copper with a funding of 26 Cr. (€ 3.3 million). The need of CNT/Cu composite is presented in the next section, which will be the topic of interest for the thesis. Thesis is mainly focused on the CNT/Cu composite, because of few motivating factors, which are discussed in the next sections.

1.4 Need of CNT/Cu Composite

Copper makes vital contributions for sustaining and improving society. Copper's chemical, physical properties like thermal conductivity, electrical conductivity and aesthetic properties make it a material of choice in a wide range of domestic, industrial and high technology applications.

The global demand for copper continues to grow: world refined usage has surged by around 300% in the last 50 years [93]. The increase in demand is all due to expanding

[3] Available at http://cordis.europa.eu/projects/rcn/108893_en.html n.d.

sectors such as electrical and electronic products, building construction, industrial machinery and equipment, transportation equipment, and consumer and general products and due to increase in population. According to Gordon et al. [94], the current per capita consumption of copper in North America is 170 *kg*, ten times more than the developing world and is increasing every year. It is also observed by Gordon et al. [94] that the cumulative extraction of copper for the world has been growing faster than cumulative discovery and they noted that it is more disturbing that cumulative extractions are now approaching cumulative discoveries as shown in Figure 1.1.

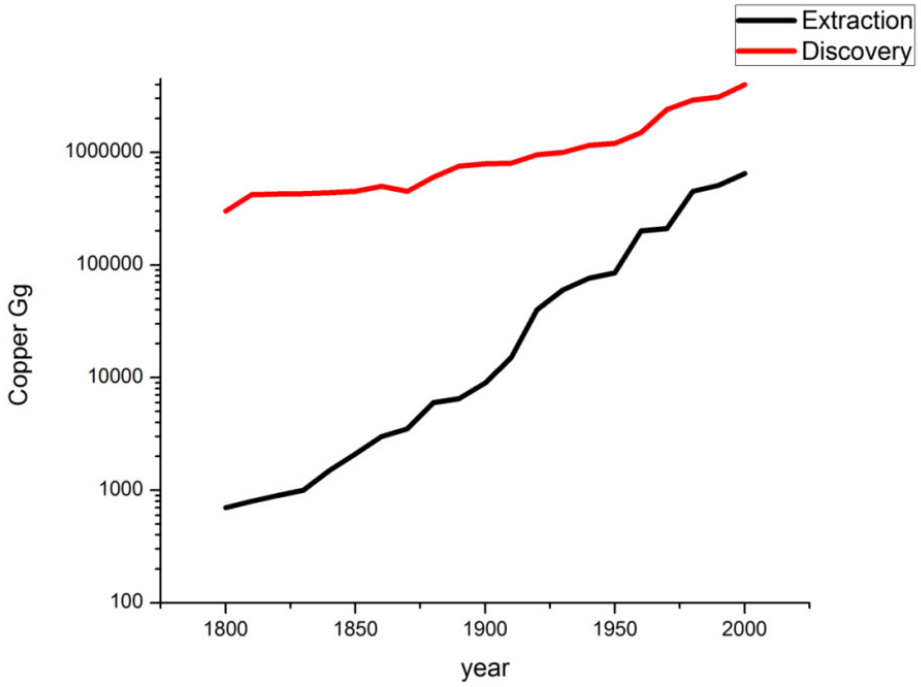

Figure 1.1: Adopted from [94]**, cumulative discovery of copper in ore and the cumulative extraction of copper worldwide in the 18th-20th centuries. (Gg on *y*-axis stands for gigagram)**

Considering the population reaches to 10 billion by the end of 21st century, the consumption will reach to 1.7 billion tons according to per capita consumption of North America. This requirement exceeds the total recoverable copper present in resources estimated at 1.6 billion tons. In addition, the present new and interesting data indicates that 26 percent of the copper available in resources has been discarded into wastes. For these reasons, we can conclude that the world will soon be running short of copper resources. Copper prices will probably extraordinarily rise over the current century.

Recycling of copper may be one way to overcome the deficiency in supply of copper, which is pursued since last couple of decades. According to Gordon et al.[94], even the recyclable copper is depleting and may not be a solution to the resource crunch for copper. The mining sector is constantly undergoing technological renovation, which besides increasing efficiency makes it possible for copper mining companies to exploit lower grade deposits, containing copper less than 0.5%. The refining and value addition to copper may be alternatives to improve efficient use of copper.

By reinforcing CNTs, the properties of the copper can be improved and the copper may be used more efficiently. CNT/Cu composite may be an excellent thermal conductor because of high thermal conductivity of the Cu (396 *W/mK*) and CNT ($\approx$3000 *W/mK*) as well as it will be lightweight. Current carrying density of the CNT is around 1000 times [95] more than the copper and hence the reinforcement of carbon nanotube in the copper may improve the current carrying capacity of the composite. But, it is difficult to convert the properties of CNT present at nano-size to the practical structural material of macro size scale. There are several challenges in the fabrication of CNT reinforced Cu composites to be used at bulk level, like agglomeration of CNT, nonuniform dispersion and misalignment of CNT in the metal matrix, damage to the CNT during fabrication process.

Researchers are trying to overcome these issues by employing various synthesis methods. Due to high melting point of copper, powder metallurgy or electrochemical deposition is preferred for mixing of CNT in the molten metal for synthesis of CNT/Cu composite. The uniform dispersion of CNTs in the metal powder is the most desired aspect of CNT/Cu composite but uniform dispersion is a great challenge towards preparing useful product. CNTs have large specific surface area and consequently lean to agglomerate and form clusters due to van der Waals forces. Uniform dispersion of the reinforcement is a necessity for harnessing the extraordinary properties of CNT as well as for obtaining isometric composite. CNT clusters have lower strength and higher porosity, and serve as discontinuities. Thus, they increase the porosity of the composite and in turn affect adversely on the composite properties. Thus, for successful processing, achieving uniform carbon nanotube dispersion in the copper matrix is one of the main challenges. The processing methods adopted are subject to the constraints of ensuring minimal damage to CNT structure. The damage may be due to applied stresses or due to reaction with the matrix material at elevated temperature. Depending on the nature of the

process, CNTs may be subjected to high temperature and stress or contact with molten metal. This may also lead to composite with high defect density.

In order to overcome these problems, some researchers used mechanical alloying (MA) method for mixing CNT and Cu powder. MA leads to the excellent dispersion of CNTs in the metal matrix but might result in the severe damage to CNTs due to intensive ball-milling for hours. Molecular level mixing is another process, which is capable of producing one-dimensional nanostructure of CNT coated with metal. However, the product of the molecular level mixing may not be directly useful for the powder metallurgy (PM) and the method is at laboratory level. Electro-co-deposition and electroless deposition are other preferred methods for fabrication of CNT/Cu coating or thin film. The thickness of composite coating or thin film by these methods will be less than $200\,\mu m$. Therefore, it is difficult to fabricate a freestanding structure by using electro-co-deposition and electroless deposition and therefore a process for bulk production of the composite may still be a distant dream.

The need is beckoning and the problem of realization of CNT/Cu composite at bulk production level looms large yet unresolved. Among many issues and challenges, the present thesis addresses uniform dispersion aspect of CNTs in the metal matrix with an innovatively modified electro-co-deposition method suitable for bulk production of composite. The next chapter presents, the detailed review on the different CNT/Cu composite synthesis processes and the properties of the CNT/Cu composite achieved by various methods. It also includes the advantages and disadvantages of the present methods and discusses the scope of improvement in the synthesis process. Based on literature review and discussion, problem statement addressed in this thesis are formed and presented.

References:

[1] Government of India Ministry of Power Central Electricity Authority New Delhi Executive Summary Power Sector. 2014.

[2] Callister WD, Rethwisch DG. Fundamentals of Material Scienec and Engineering An Integrated Approach. 4 th. John wiley and Sons, Inc; 2012.

[3] Herakovich CT of V. Mechanics of Fibrous Composites. New York: John wiley and Sons, Inc; 1998.

[4] Tjong SC. Carbon Nanotube Reinforced Composites. WILEY-VCH Verlag GmbH and Co. KGaA; 2009.

[5] Capek I. Nanocomposite Structures and Dispersions Science and Nanotechnology- Fundamental Principles and colloidal Particles. 1st ed. Elsevier; 2006.

[6] Iijima S. Helical microtubules of graphitic carbon. Nature 1991;354:56–8.

[7] Radushkevich L, Lukyanovich V. O strukture ugleroda, obrazujucegosja pri termiceskom razlozenii okisi ugleroda na zeleznom kontakte. Zurn Fis Chim 1952;26:88–95.

[8] Bollmann W, Spreadborough J. Action of Graphite as a Lubricant. Nature 1960;186:29–30.

[9] Oberlin A, Endo M, Koyama T. Filamentous growth of carbon through benzene decomposition. J Cryst Growth 1976;32:335–49.

[10] Iijima S, Ichihashi T. Single- shell carbon nanotube of 1-nm diameter. Nature 1993;363:603–5.

[11] Bethune DS, Klang CH, de Vries MS, Gorman G, Savoy R, Vazquez J, et al. Cobalt-catalysed growth of carbon nanotubes with single-atomic-layer walls. Nature 1993;363:605–7.

[12] Yao N, Lordi V, Introduction I. Young's modulus of single-walled carbon nanotubes. J Appl Phys 1998;84:1939–43.

[13] Meo M, Rossi M. A molecular-mechanics based finite element model for strength prediction of single wall carbon nanotubes. Mater Sci Eng A 2007;455:170–7.

[14] Meo M, Rossi M. Prediction of Young's modulus of single wall carbon nanotubes by molecular-mechanics based finite element modelling. Compos Sci Technol 2006;66:1597–605.

[15] Krishnan A, Dujardin E, Ebbesen TW, Yianilos PN, Treacy MMJ. Young's modulus of single-walled nanotubes. Phys Rev 1998;58:13–9.

[16] Li C, Ruoff R, Chou T. Modeling of carbon nanotube clamping in tensile tests. Compos Sci Technol 2005;65:2407–15.

[17] Yu M, Files B, Arepalli S, Ruoff R. Tensile loading of ropes of single wall carbon nanotubes and their mechanical properties. Phys Rev Lett 2000;84:5552–5.

[18] Buongiorno Nardelli M, Yakobson B, Bernholc J. Mechanism of strain release in carbon nanotubes. Phys Rev B 1998;57:R4277–R4280.

[19] Yu M, Lourie O, Dyer MJ, Moloni K, Kelly TF, Ruoff RS. Strength and Breaking Mechanism of Multiwalled Carbon Nanotubes Under Tensile Load. Science (80-) 2000;287:637–40.

[20] Wang D, Song P, Liu C, Wu W, Fan S. Highly oriented carbon nanotube papers made of aligned carbon nanotubes. Nanotechnology 2008;19:075609.

[21] Xie H. Thermal and electrical transport properties of a self-organized carbon nanotube pellet. J Mater Sci 2007;42:3695–8.

[22] Lusti HR, Gusev A a. Finite element predictions for the thermoelastic properties of nanotube reinforced polymers. Model Simul Mater Sci Eng 2004;12:S107–S119.

[23] Manafi S a., Amin MH, Rahimipour MR, Salahi E, Kazemzadeh a. Carbon nanotubes synthesized by mechanothermal method. New Carbon Mater 2009;24:39–44.

[24] Goddard III WA, Che J, Ca T. Thermal conductivity of carbon nanotubes. Nanotechnology 2000;11:65–9.

[25] Venkata Sastry NN, Bhunia A, Sundararajan T, Das SK. Predicting the effective thermal conductivity of carbon nanotube based nanofluids. Nanotechnology 2008;19:055704.

[26] Berber S, Kwon Y, Tomanek D. Unusually high thermal conductivity of carbon nanotubes. Phys Rev Lett 2000;84:4613–6.

[27] Yang D, Zhang Q, Chen G, Yoon S, Ahn J, Wang S, et al. Thermal conductivity of multiwalled carbon nanotubes. Phys Rev B 2002;66:165440.

[28] Fujii M, Zhang X, Xie H, Ago H, Takahashi K, Ikuta T, et al. Measuring the Thermal Conductivity of a Single Carbon Nanotube. Phys Rev Lett 2005;95:065502.

[29] Dresselhaus MS, Dresselhaus G, Charlier JC, Hernández E. Electronic, thermal and mechanical properties of carbon nanotubes. Philos Trans A Math Phys Eng Sci 2004;362:2065–98.

[30] Hone J, Whitney M, Piskoti C, Zettl a. Thermal conductivity of single-walled carbon nanotubes. Phys Rev B 1999;59:R2514–R2516.

[31] Hepplestone SP, Srivastava GP. Low-temperature mean-free path of phonons in carbon nanotubes. J Phys Conf Ser 2007;92:012076.

[32] Chai Y, Member S, Chan PCH, Fu Y, Chuang YC, Liu CY. Electromigration Studies of Cu / Carbon Nanotube Composite Interconnects Using Blech Structure. IEEE ELECTRON DEVICE Lett 2008;29:1001–3.

[33] Cho S, Kikuchi K, Kawasaki A, Kwon H, Kim Y. Effective load transfer by a chromium carbide nanostructure in a multi-walled carbon nanotube/copper matrix composite. Nanotechnology 2012;23:315705.

[34] Kim KT, Eckert J, Menzel SB, Gemming T, Hong SH. Grain refinement assisted strengthening of carbon nanotube reinforced copper matrix nanocomposites. Appl Phys Lett 2008;92:121901.

[35] Uddin SM, Mahmud T, Wolf C, Glanz C, Kolaric I, Volkmer C, et al. Effect of size and shape of metal particles to improve hardness and electrical properties of carbon nanotube reinforced copper and copper alloy composites. Compos Sci Technol 2010;70:2253–7.

[36] Kim KT, Cha S Il, Gemming T, Eckert J, Hong SH. The role of interfacial oxygen atoms in the enhanced mechanical properties of carbon-nanotube-reinforced metal matrix nanocomposites. Small 2008;4:1936–40.

[37] Chai G, Sun Y, Sun J “Jenny”, Chen Q. Mechanical properties of carbon nanotube–copper nanocomposites. J Micromechanics Microengineering 2008;18:035013.

[38] Wang F, Arai S, Endo M. Metallization of multi-walled carbon nanotubes with copper by an electroless deposition process. Electrochem Commun 2004;6:1042–4.

[39] Belgamwar SU, Sharma NN. Method of Producing Uniform Mixture of Copper and Carbon Nanotube in Bulk for Copper Metal Nanocomposite. 2454/DEL/2102A, 2012.

[40] Baik S, Lim B, Ryu S, Choi D, Kim B, Oh S, et al. Mechanical and electrical properties of Carbon nanotubes in copper matrix nanocomposites. Solid State Phenom 2007;120:285–8.

[41] Kim C, Lim B, Kim B, Shim U, Oh S, Sung B, et al. Strengthening of copper matrix composites by nickel-coated single-walled carbon nanotube reinforcements. Synth Met 2009;159:424–9.

[42] Belgamwar SU, Sharma NN. Synergistic electro-co-deposition and molecular mixing for reinforcement of multi-walled carbon nanotube in copper. Mater Sci Eng B 2013;178:1452–7.

[43] Yang YL, Wang YD, Ren Y, He CS, Deng JN, Nan J, et al. Single-walled carbon nanotube-reinforced copper composite coatings prepared by electrodeposition under ultrasonic field. Mater Lett 2008;62:47–50.

[44] Chu K, Guo H, Jia C, Yin F, Zhang X, Liang X, et al. Thermal properties of carbon nanotube-copper composites for thermal management applications. Nanoscale Res Lett 2010;5:868–74.

[45] Wang J, Chen G, Wang M, Chatrathi MP. Carbon-nanotube/copper composite electrodes for capillary electrophoresis microchip detection of carbohydrates. Analyst 2004;129:512–5.

[46] Kim KT, Cha S Il, Hong SH. Hardness and wear resistance of carbon nanotube reinforced Cu matrix nanocomposites. Mater Sci Eng A 2007;449-451:46–50.

[47] Peng Y, Chen Q. Ultrasonic-assisted fabrication of highly dispersed copper/multi-walled carbon nanotube nanowires. Colloids Surfaces A Physicochem Eng Asp 2009;342:132–5.

[48] Esawi a., Morsi K. Dispersion of carbon nanotubes (CNTs) in aluminum powder. Compos Part A Appl Sci Manuf 2007;38:646–50.

[49] Xu CL, Wei BQ, Ma RZ, Liang J, Ma XK, Wu DH. Fabrication of aluminum – carbon nanotube composites and their electrical properties. Carbon N Y 1999;37:855–8.

[50] Kuzumaki T, Miyazawa K, Ichinose H, Ito K. Processing of Carbon Nanotube Reinforced Aluminum Composite. J Mater Res 1998;13:2445–9.

[51] Thuaire A, Goujon C, Gauvin R, Drew R a. L. Study on the Fabrication of Aluminum Matrix Nanocomposites Reinforced with Carbon Nanotubes. Microsc Microanal 2004;10:574–5.

[52] Morsi K, Esawi a. Effect of mechanical alloying time and carbon nanotube (CNT) content on the evolution of aluminum (Al)–CNT composite powders. J Mater Sci 2007;42:4954–9.

[53] Ci L, Ryu Z, Jin-Phillipp NY, Rühle M. Investigation of the interfacial reaction between multi-walled carbon nanotubes and aluminum. Acta Mater 2006;54:5367–75.

[54] Kwon H, Leparoux M. Hot extruded carbon nanotube reinforced aluminum matrix composite materials. Nanotechnology 2012;23:415701.

[55] Lahiri D, Bakshi SR, Keshri a. K, Liu Y, Agarwal A. Dual strengthening mechanisms induced by carbon nanotubes in roll bonded aluminum composites. Mater Sci Eng A 2009;523:263–70.

[56] Bakshi SR, Singh V, Balani K, McCartney DG, Seal S, Agarwal A. Carbon nanotube reinforced aluminum composite coating via cold spraying. Surf Coatings Technol 2008;202:5162–9.

[57] Deng CF, Ma YX, Zhang P, Zhang XX, Wang DZ. Thermal expansion behaviors of aluminum composite reinforced with carbon nanotubes. Mater Lett 2008;62:2301–3.

[58] Deng C, Zhang P, Ma Y, Zhang X, Wang D. Dispersion of multiwalled carbon nanotubes in aluminum powders. Rare Met 2009;28:175–80.

[59] Deng CF, Wang DZ, Zhang XX, Ma YX. Damping characteristics of carbon nanotube reinforced aluminum composite. Mater Lett 2007;61:3229–31.

[60] Bakshi SR, Keshri AK, Singh V, Seal S, Agarwal A. Interface in carbon nanotube reinforced aluminum silicon composites: Thermodynamic analysis and experimental verification. J Alloys Compd 2009;481:207–13.

[61] Bakshi SR, Patel RR, Agarwal A. Thermal conductivity of carbon nanotube reinforced aluminum composites: A multi-scale study using object oriented finite element method. Comput Mater Sci 2010;50:419–28.

[62] Esawi a. MK, Morsi K, Sayed a., Gawad a. A, Borah P. Fabrication and properties of dispersed carbon nanotube–aluminum composites. Mater Sci Eng A 2009;508:167–73.

[63] Bakshi SR, Singh V, Seal S, Agarwal A. Aluminum composite reinforced with multiwalled carbon nanotubes from plasma spraying of spray dried powders. Surf Coatings Technol 2009;203:1544–54.

[64] Kwon H, Estili M, Takagi K, Miyazaki T, Kawasaki A. Combination of hot extrusion and spark plasma sintering for producing carbon nanotube reinforced aluminum matrix composites. Carbon N Y 2009;47:570–7.

[65] Deng C, Zhang X, Wang D, Lin Q, Li A. Preparation and characterization of carbon nanotubes/aluminum matrix composites. Mater Lett 2007;61:1725–8.

[66] Kim I-Y, Lee J-H, Lee G-S, Baik S-H, Kim Y-J, Lee Y-Z. Friction and wear characteristics of the carbon nanotube–aluminum composites with different manufacturing conditions. Wear 2009;267:593–8.

[67] Choi H, Kwon G, Lee G, Bae D. Reinforcement with carbon nanotubes in aluminum matrix composites. Scr Mater 2008;59:360–3.

[68] Deng CF, Wang DZ, Zhang XX, Li a. B. Processing and properties of carbon nanotubes reinforced aluminum composites. Mater Sci Eng A 2007;444:138–45.

[69] Li Q, Viereckl A, Rottmair C a., Singer RF. Improved processing of carbon nanotube/magnesium alloy composites. Compos Sci Technol 2009;69:1193–9.

[70] Thakur SK, Srivatsan TS, Gupta M. Synthesis and mechanical behavior of carbon nanotube–magnesium composites hybridized with nanoparticles of alumina. Mater Sci Eng A 2007;466:32–7.

[71] Goh CS, Wei J, Lee LC, Gupta M. Development of novel carbon nanotube reinforced magnesium nanocomposites using the powder metallurgy technique. Nanotechnology 2006;17:7–12.

[72] Shimizu Y, Miki S, Soga T, Itoh I, Todoroki H, Hosono T, et al. Multi-walled carbon nanotube-reinforced magnesium alloy composites. Scr Mater 2008;58:267–70.

[73] Chen D, Chen L, Liu S, Ma CX, Chen DM, Wang LB. Microstructure and hydrogen storage property of Mg/MWNTs composites. J Alloys Compd 2004;372:231–7.

[74] Chen XH, Chen CS, Xiao HN, Cheng FQ, Zhang G, Yi GJ. Corrosion behavior of carbon nanotubes–Ni composite coating. Surf Coatings Technol 2005;191:351–6.

[75] Dai P-Q, Xu W-C, Huang Q-Y. Mechanical properties and microstructure of nanocrystalline nickel-carbon nanotube composites produced by electrodeposition. Mater Sci Eng A 2008;483-484:172–4.

[76] Hwang JY, Neira a., Scharf TW, Tiley J, Banerjee R. Laser-deposited carbon nanotube reinforced nickel matrix composites. Scr Mater 2008;59:487–90.

[77] Guo C, Zuo Y, Zhao X, Zhao J, Xiong J. Effects of surfactants on electrodeposition of nickel-carbon nanotubes composite coatings. Surf Coatings Technol 2008;202:3385–90.

[78] Chen XH, Peng JC, Li XQ, Deng FM, Wang JX, Li WZ. Tribological behavior of carbon nanotubes — reinforced nickel matrix. J Mater Sci Lett 2001;20:2057–60.

[79] Sung D, Park N, Kim G, Hong S. Enhanced binding strength between metal nanoclusters and carbon nanotubes with an atomic nickel defect. Nanotechnology 2012;23:205204.

[80] Chen XH, Cheng FQ, Li SL, Zhou LP, Li DY. Electrodeposited nickel composites containing carbon nanotubes. Surf Coatings Technol Technol 2002;155:274–8.

[81] Sun Y, Sun J, Liu M, Chen Q. Mechanical strength of carbon nanotube–nickel nanocomposites. Nanotechnology 2007;18:505704.

[82] Tan J, Yu T, Xu B, Yao Q. Microstructure and wear resistance of nickel–carbon nanotube composite coating from brush plating technique. Tribol Lett 2006;21:107–11.

[83] Titus E, Cabral G, Madaleno JCC, Neto VFF, Shokuhfar T, Blau WJJ, et al. Synthesis of highly oriented carbon nanotube thin films by nickel functionalisation. Diam Relat Mater 2007;16:1195–9.

[84] Alimohammadi F, Gashti MP, Shamei A, Kiumarsi A. Deposition of silver nanoparticles on carbon nanotube by chemical reduction method: Evaluation of surface, thermal and optical properties. Superlattices Microstruct 2012;52:50–62.

[85] Feng Y, Yuan HL, Zhang M. Fabrication and properties of silver-matrix composites reinforced by carbon nanotubes. Mater Charact 2005;55:211–8.

[86] Oh Y, Suh D, Kim Y, Lee E, Mok JS, Choi J, et al. Silver-plated carbon nanotubes for silver/conducting polymer composites. Nanotechnology 2008;19:495602.

[87] Gingery D, Bühlmann P. Formation of gold nanoparticles on multiwalled carbon nanotubes by thermal evaporation. Carbon N Y 2008;46:1966–72.

[88] Shi Y, Yang R, Yuet PK. Easy decoration of carbon nanotubes with well dispersed gold nanoparticles and the use of the material as an electrocatalyst. Carbon N Y 2009;47:1146–51.

[89] Yogeswaran U, Thiagarajan S, Chen S. Nanocomposite of functionalized multiwall carbon nanotubes with nafion , nano platinum , and nano gold biosensing film for simultaneous determination of ascorbic acid , epinephrine , and uric acid. Anal Biochem 2007;365:122–31.

[90] Tello A, Cárdenas G, Häberle P, Segura R a. The synthesis of hybrid nanostructures of gold nanoparticles and carbon nanotubes and their transformation to solid carbon nanorods. Carbon N Y 2008;46:884–9.

[91] Jiang H-J, Zhao Y, Yang H, Akins DL. Synthesis and electrochemical properties of single-walled carbon nanotube–gold nanoparticle composites. Mater Chem Phys 2009;114:879–83.

[92] Pang L-X, Sun K-N, Ren S, Sun C, Fan R-H, Lu Z-H. Fabrication and microstructure of Fe3Al matrix composite reinforced by carbon nanotube. Mater Sci Eng A 2007;447:146–9.

[93] World T, Factbook C. The world copper factbook 2012. Internatioanl Copp Study Gr 2012.

[94] Gordon RB, Bertram M, Graedel TE. Metal stocks and sustainability. Proc Natl Acad Sci U S A 2006;103:1209–14.

[95] Hong S, Myung S. NANOTUBE ELECTRONICS A fl exible approach to mobility. Nat Nanotechnol 2007;2:207–8.

Chapter 2

Literature Review

2.1 Introduction

In the previous chapter, we discussed the need for composite, and advantages of composite with nanomaterials. We also elaborated use of CNTs as a competitive nanomaterial for reinforcement in composite. Different types of composites like Polymer matrix composite (PMC), ceramics matrix composite (CMC) and metal matrix composite (MMC) and advantages and disadvantages of each were presented and we have also detailed the development of nanomaterials and different type of metal nano-composite. For different types of composite the carbon nanotubes seemingly is a boon nanomaterial for reinforcement.

Carbon nanotubes (CNTs) have higher tensile strength, stiffness, and flexibility and are far superior to carbon fibers (CFs) as reinforcements for metals. Normally, carbon nanotubes are obtained in the form of a black powder similar to metallic powders. The powders are made up of lumps, which are made up of entangled CNTs. When looking inside a scanning electron microscope (SEM), one can see the CNTs twisted and entangled with each other as shown in Figure 2.1.

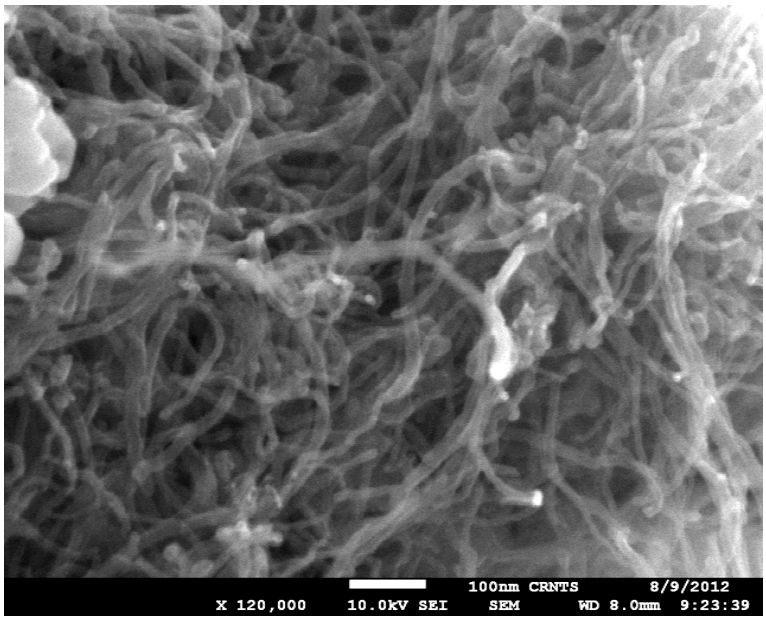

Figure 2.1: Scanning electron microscopy (SEM) image of MWCNT

The type of synthesis of CNTs is also very important in context to the quality of CNTs. In case of chemical vapor deposition (CVD) grown CNTs, the catalyst particles get trapped inside the CNTs. This trapped particles effect the properties of not only CNTs but also that of composite formed by reinforcement with such CNTs. Transmission electron microscope (TEM) images as shown in Figure 2.2, shows the trapped catalyst in the CNT when synthesized using CVD route.

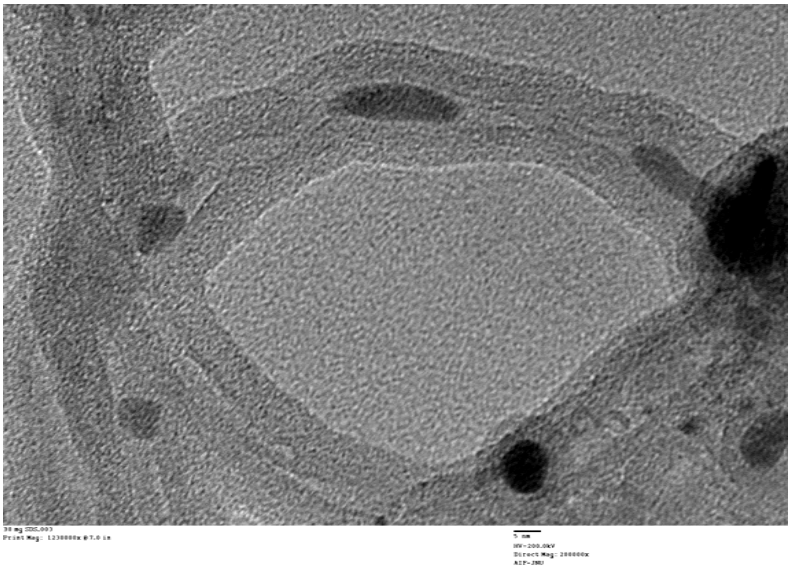

Figure 2.2: TEM image showing catalytic particles encapsulated in the carbon nanotube lumen

The addition of low loading level of CNTs to metals enhances the strength and stiffness of composites. In certain cases, a dramatic improvement in tensile strength and ductility in CNT/metal composites over unreinforced metals has been reported [1,2]. Furthermore, CNTs with excellent thermal conductivity are effective heat dissipating fillers for metals, which are very useful as thermal management components in electronic devices [3]. At present, ceramic particle-reinforced Aluminum (Al)-based metal matrix composites are widely used in electronic packaging and thermal management applications. In place of Al-based metal matrix composite, Cu-based composites are also used for the thermal management system. Recently, the escalations of fossil fuel prices for the generation of electrical power and the need to minimize the transmission losses have driven the search for high ampacity and low resistivity material for fabrication of wires, which will reduce losses in electrical transmission and in appliances. In the last chapter, we discussed a possibility of better

conductivity copper being developed by reinforcing the copper matrix with carbon nanotubes to salvage the problem of electric power losses. The metal composite of interest in this work therefore is copper metal reinforced with carbon nanotube and this metal composite of interest will be referred to as MWCNT reinforced copper matrix represented as MWCNT/Cu throughout this thesis.

The CNT may help in taking the properties of copper to the next level. However, it has been extremely difficult to turn this potential into a method for producing practically structural material in the form of a bulk product. In context to realization of composite obtained by reinforcing copper metal matrix with CNTs, there are few issues. The issues which need to be addressed and tailored namely are (i) nonuniform distribution of the CNT in the metal matrix, (ii) misalignment of CNT in the metal matrix, (iii) weak interfacial bonding between CNT and metal matrix, and (iv) damage to the properties of CNT during processing. Many researchers are working extensively since last two decades to improve the prospect of achieving better metal composite. Number of methods with alterations and omission are being developed, modelling and simulation to understand the basics of mixing and synthesis are being carried out and nonetheless, newer nanomaterials are being tried to reinforce the metal matrices to achieve the better product in bulk quantities. Method adopted to synthesize the metal composite plays an important role in deciding the properties of final product. First, the microstructure of the product is controlled by adopted method and second, the adopted method only will decide if the product can be synthesized in bulk or not. Therefore, among three of the possible investigations to achieve the better metal composite namely [i] method, [ii] nanomaterial itself, and [iii] modelling and simulation, we have focussed this thesis on investigation of methods available and alteration of method to overcome issues to obtain uniform and better dispersion of CNT in the metal matrix and bulk formation of product i.e. metal composite. The chosen metal as explained earlier is copper and the chosen nanomaterial for reinforcement is multiwalled carbon nanotube. We, therefore, first compile the available literature on methods for synthesizing metal composite in next sections starting with the enlisting of various type of methods and thereafter compiling chronologically available literature for all these methods.

2.2 Methods for Reinforcing Carbon Nanotube in Copper Matrix

Several physical methods for synthesis of composite are there like powder metallurgy, casting, metal infiltration, plasma spraying, cold spraying, sandwich processing, melt spinning etc. However, powder metallurgy and sandwich process are most popular and widely used method for the synthesis of CNT/Cu composite. Electrochemical methods, molecular level mixing method, nanoscale dispersion, mixing as a paste, chemical vapour deposition are the chemical processes. Electrochemical process and molecular level mixing process are the most often used and extremely reported methods used for synthesis of metal composite. A hierarchical classification of the processes used for the synthesis of CNT/Cu composite is shown in Figure 2.3.

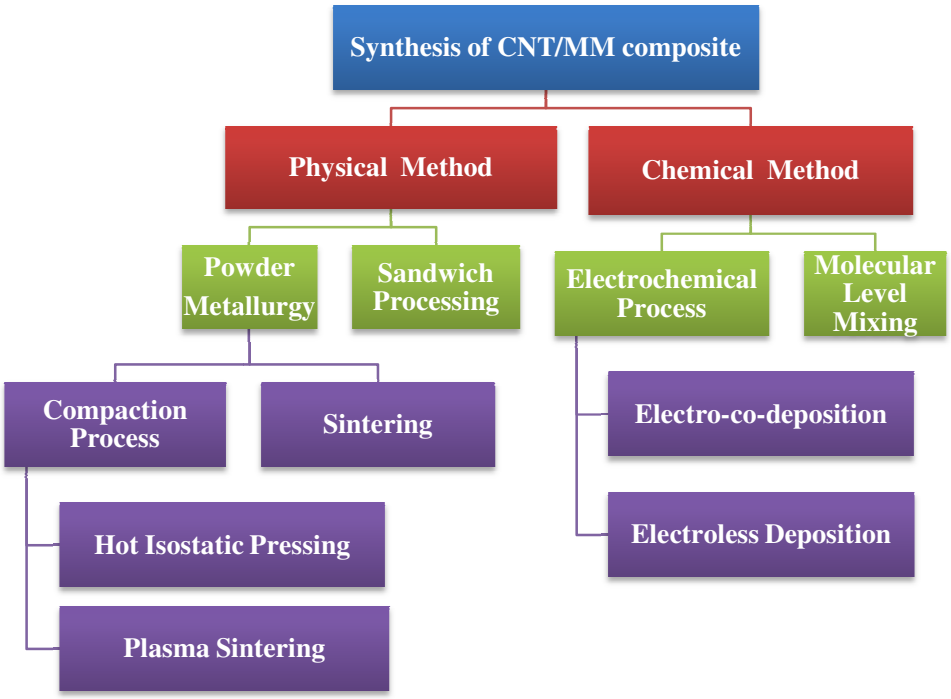

Figure 2.3: Classification of fabrication methods

As per the Figure 2.3, the synthesis processes are mainly divided in to two subgroups i.e. physical methods and chemical methods. In physical methods namely powder metallurgy, different compaction, sintering or the combinations of both are used which is shown in the classification. Compaction and then sintering is a general method for synthesis of green compact[1]. In order to achieve higher density,

[1] The weak metal part created after compacting in powder metallurgy die before sintering.

simultaneous sintering and compaction process is used which are named as hot isostatic pressing and plasma sintering. Details about these processes are discussed in the next section.

Chemical methods are classified as electrochemical and molecular level mixing. The electrochemical process is again divided in two sub groups like electro-co-deposition and electroless deposition process. The details about these processes are discussed in the next section.

2.2.1 Physical Methods

Physical methods include powder metallurgy technique (PM), melting and solidification, stirring and die casting of metal, sputtering of metal, vapour decomposition and spray coating. The available literature and details on these processes is given in the next subsection.

2.2.1.1 *Powder metallurgy*

Powder metallurgy [PM] is a method by which a freestanding structure of composite can be synthesized. There are three major processing stages in PM technique. For synthesis of CNT/Metal composite, first, the primary materials are physically powdered and mixed. Next, compaction of the fine powder formed in the previous stage is done which is followed finally by sintering and sizing. All these stages are important, but from point of view of uniform distribution of CNT in the metal matrix, first stage of mixing two components is more important. In order to have uniform distribution of the CNT in the metal matrix most of the research groups used ball milling of the CNT and copper.

In 1998, T. Kuzumaki et al. [4], have used the powder metallurgy process for the first time to fabricate CNT/Al composite. They used carbon powder containing approximately 60 vol% of carbon nanotube. They mixed 5 to 10% of carbon powder with aluminium powder having 99.99% purity and with 40 μm size. The mix then was agitated in the ethanol solution at 300 rpm for 30 mins. Then the composite powder was removed from the solution and prepared by vacuum drying method. Due to impurity of the CNT, non-uniform dispersion is observed in the aluminium powder. In 1999, C.L.Xu et al. [5], mixed the pure carbon nanotube produced by catalytic decomposition of propylene, with 99.5% pure aluminium powder with an average size of 70 μm. Different wt% of carbon nanotubes were mixed with 35 gm of aluminium powder by hand grinding for 30 min.

They observed some agglomeration of CNT at the grain boundary of the aluminium; this agglomeration was probably due to hand grinding process. However, unlike Kuzumaki, C.L. Xu could see some interfacial reaction in the form of carbide between aluminium and CNT. Several other research groups have done work on CNT/Al, CNT/Ag, CNT/Mg and CNT/Fe_3Al composite by powder metallurgy. The detail of the researches is arranged chronologically in the following Table 2.1

Table 2.1: Chronologically arranged research in CNT/Metal composite by powder metallurgy method

SN.	Year	Author	Ref.	Remarks
				CNT/Al
1.	2003	Rong Zhong et al.	[6]	The mixture of nano-Al particles and CNT are compacted into a disc under a pressure of 1.5 GPa and then consolidated under 1 GPa pressure for 30min in the temperature range of 260-480°C.
2.	2004	Yongbing Tang et al.	[7]	Fabrication process is similar as above.
3.	2004	Toru Noguchi et al.	[8]	They form the MWCNT/Al composite by nanoscale dispersion method by physically mixing the Al powder, Mg powder and a required amount of MWCNT powder in succession into 100 g of Natural Rubber.
4.	2005	R. George et al.	[9]	A mixture of CNT and aluminum powder were ball milled and the milled powder was compacted in a circular die with a load of 120 kN; the billets thus obtained were sintered in an inert gas environment for 45 min at 580°C and finally hot extruded at 560°C.
5.	2006	Lijie Ci et al.	[10]	Vertically aligned multi-walled CNT films of thickness 500 μm and of 4cm × 8cm area were prepared by CVD method. One micrometer thick pure Al was deposited on CNT film by magnetic sputtering, and this composite film is known as-deposited Al/CNT film. After this annealing, hot pressing and sintering is carried out to fabricate Al/CNT composite.
6.	2007	Chunfeng Deng et al.	[11]	Carbon nanotube reinforced 2024Al matrix composite was fabricated by cold isostatic pressing, followed hot extrusion techniques.
7.	2008	Chunfeng Deng et al.	[12]	Followed the same method as in SN.8
8.	2008	H.J. Choi et al.	[13]	The ball-milled mixture of aluminum and MWNT was placed in a copper can

SN.	Year	Author	Ref.	Remarks
				(Φ30 mm × 70 mm), compacted under high pressure. The sample was heated to a pre-determined temperature of 470°C with a heating rate of 20 °C min^{-1} within the furnace installed in the extruder. Extrusion was conducted with an extrusion ratio of 15:1 at a ram speed of 2.3 mm s^{-1}.
9.	2008	A.M. K. Esawi et al.	[14]	Al/CNT was ball milled in argon atmosphere at a rotary speed of 300 rpm. The balled milled powder was compacted followed by rolling.
10.	2009	A.M. K. Esawi et al.	[15]	Al Powder and 2 wt% MWNT were ball milled at 200rpm for 3 and 6 h in argon gas atmosphere. The ball-milled powder was mix compacted in a 20mm diameter compaction die at 475MPa. Hot extrusion of the homogenized compact was conducted at 500°C to produce 10mm diameter extrude.
11.	2009	Hansang Kwon et al.	[16]	Al powder, multi-walled carbon nanotubes and natural rubber (NR) were heat treated at 500 °C for 2 h in an argon atmosphere to evaporate the NR. The obtained Al–CNT mixture powder was sintered in a carbon mold using a spark plasma sintering device The sintered compact is the extruded through a conical die.
12.	2009	Chunfeng Deng et al.	[17]	Followed the same method as in SN.8
13.	2009	I. Kim et al.	[18]	1.**By HP method**: The Al powder and CNT were heated to the sintering temperature of 600°C at a constant rate of 10°C/min in the vacuum condition and were maintained for 30 min at 600°C and compacted with a pressure of 50 MPa. **2. By SPS method**: The Al powder and CNT were heated to the sintering temperature of 600°C at a constant rate of 50°C/min in the vacuum condition and were maintained for 10 min at 600°C, and then, compacted with a pressure of 50 MPa.
14.	2009	D. Poirier et al.	[19]	A mixture of 10 vol% CNT and Al was milled using the high energy mill. The milling was performed under argon atmosphere and 2 wt% stearic acid was added as a process control agent to avoid excessive sticking and agglomeration of the Al. After 5 hours of milling, some of the powder was heat treated at 630°C in a tubular furnace under vacuum for one hour and then the 10 vol% CNT/Al mixture was cold compacted in a 2 cm

SN.	Year	Author	Ref.	Remarks
				diameter cylinder and sintered at 630°C in a tubular furnace under vacuum for one hour to obtain a bulk
15.	2012	H.Kwon et al.	[20]	Followed same method as SN.13
				CNT/Mg
16.	2004	D. Chen et al.	[21]	MWCNT/Mg composite was formed by mechanical milling using a ball miller (GN-2 type) under a high-purity hydrogen atmosphere (0.1 MPa).
17.	2004	Carreno-Morelli, E. et al.	[22]	CNT/Mg composite have been processed by powder metallurgy. Blends of metal powders and multi-wall carbon nanotubes were compacted by uniaxial hot pressing followed by hot isostatic pressing.
18.	2006	C.S. Goh et al.	[23]	The Mg powder was homogeneously mixed with the carbon nanotubes using a V-blender for 10 h. The homogenized powder mixtures of Mg and carbon nanotubes were then compacted at a pressure of 728 MPa to form billets and the compacted billets were then sintered in a tube furnace at 630°C with argon gas atmosphere for 2 h.
19.	2007	Y. Shimizu et al.	[24]	The physically blended magnesium alloy (AZ91D) powders containing 0.5–5% carbon nanotubes were hot-pressed in a molder to form a precursor at 823 K for 5 h by applying a pressure of 25.5 MPa in a vacuum <10 Pa. The carbon nanotube- reinforced magnesium alloy composites were finally obtained in the form of rods by extruding precursors at 723 K with an extrusion ratio of 9:1
20.	2007	S. Thakur et al.	[25]	Mg and CNT were blended in a horizontal blending machine. The blended powder mixture was compacted using a 50 tonnes machine to produce billets having a 35 mm diameter. All of the compacted billets were spray-coated with graphite and then sintered in a microwave.
21.	2008	C.S.Goh et al.	[26]	Followed similar as SN.20
22.	2010	K.Kondoh et al.	[27]	Ball milling of Mg and CNT was carried out to form a uniform mixture of CNT/Mg composite powder. Then the CNT/Mg composite powder was extruded at 600°C to form a composite rod.
				CNT/Ag
23.	2005	Y.Feng et al.	[28]	Carbon nanotube and silver metal powder are homogeneously mixed in hand grinder. Then this mixture was uniaxially pressed in steel

SN.	Year	Author	Ref.	Remarks
				dies under a pressure of 320 MPa for 2 min and then isothermally sintered at 700°C for 1 h to form CNT–silver composites. The composites were then repressed at 400 MPa
CNT/Fe_3Al				
24.	2007	L.Pang et al.	[29]	Iron Aluminide and CNT composite has been fabricated by spark plasma sintering (SPS) that retains the integrity of CNT in the matrix. Samples were synthesized at pressure of 30 MPa, and temperature of 1273 K

S.R. Dong et al. [30] appear to be the first research group who fabricated the CNT/Cu composite in 2001 by powder metallurgy process. They synthesized the carbon nanotube by thermal decomposition of acetylene. Unlike Kuzumaki and Xu, they did chemical nickel plating on the CNT surface to improve the wet-ability of the CNT. Carbon nanotubes and pure copper powder with less than 9 μm particle size were ball milled for 30 min to improve the mixing. To avoid oxidation an organic liquid was added to the powder. However, they did not observed any chemical reaction between copper and CNT.

In order to have proper bonding between copper and CNT J. P. Tu et al. in 2001 [31] plated CNT by nickel using electroless method and the mixed with the 70 μm size copper particles and the hot pressed and sintered isothermally at 800°C for 2 hr. They observed uniform plating of nickel on the surface of CNT and good bonding between nickel plated carbon nanotube and copper matrix [31].

On the same basis, W. X. Chen et al. [32] in 2003, coated CNT surface with nickel by electroless plating and then they mixed the copper powder with nickel coated CNT by ball milling process. They observed proper coating of nickel as well as uniform dispersion of CNT in the copper matrix.

Similar attempt was done by S.I Cha et al. [33], in 2005, but in place of nickel coating they functionalized the CNT surface and mixed in the copper ion solution. The process was followed by drying, calcination and reduction to form the CNT/Cu composite. The process was named as molecular-level mixing, by which they achieved uniform distribution of the CNT in the metal matrix and proper bonding between CNT and Cu matrix. The process is described in the section 2.2.2.2. G. Wenli et al. [34] in 2006, used the similar method like molecular-level mixing for synthesis of one dimensional copper rod. They synthesized the MWCNT by pyrolysis of propylene-hydrogen (C_3H_6:H_2 = 2:1)

at 750°C with nickel particle as catalyst. The prepared MWCNTs were treated with concentrated nitric acid at 60°C to attach some functional group like hydroxyl and carboxyl on the surface of MWCNT. These functionalized MWCNTs (1 gm) were added to the solution of 1.5 gm $Cu(C_5H_7O_2)_2$ (copper (II) acetylacetonate) and 50 ml acetyl acetone. The mixture was ultrasonicated for 60 min and then it was filtered and dried at 60°C. They observed that the copper precursor was adsorbed on the surface of MWCNT. In the next process the copper precursor was reduced to copper by reduction process in hydrogen atmosphere. They observed good adsorption of copper on the surface of MWCNT.

B. Lim et al. [35], in 2006, synthesized composite by two different methods: mechanical mixing of carbon nanotube with copper powder and nickel coated carbon nanotube with copper powder. In the first process, SWCNT and copper powder were mixed in the ethanol and ultrasonicated at a power level of 5 W. The solution was then heated to a temperature of 50°C and ultrasonicated until most of the ethanol was evaporated. They observed uniform dispersion of the CNT in the copper matrix. In the second process, they plated the carbon nanotube with nickel by electroless method and then they mechanically mixed the plated CNT with the copper powder. They observed 60 to 170 nm thick layer of nickel on the surface of carbon nanotube. They observed better mechanical bonding between copper and carbon nanotube.

K.T Kim et al. [36, 37] in 2004 and 2006, used an innovative method for extracting the nano-sized Cu powders from $[Cu(NO_3)_2]\cdot 3H_2O$. They sprayed the water solution of $[Cu(NO_3)_2]\cdot 3H_2O$ on hot wall with 15,000 rpm and then burn dried powder at 300°C to fabricate oxide powder. The oxide powder was reduced into Cu powder at 200°C in H_2 atmosphere. The powder size of Cu was ranged from 200 to 300 nm. The nano-sized Cu powder and CNTs were mixed into composite powder through high-energy ball milling process using planetary miller (Fritsch GmbH) for 24 h with 150 rpm. They observed homogeneous dispersion of CNT in the copper matrix.

In their succession work, K.T. Kim et al. [38–40] in 2007, used molecular level mixing method for synthesis of CNT/Cu composite. In the first step, they purified and functionalised the MWCNT by acid treatment. Due to this treatment, the functional groups like carboxyl or hydroxyl were attached on the surface of CNTs. Then the Cu acetate monohydrate $[Cu(CH_3COO)_2\cdot H_2O]$ was added to the CNT suspension and ultrasonicated for 2 h. Then the solution of CNT/Cu ion precursor was vaporized at

100°C, and the vaporized CNT/Cu ion precursor powders were calcinated into CNT/CuO composite powder at 350°C in air and finally the calcinated CNT/CuO composite powder samples were reduced into CNT/Cu composite powder under hydrogen atmosphere. They observed the homogeneous dispersion of carbon nanotube in the copper matrix.

In 2007, S. Baik et al. [41], synthesized MWCNT/Cu composite by two methods: a mechanical mixing process and a molecular-level mixing process. They observed better mechanical and electrical properties in mechanically mixed powder composite compare to composite formed by molecular-level-mixing method. C.Kim et al. [42] in 2009, use the method similar to B. Lim [35] for coating the CNT surface with nickel. They also observed homogeneous dispersion of CNT in the copper matrix and proper bonding between copper and CNT.

Similarly Walid M Daoush [43] in 2009, used a method for sensitization and functionalization of MWCNT by hydroxyl and carboxyl group and then the MWCNTs were mixed with the Cu salt solution to form MWCNT/Cu composite. A. Isra et al. [44] adopted a simple method for synthesis of MWCNT/Cu composite in 2009. They mixed the Cu powder and MWCNT by using high energy ball mill in the argon atmosphere. They observed uniform dispersion of CNT through TEM.

K. Chu et al. [45,46] in 2010, used a mechanical mixing of CNT and copper particles in PCS (Particles compositing process), they observed homogeneous dispersion of CNT in the copper matrix.

In 2011, C. Guiderdoni et al. [47] synthesized CuO powder by the oxalate precipitation/calcination method. The suitable amounts of copper nitrate hexahydrate ($Cu(NO_3)_2.6H_2O$) and ammonium oxalate dihydrate ($(NH4)_2C_2O_4.2H_2O$) were dissolved in deionized water. The solution was mixed with the ethanol, where precipitation of copper oxalate (CuC_2O_4) occurred immediately. Copper oxalate powder was separated from the ethanol and dried overnight at 80°C. This powder was decomposed in air at 400°C, producing a cupric oxide (CuO) powder. A Cu powder was prepared by reduction of CuO in H_2 at 400°C. This powder was mixed with the double walled carbon nanotube (DWCNT) and the mixture was dispersed in the deionised water. The solution was ultrasonicated for 1 min and the flask containing solution of carbon nanotube and copper powder was dipped in the liquid nitrogen and freeze-dried at -40°C for 48 h in a primary vacuum (12 Pa) to form CNT/Cu composite powder.

P. Jenei [48], in 2013, used high energy planetary ball milling for homogeneous dispersion of MWCNT in the copper matrix.

The second step of powder metallurgy is compaction using powder precursor formed in the first step, as the starting material and can be classified as (A) conventional sintering, (B) hot pressing, and (C) spark plasma sintering**.**

A Conventional compaction and sintering

Compaction is a simple method of compressing the mixed metal powder in the die under high pressure. The work part after compaction is called a green compact or simply a green, the word green meaning not yet fully processed. S.R. Dong et al., in 2001 [30] used the conventional compacting and the sintering process. The copper powder and nanotubes were mixed and ball-milled for 30 min in the presence of organic liquid to avoid possible oxidation. The powders was dried and were isostatically pressed at 350 MPa for 5 min and then isothermally sintered for 2 h at 850°C in vacuum to form CNT/Cu composite. In some cases, pressure is applied from all the direction against the powder, which is placed in a flexible die is called isostatic pressing.

W.X. Chen, in 2003, [32,49] also followed the similar method as that of S.R. Dong et al. [30] for fabrication of CNT/Cu composite, but they plated the carbon nanotube by nickel using electroless method and then they compacted the CNT and copper powder mixture isostaically. Compressed metal powder is heated in a controlled-atmosphere furnace to a temperature below its melting point, but high enough to allow bounding of the particles[50]. This process is used mainly for CNT/Al and CNT/Cu composites.

In order to have better density in the green compact of CNT/Cu powder, P. Quang et al. In 2006, and 2007 [51,52] used ECAP (equal channel angular pressing), the most promising method in SPD (severe plastic deformation) and they observed good mechanical properties in the product. Conventional compaction and sintering is one of the oldest techniques utilized for fabrication of CNT/Cu composites, but it met limited success due to the poor densities of the final structure.

A. Isra et al. in 2009 [44] used compaction and sinterings method for forming 10mm diameter disc and then compressed the disc by the high pressure torsion method (HPT). Even, H. Li et al. in 2009 [53,54] Use the HPT method to form a10 mm diameter pellet

from the ball-milled powders under 6 GPa for five revolutions. All the process of fabrication were performed at room temperature.

P. Jenei et al. in 2012 [55] also used the similar method for fabrication of CNT/Cu composite. The powder blend was pre-compacted by cold isostatic pressing. The pre-compacted discs were finally consolidated by HPT at room temperature or 373 K with an applied pressure of 2.5 GPa and 10 number of revolution. Second method of compaction is hot pressing which is discussed in the next section.

B Hot pressing

Hot pressing is a technique patented by G.F Taylor [56] in 1933, which was later modified by E.P. Bernard et al. [57] and filed a patent in 1966. In this process, heat is produced within the mould by using an induction coil. The mold is made out of graphite or steel, as shown in Figure 2.4. The process comprises compacting powder at an elevated temperature while being pressed in a die between two axially aligned punches, the punches being entered into the bore of the die from opposite ends as depicted in the Figure 2.4. Simultaneous heating in which temperature of the powder increase in the range of 500-800°C and pressure in the range of 50 to 100 MPa is applied to the powder. The process will be carried out for 30 to 50 min. The high temperature and high pressure applied during the process causes sintering and creep of metal powder concurrently. By this method, high density of the material can be achieved. The densification works through particle rearrangement and plastic flow at the particle contacts. Most of the time, the moulds are made up of graphite which facilitates induction or resistance heating of the powder up to 2400°C. Hot-pressing was adapted in several studies like T. Kuzumaki et al. in 1998 [4], C.L. Xu et al. In 1999 [5], in 2007 D. Chunfeng et al. [58], S.K. Thakur et al. [25], Sheng-ming Zhou et al. [59], I. Kim et al. in 2009 [18] etc and the all used hot pressing to synthesize CNT/metal composite.

F. Chastel et al. in 2000 [60] and T. Zhang et al. used hot pressing to synthesize CNT/metal oxide in 2009 [61]. Few researchers also used hot pressing method to synthesize; carbon nanotube reinforced copper matrix composites, which are discussed in detail next. Typically, hot-pressing was performed in a graphite mould by uniaxial pressurization in a vacuum of 10^{-3} Torr [37,42,62] to prevent oxidization of the powder mixtures. Disc-shaped specimens for the displacement rate tests were hot-pressed at

45 MPa, which is the maximum pressure of the apparatus. The diameter of the specimens was 15 mm and the thickness was 0.8 mm. The temperature was ramped to 600°C in 40 min. and kept constant for 30 min. Finally, the temperature was cooled down to room temperature in 20 min.

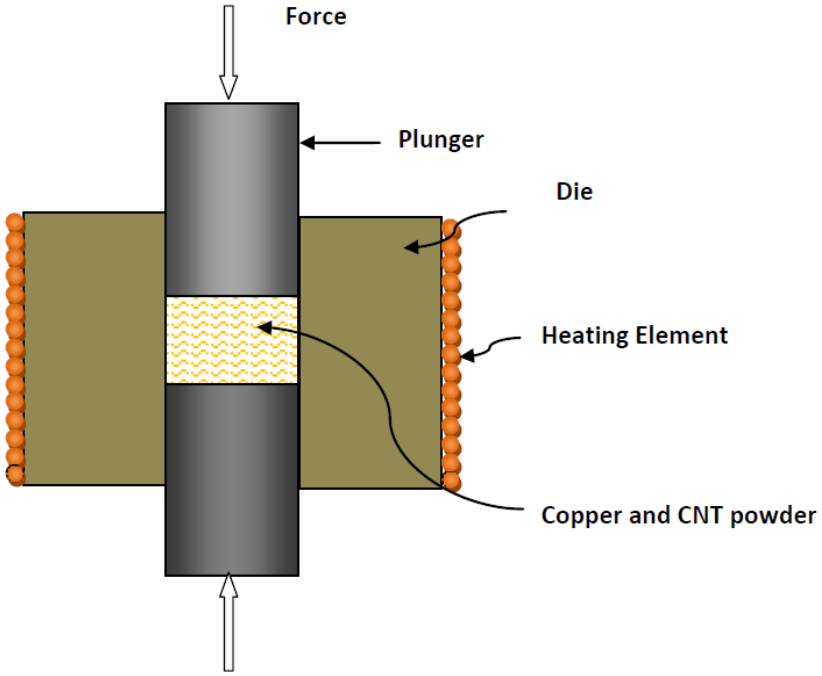

Figure 2.4: Schematic of hot pressing set up

J.P. Tu et al. [31] in 2001, fabricated the specimen by PM technique. The powders of 70 μm particle size copper powder and nickel plated CNT were mixed in a ball mill for 30 min. After ball milling the powder was isostatically pressed at a pressure of 600MPa at 100°C for 10 min under vacuum (10^{-2} Pa), and then sintered at 800°C for 2 h.

C. Kim et al. [42] in 2009, repeated the above experiment for fabrication of copper matrix composites reinforced by nickel-coated single walled carbon nanotubes (SWCNT) and formed disk-shaped specimens by the hot pressing method. C. Kim used electroless method for coating the CNT with nickel and due to which agglomeration of the CNT was avoided. As discussed in section 2.2.1.1, generally mixing of CNT and copper was carried out in the ball mill [63,64] and then the compaction of the powder is done in the hot press.

S. M. Uddin et al. in 2010 [63] done the scanning electron microscopic (SEM, JEOL 6500) investigations of the composite to evaluate the dispersion of CNT in the copper matrix. They observed two different phase one without CNT and other with CNT. This non-uniform distribution was attributed to inappropriate milling process.

K. Chu et al. in 2010 [64] fabricated CNT/Cu and CNT/ Cu-Ti composite by the hot pressing. The mixed powders were put into a cylindrical graphite die with an inner diameter of 30 mm. With the aim to prevent powders from sticking to the inner wall of the die during the sintering, the die was covered with a 2-mm thick layer of graphite felt. The compact powders were sintered at 760°C for 20 min under a pressure of 40 MPa. After sintering, the surfaces of samples were ground to remove the graphite layer. They achieved the relative density[2] up to 98% and observed that the relative density decreasesed with increase in the vol% of CNT in the copper matrix. In the hot pressing process the compaction and heating is carried out up to 45 min during which there is possibility of formation of inter-metallic compound. Such type of compounds are not reported for the CNT/Cu composite but there is formation of carbide in case of CNT/Al composite like in case of C.L. Xu in 1999 [5].

C Spark plasma sintering

The pioneering works related to the spark plasma sintering (SPS) process started in 1906 when the first direct current (DC) resistance sintering (RS) apparatus was developed by A.G. Bloxam, subsequently carried forward by A.L. Duval D'Adrian in 1922 and G.F. Taylor in 1933. In Japan, based on the idea of using the plasma on electric discharge machine for sintering metals and ceramics, a similar process was developed and patented in the early 1960's by K. Inoue [65]. However, because of the lack of application technology at that time, limited fields where it could be applied and unsolved problems associated with industrial production, equipment cost and sintering efficiency, it was not put to wide use. From the beginning of 1990 to now, the SPS process has been developed to the third generation. Now it is used for the consolidation of CNT/metal composite powder. Several research groups have used this method for consolidation of composite powder like in 2003 S.I. Cha [66] used SPS for CNT/WC composite and in 2005

[2] *Relative density* is the density of the MWCNT/Cu nanocomposite with respect to pure copper.

S.I. Cha et al. [67] for CNT/ Al_2O_3, in 2007 Lai-xue Pang [29] for CNT/Fe_3Al, in 2009 T. Zhang et al. [61] used for CNT/ Fe_3Al nanocmposite , in 2009 Hansang Kwon et al. [16] and I. Kim et al. [18] used SPS for CNT/Al, 2011 S. Bakshi [68] for CNT/Tantalum carbide.

SPS or pulsed electric current sintering (PECS) is a sintering technique which utilizes uniaxial force and it has got many advantages over conventional systems like compaction , hot press or hot isostatic press [69]. The advantages are like ease of operation, control of the sintering energy, high speed of production, high reproducibility, more safety and more reliability. This direct way of heating allows the application of very high heating and cooling rates (up to 1000 K/min), enhancing densification over grain growth promoting diffusion mechanisms, allowing maintaining the intrinsic properties of nano-powders in their fully dense products. As discussed above SPS is very good process for CNT/Cu nano-composite powder due to its fast nature, which helps in restricting the reactions between the copper matrix and CNTs. Figure 2.5 shows the schematic of the spark plasma sintering process.

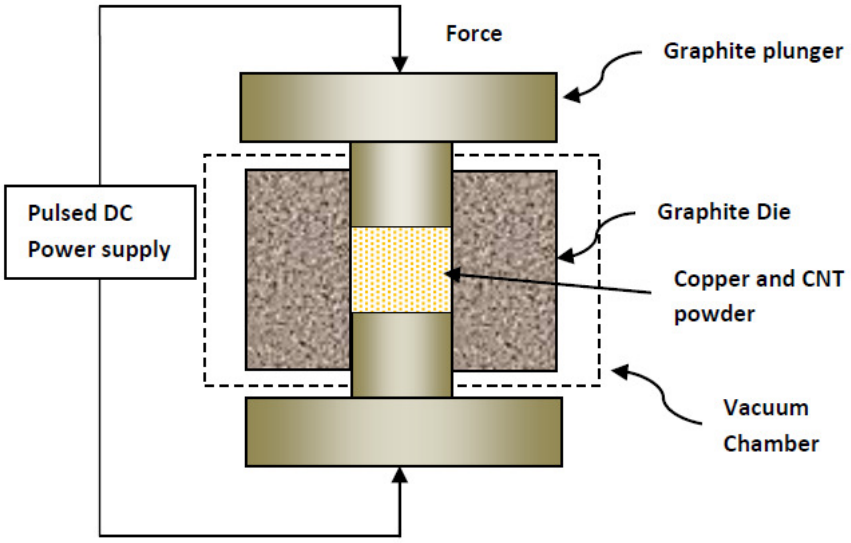

Figure 2.5: Schematic of spark plasma sintering set up

As shown in Figure 2.5, the pulsed direct current pass through the graphite die as well as the CNT/metal composite powder. Resistance heating of the CNT/metal powder takes place and due to movement of the piston, densification of the CNT/metal powder

occurs. It is observed that the density of the CNT/metal composite reaches to the theoretical density at lower sintering temperature as compared to the conventional sintering process. In this process, the heat is generated within the CNT/metal composite powder unlike heating from outside in hot press.

First time, S.I. Cha et al. in 2005 [33] used this method effectively for synthesis of CNT/Cu composite. They synthesized the CNT/Cu composite powder by molecular level mixing method and consolidated the form powder by SPS. They observed that the carbon nanotube form the network within the copper grain and observed very less dislocation density due to carbon nanotube reinforcement. In SPS consolidation, CNTs were ultra-sonicated in the ethanol for segregation of CNT, which were in the agglomerated form [70]. After drying, the copper powder was mixed with the CNTs to obtain different volume percentage (vol%) of CNT. The powder mixture was ball milled for 24 h using alumina balls [37] or mixed by particle composite system (PCS) for 40 min at 15000 rpm [46] and the resulting mixture was consolidated by SPS at 750^{o}C for hold time of 1 min – 5 min at a pressure of 40 MPa–60 MPa.

K.T. Kim et al. in 2004 [36], 2006 [37] and 2007 [38] used SPS method for synthesis of CNT/Cu composite from the powder synthesized by using molecular level mixing method. They got relative density of the composite upto 98%.

Walid M. Daoush et al. [43,62] in 2009 used SPS for consolidation of CNT/Cu composite powder. The observations indicated that the shrinkage of the CNT/Cu stopped in one minute when the sintering temperature was 600°C and the compaction pressure was 20 MPa under vacuum of 10^{-3} torr. The sintering occurred in a uniaxial graphite mold of 10 mm in diameter to produce a 2-mm thick sintered sample.

K. Chu et al. [46] in 2010 mixed CNT and Cu particles by PCS and used SPS for consolidation of the powder. The heating rate was 100^{o}C/min, and a pressure of 40–60 MPa was applied from the start to the end of the sintering. The sintering temperatures were set at 550–650^{o}C with holding times of 5–10 min. They observed relative density of the product up to 98.5%.

In 2011, Guiderdoni et al. [47] synthesized the CuO powder by the oxalate precipitation/calcination route. After reduction of CuO powder, the Cu and DWCNT powder was formed by freeze drying method and the form powder was sintered by SPS

method. They observed uniform distribution of DWCNT in the metal matrix composite, which was attributed to the very short times involved in the ultrasonication and dispersion process, together with freeze-drying and SPS.

2.2.1.2 *Sandwich processing*

Researchers have tried to prepare MM-CNT composites by putting alternate layers of CNT and metal like a sandwich structure and then consolidated by applying very high pressure. The sandwich processing technique steps are schematically shown in Figure 2.6. and the Figure is adopted form review done by S. Bakshi et al. [71]. The first step of the method shows that the CNT and acetone mixture was sprayed on the thin copper sheet. The sprayed CNT stuck to the copper surface. Then another thin foil of copper was placed on the CNT sprayed copper sheet as shown in step two in the Figure 2.6. In this way, the layering of CNT and the copper sheet was prepared like a sandwich. The process therefore is named as sandwich technique. The uppermost and the lowermost layer meant of copper foil. The prepared sandwich of CNT and copper foil was rolled and annealed at very high temperature below melting point of copper as shown in step three of Figure 2.6

Y. Li et al. in 2007 [1] demonstrated a successful fabrication of SWCNT/Cu laminate composites by combined techniques of cold rolling and annealing. Acetone-sprayed thin film (450 nm) of SWCNT was formed on Copper foil of 10 μm thick. Nineteen layers of large-area SWCNT films sandwiched between 20 layers of Cu thin foils were stacked in this way. Both pure Cu and SWCNT/Cu laminates were cold rolled using a Durston Rolling Mills, with fixed roller gaps of 0.075 and 0.05 mm, respectively. After rolling, some laminate composites were annealed at 1050°C for 10 h under mixed gases of Ar and H_2, and were cold rolled again with a reduced roller gap of 0.025 mm. The measurement shows that the Young's modulus of the resultant laminate composites is improved by 13%± 5%, exhibiting an improvement over the comparative pure Cu foils processed under identical conditions. These results suggested that good interfacial adhesions between nanotubes and the Cu matrix have been achieved after the rolling annealing-rolling processes.

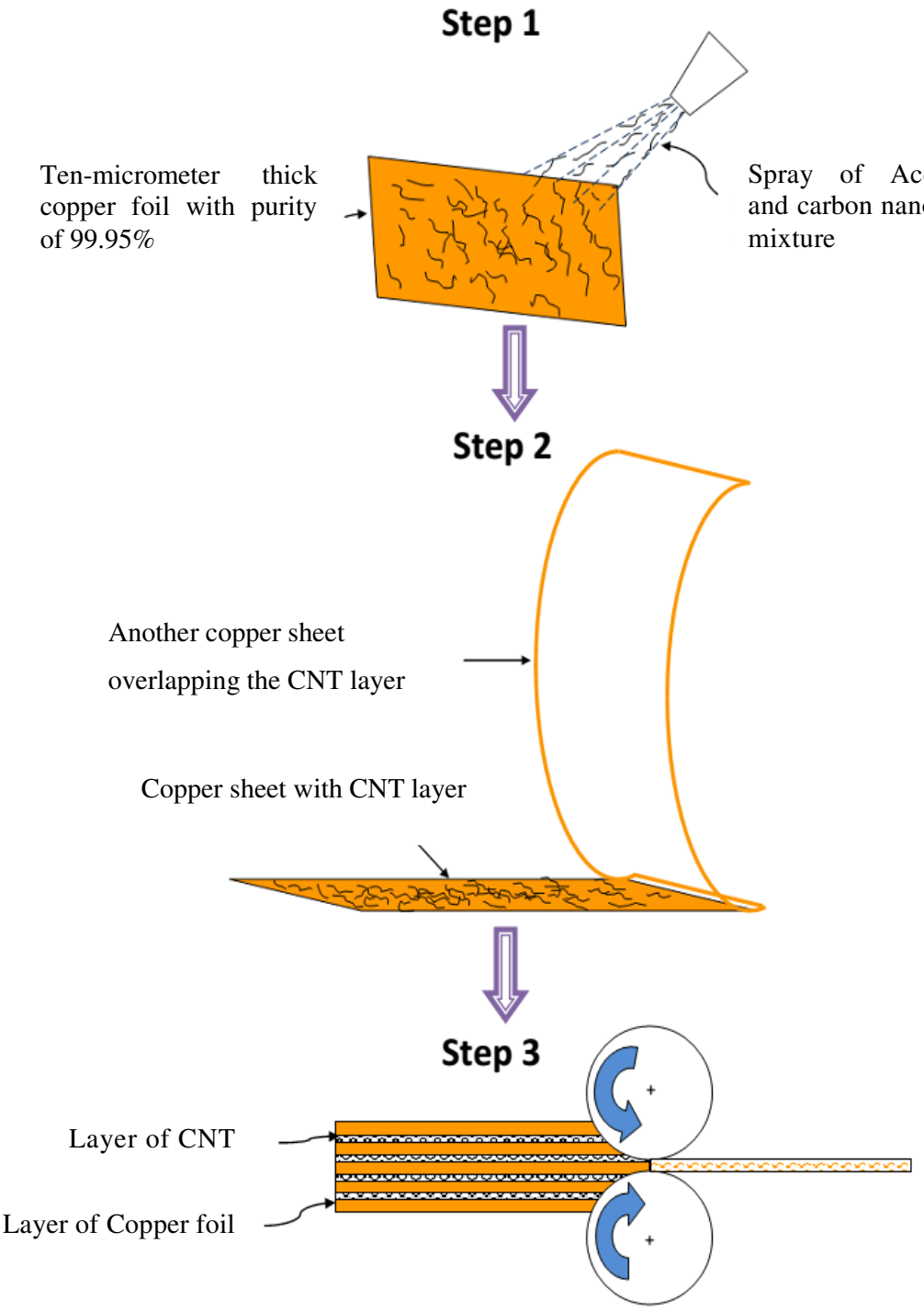

Figure 2.6: Schematic showing sandwich processing of carbon nanotube and copper composite [72]

2.2.2 Chemical Methods

The major chemical processes used for making metal composite are electrochemical process and molecular level mixing

2.2.2.1 *Electrochemical process*

This is the second most popular route after powder metallurgy. The electrochemical method is primarily used for formation of thin composite coatings with a reported thickness of 20 to 180 μm . G. Chai et al. in 2008 [2] fabricated a layer of CNT/Cu composite with a thickness 40 μm and J. Tan et al. [73] in 2006 fabricated a layer of CNT/Ni composite with thickness of 180 μm . Metal is deposited on the uniform, aligned CNTs and consistent distribution of CNT in the metal matrix is achievable. Electrochemical route mainly consists of two techniques. The first technique, Electro-co-deposition requires the traditional electrochemical cells in which composite film is deposited by current flow between anode and cathode. The second technique, known as electroless plating, does not require any external energy source. This is a chemical process, in which thermo-chemical decomposition of metallic salts takes place in the bath to release metallic ions that forms composite with CNTs.

A Electro-co-deposition

The process in which two or more elements are electroplated is called electro-co-deposition. It is analogous to an electrochemical cell and it works in reverse direction. The part to be electro-co-deposited is the cathode in the circuit as shown in Figure 2.7. The anode may be made up of the metal to be plated or it may be an inert electrode like platinum. Both anode and cathode components are immersed in an electrolyte containing one or more dissolved metal salts and other elements (in present case nano-particles) as well as acid which increase the concentration of H^+ ions that permit the flow of electricity as seen in Figure 2.7. A power supply supplies a direct current to the anode, oxidizing the metal atoms that comprise it and allowing them to dissolve in the solution. At the cathode, the dissolved metal ions in the electrolyte solution are reduced at the interface between the solution and the cathode and the nanoparticles are co-deposited with the metal ions, such that they "plate out" onto the cathode. Schematic of the electro-co-deposition is shown in the Figure 2.7. In the case of co-deposition of CNTs and metals, good suspension and uniform dispersion of CNTs in the bath are the key factor

for getting coatings with homogeneous CNT distribution. This is challenging because CNTs have a tendency of agglomeration because of very high surface energy owing to large surface area. In 2010 and in 2013 K. Chu et al. used acid cleaning [46,64] process to avoid the agglomeration, in 2004 E. Carreno-Morelli et al. [22] for CNT/Mg, in 2007 E. Titus et al. [74] and C. Guo et al. [75] for CNT/Ni, in 2007 B. M. Praveen [76] for CNT/Zn, in 2008 Y. L. Yang [77] for CNT/Cu, in 2008 A. Tello [78] for CNT/Au, used surfactants to avoid agglomeration.

In 2009, C. Kim [42] did nickel coating for uniform dispersion as well as to improve wet-ability of the CNT with copper, in 2011 Ch. Guiderdoni [47] also coated CNT surface by electroless nickel coating to improve suspension of CNTs in the electrolyte. The electrolytic bath agitation by means of magnetic stirrer as shown in Figure 2.7 or mechanical stirrer or ultrasonication are also the commonly used techniques for uniform dispersion of CNTs in the electrolyte. Electro-co-deposition technique has been reported as a processing route for mainly CNT/Ni [49,73,75,79–89] and CNT/Cu [2,77,90–95] composites.

X. H. Chen et al. [83,84] in 2001 used the electro-co-deposition method for coating of CNT/Ni for the first time. The CNT/Cu composite coatings by electro-co-deposition method was first synthesized by Q. Chen et al. in 2006 [91], again they used the electro-co-deposition method for CNT/Ni composite in 2007 [80] and in 2008 and in 2009 for CNT/Cu composite [2,93,94]. The process of electro-co-deposition was mainly used for micro-fabrication. In this process silicon wafer with a seed layer of copper was used as a cathode and the co-deposition of the copper and carbon nanotube was carried out on it. They concluded better bonding between copper and carbon nanotube as well as uniform dispersion of carbon nanotubes in the copper matrix from SEM images.

In 2006, N. Ferrer Anglada et al. [90] prepared a SWCNT/Cu composite by electro-deposition process rather than electro-co-deposition process. They used a bucky paper (a thick netwok of SWCNT) as a cathode and electro-deposited copper on it. They obtained samples with 30% to 55% Cu in weight.

In 2007, Y. L. Yang et al. [77] prepared a single walled carbon nanotube copper composite coating by electro-co-deposition method in the ultrasonic field for uniform dispersion. Due to axial properties of carbon nanotube, alignment of carbon nanotube is also an important issue. In order to have alignment of carbon nanotube in the metal

matrix electro-co-deposition of the copper is carried on the align CNT forest grown by chemical vapour deposition. D. Wang et al. in 2008 synthesized a bucky-paper by using CVD grown aligned CNT [96].

In 2008, Y. Chai used a plasma enhanced CVD system to grow a low density carbon nanotube on the silicon substrate wafer having oxide on the surface [92]. Then, copper was deposited by electro-chemical method, which infiltrated to the base of the CNT through the low density CNT forest to synthesize a CNT/Cu composite. In 2013, C. Subramaniam used similar method like bucky-paper synthesis. They had grown the CNT forest by water assisted super-growth technique [95]. Then the vertically aligned CNTs were shear between two glass plate to change the alignment direction. The assembly was placed in the electrolyte and copper was electrodeposited on it to form a CNT/Cu composite [95]. During electro-co-deposition the voids presents in the CNT forest will be filled by the electro-co-deposited copper and alignment of the CNT can be achieved. Such type of the composite will have low thickness 50 μm [92].

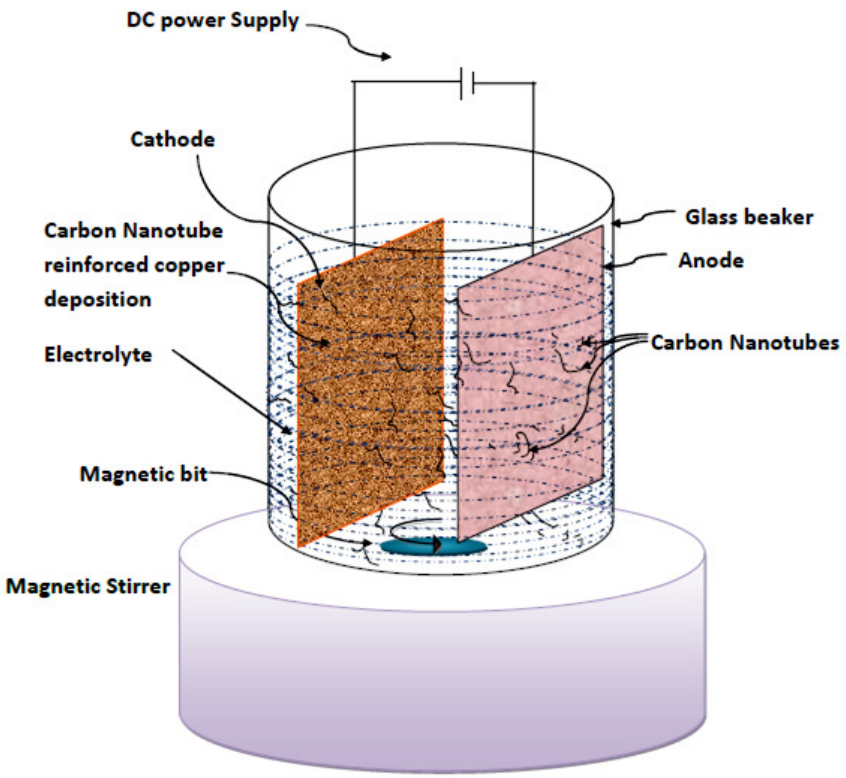

Figure 2.7: Schematic electro-co-deposition of CNT/metal plating setup

B Electroless deposition

Electroless or autocatalytic plating involves the presence of a chemical reducing agent in solution to reduce metallic ions to the metal state. However, the name electroless is somewhat misleading. There are no external electrodes present, but there is electric current (charge transfer) involved. Instead of an anode, the metal is supplied by the metal salt; replenishment is achieved by adding either salt or an external loop with an anode of the corresponding metal that has higher efficiency than the cathode. There is therefore, instead of a cathode to reduce the metal, a substrate serving as the cathode, while the electrons are provided by a reducing agent. The process takes place only on catalytic surfaces rather than throughout the solution.

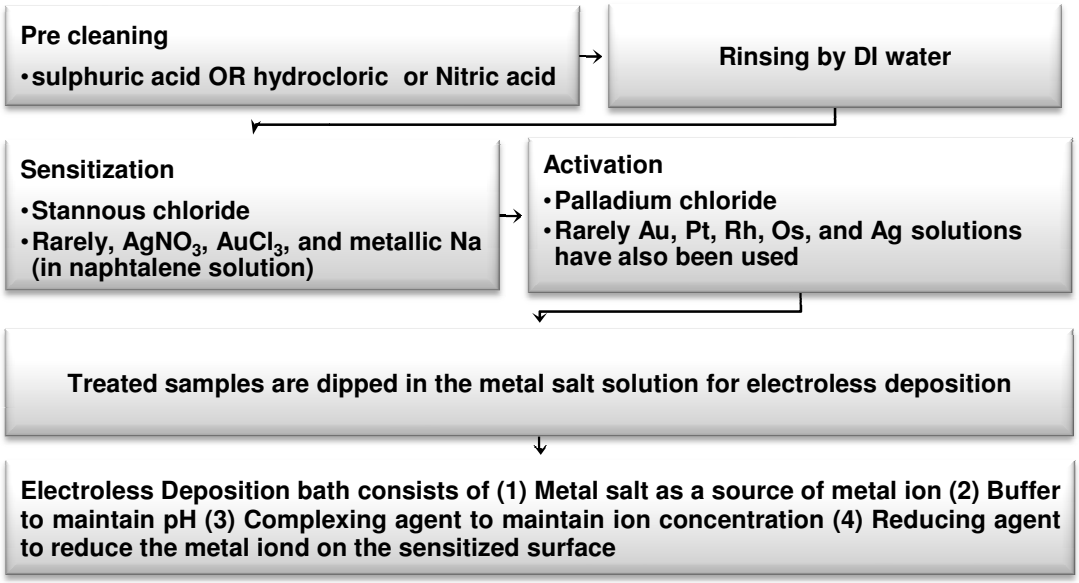

Figure 2.8: Process steps in electroless deposition

There has been great interest in the metallization of MWCNTs for creating new metal-matrix-based carbon nanotube composites. Such metallization of MWCNTs can be achieved via an electroless deposition process at normal temperature state. This very special process involves a continuous build-up of metal coating on a MWCNT by the mere immersion in a suitable aqueous solution. A chemical reducing agent in solution supplies the electrons for converting metal ions to the metal form,

$$M^{2+} + 2e^{-}(\text{supplied by the reducing agent}) \xrightarrow{\text{Catalytic surface}} M^{0}$$

To obtain the MWCNTs covered with a continual Cu layer, pre-treatment of CNT is very essential. Pre-treatment not only helps in cleaning the MWCNT but it also helps in increasing the catalytic sites on the surface of CNT. In general, electroless deposition comprised of (1) cleaning, (2) surface modification, (3) sensitization, and (4) activation (acceleration) [97,98]. Pre-cleaning of MWCNT is carried out by HNO_3 solution whereas the sensitization and activation of pre-cleaned MWCNTs will be done in the aqueous solution of $SnCl_2$ (Stannous chloride) and HCl and an aqueous solution containing $PdCl_2$ (Palladium chloride) and HCl respectively.

Several researchers like, in 2000, X. Chen et al. [99], in 2004 F. Wang et al. [97], in 2006 Lim et al. [35], in 2008 Oh et al. [100], in 2009 Peng et al. [93] and C. Kim et al. [42] etc. used the same method for sensitization and activation of pre-cleaned CNT. The electroless coated CNTs were used for the fabrication of CNT/Cu composite. In 2004 F. Wang et al. [97] , in 2009 C. Kim et al. [42] , Peng et al. [93], Walid M. Daoush [62], Daoush et al. [43], L. Xia et al. [101] etc have used the electroless plating technique to coat the CNT.

For electroless deposition of Cu, researchers like F Wang et al. in 2004 [97] and in 2009 Daoush et al. [43,62] have used the deposition bath comprises of copper sulphate-penta hydrate ($CuSO_4.5H_2O$) as a copper source, $EDTANa_2$ as a complexing agent and glyoxylic acid (CHOCOOH) as a reducing agent. Copper was deposited on the surface of the CNT by electroless plating.

In 2004, F. Wang et al. [97] mixed the treated MWCNT in the Cu plating bath with magnetic stirrer agitation. The deposition time was 10 min and the temperature of deposition was 60°C. The deposited MWCNTs were filtered and cleaned with deionised water, then dried in vacuum desiccator. They observed, 80 to 100 nm thickness of Copper on the surface of CNT.

Walid M. Daoush et al. in 2009, [43,62] deposited Cu on the CNT to improve the interfacial bonding strength between Cu and CNTs by acid treatment and electroless copper coating. Concentrated hydrochloric, nitric, sulphuric acids were used for CNTs surface cleaning and acid treatment. After cleaning, the CNTs are sensitized and activated by the aforementioned method. The sensitized CNTs were stirred in the copper sulphate penta-hydrate solution for 2 h. After completion of the electroless copper deposition reaction, the coated CNT underwent washing with distilled water and acetone, filtration and drying in vacuum dryer for 2 h at 80°C. The produced composite powders

were sintered using spark plasma technique. The prepared sintered materials were underwent microstructure investigations, physical and mechanical properties measurements to evaluate each composite. First, electro-co-deposition and electroless deposition methods are mainly developed for Ni and Ni-alloys, with a very few investigations on Cu and Co. These methods require more research to optimize the process for other metals including Cu. Second limitation of this method is the synthesis of freestanding structure. Electro-co-deposition and electroless method are used mainly for synthesizing the CNT/MM composite in the form of thin coating or sheet with less than 200 μm thickness. With the current knowledge, it is almost impossible to produce thick and freestanding CNT/MM composites for structure applications by electrochemical processing.

2.2.2.2 *Molecular level mixing*

In 2005, Cha S.I. et al. [33,38,67] developed the molecular level mixing method for synthesis of MWCNT reinforced Cu composite. The method begins with functionalization of CNT before dispersing MWCNTs in copper acetate (II) monohydrate [$Cu(CH_3COO)_2.H_2O$] solution. The cleaning of the MWCNT was done with the help of hydrofluoric acid. In order to attach a carboxyl functional group, CNTs are cleansed in the aqua-regia (solution of H_2SO_4/HNO_3 in 3:1 ratio). The Functionalized MWCNT was added oleylamine and dispersed in an ultrasonic bath for 3 h. Copper acetate (II) monohydrate [Cu $(CH_3COO)_2$. H_2O] was added into that flask and then the mixture was sealed and purged with argon for 1 h. The mixture was heated to 523 K and maintained at this temperature for 10 min through heating the flask in a heating mantle with a uniform heating rate of 10 K/min. The salt was converted to CuO by calcining. After slow cooling to room temperature, CNT/Cu-oxide composite powders consisting of CuO and Cu_2O were obtained from the reaction. Then, the CNT/Cu-oxide composite powders were reduced at 573 K for 2 h under hydrogen atmosphere, to form CNT/ Cu composite.

K.T. Kim et al. in 2007 [38] also synthesized CNT/ Cu composite by the molecular level mixing method and studied the hardness and wear resistance of the composite. In the subsequent work of the same group in 2008 [39], they studied the effect of grain refinement and reinforcement of CNT on the mechanical properties of CNT/Cu composite. S. Baik et al. in 2007 [41] also fabricated the CNT/Cu composite by

molecular level mixing method and they studied the mechanical and electrical properties and observed that the mechanical properties were improved and the electrical resistance was also decreased. As described above, the molecular-level mixing was a promising technique for the production of metal powders containing dispersed CNTs. Although, there are chances of incomplete reduction of the CNT/copper oxide powder due to which, there is possibility of oxygen impurity in the powder. K.T. Kim et al. in 2008 [40] have discussed the unreduced oxygen is good for the interfacial stress transfer, which aids in effective strengthening and this may helpful for thermal conductivity. However, for electrically conductive applications the presence of oxygen may not be suitable.

2.2.2.3 *Mixing as paste*

A few studies have reported production of CNT/MM paste mixture. The paste of Cu and CNT may not be classified as composites truly. A paste of Cu particles and CNTs, mostly in mineral oil, was made to be used as biosensors [102,103]. All these composites are reported to have increased sensitivity, stability and reproducibility.

2.3 Properties of Carbon Nanotube-Copper Composite

Various methods used to form CNT/Cu metal composite have their own advantages and disadvantages. The electrical and mechanical properties obtained using various synthesis methods discussed in the previous section shows wide variation not only among methods used but as prepared by individual researchers. The next section elaborates on mechanical and electrical properties of CNT/Cu metal composite achieved by different methods.

2.3.1 Mechanical properties of carbon nanotube-copper composite

Carbon nanotube improves the mechanical properties as well as thermal properties. However is has been extremely difficult to turn this potential into a method for practical structural materials. Any real structural material can be fabricated from arrays or networks of fibres or from composites of fibre embedded in a matrix. In either case, the resulting mechanical properties will depend strongly on the stress transfer between matrix and fibre. Transfer of the stress strongly depends on the bonding between matrix and the fibres. Sometimes the chemical bond and sometimes only physical van der Waals bond is observed between the matrix and fibre. It is obvious to have better stress transfer in chemical bonding. Another factor on which stress transfer depends is the critical fibre length (L_c), which is necessary for effective transfer of stress. Critical

length of the fibre depends on fibre diameter d, fibre tensile strength σ_f and on the fibre-matrix bond strength τ_c according to $L_c = (\sigma_f \, d/2\tau_c)$ [104] (L_c/d ratio is called aspect ratio). The average length of carbon nanotube is much higher than the critical length hence the transfer of the load will be significant and therefore, it is expected to have better mechanical properties in the composite.

Mechanical properties

Most of the research groups have studied the tribological properties of the CNT/Cu composite. CNT not only helps in improving the strength of the composite but also helps in reducing the wear of the material. In between two mating surfaces, the CNT form a graphitic layer as well as CNT will act as a spacer, which will result in lubrication and sometimes it will avoid the direct contact between the two meting surfaces. This improves the coefficient of friction and decreases the wear rate of the composite, in turn reduces the material loss by wear. There are several methods like ring-on-block which was used by several researchers like S.R. Dong et al. in 2001 [30] , W.X. Chen et al. in 2003 [49], P.Q. Dai et al. in 2008 [105], Men et al. in 2008 [106], Second method is ball-on-disk which was used by X.H. Chen in 2001 [83], Z. Yang et al. in 2004 [79], Lim et al. in 2006 [35], Kinoshita et al. in 2007 [107], C. Kim et al. in 2009 [42], the third method is pin-on-disk which was used by J.P. Tu et al. in 2001 [31], Wang et al. in 2003 [86], Zhou et al. in 2007 [59], K.T. Kim et al. in 2007 [36,38], I.Y. Kim et al. in 2009 [18], Praveen et al. in 2009 [85], Guiderdoni et al. in 2011[47], Alishahi et al. [82] etc by which tribological properties can be measured. S.R. Dong et al. [30]. In 2001 [30] are the pioneer in the production of CNT/Cu composite by powder metallurgy method. The form composite by PM method is tested for hardness and wear resistance. It is clear that the hardness of the composite increases up to ~12 vol% volume fraction of the CNT and then it decreases. In the same way, wear rate and coefficient of friction decreases up to ~12 vol% and it is observed that with increase in volume percentage the wear resistance and coefficient of friction slightly increases. Due low wet-ability of the CNT, no CNT/Cu compound is observed on the surface of CNT. In order to increase the wet-ability of the CNT, these are coated with nickel and then W.X. Chen et al. in 2003 [32] used coated CNTs to form composite. They have tested this composite for the hardness, coefficient of friction and the wear rate. They also observed the result similar to S. R. Dong and found that the optimum volume percentage of CNT as 10-12. However, due to the bonding in CNT and Cu matrix it is expected that the yield strength and the ultimate tensile strength will increase.

K.T. Kim et al. in 2006 [37] measured the hardness of the CNT/Cu composite by nanoindentation method. The hardness of the CNT/Cu composite was 1.75 GPa with 10 vol% of CNT and the hardness of the pure copper synthesized by the same protocol was 0.57 GPa. From this, it was clear that the hardness of CNT/Cu was three times higher than the pure copper. They calculated the yield strength from the hardness value data and they observed that the yield strength of CNT/Cu (587 MPa) was three times higher than the pure copper yield strength (190 MPa). In their subsequent work[38], they measured the hardness value by Vicker hardness tester and they observed that the hardness of the CNT/Cu composite was 1.1 GPa (with 10 vol% of CNT), which was about 1.8 times higher than the pure copper.

In their succeeding work, K.T. Kim et al. in 2008 [39] have also used the molecular level-mixing process in order to have homogeneous dispersion of CNT in fine grained metal matrix. They have studied the effect of grain size on the mechanical properties of CNT/Cu composite. They observed, yield strength of the 5 vol% CNT reinforced composite (460 MPa) is enhanced by 2.35 times than that of unreinforced Cu (195MPa). Due to reduction in the grain size, the yield strength of unreinforced Cu as well as CNT reinforced copper is enhanced. This result shows that for better property of the reinforced composite, it should be accompanied by work hardening process.

C. Kim et al. in 2009 [42] investigated the nickel coated SWNT reinforced copper matrix composite. The composite was fabricated by PM. Due to similar density of copper and nickel the uniform distribution of the CNT was observed.

S.I. Cha et al. in 2005 [67] have fabricated the CNT/Cu composite by molecular level mixing of functionalize CNT with Cu ion followed by spark plasma sintering. The form composite have shown good yield strength. The yield strength of the CNT/Cu (10 vol%) composite was 455 MPa, which was more than three times higher than the pure Cu (150 MPa). The Young's modulus compared to Cu matrix was 1.5 times higher than the pure copper. The improvement in the properties was attributed to the uniform dispersion and interfacial strength between CNT and the copper matrix.

With this view, B. Lim et al. in 2006 [35] have carried out high temperature displacement rate test to evaluate the interfacial strength between the copper particle and the carbon nanotube. The specimen (composite CNT/Cu) with 0.5 vol% of CNT show very high displacement rate with low rupture time. The other specimen with nickel-coated nanotube reinforced copper matrix composite demonstrated the slowest displacement rate and took

long time to rupture and it was about six times longer than the pure copper specimen. From this, it was concluded that this outstanding strength was due to the transfer of stress from metal matrix to the carbon nanotube and it is possible only because of improved interfacial strength between nickel-coated carbon nanotubes and copper particles.

In 2007, Seunghyun Baik et al. [41] have used two different methods i.e. mechanical mixing and molecular level mixing process for fabrication of the carbon nanotube reinforced copper composite. They carried out tests to check the mechanical properties of the composite. It is observed that there is significant improvement in the mechanical properties of the composite.

Some of the research groups used electro-chemical method for fabrication of the CNT/Cu composite. In 2008, G. Chai et al. [2] synthesized the CNT reinforced Cu composite by electrochemical-co-deposition. It was observed that the distribution of the CNT in the copper matrix is uniform. The mechanical properties of the form composite were studied. They noticed that the yield strength (measured as 420 MPa) of the CNT/Cu was five times and ultimate strength was three times more than the pure copper (measured as 75 MPa).

In 2008, Y. L. Yang et al. [77] also synthesized the CNT reinforced Cu composite by electrochemical-co-deposition and studied the micro-hardness of the composite. A significant enhancement in micro-hardness (1.18 GPa to 1.6 GPa approximately by 36%) was observed in the SWNT/Cu composites.

In 2009, Walid M Daoush [62] deposited copper on the CNT by using electroless Cu deposition method in alkaline copper sulphate and trisodium citrate bath. The formed powder copper coated CNTs were sintered by SPS process. He forms the composite with different vol% of CNT and during characterization he observed that the yield strength and the ultimate strength increases up to 15 vol% of CNT. The hardness of the composite also increases with increase in vol% of CNT up to 20 vol%.

In 2013, K. Chu et al. [64] synthesized the CNT/Cu composite and they observed that the yield strength of Cu/CNT composite with 10 vol% CNTs, is up to 278 MPa and the yield strength of the pure copper sample is 168 MPa; i.e., the yield strength increased by 65%. This enhancement in the properties was attributed to the uniform dispersion of the CNT in the copper matrix.

2.3.2 Electrical and thermal properties of CNT/Cu composites

Due to remarkable electrical properties and thermal properties of the carbon nanotube, researchers believe that the carbon nanotube can be reinforced to also improve the thermal as well as electrical properties of the CNT/metal composite. In 2007, S. Baik [41] claim that the electrical resistance of the CNT/Cu composite was decreased due to reinforcement of CNT in copper matrix.

In 2008, Yang Chai et al. [92] studied the electro-migration [EM] properties of pure Cu and CNT/Cu composite. They observed slower EM rate in the CNT/Cu composite and this is attributed to the reinforced CNT. Slow EM rate will cause high electrical conductivity of the composite. In contrary to this observation, in 2009, W. M. Daoush et al. [43] have tested the form CNT/Cu composite for electrical conductivity and observed that the electrical conductivity decrease with the increase in the CNT vol%. During synthesis of CNT/Cu composite the CNT occupy the grain boundary region, which causes obstacle for the movement of electrons across the grain and hence they claim that the electrical conductivity of the composite was decreases. In support to this observation, in 2013, K. Chu et al. [64] also observed noticeable decrease in the electrical conductivity.

It is quite interesting to note from the literature review in the previous sections that despite various methods having being used for synthesis of CNT/Cu metal composite none have been commercialised or was able to put to bulk production till date. After electrical and mechanical testing of the samples, it was observed that the widely varied values were achieved for different electrical and mechanical properties of the formed metal composite. A comparison of different methods and the properties obtained of the formed composite is shown in Table 2.2. The possibility of method variation to obtain better properties is obvious and this can be figured out from Table 2.2, which is obtained from the extensive literature survey. By the powder metallurgy method, uniform dispersion of the CNT in the metal matrix is possible. However, the mixing of the metal powder and carbon nanotube, in ball milling or in particles compositing process, is a very severe process by which the CNT will break and will lose its properties. Definitely, form the table it is clear that the improvement in mechanical properties is good, this is because of the hindrances to the movement of dislocation caused by CNTs (may be in a broken state) present in the metal matrix. Nevertheless, none of the studies shows any improvement in the electrical properties of the composite, even none of the group has carried out any investigation on electrical properties of the composite simultaneously with the investigation of mechanical properties.

Table 2.2: Comparative statement of mechanical and electrical properties of CNT/Cu composite by different group of researchers

Method	Author	Year	Ref	Mechanical property		Electrical properties	
				Young's Modulus, Ultimate tensile strength, Hardness			
				with CNT	without CNT	with CNT	without CNT
Physical methods	S.R.Dong et al.	2001	[30]	with 15 vol.% CNT Vicker hardness=118 VHN	vicker hardness=98 VHN	-	-
	Tu, J. P et al.	2001	[31]	with 12 vol.% CNT Rockwell hardness=12.5 HRB	Rockwell hardness=10.2 HRB	-	-
	Chen,W. X et al.	2003	[32]	with 12 vol.% CNT Rockwell hardness=21.5 HRB	Rockwell hardness=10.2 HRB	-	-
	Kim, K. T. et al.	2004	[36]	with 10 vol.% CNT hardness=100 MPa	Hardness=56 MPa	-	-
	Quang, P. et al.	2006	[51]	with 5 vol.% CNT Vicker hardness=280 VHN and after 8 passes	-	-	-
	Kim, K. T. et al.	2006	[37]	with 10 vol.% CNT, Yield strength = 197 MPa Young's Modulus= 137 GPa Tensile strength = 281 MPa Hardness=1.75 GPa	Yield strength = 150MPa Young's modulus= 80 GPa Tensile strength = 175 MPa Hardness =0.57 GPa	-	-
	Quang, P. et al.	2007	[52]	with 1 vol.% CNT H=115 VHN and after 8 passes	-	-	-
	Kim, K. T. et al.	2007	[38]	with 10 vol.% CNT, Hardness =1.1 GPa	Hardness =0.8 GPa	-	-
	Kim, K. T. et al.	2008	[40]	Yield strength = 455 MPa Young's modulus= 138 GPa	Yield strength = 150 MPa Young's modulus = 100 GPa		
	Li, H. et al.	2009	[54]	Hardness = 3.5 GPa	Hardness =2.8 GPa		
	Li, H. et al.	2009	[53]	Compressive Yield strength = 1125 MPa	Compressive yield strength = 738 MPa		

Method	Author	Year	Ref	Mechanical property		Electrical properties	
	Guiderdoni, Ch. et al.	2011	[47]	Microhardness=103 Hv	Microhardness=50 Hv		
Chemical method	Chai, G et al.	2008	[2]	Yield strength = 420 MPa Tensile strength =710 MPa	Yield strength = 75 MPa Tensile strength =230 MPa		
	Cha, S. I. et al.	2008	[33]	with 10 vol.% CNT, Yield strength = 455MPa Young's Modulus= 135 GPa	Yield strength = 150MPa Young's Modulus= 80 GPa	-	-
	Ferrer-Anglada , N. et al.	2006	[90]	-	-	No change in Electrical conductivity	
	Li,Y-H. et al.	2007	[1]	Yield Strength= 132 GPa Tensile Strength = 361 MPa	Yield Strength = 117 GPa Tensile Strength = 334 MPa		
	Yang, Y. L. et al.	2008	[77]	with 10 vol.% CNT, hardness =1.61 GPa	hardness =1.18 GPa	Electrical conductivity was comparable to the pure copper	
	Daoush, W. M. et al.	2009	[43]	Yield strength = 350 MPa Young's modulus= 105 GPa hardness =1.5 GPa	Yield strength = 120MPa Young's modulus= 51.6 GPa hardness =0.7 GPa	Electrical conductivity decreases with increase in CNT content	
	Kim, C. et al.	2009	[42]			No change in electrical conductivity	
	Sun, Y. et al.	2009	[94]	Tensile Strength= 670 MPa	Tensile Strength= 230 MPa		
	C. Subramaniam et al.	2013	[95]			Current carrying capacity = 600 MA/cm²	Current carrying capacity =6.1 MA/cm²

The electrochemical methods are more feasible and comparable because during the electrochemical process there is very less possibility of CNT breakage. It means the pristine CNTs will be reinforced in the CNT/Cu composite, which will preserve the properties of CNT in the composite. The electrochemical method will help in improving other properties like electrical properties, which is associated with the pristine CNT. Most of the research groups, who are working in the CNT/Metal matrix composite field, studied of mechanical properties of the composite extensively. Very few research groups [28,42,43,77,90,100] have studied the electrical properties. However, their results on electrical properties of the form composite are contradicting to each other.

There is a possibility of improvement in the electrochemical process and obtain simultaneously improvement in electrical and mechanical property of the form CNT/Cu composite. We formulated our investigation statement for this thesis on this possibility and the workdone to devise a better method. The detailed problem statements are is given in the next section.

2.4 Scope of the Present Work

In this and previous chapter we have noted from the literature that carbon nanotubes are one of the best reinforcing nanomaterial in metal matrix for improvisation of metal properties. Most of the early research on fabrication of CNT composites used blending by adding CNTs to metals. Researchers have observed that CNTs are not dispersed uniformly by blending of larger concentration of CNTs, which results in deterioration in mechanical properties.

- Ball milling is a general method for uniform dispersion of CNTs but the ball milling will cause damage to the CNTs and the length of CNTs get shortens. The length of the CNTs is one of the important factors for the improvement in mechanical properties like yield strength, tensile strength etc.
- Molecular level mixing is a new method for uniform dispersion of CNT in metal matrix. Uniform dispersion of CNT in metal matrix is observed but the process is at laboratory level.
- Some of the research groups used Electro-chemical method for fabrication of the Metal/CNT composite. In case of electro-co-deposition method, it is difficult to get a freestanding structure. The process limits the thickness of the composite up to 200 μm.

- The methods suggested have drawbacks like in case of molecular level mixing incomplete reduction of the CNT/Cu oxide may lead to the oxide impurity. Ball milling will result in damage to the CNTs. The electro-co-deposition method is described for the micro-fabrication process.

Moreover, as the quality of dispersion of MWCNT is also important, at the same time the process should be easily scalable for bulk production of composite.

Considering state of art after comprehensive literature review, we narrowed our scope of investigation on the following aspect of the issues challenging synthesis for the composite.

i Is it possible to tweak an existing method, which may enable a feasible newer modified method and ensure a way to obtain a bulk production? In this attempt, we need to relook at all existing methods, their relative advantages/disadvantage, figured out one best method and try to improve that particular method. A thorough work out and combining two existing methods, we improved and form a modified method, which enables bulk production of CNT/Cu metal composite in powder form. The new modified method proposed was described in Chapter 3.

ii Non-uniform dispersion of CNT in the copper matrix formed by the newer method has to be ensured. This needs a study of microstructure of the form CNT/Cu composite and is investigated in Chapter 4.

iii The bulk produced CNT/Cu composite need to be investigated for the betterment of mechanical properties. The properties will improve if there is uniform dispersion of CNT. An investigation on improvement of mechanical properties is quite essential for any such proposal of bulk production and this was done and presented in Chapter 5.

iv On similar argument as in (iii), investigation of the electrical properties of the composite is also quite essential, which was done and presented in Chapter 6. The chapter also statistically figure out the process parameters significantly affecting the variation in the electrical properties of the product.

In Chapter 7 we give, conclusion and also present the scope of the future work and conclusions obtained by work out in this thesis.

In the next chapter, we present the modified method and characterization of the MWCNT/Cu composite powder.

References:

[1] Li Y-H, Housten W, Zhao Y, Zhu YQ. Cu/single-walled carbon nanotube laminate composites fabricated by cold rolling and annealing. Nanotechnology 2007;18:205607.

[2] Chai G, Sun Y, Sun J "Jenny", Chen Q. Mechanical properties of carbon nanotube–copper nanocomposites. J Micromechanics Microengineering 2008;18:035013.

[3] Goddard III WA, Che J, Ca T. Thermal conductivity of carbon nanotubes. Nanotechnology 2000;11:65–9.

[4] Kuzumaki T, Miyazawa K, Ichinose H, Ito K. Processing of Carbon Nanotube Reinforced Aluminum Composite. J Mater Res 1998;13:2445–9.

[5] Xu CL, Wei BQ, Ma RZ, Liang J, Ma XK, Wu DH. Fabrication of aluminum – carbon nanotube composites and their electrical properties. Carbon N Y 1999;37:855–8.

[6] Zhong R, Cong H, Hou P. F abrication of nano-Al based composites reinforced by single-walled carbon nanotubes. Carbon N Y 2003;41:848–51.

[7] Tang Y, Cong H, Zhong R, Cheng H-M. Thermal expansion of a composite of single-walled carbon nanotubes and nanocrystalline aluminum. Carbon N Y 2004;42:3260–2.

[8] Noguchi T, Magario A, Fukazawa S, Shimizu S, Beppu J, Seki M. Carbon Nanotube/Aluminium Composites with Uniform Dispersion. Mater Trans 2004;45:602–4.

[9] George R, Kashyap KT, Rahul R, Yamdagni S. Strengthening in carbon nanotube/aluminium (CNT/Al) composites. Scr Mater 2005;53:1159–63.

[10] Ci L, Ryu Z, Jin-Phillipp NY, Rühle M. Investigation of the interfacial reaction between multi-walled carbon nanotubes and aluminum. Acta Mater 2006;54:5367–75.

[11] Deng CF, Wang DZ, Zhang XX, Ma YX. Damping characteristics of carbon nanotube reinforced aluminum composite. Mater Lett 2007;61:3229–31.

[12] Deng CF, Ma YX, Zhang P, Zhang XX, Wang DZ. Thermal expansion behaviors of aluminum composite reinforced with carbon nanotubes. Mater Lett 2008;62:2301–3.

[13] Choi H, Kwon G, Lee G, Bae D. Reinforcement with carbon nanotubes in aluminum matrix composites. Scr Mater 2008;59:360–3.

[14] Esawi AMK, El Borady M a. Carbon nanotube-reinforced aluminium strips. Compos Sci Technol 2008;68:486–92.

[15] Esawi a. MK, Morsi K, Sayed a., Gawad a. A, Borah P. Fabrication and properties of dispersed carbon nanotube–aluminum composites. Mater Sci Eng A 2009;508:167–73.

[16] Kwon H, Estili M, Takagi K, Miyazaki T, Kawasaki A. Combination of hot extrusion and spark plasma sintering for producing carbon nanotube reinforced aluminum matrix composites. Carbon N Y 2009;47:570–7.

[17] Deng C, Zhang P, Ma Y, Zhang X, Wang D. Dispersion of multiwalled carbon nanotubes in aluminum powders. Rare Met 2009;28:175–80.

[18] Kim I-Y, Lee J-H, Lee G-S, Baik S-H, Kim Y-J, Lee Y-Z. Friction and wear characteristics of the carbon nanotube–aluminum composites with different manufacturing conditions. Wear 2009;267:593–8.

[19] Poirier D, Gauvin R, Drew R a. L. Structural characterization of a mechanically milled carbon nanotube/aluminum mixture. Compos Part A Appl Sci Manuf 2009;40:1482–9.

[20] Kwon H, Leparoux M. Hot extruded carbon nanotube reinforced aluminum matrix composite materials. Nanotechnology 2012;23:415701.

[21] Chen D, Chen L, Liu S, Ma CX, Chen DM, Wang LB. Microstructure and hydrogen storage property of Mg/MWNTs composites. J Alloys Compd 2004;372:231–7.

[22] Carreno-Morelli E, Yang J, Couteau E, Hernadi K, Seo JW, Bonjour C, et al. Carbon nanotube/magnesium composites. Phys Status Solidi 2004;201:R53–R55.

[23] Goh CS, Wei J, Lee LC, Gupta M. Development of novel carbon nanotube reinforced magnesium nanocomposites using the powder metallurgy technique. Nanotechnology 2006;17:7–12.

[24] Shimizu Y, Miki S, Soga T, Itoh I, Todoroki H, Hosono T, et al. Multi-walled carbon nanotube-reinforced magnesium alloy composites. Scr Mater 2008;58:267–70.

[25] Thakur SK, Srivatsan TS, Gupta M. Synthesis and mechanical behavior of carbon nanotube–magnesium composites hybridized with nanoparticles of alumina. Mater Sci Eng A 2007;466:32–7.

[26] Goh CS, Wei J, Lee LC, Gupta M. Ductility improvement and fatigue studies in Mg-CNT nanocomposites. Compos Sci Technol 2008;68:1432–9.

[27] Kondoh K, Fukuda H, Umeda J, Imai H, Fugestu B, Endo M. Microstructural and mechanical analysis of carbon nanotube reinforced magnesium alloy powder composites. Mater Sci Eng 2010;527:4103–8.

[28] Feng Y, Yuan HL, Zhang M. Fabrication and properties of silver-matrix composites reinforced by carbon nanotubes. Mater Charact 2005;55:211–8.

[29] Pang L-X, Sun K-N, Ren S, Sun C, Fan R-H, Lu Z-H. Fabrication and microstructure of Fe3Al matrix composite reinforced by carbon nanotube. Mater Sci Eng A 2007;447:146–9.

[30] Dong SR, Tu JP, Zhang XB. An investigation of the sliding wear behavior of Cu-matrix composite reinforced by carbon nanotubes. Mater Sci Eng A 2001;313:83–7.

[31] Tu JP, Yang YZ, Wang LY, Ma XC, Zhang XB. Tribological properties of carbon-nanotube-reinforced copper composites. Tribol Lett 2001;10:225–8.

[32] Chen WX, Tu JP, Wang LY, Gan HY, Xu ZD, Zhang XB. Tribological application of carbon nanotubes in a metal-based composite coating and composites. Carbon N Y 2003;41:215–22.

[33] Cha SI, Kim KT, Arshad SN, Mo CB, Hong SH. Extraordinary Strengthening Effect of Carbon Nanotubes in Metal-Matrix Nanocomposites Processed by Molecular-Level Mixing. Adv Mater 2005;17:1377–81.

[34] Wenli G, Yue Z, Tongxiang L. Preparation of copper coated carbon nanotubes by decomposition of Cu(II)acetylacetonate in hydrogen atmosphere. J Mater Sci 2006;41:5462–6.

[35] Lim B, Kim C, Kim B, Shim U, Oh S, Sung B, et al. The effects of interfacial bonding on mechanical properties of single-walled carbon nanotube reinforced copper matrix nanocomposites. Nanotechnology 2006;17:5759–64.

[36] Kim KT, Lee KH, Cha S I, Mo CB, Hong SH. Characterization of Carbon Nanotubes/Cu Nanocomposites Processed by Using Nano-sized Cu Powders. MRS Proceeding 2004;821:2004.

[37] Kim KT, Cha S I, Hong SH, Hong SH. Microstructures and tensile behavior of carbon nanotube reinforced Cu matrix nanocomposites. Mater Sci Eng A 2006;430:27–33.

[38] Kim KT, Cha S Il, Hong SH. Hardness and wear resistance of carbon nanotube reinforced Cu matrix nanocomposites. Mater Sci Eng A 2007;449-451:46–50.

[39] Kim KT, Eckert J, Menzel SB, Gemming T, Hong SH. Grain refinement assisted strengthening of carbon nanotube reinforced copper matrix nanocomposites. Appl Phys Lett 2008;92:121901.

[40] Kim KT, Cha S Il, Gemming T, Eckert J, Hong SH. The role of interfacial oxygen atoms in the enhanced mechanical properties of carbon-nanotube-reinforced metal matrix nanocomposites. Small 2008;4:1936–40.

[41] Baik S, Lim B, Ryu S, Choi D, Kim B, Oh S, et al. Mechanical and electrical properties of Carbon nanotubes in copper matrix nanocomposites. Solid State Phenom 2007;120:285–8.

[42] Kim C, Lim B, Kim B, Shim U, Oh S, Sung B, et al. Strengthening of copper matrix composites by nickel-coated single-walled carbon nanotube reinforcements. Synth Met 2009;159:424–9.

[43] Daoush WM, Lim BK, Mo CB, Nam DH, Hong SH. Electrical and mechanical properties of carbon nanotube reinforced copper nanocomposites fabricated by electroless deposition process. Mater Sci Eng A 2009;513-514:247–53.

[44] Isra A, Zhu YT, Horita Z, Koch CC. Processing and characterization of nanostructured Cu-Carbon nanotube composite. Mater Sci Eng 2009;523:60–4.

[45] Chu K, Wu Q, Jia C, Liang X, Nie J, Tian W, et al. Fabrication and effective thermal conductivity of multi-walled carbon nanotubes reinforced Cu matrix composites for heat sink applications. Compos Sci Technol 2010;70:298–304.

[46] Chu K, Guo H, Jia C, Yin F, Zhang X, Liang X, et al. Thermal properties of carbon nanotube-copper composites for thermal management applications. Nanoscale Res Lett 2010;5:868–74.

[47] Guiderdoni C, Estournès C, Peigney A, Weibel A, Turq V, Laurent C. The preparation of double-walled carbon nanotube/Cu composites by spark plasma sintering, and their hardness and friction properties. Carbon N Y 2011;49:4535–43.

[48] Jenei P, Yoon EY, Gubicza J, Kim HS, Lábár JL, Ungár T. Microstructure and Thermal Stability of Copper - Carbon Nanotube Composites Consolidated by High Pressure Torsion. Mater Sci Forum 2012;729:228–33.

[49] Chen W., Tu J., Xu Z., Chen W., Zhang X., Cheng D. Tribological properties of Ni P multi walled carbon nanotubes electroless composite coating. Mater Lett 2003;57:1256–60.

[50] Goudah G, Ahmad F, Mamat O. Microstructural studies of sintered carbon nanotubes reinforced copper matrix composite. J Eng Sci Technol 2010;5:272–83.

[51] Quang P, Jeong YG, Hong SH, Seop H. Equal Channel Angular Pressing of Carbon Nanotube Reinforced Metal Matrix Nanocomposites. Key Eng Mater 2006;326-328:325–8.

[52] Quang P, Jeong YG, Yoon SC, Hong SH, Kim HS. Consolidation of 1vol.% carbon nanotube reinforced metal matrix nanocomposites via equal channel angular pressing. J Mater Process Technol 2007;187-188:318–20.

[53] Li H, Misra A, Horita Z, Koch CC, Mara N a., Dickerson PO, et al. Strong and ductile nanostructured Cu-carbon nanotube composite. Appl Phys Lett 2009;95:071907.

[54] Li H, Misra A, Zhu Y, Horita Z, Koch CC, Holesinger TG. Processing and characterization of nanostructured Cu-carbon nanotube composites. Mater Sci Eng A 2009;523:2009.

[55] Jenei P, Yoon EY, Gubicza J, Kim HS, Lábár JL, Ungár T. Microstructure and Thermal Stability of Copper - Carbon Nanotube Composites Consolidated by High Pressure Torsion. Mater Sci Forum 2012;729:228–33.

[56] Taylor GF. Apparatus for making hard metal composites. US 1896854 A, 1933.

[57] Bernard EP, Simpson LW. PROCESS FOR HOT PRESSING POWDER. US3231648 A, 1966.

[58] Deng C, Zhang X, Wang D, Lin Q, Li A. Preparation and characterization of carbon nanotubes/aluminum matrix composites. Mater Lett 2007;61:1725–8.

[59] Zhou S, Zhang X, Ding Z, Min C, Xu G, Zhu W. Fabrication and tribological properties of carbon nanotubes reinforced Al composites prepared by pressureless infiltration technique. Compos Part A Appl Sci Manuf 2007;38:301–6.

[60] Chastel F, Flahaut E, Peigney A, Rousset A. Carbon Nanotube – Metal – Oxide Nanocomposites: Microstructure , Electrical Conductivity and Mechanical properties. Acta Mater 2000;48:3803–12.

[61] Zhang T, Kumari L, Du GH, Li WZ, Wang QW, Balani K, et al. Mechanical properties of carbon nanotube–alumina nanocomposites synthesized by chemical vapor deposition and spark plasma sintering. Compos Part A Appl Sci Manuf 2009;40:86–93.

[62] Daoush WM. Processing and characterization of CNT/Cu nanocomposites by powder technology. Powder Metall Met Ceram 2009;47:531–7.

[63] Uddin SM, Mahmud T, Wolf C, Glanz C, Kolaric I, Volkmer C, et al. Effect of size and shape of metal particles to improve hardness and electrical properties of carbon nanotube reinforced copper and copper alloy composites. Compos Sci Technol 2010;70:2253–7.

[64] Chu K, Jia C, Li W, Wang P. Mechanical and electrical properties of carbon-nanotube-reinforced Cu-Ti alloy matrix composites. Phys Status Solidi 2013;210:594–9.

[65] Xie G. Spark Plasma Sintering: A Useful Technique to Develop Large-Sized Bulk Metallic Glasses. J Powder Metall Min 2013;02:2–4.

[66] Cha SI, Hong SH. Microstructures of binderless tungsten carbides sintered by spark plasma sintering process. Mater Sci Eng A 2003;356:381–9.

[67] Cha SI, Kim KT, Lee KH, Mo CB, Hong SH. Strengthening and toughening of carbon nanotube reinforced alumina nanocomposite fabricated by molecular level mixing process. Scr Mater 2005;53:793–7.

[68] Bakshi SR, Musaramthota V, Virzi D a., Keshri AK, Lahiri D, Singh V, et al. Spark plasma sintered tantalum carbide–carbon nanotube composite: Effect of pressure, carbon nanotube length and dispersion technique on microstructure and mechanical properties. Mater Sci Eng A 2011;528:2538–47.

[69] Suárez M, Fernández A, Menéndez JL, Torrecillas R, Kessel HU, Hennicke J, et al. Challenges and Opportunities for Spark Plasma Sintering: A Key Technology for a New Generation of Materials. In: Ertug B, editor. Sinter. Appl., 2013, p. 319–42.

[70] Cho S, Kikuchi K, Kawasaki A, Kwon H, Kim Y. Effective load transfer by a chromium carbide nanostructure in a multi-walled carbon nanotube/copper matrix composite. Nanotechnology 2012;23:315705.

[71] Bakshi SR, Lahiri D, Agarwal a. Carbon nanotube reinforced metal matrix composites – a review. Int Mater Rev 2010;55:41–64.

[72] Agarwal A, Bakshi SR, Lahiri D. Carbon Nanotubes Reinforecd Metal Matrix Composite. Boca Raton, Florida: CRC Press, Taylor and Francis Group; 2011.

[73] Tan J, Yu T, Xu B, Yao Q. Microstructure and wear resistance of nickel–carbon nanotube composite coating from brush plating technique. Tribol Lett 2006;21:107–11.

[74] Titus E, Cabral G, Madaleno JCC, Neto VFF, Shokuhfar T, Blau WJJ, et al. Synthesis of highly oriented carbon nanotube thin films by nickel functionalisation. Diam Relat Mater 2007;16:1195–9.

[75] Guo C, Zuo Y, Zhao X, Zhao J, Xiong J. Effects of surfactants on electrodeposition of nickel-carbon nanotubes composite coatings. Surf Coatings Technol 2008;202:3385–90.

[76] Praveen BM, Venkatesha TV, Arthoba Naik Y, Prashantha K. Corrosion studies of carbon nanotubes–Zn composite coating. Surf Coatings Technol 2007;201:5836–42.

[77] Yang YL, Wang YD, Ren Y, He CS, Deng JN, Nan J, et al. Single-walled carbon nanotube-reinforced copper composite coatings prepared by electrodeposition under ultrasonic field. Mater Lett 2008;62:47–50.

[78] Tello A, Cárdenas G, Häberle P, Segura R a. The synthesis of hybrid nanostructures of gold nanoparticles and carbon nanotubes and their transformation to solid carbon nanorods. Carbon N Y 2008;46:884–9.

[79] Yang Z, Xu H, Li M-K, Shi Y-L, Huang Y, Li H-L. Preparation and properties of Ni/P/single-walled carbon nanotubes composite coatings by means of electroless plating. Thin Solid Films 2004;466:86–91.

[80] Sun Y, Sun J, Liu M, Chen Q. Mechanical strength of carbon nanotube–nickel nanocomposites. Nanotechnology 2007;18:505704.

[81] Tsai L-N, Cheng Y-T, Hsu W, Fang W. Ni-carbon nanotubes nanocomposite for robust microelectromechanical systems fabrication. J Vac Sci Technol B Microelectron Nanom Struct 2006;24:205–10.

[82] Alishahi M, Monirvaghefi SM, Saatchi A, Hosseini SM. The effect of carbon nanotubes on the corrosion and tribological behavior of electroless Ni–P–CNT composite coating. Appl Surf Sci 2012;258:2439–46.

[83] Chen XH, Peng JC, Li XQ, Deng FM, Wang JX, Li WZ. Tribological behavior of carbon nanotubes — reinforced nickel matrix. J Mater Sci Lett 2001;20:2057–60.

[84] Chen XH, Cheng FQ, Li SL, Zhou LP, Li DY. Electrodeposited nickel composites containing carbon nanotubes. Surf Coatings Technol Technol 2002;155:274–8.

[85] Praveen BM, Venkatesha TV. Electrodeposition and properties of Zn–Ni–CNT composite coatings. J Alloys Compd 2009;482:53–7.

[86] Wang LY, Tu JP, Chen WX, Wang YC, Liu XK, Olk C, et al. Friction and wear behavior of electroless Ni-based CNT composite coatings. Wear 2003;254:1289–93.

[87] Chen XH, Chen CS, Xiao HN, Cheng FQ, Zhang G, Yi GJ. Corrosion behavior of carbon nanotubes–Ni composite coating. Surf Coatings Technol 2005;191:351–6.

[88] Wang F, Arai S, Endo M. Preparation of nickel–carbon nanofiber composites by a pulse-reverse electrodeposition process. Electrochem Commun 2005;7:674–8.

[89] Arai S. Ni-deposited multi-walled carbon nanotubes by electrodeposition. Carbon N Y 2004;42:641–4.

[90] Ferrer-Anglada N, Gomis V, El-Hachemi Z, Weglikovska UD, Kaempgen M, Roth S. Carbon nanotube based composites for electronic applications: CNT-conducting polymers, CNT-Cu. Phys Status Solidi 2006;203:1082–7.

[91] Chen Q, Chai G, Li B. Exploration Study of Multifunctional Metallic Nanocomposite Utilizing Single-Walled Carbon Nanotubes for Micro/Nano Devices. Proc Inst Mech Eng Part N J Nanoeng Nanosyst 2006;219:67–72.

[92] Chai Y, Member S, Chan PCH, Fu Y, Chuang YC, Liu CY. Electromigration Studies of Cu / Carbon Nanotube Composite Interconnects Using Blech Structure. IEEE ELECTRON DEVICE Lett 2008;29:1001–3.

[93] Peng Y, Chen Q. Ultrasonic-assisted fabrication of highly dispersed copper/multi-walled carbon nanotube nanowires. Colloids Surfaces A Physicochem Eng Asp 2009;342:132–5.

[94] Sun Y, Chen Q. Diameter dependent strength of carbon nanotube reinforced composite. Appl Phys Lett 2009;95:021901.

[95] Subramaniam C, Yamada T, Kobashi K, Sekiguchi A, Futaba DN, Yumura M, et al. One hundred fold increase in current carrying capacity in a carbon nanotube-copper composite. Nat Commun 2013;4:2202.

[96] Wang D, Song P, Liu C, Wu W, Fan S. Highly oriented carbon nanotube papers made of aligned carbon nanotubes. Nanotechnology 2008;19:075609.

[97] Wang F, Arai S, Endo M. Metallization of multi-walled carbon nanotubes with copper by an electroless deposition process. Electrochem Commun 2004;6:1042–4.

[98] Schlesinger M. Electroless deposition of nickel. 5th ed. John wiley and Sons, Inc; 2010.

[99] Chen X, Xia J, Peng J, Li W, Xie S. Carbon-nanotube metal-matrix composites prepared by electroless plating. Compos Sci Technol 2000;60:301–6.

[100] Oh Y, Suh D, Kim Y, Lee E, Mok JS, Choi J, et al. Silver-plated carbon nanotubes for silver/conducting polymer composites. Nanotechnology 2008;19:495602.

[101] Xia L, Jia B, Zeng J, Xu J. Wear and mechanical properties of carbon fiber reinforced copper alloy composites. Mater Charact 2009;60:363–9.

[102] Arribas AS, Bermejo E, Chicharro M, Zapardiel A, Luque GL, Ferreyra NF, et al. Analytical applications of a carbon nanotubes composite modified with copper microparticles as detector in flow systems. Anal Chim Acta 2006;577:183–9.

[103] Wang J, Chen G, Wang M, Chatrathi MP. Carbon-nanotube/copper composite electrodes for capillary electrophoresis microchip detection of carbohydrates. Analyst 2004;129:512–5.

[104] William D. Callister DGR. Fundamentls of Material Science and Engineering An Integrated approach. 4th ed. John wiley and Sons, Inc; 2012.

[105] Dai P-Q, Xu W-C, Huang Q-Y. Mechanical properties and microstructure of nanocrystalline nickel-carbon nanotube composites produced by electrodeposition. Mater Sci Eng A 2008;483-484:172–4.

[106] Men XH, Zhang ZZ, Song HJ, Wang K, Jiang W. Functionalization of carbon nanotubes to improve the tribological properties of poly(furfuryl alcohol) composite coatings. Compos Sci Technol 2008;68:1042–9.

[107] Kinoshita H, Ippei I, Sakai H, Ohmae N. Synthesis and mechanical properties of carbon nanotube diamond like carbon composite films. Diam Relat Mater 2007;16:1940–4.

Chapter 3

Process Development and Experiment

3.1 Conventional Synthesis Techniques of CNT/Cu Composites

In the previous chapter, the two main methods for fabrication of CNT/Cu composite were discussed namely (1) powder metallurgy and (2) electrochemical process. Due to high melting point of copper, the fabrication of copper-matrix composites is commonly done by PM or electrochemical-co-deposition. Both methods are widely used for the fabrication of CNT/Cu composite. However, each one is having its advantages and disadvantages. The advantages and disadvantages of each fabrication process are discussed in the next section. A quest for a method, which can give a CNT/Cu composite with a betterment in electrical and mechanical properties keeps researchers working towards this objective. In this context, we developed a new modified electro-co-deposition method, which is discussed and compared with the other methods. Its attributes are later given and compared with the other conventional method.

3.1.1 Electrochemical technique

Comprehensive literature review on electrochemical techniques have been discussed in the previous chapter. Electrochemical and electroless deposition techniques are utilized to synthesize CNT/Cu composite coatings and thin films. Primarily the electrochemical technique for fabrication of the CNT/Cu composite can be divided as [1]:

(i) The electrochemical deposition technique used to form a thin layer of CNT/Cu composite by co-depositing the CNT and copper ions on the surface.

(ii) The electroless deposition or auto catalytic technique method used for fabrication of one dimensional (1-D) structure by depositing copper on the CNT surface.

(iii) The electro deposition technique was also used for depositing only copper on the aligned CNT forest grown by chemical vapor deposition method in order to get an aligned CNT/ Cu composite.

(iv) In molecular level mixing, copper salt is dissolved in the stable solution of the functionalized CNTs with DI water or ethanol. Copper ions are attached with the functionalized CNT and after drying, forms a layer of copper oxide on the surface of CNT. The formed layer is converted to CNT/Cu 1-D structure after reduction in the presence of hydrogen.

In the first kind of classification, the CNT/Cu composites are synthesized by electrochemical co-deposition [2], where the CNTs can be driven and deposited onto a cathode, together with copper ions. It produces the composite coating on the surface of the cathode. Figure 3.1 and Figure 3.2 is the schematic representation of the electro-co-deposition method. The cathode in the circuit is the part, which is to be electro-co-deposited as shown in Figure 3.1. The anode may be made up of the metal to be plated, to replenish the metal ions in the electrolyte after deposition, or it may be an inert electrode like platinum. Both anode and cathode components are immersed in an electrolyte containing one or more dissolved metal salts and other elements (in present case carbon nanotubes) as well as acid which increase the concentration of H^+ ions that permit the flow of electricity as seen in Figure 3.1.

A power source supplies a direct current to the anode, oxidizing the metal atoms that comprise it and allowing them to dissolve in the solution. At the cathode, the dissolved metal ions in the electrolyte solution are reduced at the interface between the solution and the cathode and the carbon nanotubes are co-deposited with the metal ions, such that they 'plate out' onto the cathode as shown in Figure 3.2.

The flow chart corresponding to the electro-co-deposition plating process is shown in the Figure 3.3. In the case of co-deposition of CNTs and metals, good suspension and uniform dispersion of CNTs in the bath are the key factor for getting coatings with homogeneous CNT distribution. Uniformly dispersed CNTs in the copper electrolyte and copper ions are deposited onto the cathode simultaneously during the deposition. The method is similar to the conventional electroplating method. Uniform CNT distribution in the copper matrix depends on the uniform dispersion in the electrolyte, which present as first challenge in the method. As presented in previous chapter section 2.2, there are several methods for uniform dispersion of CNT in the electrolyte.

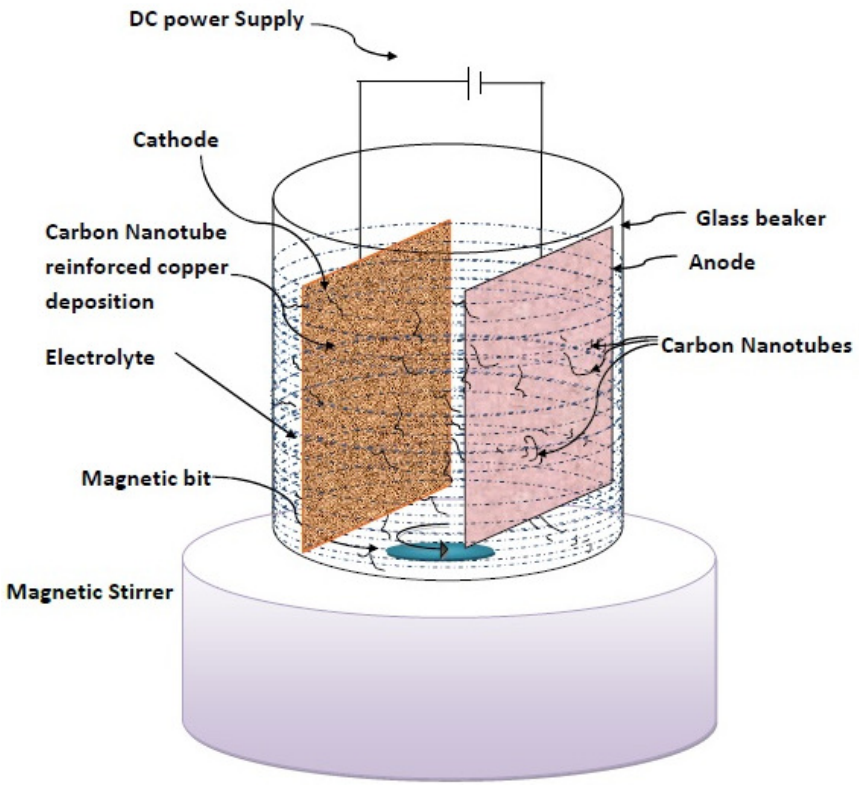

Figure 3.1: Schematic showing electro-co-deposition of copper and carbon nanotube

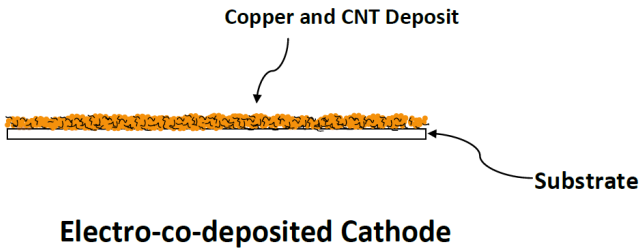

Figure 3.2: Schematic showing electro-co-deposited cathode

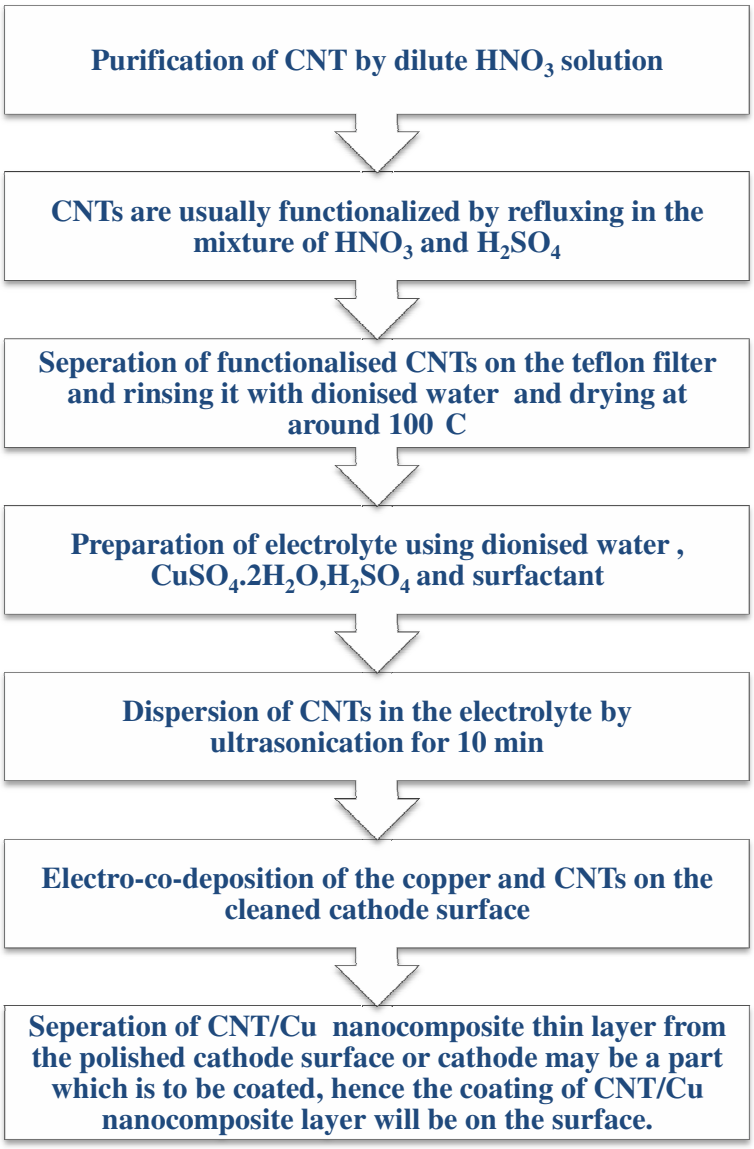

Figure 3.3: Flow chart for electro-co-deposition process

In the second kind of classification known as electroless or autocatalytic plating, the process involves the presence of a chemical reducing agent in solution to reduce metallic ions to the metal state. Instead of an anode, the metal is supplied by the metal salt. In case of CNT/Cu composite formation by electroless method, CNTs in the solution act as cathode instead of a separate metallic cathode and the electrons are provided by a reducing agent. The process takes place only on activated surface of CNT rather than throughout the solution. The method is very good for synthesis of one dimensional CNT/Cu composite wire but the method is at laboratory level and the amount, which will form by this method, is very small. The flowchart for electroless deposition is shown in Figure 3.4

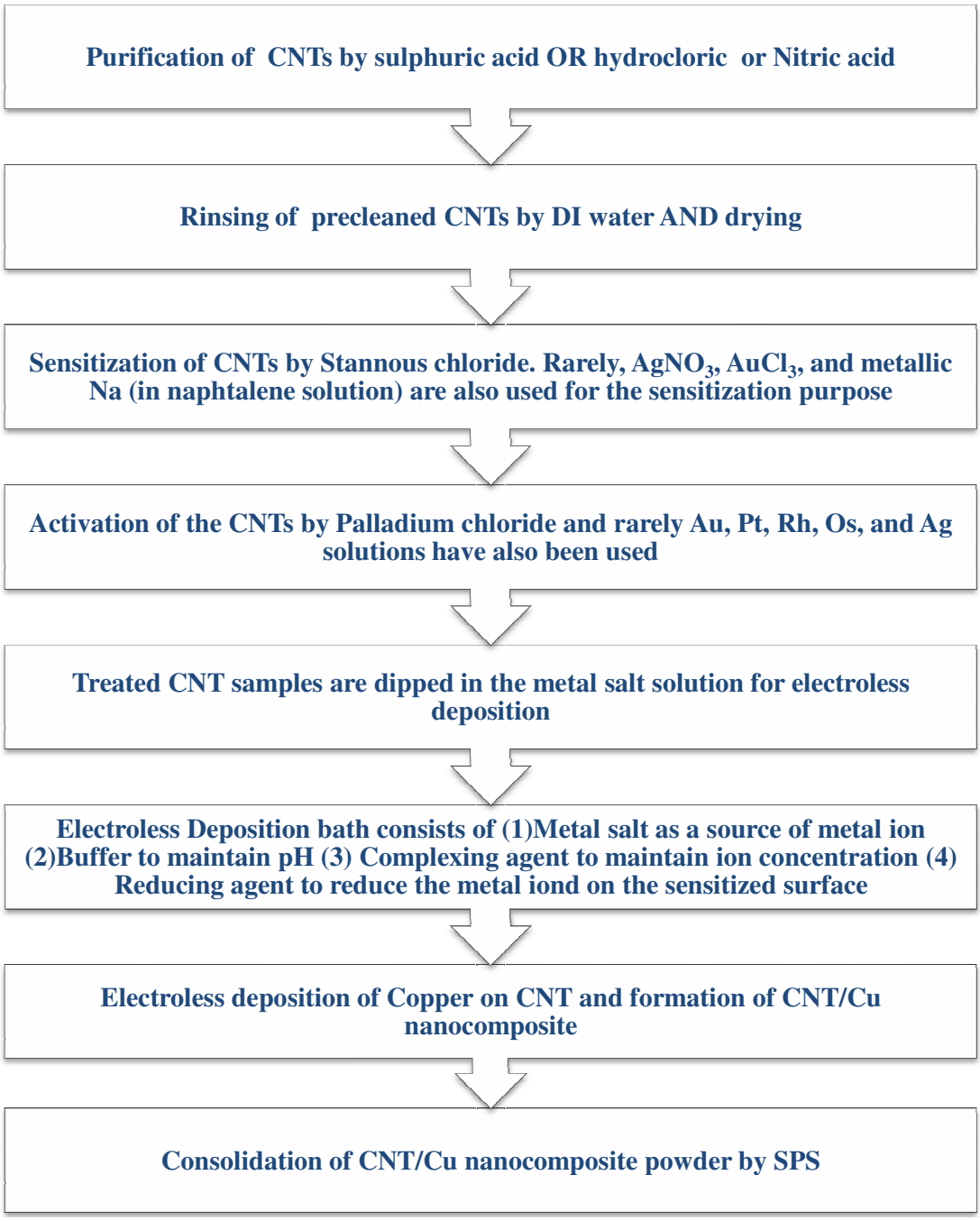

Figure 3.4: Flow chart for electroless deposition process

In the third kind of classification, copper is deposited on the CVD grown aligned CNT, which looks like a CNT forest as seen in Figure 3.3 step-1. During electro deposition the copper occupies the voids between the CNT and form a composite with aligned CNT.

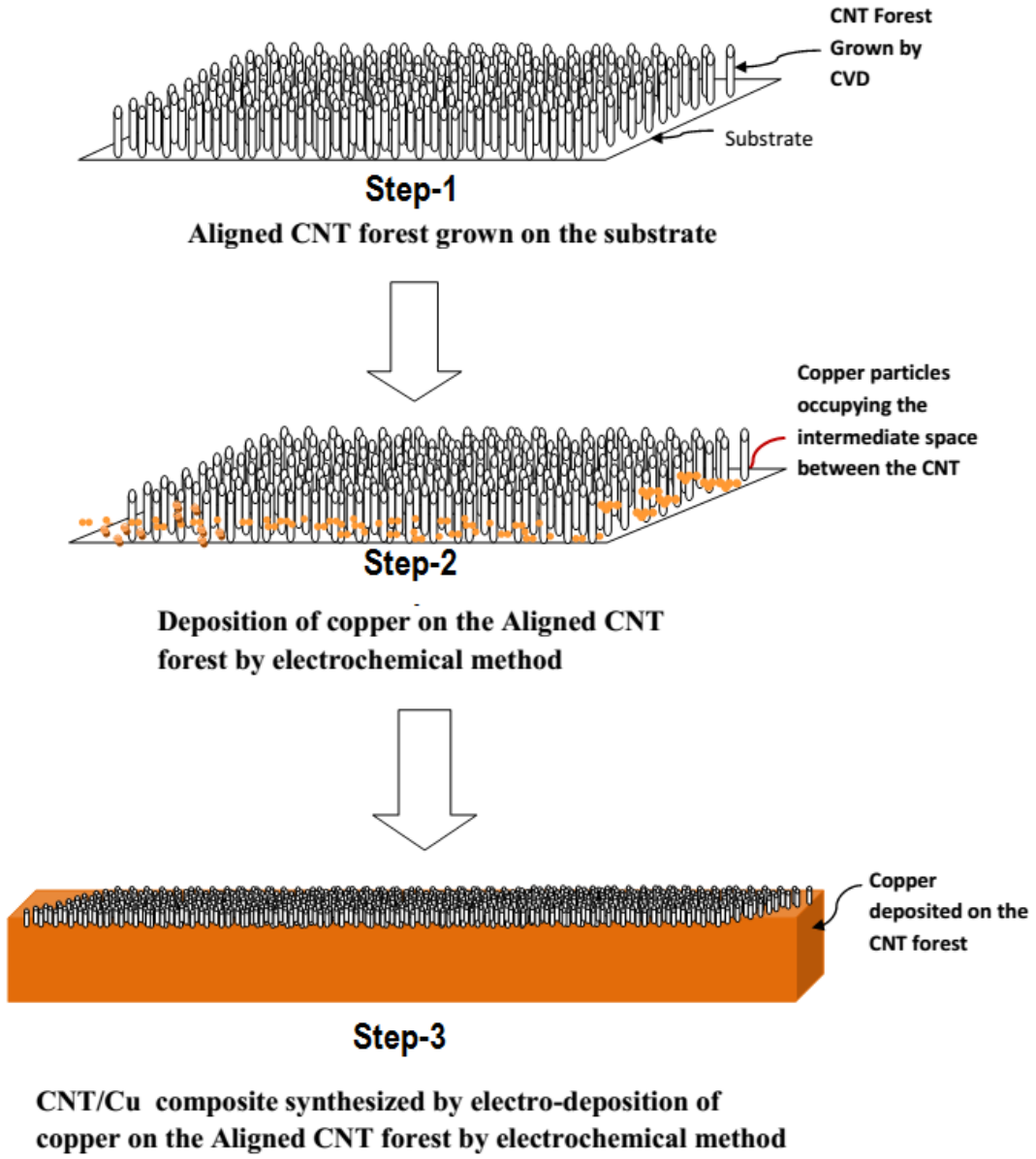

Figure 3.5: Different steps for synthesis of CNT/Cu composite by depositing copper on the CNT forest by electrochemical method

The method has advantage that alignment of carbon nanotube in the composite comes noteworthy and the composite will have directional properties. This technique is very useful for the micro-fabrication process. By using this technique component of different micro devices like nano-sensors, actuators, RF switches, interconnect etc can be fabricated. However, the product size of this composite is constrained by cathode size on which CNTs are grown in the CVD. Hence, bulk production of this type of composite is

difficult as well as costlier. Different steps associated with the above-mentioned method are shown in Figure 3.5.

In the fourth kind of the classification, the reduction of copper oxide present on the surface of CNT is carried out in the presence of hydrogen. The molecular level mixing method is thoroughly discussed in Chapter 2 section 2.2.2.2. This is very good for the dispersion of carbon nanotube in the copper matrix. Molecular level mixing method is most suitable for production of one-dimensional CNT/Cu composites. This method is at laboratory level and may not be the suitable method for the bulk production of CNT/Cu composite. The flowchart for this method is shown in Figure 3.6

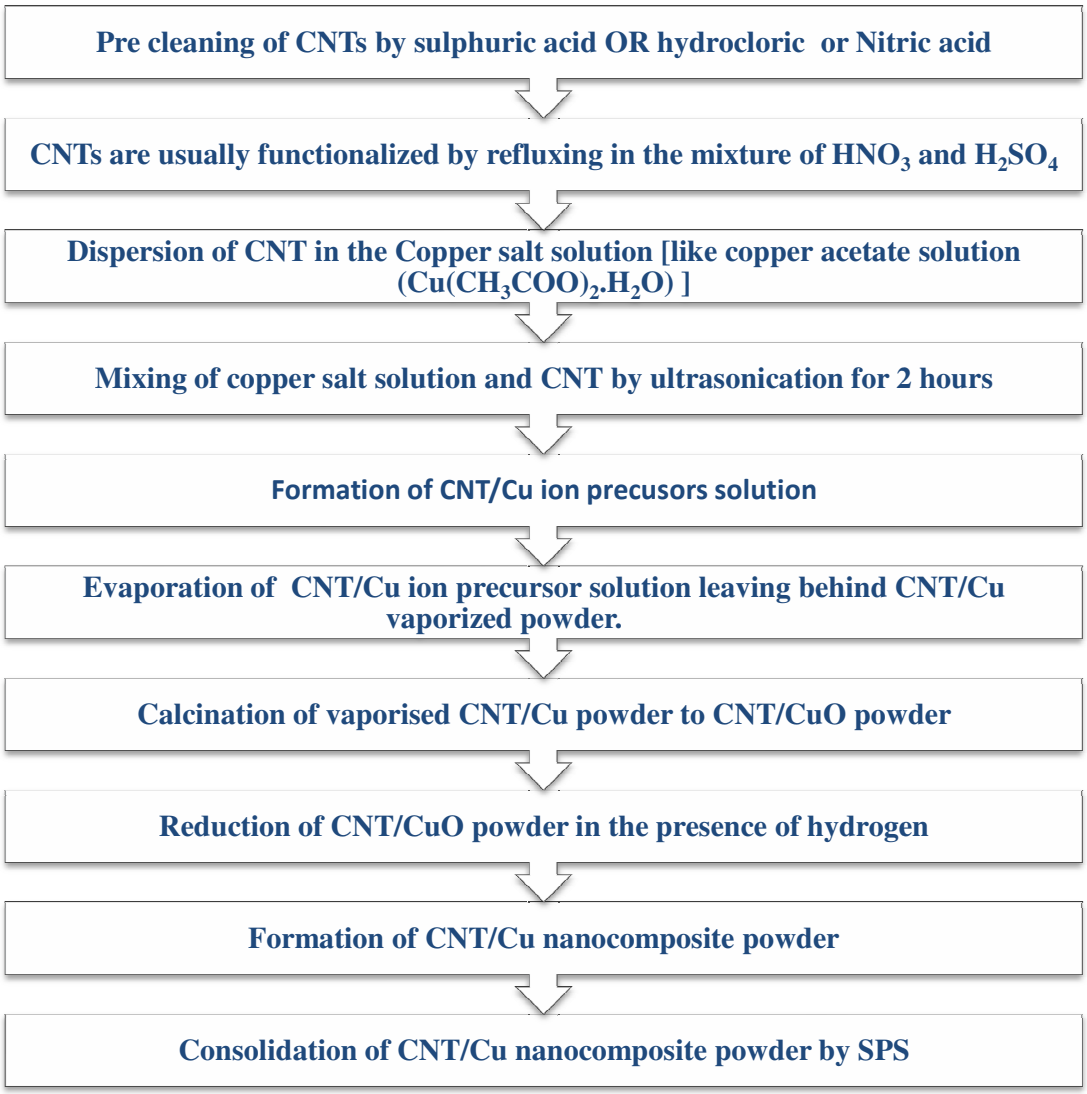

Figure 3.6: Flowchart for molecular level mixing method

All above techniques are very effective in producing thin CNT/Cu composites and coatings with good dispersion of CNTs. In all the above process the deposition and mixing of carbon nanotube in the metal matrix takes place at low temperature and without mechanical mixing and therefore damage to the CNT will be very less and properties of CNT will be maintained during mixing process. These factors are very important in context to the properties exhibited by the composites and their performance in service condition. However, there are few foremost limitations of all above methods. Molecular level mixing is a good method for uniform dispersion of CNTs in metal matrix but the process is still at laboratory level. During reduction of copper oxide, which is present on the CNT surface, complete copper oxide may not be exposed to the hydrogen and hence, there is a possibility of incomplete reduction of the composite. Due to incomplete reduction of the copper oxide, there is possibility of oxide presence in the composite form using molecular level mixing method. Some of the research groups used electro-chemical method for fabrication of the CNT/Cu composite. In case of electro-co-deposition and electroless method, it is difficult to get a freestanding structure. The process limits the thickness of the composite up to 200 μm.

3.1.2 Powder metallurgy

Powder metallurgy [PM] is common method for fabrication of CNT/Cu composite. The PM method consists of three processes as shown in Figure 3.7. Several research groups have observed uniform dispersion of the carbon nanotube in the metal matrix at the same time, a freestanding structure of CNT/Cu composite can be easily synthesized. However, the major disadvantage of PM technique is at the mixing process. The precursors are physically mixed in the ball mill for long period some time upto 48 hrs [3] as shown in Figure 3.7 (step-1). During ball milling of the precursor powder, the particles are welded, dewelded, rewelded and fragmented. These processes may cause damage to the CNT and hence the CNT may lose its electrical and thermal properties. The process flow chart for PM method is shown in Figure 3.8.

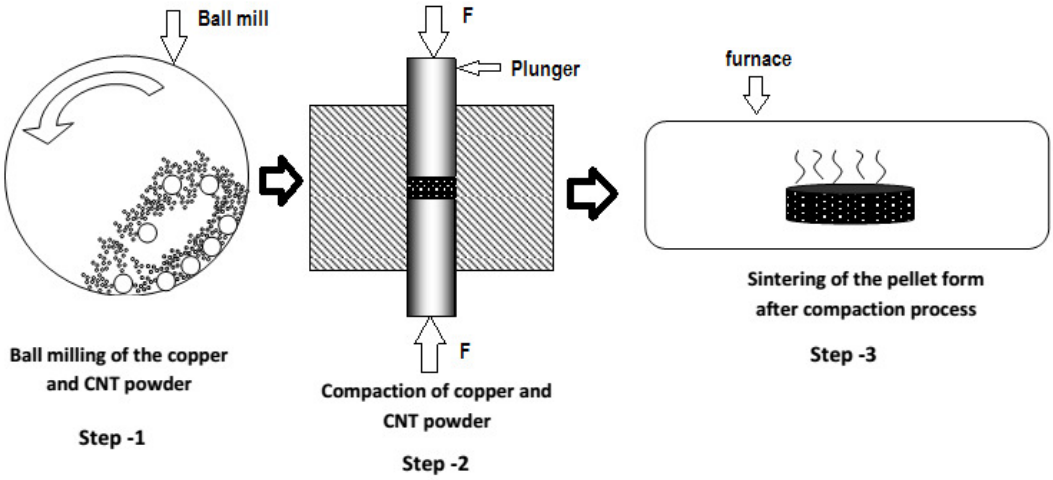

Figure 3.7: Different steps for synthesis of CNT/Cu composite by powder metallurgy method

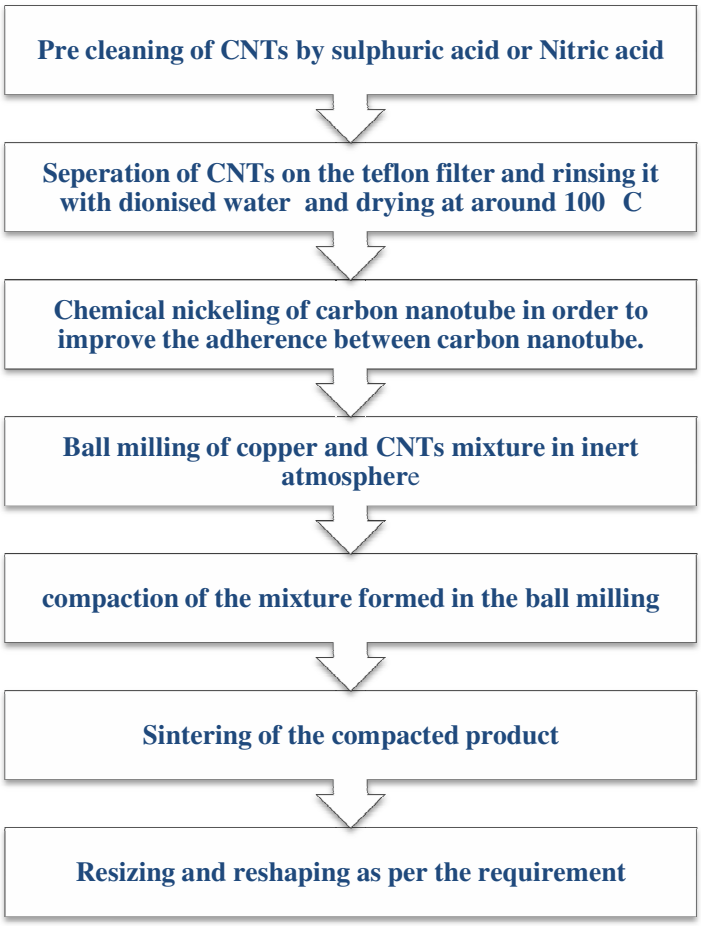

Figure 3.8: Flow chart for powder metallurgy process

Form the table 2.2 in chapter 2, it is quite clear that the mechanical properties improves by powder metallurgy method and this is because of the impediment to the movement of dislocation caused by CNTs (may be in a broken state) present in the metal matrix.

Although above methods are promising ways for CNT/Cu composite synthesis, for reasons mentioned above, none of the processes has been commercialised yet. To develop a synthesis process to be commercially competitive, it is required to have proper mixing of CNT at low temperature, less damage to the CNT, CNTs should be almost in pristine form, ability to fabricate freestanding structure, and the process should be easily scalable to bulk production level.

Considering the relative advantages and disadvantages, a close study of electro-deposition, electroless deposition and powder metallurgy paves way for realization of a method for reaping benefits of three methods. In electro-co-deposition, there is always a possibility of non-uniform CNT embedment in copper matrix because of non-uniform dissolution of CNTs, differential drag and approach to metal cathode by CNTs in comparison to copper ions and less time availability for deposited CNTs to capture and adhere to the co-deposited copper. These drawbacks are somewhat attenuated in electroless deposition. In electroless deposition, the CNTs in the solution attached themselves to the copper ions. In fact, copper ions in the solution consider CNTs as cathode. There are many opportunities and enough time for CNTs to capture copper ions. For a better attachment both in number and uniformity of copper ions or atoms on CNT, scientist have tried to raise the surface energy of CNT by coating it with materials like nickel or by functionalising CNT surface with hydroxyl or carboxyl ions. In this context, we considered that the roughness of the surface also alters the surface energy. The roughness of the CNT is possible by exposing and creating defects on the surface of CNT. The created defects may play a vital role in better attachment of copper to CNT and may reduce the need of a coating material like nickel and still enhance the attachment of the copper. We consider this phenomenon as copper-philicity on CNT surface. The defects on CNT, which can increase copper-philic sites due to enhancement of the roughness, can be created by critically damaging the bonds regularly on the surface of CNT. A regular arrangement of such damaged sites on the surface can be more useful. One of the method to create such sites can be by use of ultrasonication. We have used aforementioned thoughts and arguments to create a modified electro-co-deposition method to synthesize CNT/Cu composite. The new method

developed, use ultrasonication for developing such active sites on the CNT surface and is discussed in the next section.

3.2 Modified Electro-Co-Deposition Method

Development of new method is by combining the good aspects of electro-co-deposition, electroless deposition and powder metallurgy, and named as modified electro-co-deposition method.

From literature survey it has been observed that the CNTs [4–6] get damaged severely due to ball milling. Li et al. [4] and K. Chu et al. [6] observed the repeated fracture and breaking of the CNTs in the ball milling process. The average length of CNTs will be reduced to shorter lengths and it looks straight because of small length. Due to ball milling, CNTs will break and will open on both sides. Oxidation of CNT occurs by air with local high temperature produced by ball milling [5].

In general, in electro-co- deposition surfactants are used for the uniform dispersion of CNTs in the electrolyte and ultrasonication is used for very small duration like 10 min [7] in order to de-agglomerate the CNTs and then the CNTs will remain uniformly dispersed in the electrolyte for few hours due to surfactant. Therefore, use of ultrasonication is restricted up to de-agglomeration of the CNTs only.

From the flow charts, for electro-co-deposition process, electroless process, molecular level mixing and powder metallurgy as shown in Figures 3.3, 3.4, 3.6 and 3.8 respectively, it has been realised that uniform mixing of the carbon nanotube in the metal matrix is possible by all the three methods. However, the electro-co-deposition method, electroless deposition and molecular level mixing in which the purity of CNT will be maintained and the damage to the CNT will be minimal. Another issue is with the freestanding structure of CNT/Cu composite, which is possible by powder metallurgy method and it is difficult to synthesis a free standing structure by electro-co-deposition and electroless method. The combination of these two methods will lead to the proper fabrication of CNT/Cu composite.

Recently[1], modified electro-co-deposition method (point electro-co-deposition method) is reported to be a suitable solution to the above problem like bulk production of CNT/Cu composite and to synthesise CNT/Cu composite with a better electrical and mechanical properties. Figure 3.9 shows a schematic for the modified electro-co-deposition (point electro-co-deposition) method.

The MWCNTs were ultrasonicated in the electrolyte and in the borosilicate beaker for 3 to 6 hours. The experimental shown in the Figure 3.9, consists of borosilicate beaker, which contains electrolyte with ultrasonicated CNTs. The beaker was placed on a magnetic stirrer and agitated continuously during deposition in order to avoid the formation of double layer on the cathode surface. Four anodes as shown in Figure 3.9 were arranged in a series and an insulated cathode was placed at the centre.

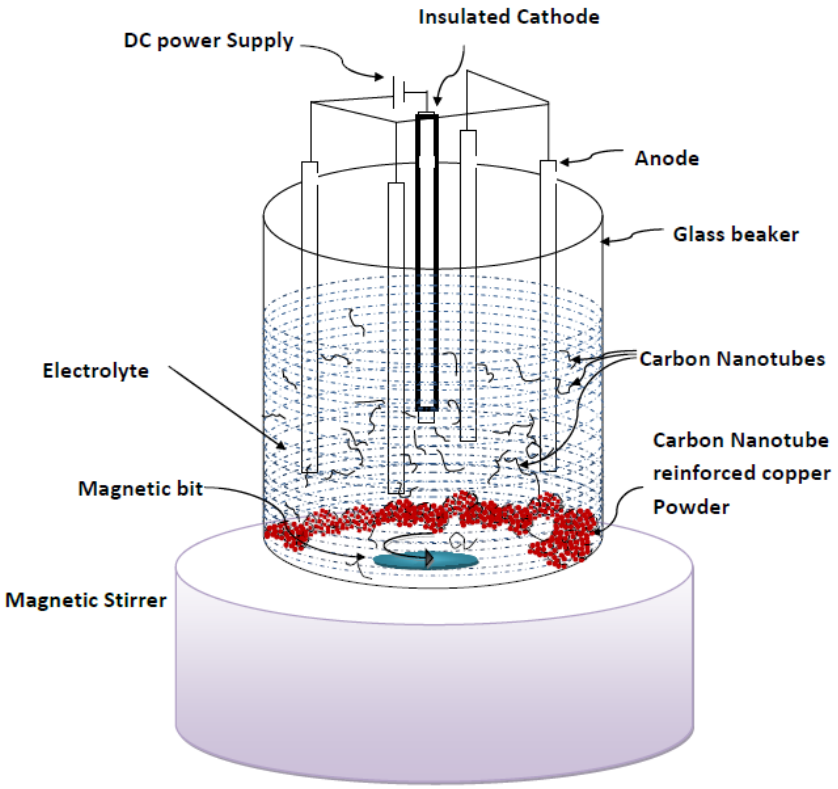

Figure 3.9: Schematic of modified electro-co-deposition technique for CNT/Cu composite

[1] Indian Patent Application, "Method of Producing Uniform Mixture of Copper and Carbon Nanotube in Bulk for Copper Composite" 2454/DEL/2012 (filed), Published on 07/12/2012.

The current was passed through the electrodes and the deposition took place at the tip of insulated cathode. The cathode was tapped several times during co-deposition of copper and CNT. The CNT/Cu composite powder was collected at the bottom of the flask. The detail process is discussed in the section 3.5.

The key difference between the new process and the conventional electro-co-deposition method, shown in Figure 3.9, for fabrication of CNT/Cu composite is synthesis of composite powder rather than simply plating [8] at the cathode. The ultrasonication time used in electro-co-deposition method is very high in comparison to all existing reports. Due to prolonged ultrasonication, the CNTs get uniformly dispersed in the solution as well as the there is a possibility of breaking the weak bonds on the CNT surface rather than complete breaking in two parts [9] as it may happens in the ball milling. The bond breakage instead of complete CNT breakage ensures that the properties of the MWCNT will be preserved. There is direct deposition of copper ions on the surface of the MWCNT at the molecular level and therefore the steps like calcination and reduction, which are necessary in case of molecular level mixing are eliminated. The new method is easy and scalable for the bulk production of carbon nanotube reinforced copper composite powder where as the earlier electro-co-deposition method is primarily used for the micro-fabrication [10] purpose only and are not easily scalable.

The form powder by modified electro-co-deposition method is then compacted and sintered at about 950°C for 60 minutes. The temperature of sintering is very less than the stability temperature of carbon nanotube which is about 2200°C [11,12] and hence the sintering at 950°C in the presence of nitrogen will not cause any damage to the CNT. In general, the thickness which was achieved in conventional electro-co-deposition method is less than 200 μm (Chai G et al. [2] claims to have fabricated composite coating of 1mm thickness). Using the newer process a freestanding structure of desired thickness can be fabricated by following the powder metallurgy process on the formed composite powder (the thickness of any structure is limited by the compaction limits). CNT content in the composite is not proportional to the CNT added in the electrolyte in conventional electro-co-deposition method whereas in the modified electro-co-deposition process it is almost proportional. By this new method, uniform dispersion of carbon nanotube in the copper matrix has been observed. Uniform dispersion will also result in improvisation of composite properties.

In summary, the modified electro-co-deposition process shows promising advantages and has a potential to become a commercial viable process. Various process attributes and the process itself are discussed in the next section.

3.3 Process Attributes

3.3.1 Versatility of material system

The flexibility in the use of metal matrix allows a wide range of metals like copper, nickel, zinc, silver, gold, tin, chromium etc. In addition, the electro-co-deposition process is able to allow for other reinforcing nano-particles like C_{60}, carbon nanotube or any other metal nanoparticles.

3.3.2 Production rate

In this process, the production rate depends on several parameters like the quantity of electrolyte, size of setup and number of electrodes. The production rate can be increased by increasing number of electrodes and increasing the size of setup. The production rate of the process can be increased by optimizing the process of continuous replenishment of the electrolyte and amount of CNT in the electrolyte.

3.3.3 The process

The process is the combination of virtues of the electro-co-deposition and the powder metallurgy due to which most of the problem related with electro-co-deposition and powder metallurgy are avoided. In conventional method, the powder is synthesized by electrolysis and the process is consists of two steps. First, the deposition of the metal is carried out on the cathode surface and then deposition is scrubbed from the surface of the electrode. During production of the copper powder care has to be taken that the product should not adhere, or adhere only weakly, to the cathode. In the suggested method, the powder synthesis is a single step process.

3.4 Experiment Setup

In conventional experimental electro-co-deposition methods, the cathode and anodes are of plate shape.

In the modified experimental setup, four platinum-coated titanium anodes (diameter 3 mm and length 10 cm) (as shown in Figure 3.10) were fixed in the 6 mm thick Perspex

sheet (as shown in Figure 3.11). In the new method, the conventional setup is tweaked up by introducing insulation over rod shape electrode. The insulation avoids the plating and allows deposition at the tip of the electrode, which was not insulated. A borosilicate container of 500 ml was used for conducting the experiment. Complete assembly of electrode and Perspex sheet was then placed on the borosilicate container. The insulation coated copper or platinum cathode (keeping the tip of the cathode open) was placed at the centre of the container as shown in Figure 3.11. Experimental setup for the modified electro-co-deposition [13] used is shown in Figure 3.12.

Figure 3.10: Image of titanium electrodes coated with platinum (four anodes and a insulation coated cathode)

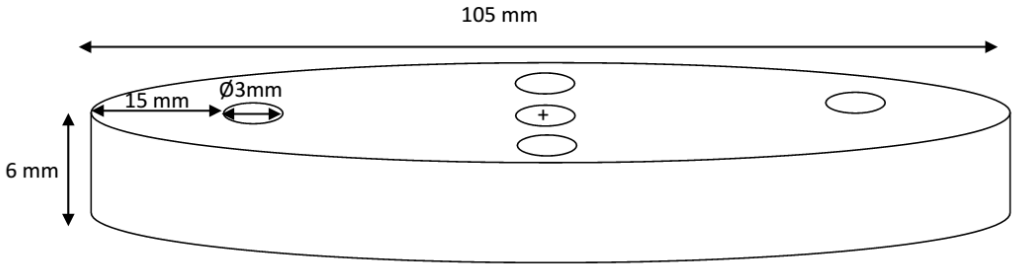

Figure 3.11: Perspex sheet (thickness 6 mm) for holding the electrodes

In the next sections, we detailed the experimental procedure, which include the materials used, sample preparation and pelletization.

3.5 Experimental Procedure

3.5.1 Materials

A The chemicals

For preparation of electrolyte, the copper (II) sulphate pentahydrate ($CuSO_4.5H_2O$) with purity of 99% and sulphuric acid with 98% concentration were obtained from Merck. Titanium electrodes coated with platinum with 10µm thickness were purchased from Titanium Tantalum Product Limited Chennai, India.

B Particulates

Multiwalled carbon nanotube (MWCNT) was obtained from Sigma aldrich (Product code 677248-5G). Multiwalled carbon nanotube with 95% purity had the outer diameter, inner diameter, and length 10-15 *nm*, 2-6 *nm*, and 0.1-10 *µm* respectively. The melting point and density of MWCNT, as per the data sheet provided by the supplier, is 3652-3607°C and ≈2.1 *g/l* at 25°C.

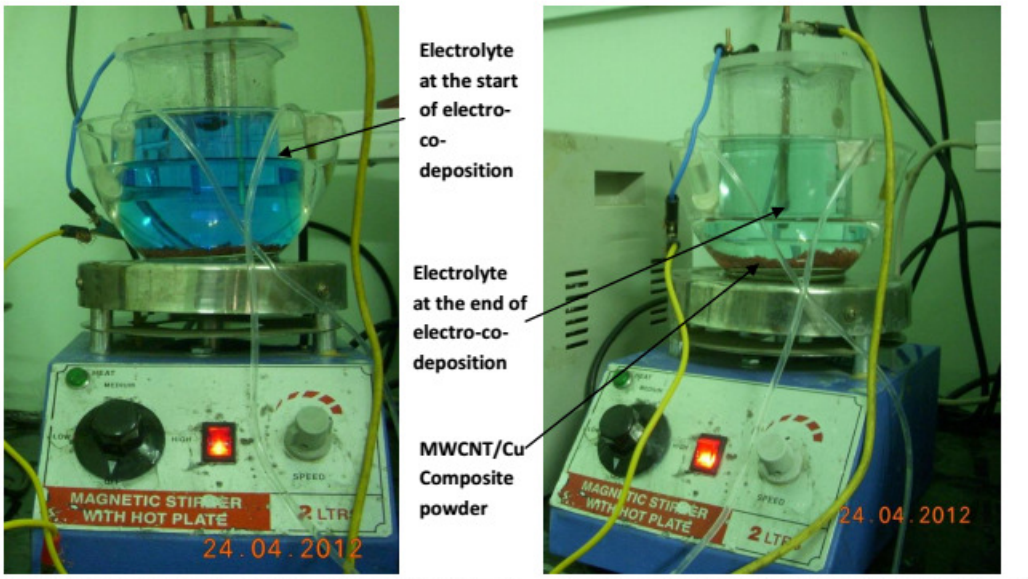

Figure 3.12: Actual setup of modified electro-co-deposition method a) Modified electro-co-deposition method at the start of process with blue coluored electrolyte b) Colourless electrolyte after complete deposition of the copper and MWCNT-co-deposition

3.5.2 Sample preparation

Powder formation by electrochemical method

Copper (II) sulphate pentahydrate ($CuSO_4.5H_2O$) in the range 75 to 125 gm/l was dissolve in the DI water and to adjust the pH value of electrolyte in the range 1 to 3, sulphuric acid was added to the electrolyte to make 400 ml solution. Solution was vacuum filtered (through Whatman ashless filter paper grade 42 with particle retention size of 2.5 µm) in order to remove the insoluble impurities. 25 to 125 mg/l of MWCNT was added to the electrolyte and the solution was agitated by magnetic stirrer for 10 min with 200 rpm, and then was followed by an ultrasonic (20 kHz, 500 W) treatment, as shown in Figure 3.13, was given to break up the CNT agglomeration and to disperse it uniformly in the solution. The ultrasonication also led to surface defects on CNTs, which becomes active sites for capturing copper ions.

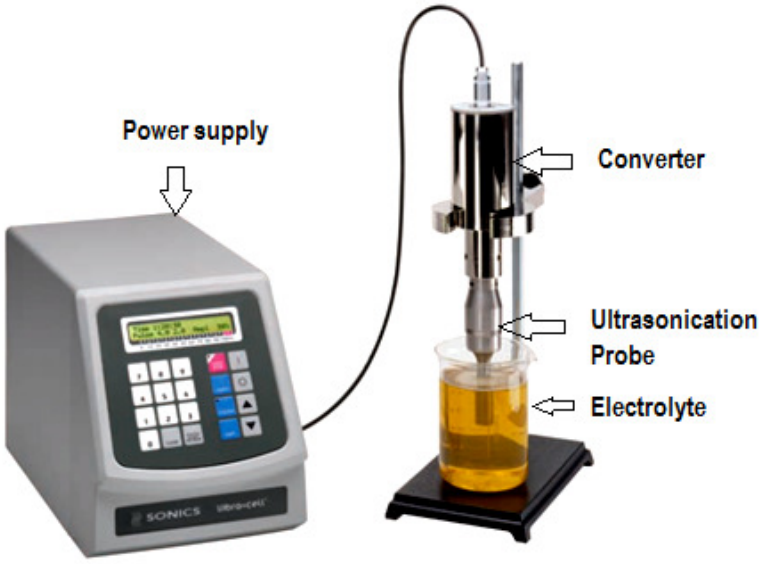

Figure 3.13: Image of ultrasonication equipment used for the ultrasonication Model: Sonics vibra cell VC 505 (20 kHz and 500 W)

Figure 3.14, shows the MWCNT before and after ultrasonication process. Form figure, it is observed that the MWCNTs are disentangled after ultrasonication treatment. As discussed earlier the ultrasonication treatment also break the weak bonds on the surface of MWCNT as well as treatment breaks the weak bonds on the cap of MWCNT. It can be realised from Figure 3.15. Figure 3.15(a) shows the MWCNT cap before ultrasonication treatment, which is in position whereas Figure 3.15(b) shows the MWCNT cap after ultrasonication treatment, which is in a broken state.

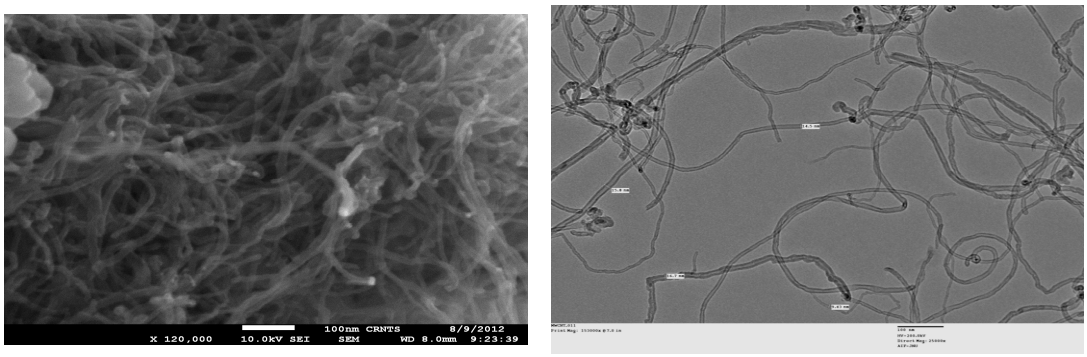

(a) (b)

Figure 3.14: (a) SEM image of MWCNT before ultra sonication treatment (b) TEM image of MWCNT after ultra sonication treatment

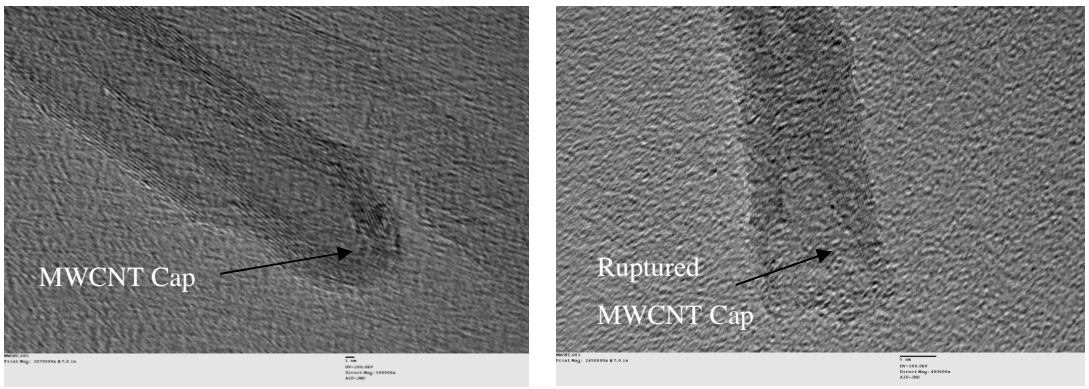

(a) (b)

Figure 3.15 (a) TEM image of MWCNT cap before ultrasonication treatment (b) TEM image of MWCNT cap after ultrasonication treatment

The experimental setup for electro-co-deposition used is shown in Figure 3.12, which facilitates co-deposition of the CNT and copper ions on the cathode. The method is referred as point electro-co-deposition method [14]. In this experimental setup, four titanium anodes coated with platinum (diameter 3 mm and length 10 cm) were dipped 50% in the solution circumferentially and insulation coated copper or platinum cathode is placed at the centre of the container as shown in Figure 3.12. The container was placed on magnetic stirrer and the solution is stirred with 400 rpm. Direct constant current of 6 ampere is connected to the electrodes. The cathode was tapped several times during the electro-co-deposition process in order to remove the reduced copper and CNT composite powder from the small tip of cathode. The mixture of

copper and CNT was separated from the electrode and settled down at the bottom of the flask. The process is continued until it is observed that the original dark blue solution of MWCNT, $CuSO_4.5H_2O$ and H_2SO_4 (Dark blue colour is due to MWCNT and $CuSO_4.5H_2O$) become colourless (Figure 3.12(b)).

The wet powder was removed from the electrolyte by vacuum filtration method and washed several times with a large amount of demineralised water in order to make the CNT/Cu powder free from acid traces. The form powder was dried in vacuum of 7 kPa at 80°C with the help of rotary evaporator (Rotary evaporator model: Buchi Rotavapor R-210). The powder was passed through a sieve (US Sieve Size No.230) of Tyler mesh size 250 having opening size of 63 μm. It has been observed that the 90% of the powder is passed through the sieve. This implies that the majority of the particles were of the size less than 63 μm. Then it was stored in nitrogen-filled vial to avoid any further oxidation of the powder. The flowchart for the modified electro-co-deposition is shown in Figure 3.16.

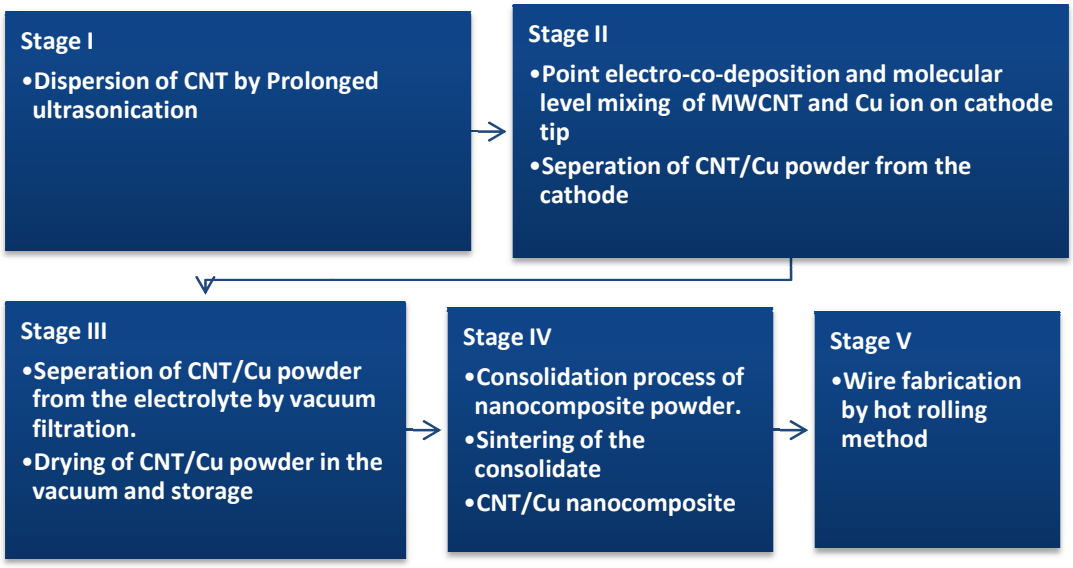

Figure 3.16: Flow chart for the modified electro-co-deposition method

The powder formed in the process was then subjected to the palletization, which is detailed in the next section.

Pellet formation by powder metallurgy

Pellet from the above powder was formed by conventional powder metallurgy process. Powder densification can be achieved through pressing to a high density followed by sintering process. Dies of different diameters (25.4 mm, 12.7 mm and 10 mm) as shown in Figure 3.17 were fabricated at institute workshop were used for the densification process.

Pellets of diameter 12.7 mm were fabricated as 12.7 mm diameter pellets were suitable for different type of characterization. The solid pellets with the dimensions of 12.7 mm diameter and 2 mm thick were fabricated by compacting the CNT/Cu powder, formed by modified electro-co-deposition, in a uniaxial die under the pressure of 650 MPa. The Pallet formed by the compaction process is called as green compacts. Sintering of the pallets were carried out in the furnace. Primary variables defining a powder sintering operation are time, temperature and furnace atmosphere. Sintering temperature is typically 70% to 90% of the metal's melting point. Therefore, the sintering temperature during the process was kept 950 °C, which is about 87% of 1083°C, which is the melting point of copper. The sintering time is dependent on material. Copper is sintered for a relatively short time and it is about 10 to 45 min. In the present case, the sintering was carried out for 55min. A controlled atmosphere is critical during powder sintering. The purpose of the controlled atmosphere in sintering is to prevent oxidation of the pellet. Common atmospheres used for industrial powder processes are inert gases such as argon or helium or nitrogen. Sometimes parts are also sintered in a vacuum. The nitrogen gas is inert below 1000°C and hence we prefer to use nitrogen gas during sintering process.

Sintering of a green compact occurs in two stages. First, the temperature is raised gradually to the sintering temperature i.e. 950°C with a ramp rate of 20°C/min in the nitrogen atmosphere and maintained for 55 min for the desired amount of bonding to occur. Temperature is lowered gradually with a rate of 5°C/min as the pallet is allowed to cool during the second stage. The pallet was kept in the controlled furnace atmosphere during cooling down.

Figure 3.17: Dies used for the fabrication of the pellets

The sintered samples underwent grinding using 1000 and 2500 grade SiC papers, respectively. The ground samples were polished using diamond paste of 3 µm particle size.

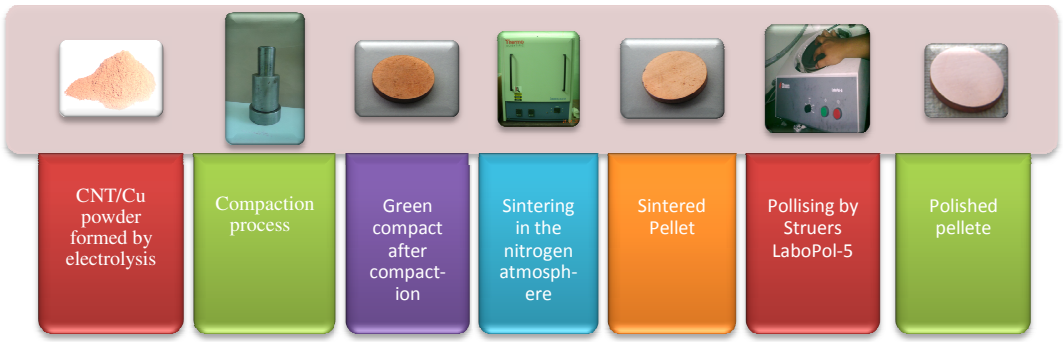

Figure 3.18: Description of pellet forming by powder metallurgy method

Conversion from powder to pallet is pictorially shown in Figure 3.18.

3.6 Conclusion

From above discussion, it has been observed that there are some key differences, which makes the modified electro-co-deposition method suitable for the bulk production. The conclusions based on the work carried out at this point are as follows:

1. We have developed a modified electro-co-deposition method wherein a prolonged ultrasonication of the CNTs was carried out for uniform dispersion of the CNT in the electrolyte. The prolonged ultrasonication helps to expose the defects on the surface of CNT as observed in TEM of MWCNT before and after ultrasonication. In conventional electro-co-deposition method, the CNTs are functionalized by mixing it with HNO_3:H_2SO_4 solution in order to disperse the MWCNT uniformly in the electrolyte and to bond metal in the electrolyte. This functionalization may cause impurity in the formed composite.
2. In modified electro-co-deposition method, electro-co-deposition of MWCNT and copper occurs at the tip of cathode. The cathode is in the form of a rod and the product will be CNT/Cu composite powder. In conventional electro-co-deposition method, electrodes are in the form of plates, on which electro-co-deposition occurs and the product will be a thin sheet of CNT/Cu composite.
3. The modified electro-co-deposition method can be easily scaled up for the bulk CNT/Cu composite fabrication whereas the conventional electro-co-deposition is used for the micro-fabrication process.
4. In the modified electro-co-deposition method prolonged ultrasionication was carried out which helps in uniform dispersion in the electrolyte as well as it helps in disentanglement of CNT agglomerates and in breaking the weak bonds on the surface like pentagonal or heptagonal structure on the CNT cap. However, in PM the mixing of carbon nanotube and copper powder is carried out in the ball milling and it was observed that the CNT get severely damaged and get shortened during the process.
5. In modified electro-co-deposition process, the deposition of copper on the surface of CNT takes place at molecular level but the calcination and reduction processes are not required in this process whereas in molecular level mixing, calcination and reduction are the two important processes. It is possible that the complete reduction of CNT/CuO composite may not take place and the oxide will remain, as it is the composite.

In the next chapter, detailed characterization of the formed CNT/Cu composite powder is discussed, which includes characterization of CNT/Cu composite by XRD analysis, SEM and TEM.

References:

[1] Agarwal A, Bakshi SR, Lahiri D. Carbon Nanotubes Reinforecd Metal Matrix Composite. Boca Raton, Florida: CRC Press, Taylor and Francis Group; 2011.

[2] Chai G, Sun Y, Sun J "Jenny", Chen Q. Mechanical properties of carbon nanotube–copper nanocomposites. J Micromechanics Microengineering 2008;18:035013.

[3] Morsi K, Esawi a. Effect of mechanical alloying time and carbon nanotube (CNT) content on the evolution of aluminum (Al)–CNT composite powders. J Mater Sci 2007;42:4954–9.

[4] Li JL, Bai GZ, Feng JW, Jiang W. Microstructure and mechanical properties of hot-pressed carbon nanotubes compacted by spark plasma sintering. Carbon N Y 2005;43:2649–53.

[5] Chen XH, Cheng FQ, Li SL, Zhou LP, Li DY. Electrodeposited nickel composites containing carbon nanotubes. Surf Coatings Technol Technol 2002;155:274–8.

[6] Chu K, Jia C, Li W, Wang P. Mechanical and electrical properties of carbon-nanotube-reinforced Cu-Ti alloy matrix composites. Phys Status Solidi 2013;210:594–9.

[7] Fiedler B, Gojny FH, Wichmann MHG, Nolte MCM, Schulte K. Fundamental aspects of nano-reinforced composites. Compos Sci Technol 2006;66:3115–25.

[8] Chen XH, Peng JC, Li XQ, Deng FM, Wang JX, Li WZ. Tribological behavior of carbon nanotubes — reinforced nickel matrix. J Mater Sci Lett 2001;20:2057–60.

[9] Ruan B, Jacobi AM. Ultrasonication effects on thermal and rheological properties of carbon nanotube suspensions. Nanoscale Res Lett 2012;7:127.

[10] Chen Q, Chai G, Li B. Exploration Study of Multifunctional Metallic Nanocomposite Utilizing Single-Walled Carbon Nanotubes for Micro/Nano Devices. Proc Inst Mech Eng Part N J Nanoeng Nanosyst 2006;219:67–72.

[11] Liew K, Wong C, He X, Tan M. Thermal stability of single and multi-walled carbon nanotubes. Phys Rev B 2005;71:075424.

[12] Kim Y a., Muramatsu H, Hayashi T, Endo M, Terrones M, Dresselhaus MS. Thermal stability and structural changes of double-walled carbon nanotubes by heat treatment. Chem Phys Lett 2004;398:87–92.

[13] Belgamwar SU, Sharma NN. Synergistic electro-co-deposition and molecular mixing for reinforcement of multi-walled carbon nanotube in copper. Mater Sci Eng B 2013;178:1452–7.

[14] Belgamwar SU, Sharma NN. Method of Producing Uniform Mixture of Copper and Carbon Nanotube in Bulk for Copper Metal Nanocomposite. 2454/DEL/2102A, 2012.

Chapter 4

Characterization of MWCNT/Cu Composite Powder

Developments of the new process as well as the advantages of the process over the conventional processes were discussed in the previous chapter. The CNT/Cu composite powder synthesized by the modified electro-co-deposition process was characterized to understand the composition, microstructure of the CNT/Cu powder and to study the effect of the MWCNT reinforcement on the density of the composite. The detail characterization of the CNT/Cu composite powder formed by the modified electro-co-deposition method is discussed in this chapter.

4.1 Characterization Result

For primary characterisation purpose, six different samples with variation in the amount MWCNT were prepared by the modified electro-co-deposition. All those powder samples were characterised by X-ray diffraction (XRD), Energy Dispersive X-ray Spectroscopy (EDAX), Scanning Electron Microscopy (SEM) and Transmission Electron Microscopy (TEM).

4.1.1 Sample preparation

The 40 gm of $CuSO_4.5H_2O$ (from Merk with purity of 99%) and 98% concentrated sulphuric acid, to adjust the pH value to 2, were dissolved in de-ionized (DI) water to make 400 ml solution. The solution was vacuum filtered (through Whatman ashless filter paper grade 42 with particle retention size of 2.5 μm) in order to remove the insoluble impurities. MWCNTs (obtained from Sigma Aldrich, India, OD 10-15 nm, ID 2-6 nm, length 1-10 μm) were added in ratios of 25, 50, 75, 100 and 125 mg/l to the electrolyte. Magnetic stirrer agitated the electrolyte solution for 10 minutes with 200 rpm. After mixing by a magnetic stirrer, an ultrasonic (20 kHz, 500 W) treatment was given for three hours to break up the MWCNT agglomeration and to disperse it uniformly in the solution. Experimental setup for the modified electro-co-deposition [1] used is shown in Figure 3.12 in Chapter 3, which facilitates the capture of the MWCNTs by copper ions in solution itself. In the experimental setup, four platinum anodes (diameter 3 mm and length 10 cm) were dipped 50% in the solution circumferentially and insulation coated

copper cathode (keeping the tip of the cathode open) was placed at the centre of the container as shown in Figure 3.12 in Chapter 3 . The container was placed on magnetic stirrer, and the solution was stirred with 400 rpm. Direct constant current of 6 ampere was connected to the electrodes. Electro-co-deposition of copper particles and the MWCNTs occurred at tip of the cathode. The cathode was tapped several times during the electro-co-deposition in order to remove the reduced MWCNT reinforced copper powder particles from tip of the cathode. The powder of MWCNT reinforced copper particles settled down at the bottom of the flask.

The process was continued for 3.5 hours, and it was observed that the original dark-blue solution of MWCNTs, $CuSO_4.5H_2O$ and H_2SO_4 (Dark blue colour was due to MWCNTs and $CuSO_4.5H_2O$) become colourless (Figure 3.13 in Chapter 3). The powder was removed from the solution and rinsed thoroughly by DI water in order to remove the acidic contact, if any in the powder. Form powder was dried in the vacuum of 4 kPa at 70^{o}C by using rotavapour (BUCHI R-210) and stored in nitrogen filled vials to avoid the oxidation of the powder. Initially, X-ray diffraction was used for the characterization.

4.1.2 Compaction and wire forming of carbon nanotube-copper composite powder

Conventional compaction and the sintering were adapted in this study to fabricate carbon nanotube reinforced copper matrix composites. The compaction of composite powder was performed in a die by uniaxial pressurization of 650 MPa. Disc-shaped specimens with diameter of 12.7 mm and the thickness of 2 mm were fabricated. The disc shape samples were sintered in an inert atmosphere furnace. The furnace temperature was ramped to 950°C with a ramp rate of 20°C/min about in 50 min and kept constant for 55 min. Finally, the samples were cooled down to room temperature in around 180 min in furnace itself. A PID controller controlled the temperature of the apparatus with an accuracy of ±5°C. Struers labopol-5 grinding and polishing machines were used to grind the sintered samples using 1000 and 2500 grade SiC papers, respectively. A home built setup was used to hot-roll these samples. The MWCNT/Cu composite sample was heated to 950°C and then it rolled down to the diameter of 1.5 mm. The rod of 1.5 mm diameter was then cold drawn through a series of tungsten carbide dies to 0.813 mm (AWG No. 20) wire. Annealing of copper wire was carried out in order to relieve the cold working stress.

4.1.3 X-ray diffraction

XRD is a non-destructive technique used for identification of orientation, determining structural properties, lattice parameters 10^{-4} Å, strain, grain size, phase composition, and even for determining atomic arrangement.

X-ray diffractometer (XRD) (Model RIGAKU MiniFlex-II) (Cu Kα: λ = 0.15418 *nm*) was used for characterization of the composite powder. Diffraction data were collected with scanning rate of 0.05°/sec at 20°C to ascertain the accuracy.

Figure 4.1, shows the XRD patterns for the pure copper fabricated by the modified electro-co-deposition. Diffraction angle is given on abscissa whereas the intensity (a.u.) is plotted on the ordinate. The sharp and prominent XRD peaks in the spectrum confirm the crystalline structure of the samples. The d-spacing (inter planer spacing) corresponding to the XRD spectrum shown in Figure 4.1, are determined using equation (4.1) [2] and are obtained as 2.08 Å, 1.80 Å and 1.28 Å for first, second and the third peak (from left on the graph).

$$d_{hkl} = \frac{n\lambda}{2\sin\theta} \tag{4.1}$$

where, n is the order of reflection, λ is the wavelength of x-ray and angle θ is half the angle between the diffracted beam and the original beam. The planar indices are determined from the Bragg's angle 43.44, 50.56, and 74.20 2θ are shown in Table 4.1 and belongs to the planar indices (111), (200), and (220). The d-spacing values of diffraction peaks in XRD pattern with strong intensities appears at Bragg's angle 43.44, 50.56, and 74.20 2θ, which corresponds to (111), (200), and (220) planes matching with amcsd 0014944 (American Mineralogist Crystal Structure Database). These observations confirm the face centered cubic structure (FCC) of pure copper synthesized by modified electro-co-deposition.

Table 4.1: Planar indices corresponding to the Bragg's angle

Peak	2θ	$\sin^2\theta$	$\sin^2\theta_n/\sin^2\theta_1 = h^2+k^2+l^2$	$h^2+k^2+l^2$	h k l
1	43.44	0.137	1 = 3/3	3	1 1 1
2	50.56	0.182	1.333 = 4/3	4	2 0 0
3	74.20	0.364	2.667 = 8/3	8	2 2 0

The unit cell geometry parameters (lattice parameter) were calculated by using equation 4.2 [2]

$$a = d_{hkl} \times \sqrt{h^2 + k^2 + l^2} \qquad (4.2)$$

in which, 'a' is lattice parameter, 'd_{hkl}' is the interplanar spacing and h, k and l are the planar indices. The calculated lattice parameters from above data and equation 4.2 are length a = 3.60 Å, b = 3.60 Å, and c = 3.60 Å. This examination confirms the face-centred-cubic crystalline structure of copper.

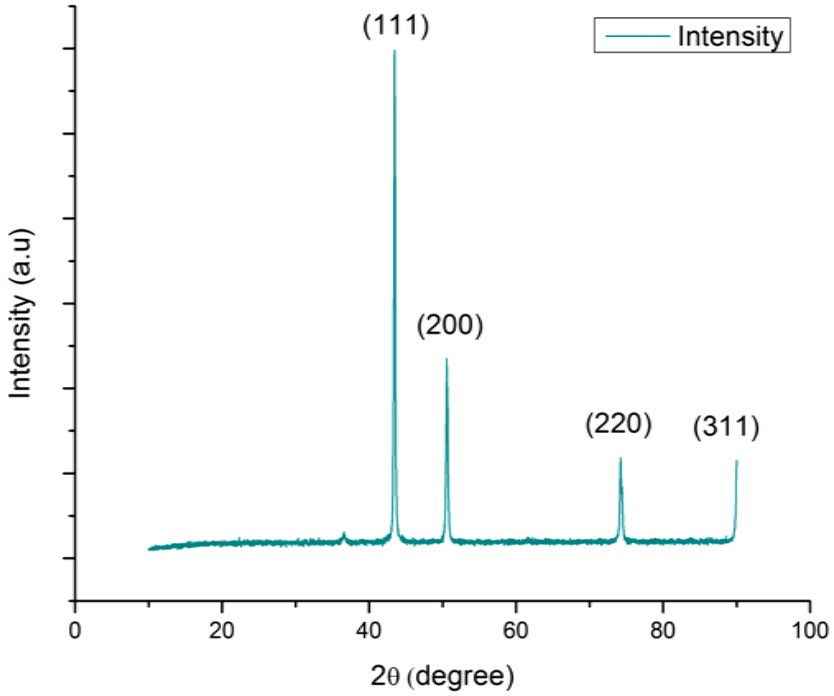

Figure 4.1: X-ray diffraction spectrum of pure copper synthesized by the modified electro-co-deposition process

4.2 Micro-Strain

The shape of the peak contains some valuable information, like width of the peak increases with decrease in crystallite size at the same time the width of the peak increase due to micro-strain and small range lattice strain caused by the crystallite defects. Therefore, the micro-strain and the crystallite size both lead to peak broadening means that either both size and strain must somehow be measured, or a way to eliminate the effect of one or the other must be found. In this experiment, both crystallite size and microstrain are measured. The Scherrer method, which gives size based broadening on

measurements of any one peak when strain is not present, is applied to all the diffraction peaks and the change in size is used for the measurement of microstrain. This analysis technique is adopted from Suryanarayana and Norton's book [3].

On close examination of a powder diffraction pattern in Figure 4.1, it was noticed that the peaks becomes broader as the 2θ increases. There are several reasons for the broadening of peaks with the 2θ, including nature of sample, nonlinear d-spacing with 2θ and focusing of X-rays onto the sample. The increase in the peak width with respect to diffraction angle is shown in the Figure 4.2.

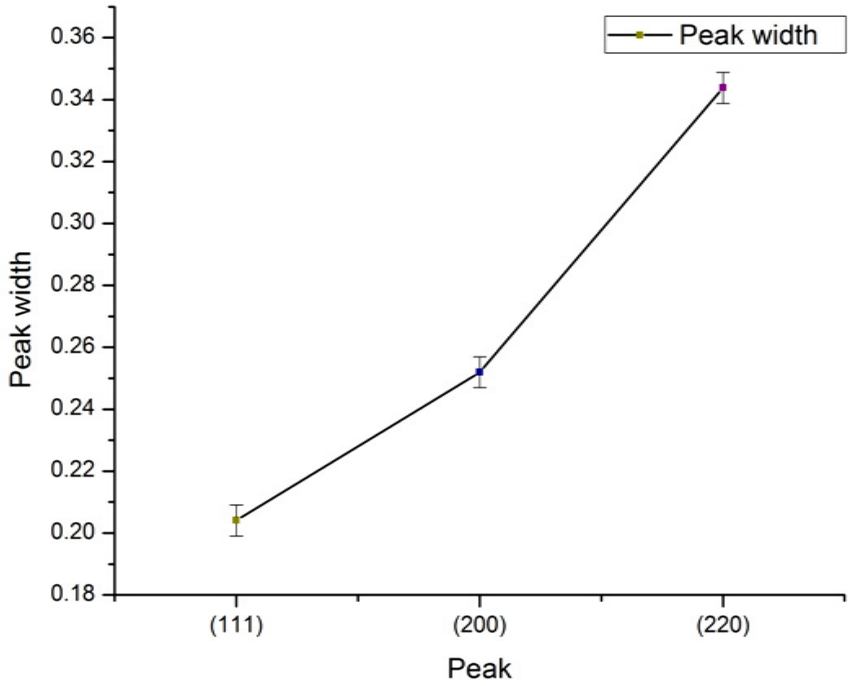

Figure 4.2: Peak width vs diffraction peaks of pure copper fabricated by modified electro-co-deposition

The broadening of the peaks i.e. peak width (β) of pure copper sample was compared with the XRD peaks of MWCNT reinforced copper composite. The broadening of a peak was determined by fitting every diffraction peak data with a Lorentzian peak function and Gaussian fit function after subtracting the $K\alpha$ component and the background. Peaks for plane (111), (200) and (220) of pure copper are shown in the Figure 4.3(a) through to (c). The broadening of each peak is attributed to the particle size, strain and instrumental broadening.

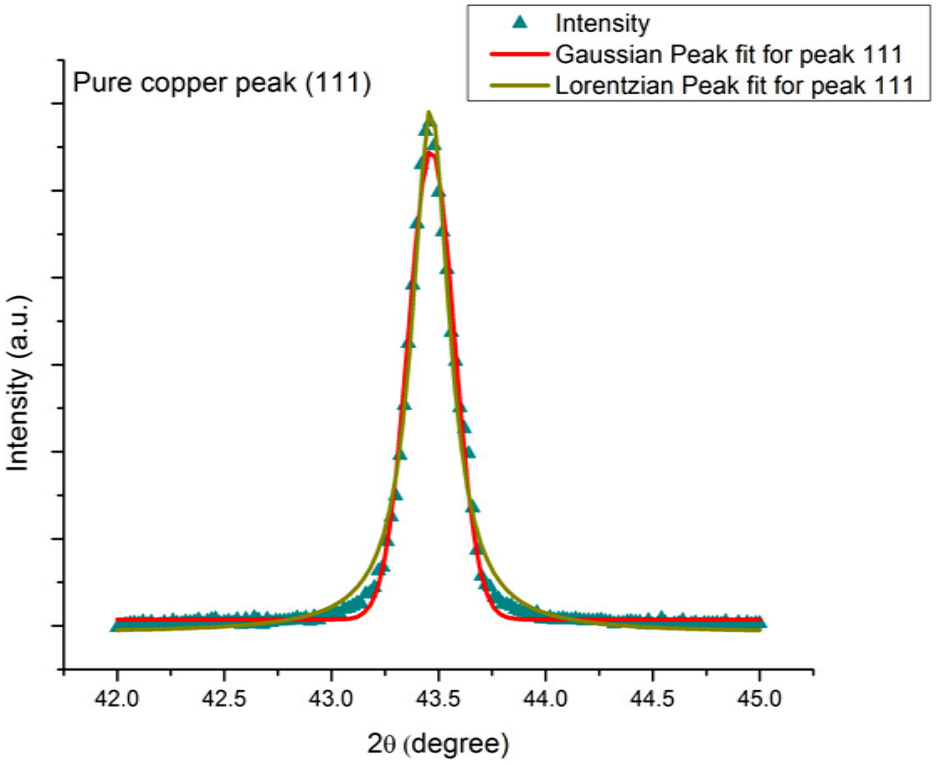
Intensity
Gaussian Peak fit for peak 111
Lorentzian Peak fit for peak 111
Pure copper peak (111)
Intensity (a.u.)
42.0
42.5
43.0
43.5
44.0
44.5
45.0
2θ (degree)

(a)

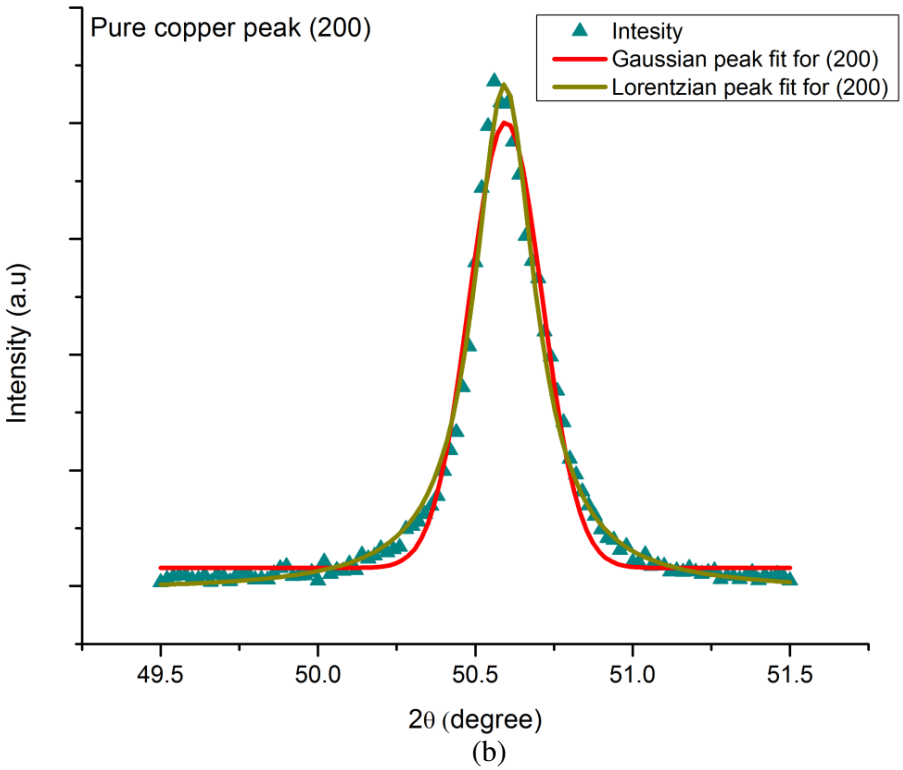
Pure copper peak (200)
Intesity
Gaussian peak fit for (200)
Lorentzian peak fit for (200)
Intensity (a.u)
49.5
50.0
50.5
51.0
51.5
2θ (degree)

(b)

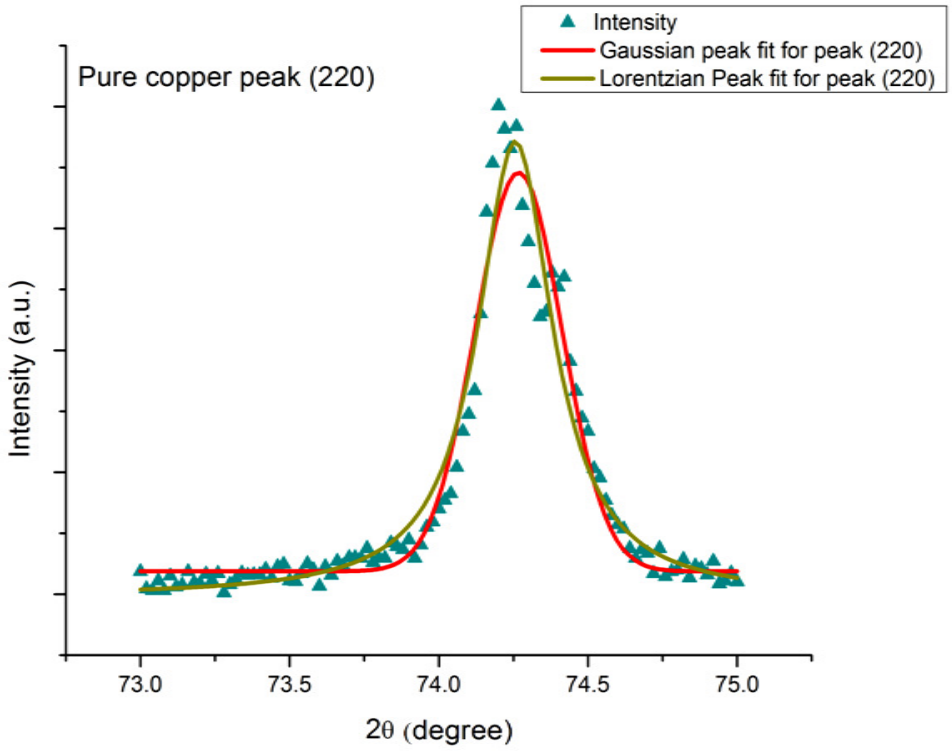

(c)

Figure 4.3: Gaussian and Lorentzian peak fit for pure copper fabricated by modified electro-co-deposition method, {111}, {200} and {220} XRD diffraction peak

The peak broadening due to grain size β_{size} in the material can be expressed by Scherrer equation [4], as

$$\beta_{size} = \frac{K\lambda}{D\cos\theta} \tag{4.3}$$

where, $K = 0.9$, λ is the wavelength of X-ray $\lambda = 0.15418$ nm, θ is Bragg's angle, and D is grain size.

Broadening due to micro-strain can be determined by using equation (4.4). Micro-strain is due to imperfection of the lattice, which may be due to vacancies, defects, impurities, dislocations, stacking faults etc. The dependence of broadening and the Braggs angle [4] is given by

$$\beta_{strain} = 4\varepsilon\tan\theta = \eta\tan\theta \tag{4.4}$$

$$\eta = 4\varepsilon$$

where , β_{strain} is the broadening of peak due to strain, ε strain and θ is Bragg's angle.

Broadening of the peak can be determined for lorentzian peak function by simply adding equation (4.3) and (4.4) [5]and it is given by

$$\beta_{\text{size+strain}} = \beta_{\text{size}} + \beta_{\text{strain}} \tag{4.5}$$

where, $\beta_{\text{size+strain}}$ is pure sample peak broadening due to particle size and strain in particle, β_{size} is peak broadening due to particle size and β_{strain} is peak broadening due to strain in the particle.

Substituting the equation (4.3) and (4.4) in (4.5) we get,

$$\beta_{\text{size+strain}} = \frac{K\lambda}{D\cos\theta} + \eta\tan\theta \tag{4.6}$$

For Guassian fit function [6] the $\beta_{\text{size+strain}}$ can be determined as

$$\beta_{\text{size+strain}} = (\beta^2_{\text{size}} + \beta^2_{\text{strain}})^{\frac{1}{2}} \tag{4.7}$$

Substituting the equation (4.3) and (4.4) in (4.7) we get

$$\beta_{\text{size+strain}} = \left[\left(\frac{K\lambda}{D\cos\theta}\right)^2 + (\eta\tan\theta)^2\right]^{\frac{1}{2}} \tag{4.8}$$

The equations (4.6) and (4.8) can be rearranged and are given as equation (4.9) and (4.10).

$$\beta_{\text{size+strain}}\cos\theta = \frac{K\lambda}{D} + \eta\sin\theta \tag{4.9}$$

$$\beta^2{}_{\text{size+strain}}\cos^2\theta = \left(\frac{K\lambda}{D}\right)^2 + (\eta\sin\theta)^2 \tag{4.10}$$

This is known as Williamson-Hall's method for determining micro-strain and size separation.

For equation (4.9), $\beta_{\text{size+strain}}\cos\theta$ is plotted against $\sin\theta$ for three XRD reflections (111), (200) and (220). As the above equations (4.9 and 4.10) are in the form of $y = mx + c$, data should be on a straight line, with a slope of η and an intercept of $k\lambda/D$. The plot is shown in Figure 4.4. Similarly, when $\beta^2{}_{\text{size+strain}}\cos^2\theta$ is plotted against $\sin^2\theta$ for equation (4.10), the result should be a straight line, with a slope of η^2

and an intercept of $(k\lambda/D)^2$. Data for $\beta_{size+strain}$ is given in Appendix-A Table A.1. The plot is shown in Figure 4.5.

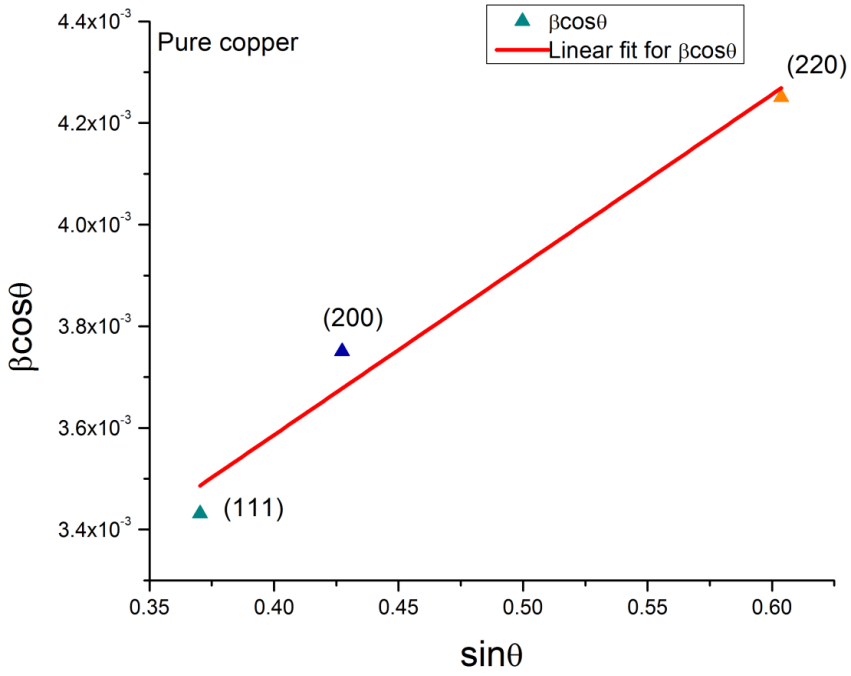

Figure 4.4: Williamson-Hall plot of pure copper sample prepared by modified electro-co-deposition method (lorentzian peak fit function)

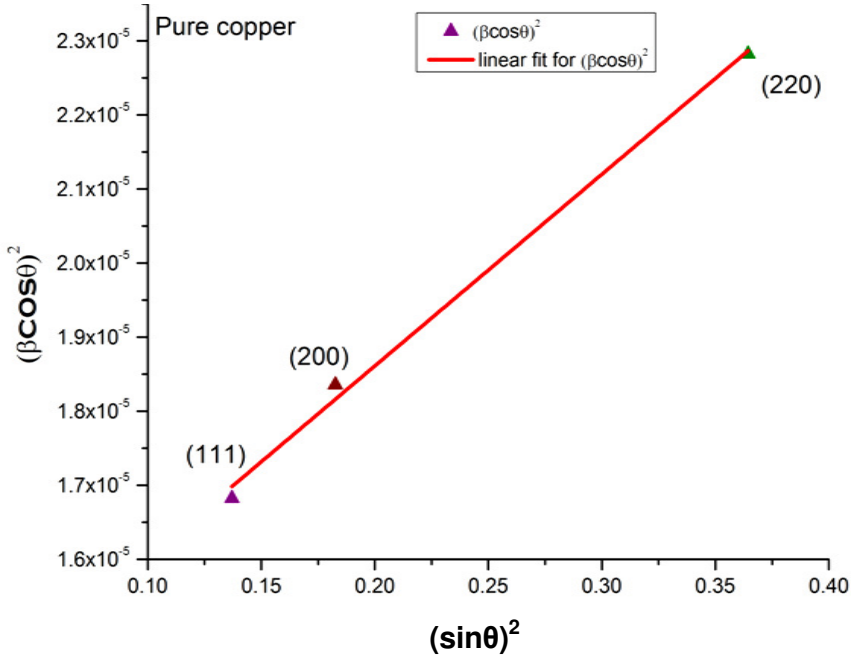

Figure 4.5: Linear fit for the Gaussian peak function of pure copper sample prepared by modified electro-co-deposition method

The initial micro-strains present in the pure copper fabricated by the modified electro-co-deposition method and copper crystallite size were estimated by performing a strain-size separation on pure copper using a Williamson-Hall plot, shown in Figure 4.4. Using equation (4.9) and the Figure 4.4 initial strain and the copper crystallite size was calculated. From the graph, the initial strain equaled 0.08%, and the copper crystallite size equaled 61.6 nm.

The strain value determined for the pure copper may be due to the particle size or due to other defects in the crystal. Figure 4.6, which is XRD spectrum of MWCNT/Cu composite synthesized by modified electro-co-deposition method with 50 mg/l concentration of MWCNT in the electrolyte, does not show any traces of MWCNT (carbon) in the spectrum or even the figure does not depict the formation of new compound. However, the reinforcement of MWCNT will cause microstrain in the copper crystal. Therefore, the MWCNT/CNT composite synthesized by electro-co-deposition method with different concentrations like 25, 50, 75, 100 and 125 mg/l in the electrolyte were analysed for the micro-strain by using Williamson-Hall plot.

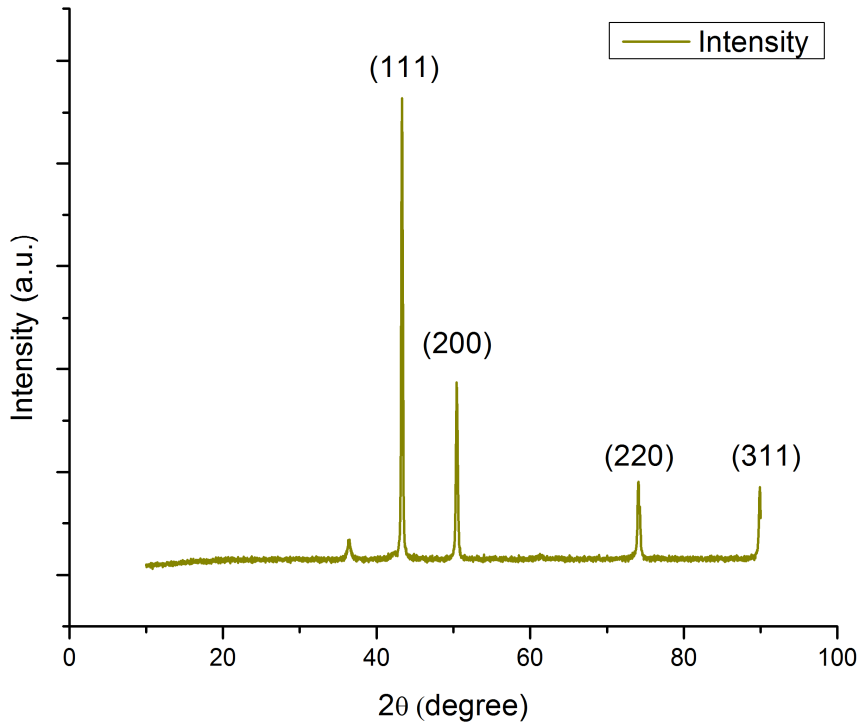

Figure 4.6: X-ray diffraction spectrum of MWCNT/Cu composite pure copper synthesized by the modified electro-co-deposition process with 50 mg/l concentration of MWCNT in the electrolyte

when $\beta_{size+strain} \cos\theta$ is plotted against $\sin\theta$ and $\beta^2_{size+strain} \cos^2\theta$ is plotted against $\sin^2\theta$, the result should be a straight line, with the slope of η and an intercept of $k\lambda/D$ and slope of η^2 and an intercept of $(k\lambda/D)^2$ respectively. Using this method, the data of the all above mentioned samples exhibit a good fit, with Pearson's correlation coefficients[1] (R) between 0.83 and 0.99. The calculated grain size and micro-strain values for all the six powder samples are shown in Table 4.2. It was observed that the strain values increases with increase in MWCNT concentration in the electrolyte. This means the reinforcement of MWCNT causes the micro-strain in the Cu/MWCNT composite powder.

Table 4.2: Calculated grain size and micro-strain of Cu and MWCNT/Cu composite powder with different wt% of MWCNT

		Lorentzian peak function			Guassian peak function		
SN.	**Sample**	**Micro-strain**	**Grain size (nm)**	**[1]Pearson's R**	**Micro-strain**	**Grain size (nm)**	**Pearson's R**
1	Pure copper	8.37×10^{-4}	61.67	0.99	12.7×10^{-4}	37.86	0.99
2	Copper with 25 mg of MWCNT per litre of electrolyte	8.40×10^{-4}	56.87	0.85	12.5×10^{-4}	35.76	0.89
3	Copper with 50 mg of MWCNT per litre of electrolyte	9.8×10^{-4}	63.07	0.99	13.8×10^{-4}	36.34	0.99
4	Copper with 75 mg of MWCNT per litre of electrolyte	$10.5\times\times10^{-4}$	57.58	0.87	13.9×10^{-4}	34.05	0.85
5	Copper with 100 mg of MWCNT per litre of electrolyte	$15\times\times10^{-4}$	80.67	0.95	18.2×10^{-4}	37.35	0.97
6	Copper with 125 mg of MWCNT per liter of electrolyte	$11.1\times\times10^{-4}$	63.95	0.85	15.7×10^{-4}	38.07	0.84

[1] Pearson's correlation coefficient is a measure of the strength and direction of the linear relationship between two variables that is defined as the covariance of the two variables divided by the product of their standard deviations.

$$R_{x,y} = \frac{\mathrm{cov}(x,y)}{\sigma_x \sigma_y} = \frac{E[(x-\mu_x)-(y-\mu_y)]}{\sigma_x \sigma_y}$$

where, cov is the covariance, σ_x is the standard deviation of x, μ_x is the mean of x, and E is the expectation

However, the particle size and micro-strain are the factors which affects the broadening of the peak [7]. Contribution of these parameters in broadening was determined by using equation (4.4) and (4.5) and are tabulated below:

Table 4.3: Broadening of the peak due to micro-strain and grain size

		Lorentzian Fit		Gaussian Fit	
Material	**Plane**	**broadening due to micro-strain (rad)**	**broadening due to grain size (rad)**	**broadening due to micro-strain (rad)**	**broadening due to grain size (rad)**
Pure copper	111	0.0014	0.0024	0.0020	0.0039
	200	0.0016	0.0025	0.0024	0.0041
	220	0.0025	0.0028	0.0039	0.0046
25 mg/l	111	0.0015	0.0026	0.0020	0.0042
	200	0.0016	0.0027	0.0023	0.0043
	220	0.0026	0.0031	0.0038	0.0048
50 mg/l	111	0.0015	0.0024	0.0022	0.0041
	200	0.0018	0.0024	0.0026	0.0042
	220	0.0029	0.0027	0.0042	0.0047
75 mg/l	111	0.0016	0.0026	0.0022	0.0044
	200	0.0019	0.0027	0.0026	0.0045
	220	0.0031	0.0030	0.0042	0.0051
100 mg/l	111	0.0024	0.0018	0.0029	0.0039
	200	0.0029	0.0019	0.0034	0.0041
	220	0.0046	0.0021	0.0055	0.0046
125 mg/l	111	0.0018	0.0024	0.0025	0.0039
	200	0.0021	0.0024	0.0030	0.0040
	220	0.0033	0.0027	0.0048	0.0046

Different Williamson-Hall plots ($\beta \cos\theta$ vs. $\sin\theta$) were drawn for all the six composite powder including pure copper. The grain sizes of the composite powder samples were determined by finding the intercept of Williamson-Hall plot ($\beta \cos\theta$ vs. $\sin\theta$) with the ordinate (i.e. $\beta \cos\theta$ axis) and equating the intercept value with $k\lambda/D$, where, $K = 0.9$, λ is the wavelength of x-ray $\lambda = 0.15418\ nm$, and D is grain size. The grain size is tabulated in Table 4.2 and is 60 ±4 nm (by lorentzian fit). Similarly, for Gaussian fit peaks, graphs for $(\beta \cos\theta)^2$ vs. $(\sin\theta)^2$ as discussed at the start of the section, were plotted for all the composite samples. The grain size of the composite samples were determined by finding the intercept of the plot with the ordinate {the vertical axis $(\beta \cos\theta)^2$ } and then equating the intercept with $(k\lambda/D)^2$. The grain size of the composite samples, which was

determined by the above method is tabulated in Table 4.2 and it is about 36±2 nm (Gaussian Fit). In both the cases, the observed variation in the particle size is less. In order to check the contribution of grain size and micro-strain on the peak broadening, the graphs are plotted with calculated data in Table 4.3, which is for the contribution of grain size and micro-strain on peak broadening. The contribution of micro-strain on peak broadening is plotted in Figure 4.7. The contribution of micro-strain on the peak broadening is plotted on the ordinate and the MWCNT concentration in the electrolyte on the abscissa. The data is plotted on the graph and fitted linearly as seen in Figure 4.7. From the Figure 4.7, it has been observed that the peak broadening increases gradually as the concentration of MWCNT in the electrolyte increases. Whereas the contribution of the grain size on the peak broadening is studied form Figure 4.8. The contribution of grain size on the peak broadening is plotted on the ordinate and the concentration of MWCNT in the electrolyte is plotted on the abscissa. From Figure 4.8, it is observed that there is a slight decrease in the peak broadening with increase in concentration of the MWCNT in the electrolyte. From these observations, it is concluded that the peak broadening is due to the micro-strain in MWCNT/Cu composite and it is attributed to the reinforcement of MWCNT in the copper matrix.

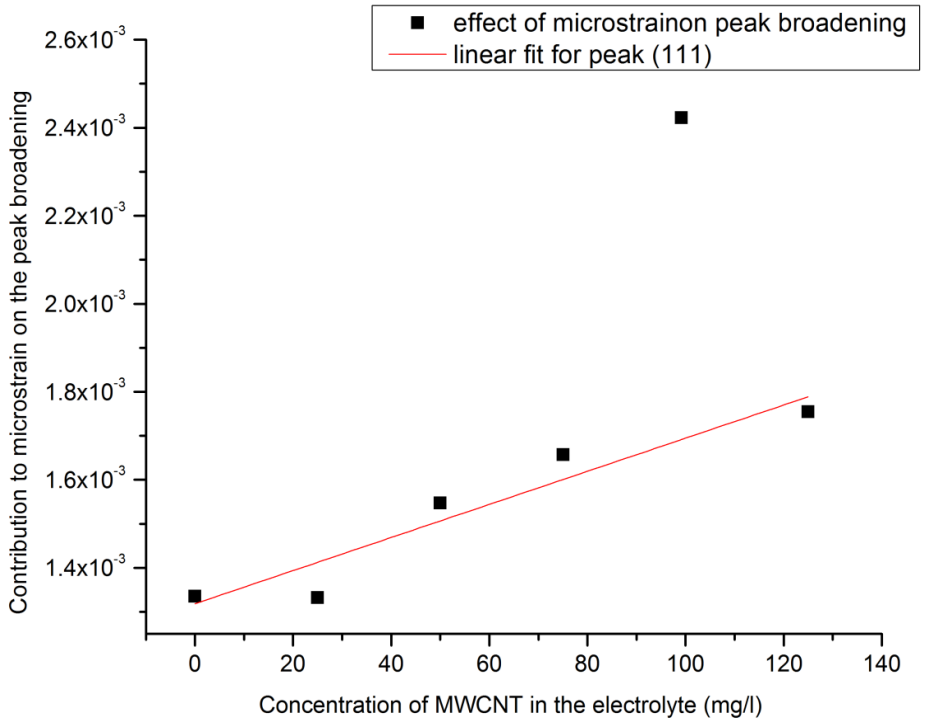

Figure 4.7 Effect of micro-strain on the peak broadening vs. MWCNT concentration in the electrolyte in mg/l

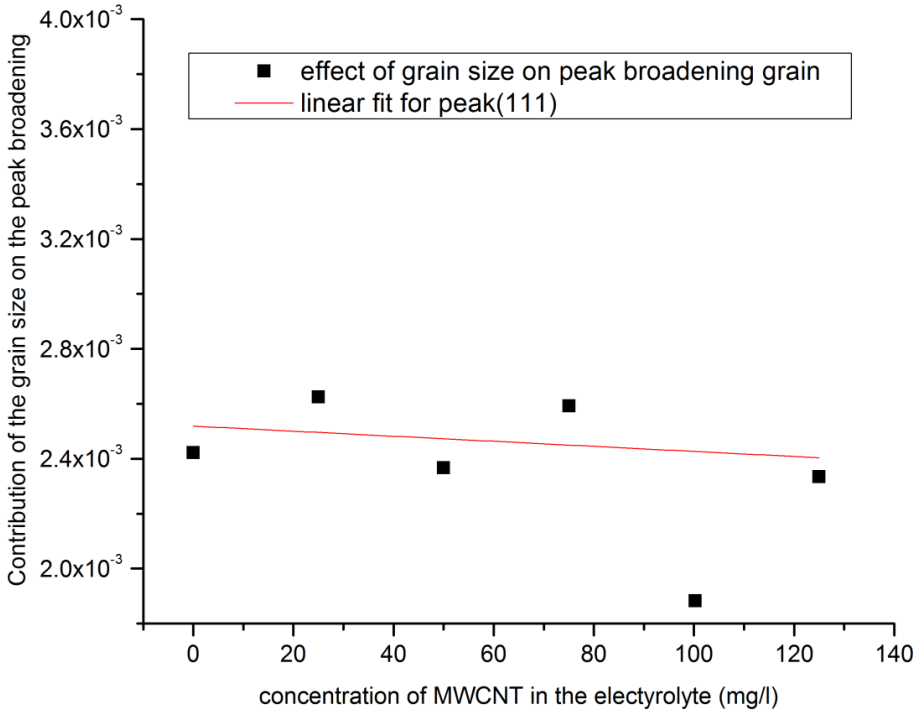

Figure 4.8: Effect of grain size on the broadening of the peak vs. concentration of MWCNT in the electrolyte

It has been observed that due to micro-stresses in the composite the peak shifts towards lower angle compare to the pure copper [4].

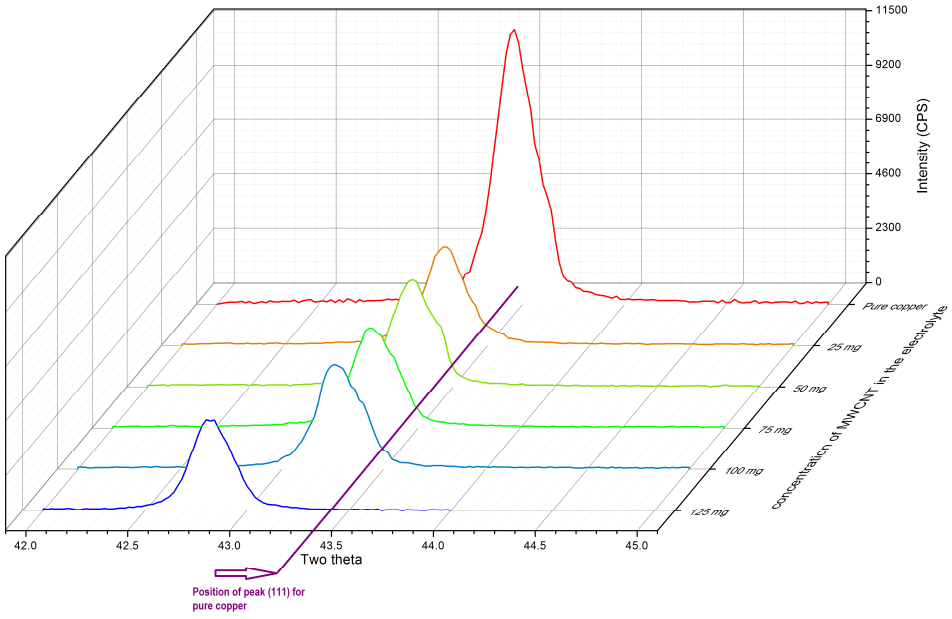

Figure 4.9: X-ray diffraction peak (111) for six samples, showing shifting of the MWCNT/Cu composite peaks towards lower angle compare to pure copper peak

Figure 4.9 shows the XRD patterns for peak (111) of pure copper and the MWCNT reinforced copper composite powders. In Figure 4.9, the Bragg's angle is plotted on abscissa, intensity (CPS) is plotted on ordinate whereas the concentration of MWCNT in the electrolyte is plotted on applicate. The position of pure copper is shown on the Figure 4.9 by an arrow. Form the figure it is seen that the peak (111) of MWCNT reinforced composite powder samples are shifted towards lower angle compared to the pure copper peak (111). This shifting of MWCNT reinforced composites peaks is attributed to the micro-stresses, which caused micro-strain due to reinforcement of MWCNTs.

4.3 Microstructure

The external morphology of the powder was studied under scanning electron microscopy (SEM). The powder samples were spread on carbon adhesive tape and then observed by SEM. SEM image of pure copper sample is shown in the Figure 4.10. The image shows the dendritic (tree like) structure of the copper particles. During electro-deposition as the overvoltage[2] increases, nucleation of copper on the cathode starts with reduction of the copper ion and which, behaves as an adatom on the cathode surface [9]. At the same time, there is increase in the number of sites suitable for instantaneous dendritic growth initiation [10] due to increase in over voltage. The number of nucleation sites on the initial surface is obviously limited all due to small area of electro deposition in the present experiment, while the nucleation on the growing grains can take place continuously, which result in the dendritic structure of the copper particles. Figure 4.10 shows a magnified image of dendritic morphology of the copper particle. Dendritic morphology is a characteristic of all copper powders got at constant current density. The observed SEM images in Figures 4.10 and 4.12 and the SEM images studied by Pavlovic et al. [11] as shown in Figure 4.11 are similar and therefore it validates that newer method also develops same microstructure of pure copper as had been observed by the conventional method.

[2] when hydrogen is evolved at the cathode or oxygen at an anode, the potential required is usually greater than the equilibrium potential of a hydrogen or oxygen electrode in that solution. This difference in potential, known as the *overvoltage* and it increases with the current density.

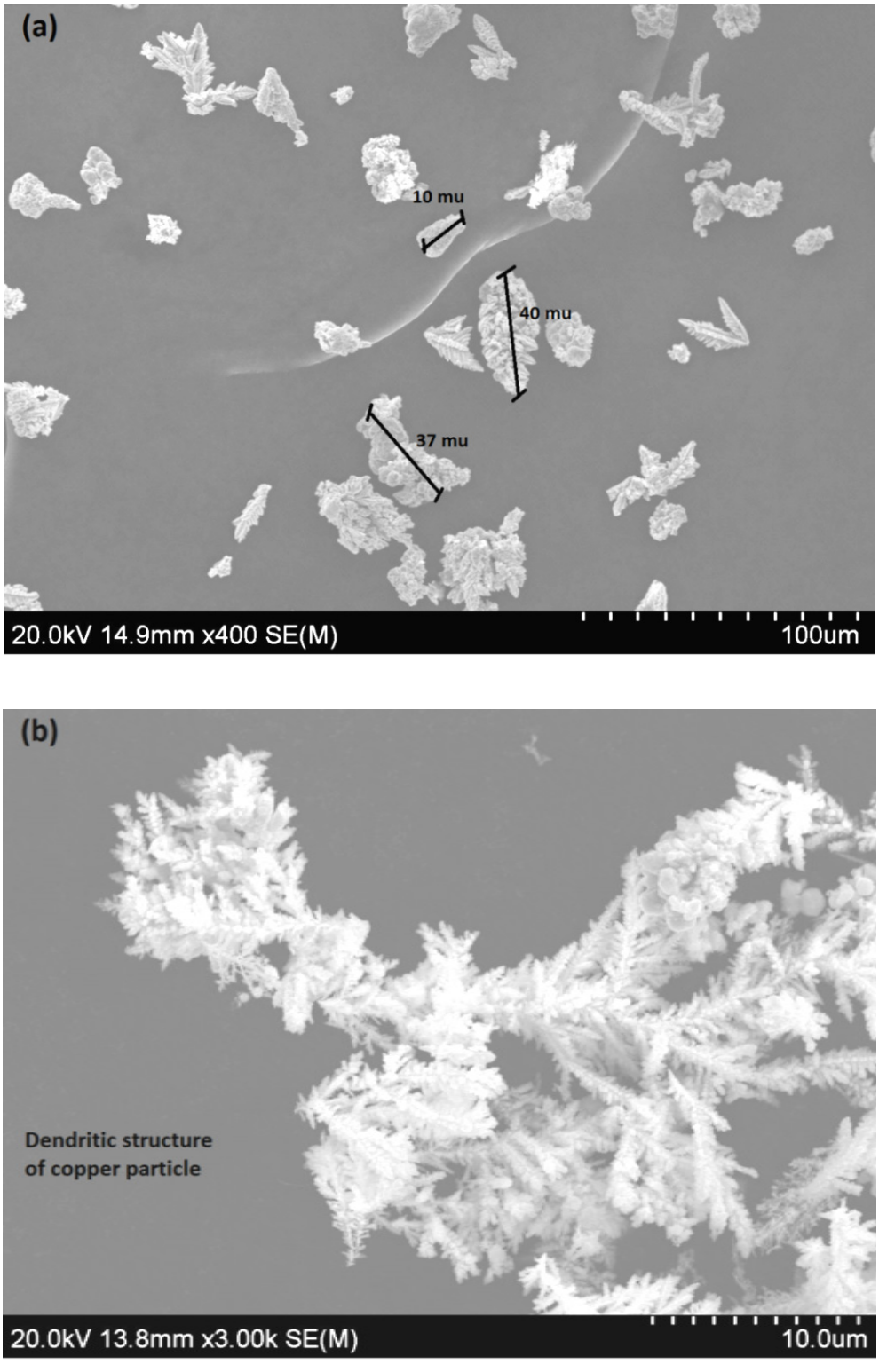

Figure 4.10: (a) SEM image of pure copper powder particles showing particle size in the range of 10-40 µm (b) SEM image of pure copper powder particle showing dendritic structure

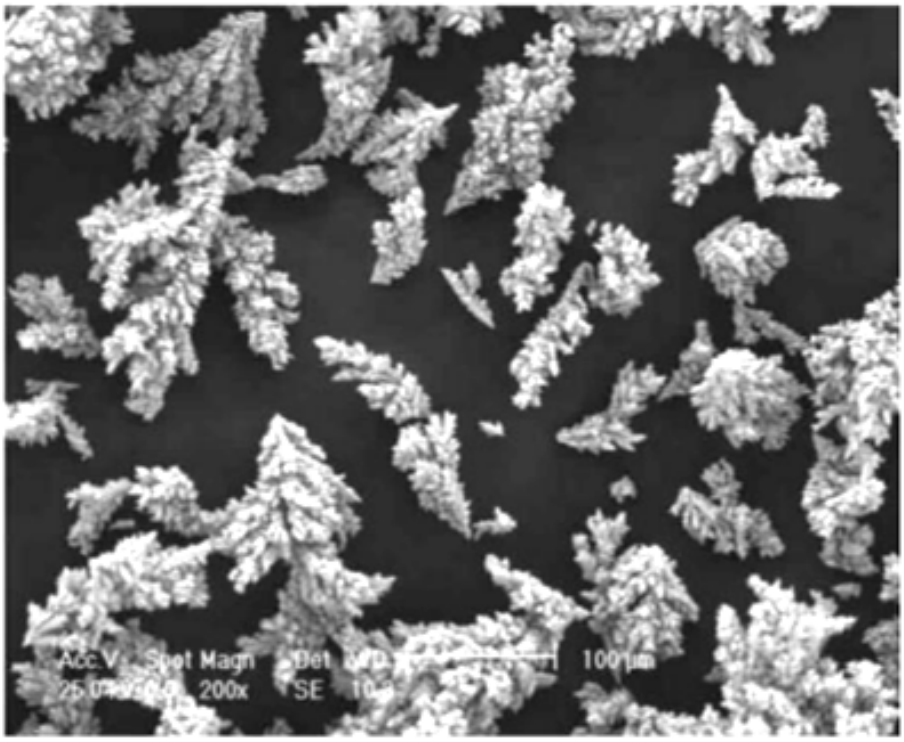

Figure 4.11: Dendritic structure of the copper by electrolysis technique. Adopted from the article by M.G. Pavlovic et al. [12]

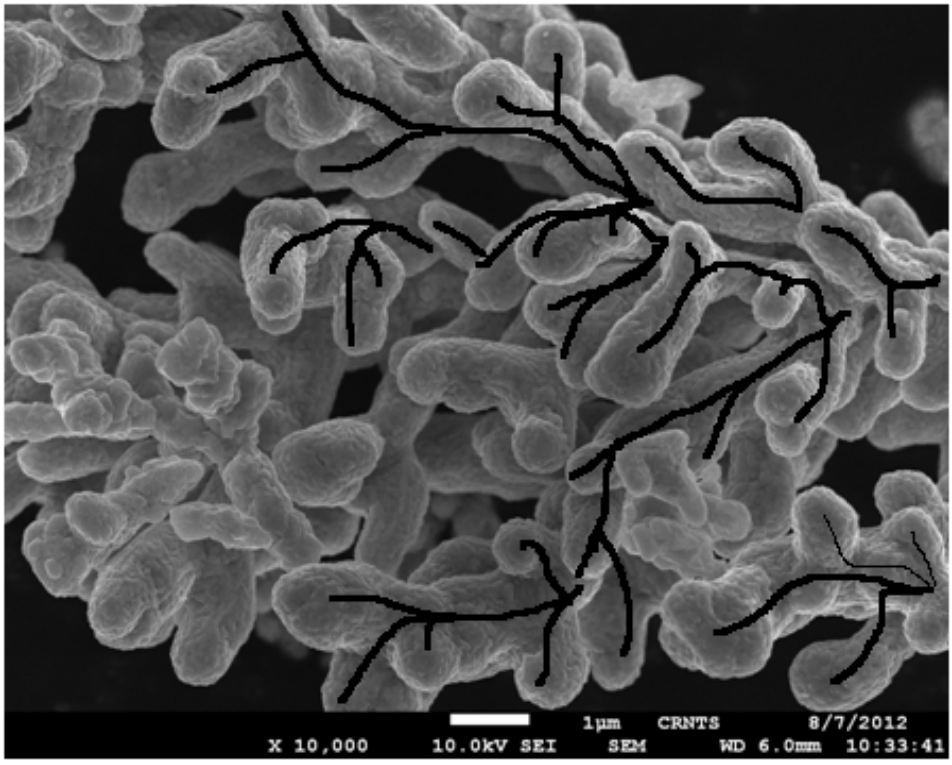

Figure 4.12: HRSEM image of dendritic structure of pure copper powder particle

The particle size of the copper observed by SEM in Figure 4.10(a) was in the range of 15-40 μm. The MWCNT/Cu composite powder synthesized by the modified electro-co-deposition route, shown in Figure 4.13, depicts the dendritic morphology [13] with MWCNT reinforced in the copper particles.

The Figure 4.13 shows the dendritic structure of copper particle and protruding MWCNT, which confirms the reinforcement of MWCNT in the copper matrix.

The most important feature of this process is uniform mixing of CNTs with Cu particles by co-deposition process. The CNTs are reinforced within Cu powders and copper nucleates on the MWCNT surface [13] rather than simply trapping in the co-deposited Cu powders particle dendrite.

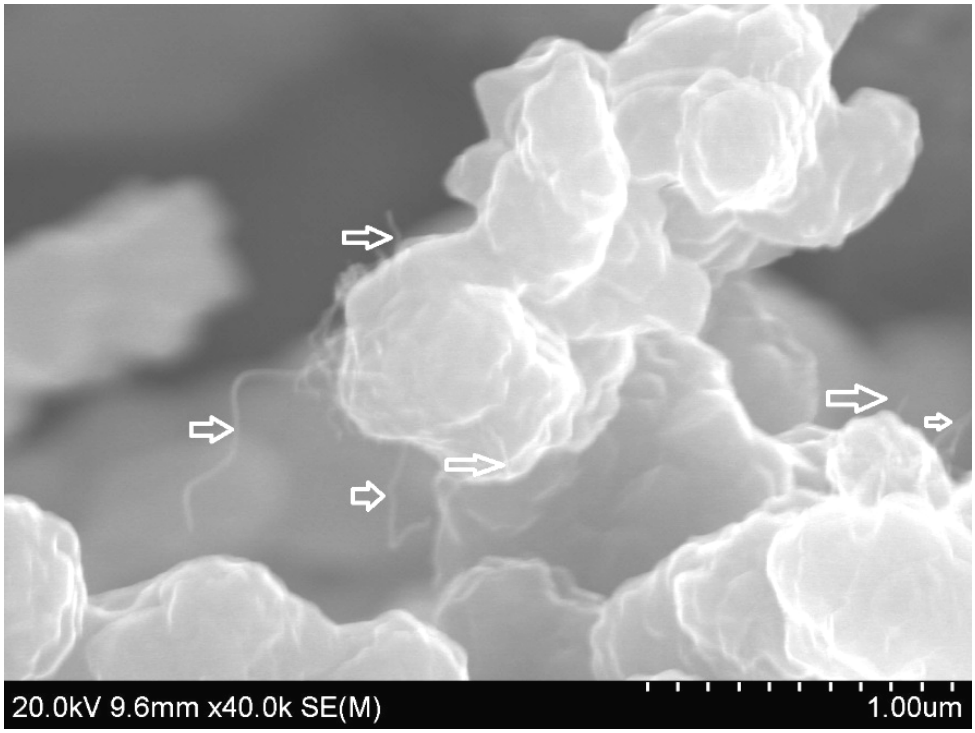

Figure 4.13: FESEM image of dendritic structure of co-deposited copper MWCNT composite powder particle

Purified MWCNT, as shown in Figure 4.14(a), were used for the fabrication of MWCNT/Cu composite, which helped in improved property of the composite. Figure 4.14(b) shows the HRTEM image of the MWCNT coated with Cu particles obtained in the newer method. The diameters of copper particles seen in the HRTEM image were in the range of 10-20 nm.

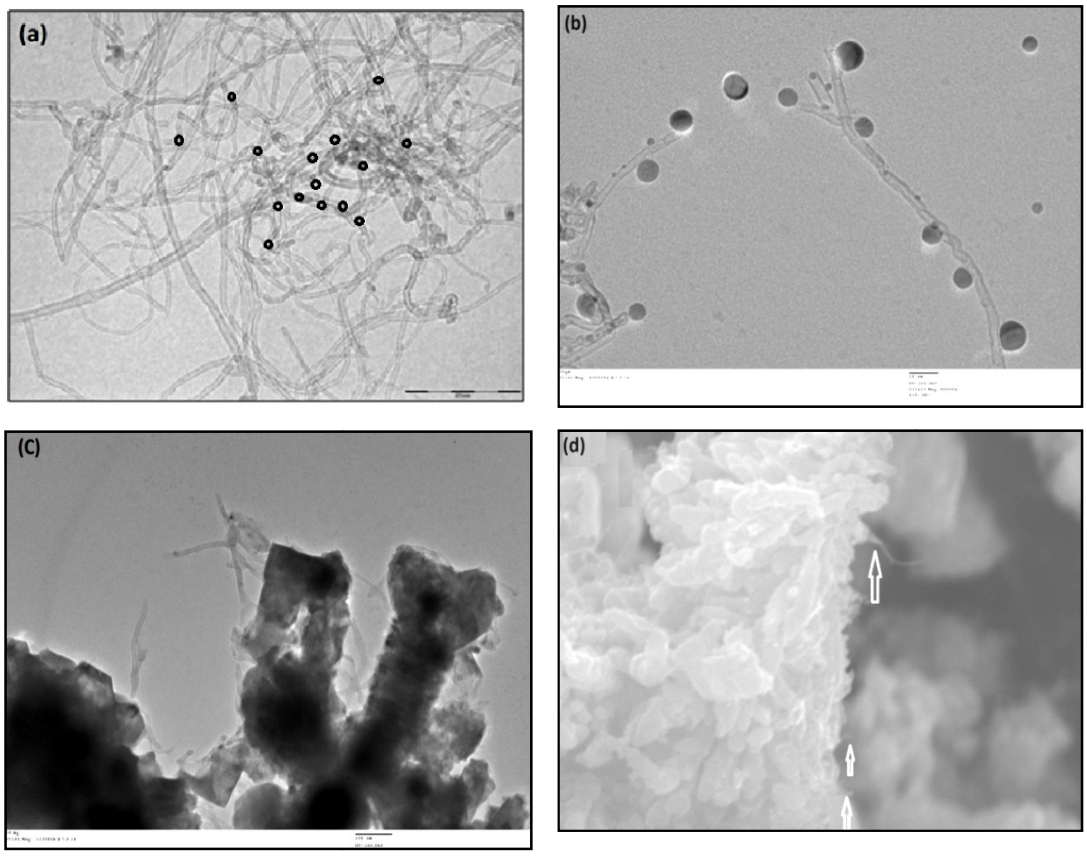

Figure 4.14: (a) HRTEM micrograph for the as received MWCNTs; (b) HRTEM micrograph of MWCNTs and the coated copper particles on the surface of MWCNT; (c) HRTEM micrograph for electro-co-deposited MWCNT/Cu composite powder showing bridging and properly reinforced MWCNT; (d) FESEM micrograph of electro-co-deposited MWCNT/Cu composite powder showing pulled out MWCNT

During co-deposition of the Cu and MWCNT, Cu^{2+} were electrodeposited at the tip of the cathode and on the surface of the MWCNT. The spherical or hemispherical structure of the copper crystal on the surface, seen in the Figure 4.14(b), is the stage before formation of dendrite [9]. This shows that the copper ions got some active sites on the surface of the MWCNT during co-deposition of MWCNT and Cu. As the deposition continues, Cu particles were deposited on the surface of MWCNTs and the MWCNTs were surrounded by the copper matrix as shown in Figure 4.14(c). It was observed from Figure 4.14(b) that the copper deposited on the surface of MWCNT, but the nucleation and deposition took place selectively at some sites like end of the MWCNT and some sites on outer surface. From Figure 4.14(a), it is seen that the ends of the MWCNT are open {few openings are highlighted in the Figure 4.14(a)}, which is a defect and hence the site becomes more active.

Therefore, Cu^{2+} ions reduce easily by accepting electrons form the dangling bond at the end of the MWCNT and deposits there. Moreover, carbon nanotubes are not perfect. Defects such as pentagons, heptagons, vacancies, dopant or catalyst particles trapped during chemical vapour deposition process, are found to modify the electronic properties of these nano-systems [17-19]. These defect sites on the outer surface are having more broken bonds and hence these sites becomes more active than other sites on the outer surface of MWNTs [17]. Thus, Cu^{2+} ions easily accept electrons and deposits on the defect sites. MWCNT/Cu composite powders were rigorously ultrasonicated in the acetone bath and then HRTEM and FESEM micrographs (Figure 4.14) were obtained. After rigorous ultrasonication, the Cu particles and MWCNTs are seen intact significantly and confirms that there is very good bonding between Cu particles and MWCNT. Some MWCNTs, which are pulled out of the Cu matrix and are shown in Figure 4.14(d), marked by arrow. They had some unique protrusion shape like triangular pyramid. This triangular pyramid shape is all due to coating of copper on the surface of MWCNT. In conventional method such as powder metallurgy, there is physical mixing of the copper and carbon nanotube.

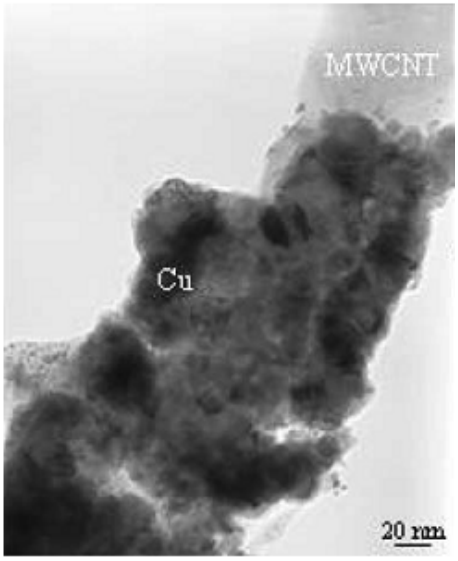

Figure 4.15: Adopted from an article by Feng Wang et al. [18]**. HRTEM image of copper coating on functionalized MWCNT**

However, in conventional electro-deposition method, in some cases deposition of copper is observed as shown in Figure 4.15 (the figure is adopted from [18]). This deposition was due to attachment of carboxyl or hydroxyl group on the surface of CNT i.e. functionalization of CNT or due to coating of Nickel on CNT.

4.4 Energy Dispersive Spectrum (EDS)

Energy dispersive x-ray spectroscopy helps in elemental analysis of the composite. Therefore, EDS analysis of the MWCNT/Cu composite was carried out in order to do the elemental analysis of the MWCNT/Cu composite. This elemental analysis is needed to confirm that the particles, which are attached on the surface of MWCNTs, are of copper only.

Figure 4.16 shows the energy dispersive spectral (EDS) map of MWCNT/Cu composite powder having 25 mg/l concentration of MWCNT in electrolyte. Initially copper is mapped by EDS which is shown in red colour and then the mapping of carbon was carried out which is shown in green colour. EDS revealed that the carbon follows the profile of the copper particle and hence it is concluded that the Cu and carbon (MWCNT) are intact. This behaviour also confirms that there is bonding, may be electrostatic bonding, between MWCNT and copper matrix. FESEM micrograph shown in Figure 4.13 of MWCNT/Cu composite powder shows uniform dispersion of MWNTs. This bonding between MWCNTs and Cu matrix and uniform dispersion of MWCNTs in the copper matrix assure better mechanical properties.

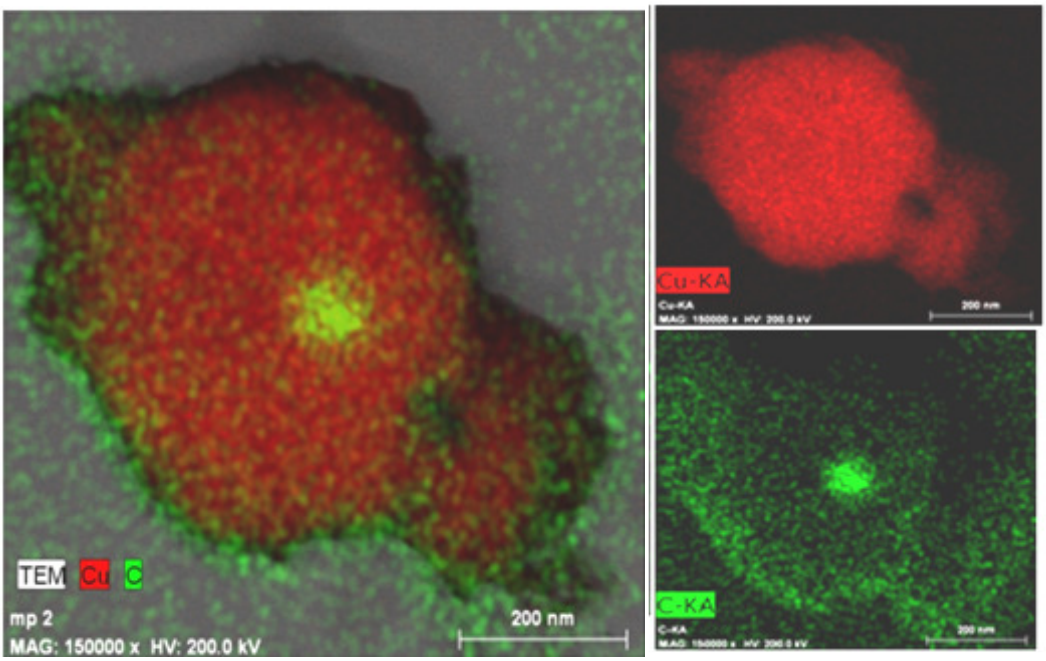

Figure 4.16: EDS mapping profile of MWCNT/Cu composites (25 mg/l concentration of MWCNT in electrolyte)

Again, in order to ensure the uniformity of MWCNT in the copper matrix, an EDS analysis of a sample with 50mg/l of MWCNT concentration was carried out at three random sites as shown in Figure 4.17(a), (b) and (c). The electro-co-deposited MWCNT/Cu composite powder was separated from the electrolyte and was then dried and fixed on an electro-conductive tape. The quantitative analysis of the MWCNT/Cu composite powder was carried out by the EDS. The EDS analysis of the sample at three different sites is shown in Figure 4.18(a), (b) and (c). The EDS spectrums are plotted for counts vs. Energy (keV). The characteristic x-ray for copper appears at 8.040 keV (Kα) and 0.930 keV (Lα) and for carbon characteristic x-ray appears at 0.277 keV (Kα). In the Figure 4.20, the presence of copper and carbon is observed and some percentage of oxygen is also observed. The copper is very unstable and get oxidise easily in the atmosphere. In the present situation, the particle size of the copper is very small (in the range of 10-40 μm) therefore the surface area of the particles is large which lead to high surface energy and hence it becomes more active. In addition to this unsophisticated handling of the MWCNT/Cu composite powder causes oxidation. From EDAX data given in Table 4.4, it can be observed that the wt% of carbon is 1.83±0.06 and copper is 96.20±0.12 similarly the at% of carbon is 8.53±0.3 and of copper is 84.51±0.51 at three random sites, which illustrates uniform mixing of MWCNT in copper matrix.

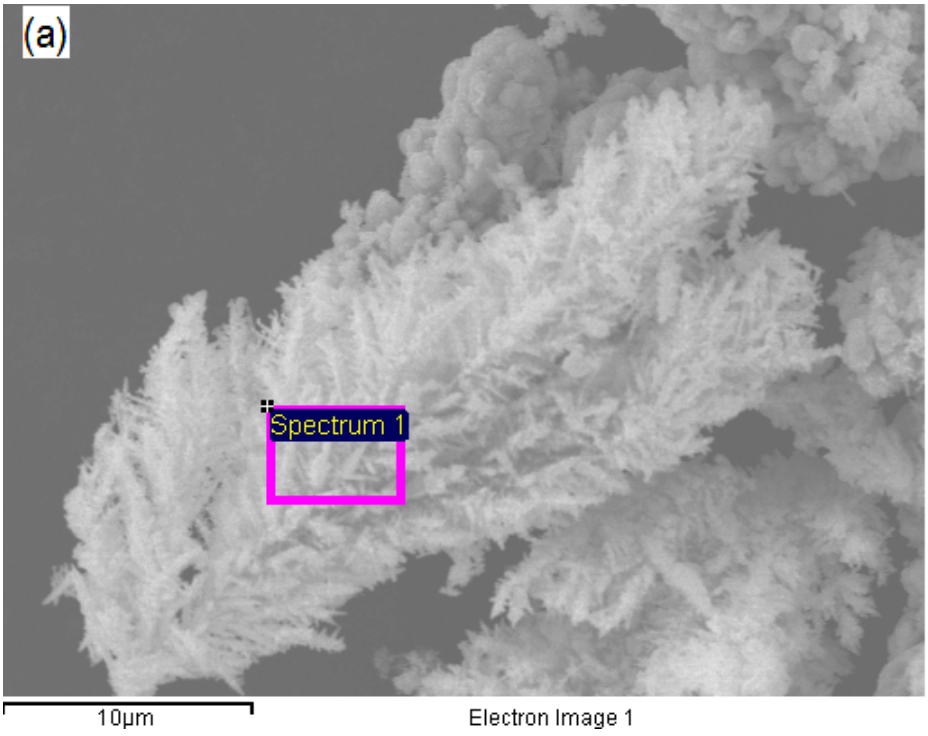

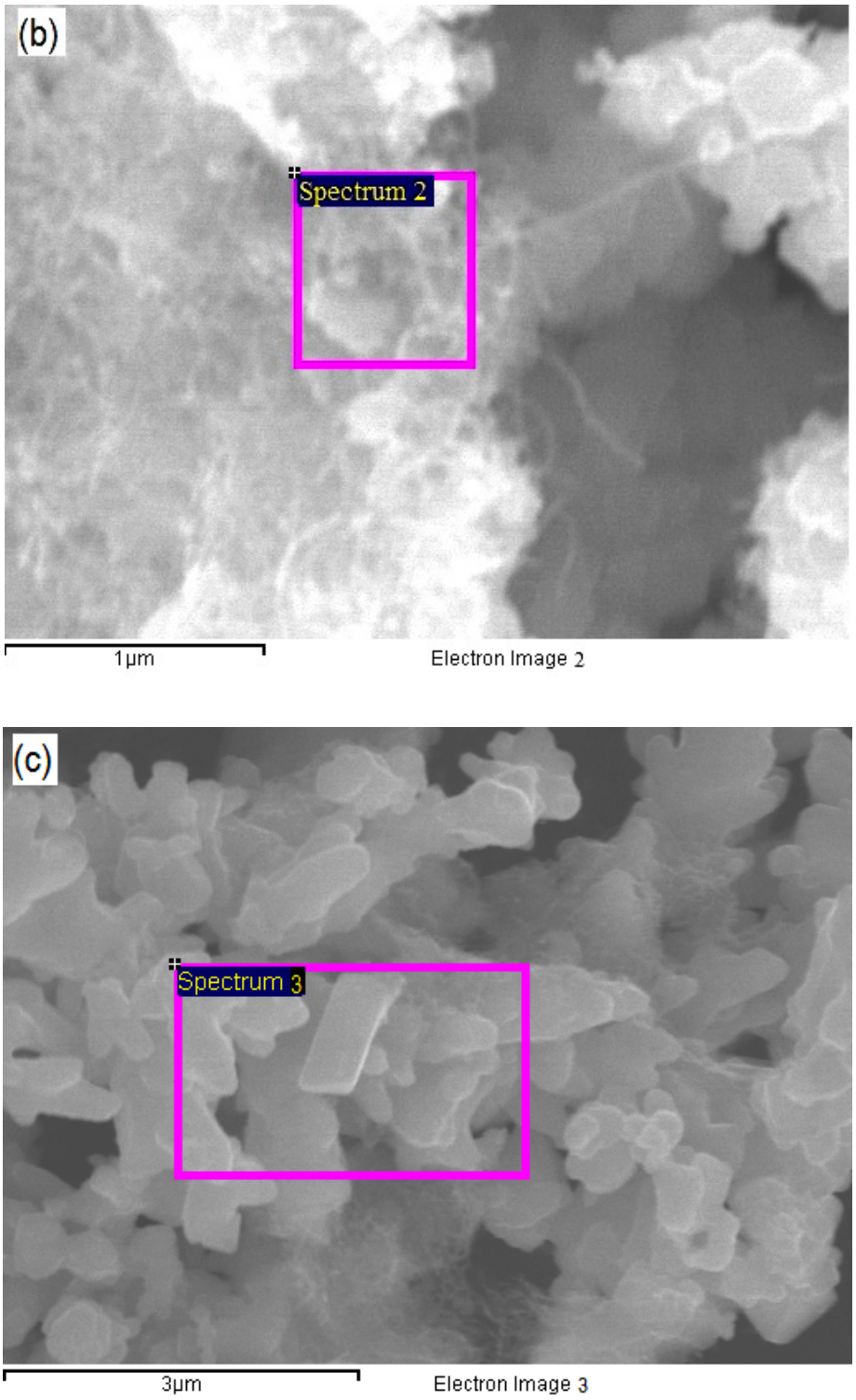

Figure 4.17: SEM micrograph showing EDS of the sample at three randomly selected sites showing presence of carbon in (a), (b) and (c)

(a)

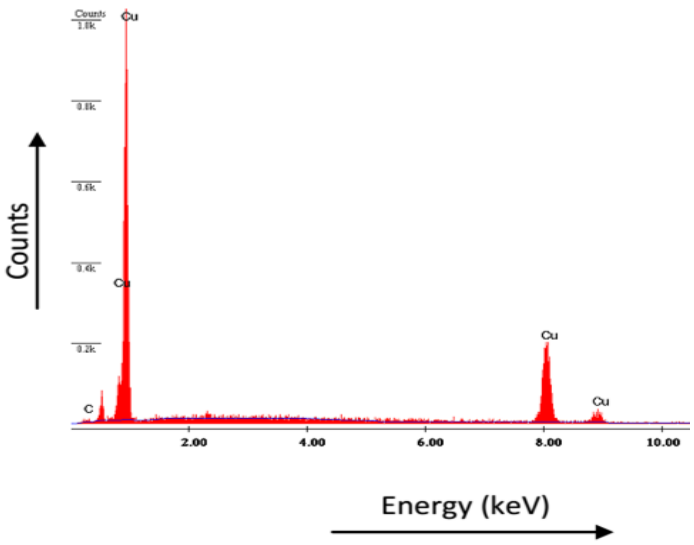

(b)

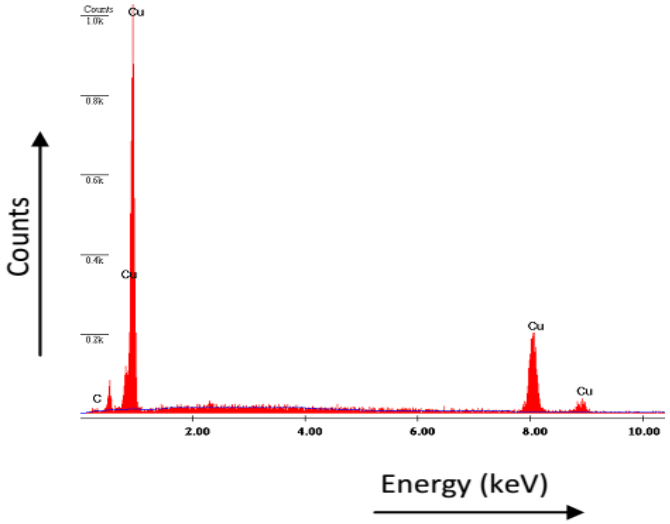

(c)

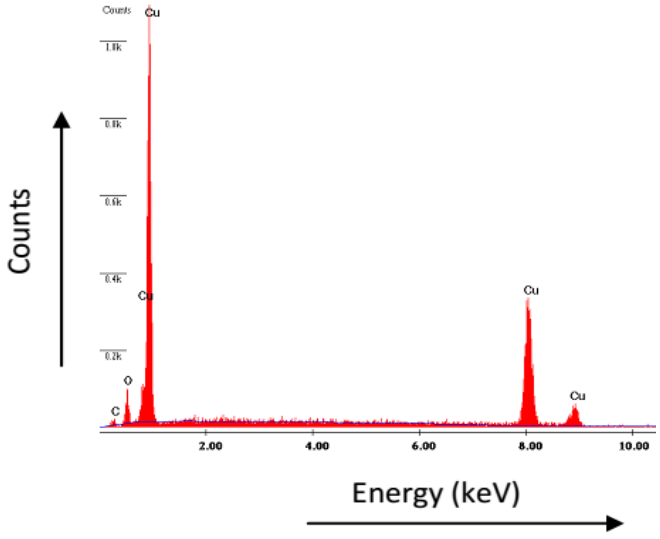

Figure 4.18: (a) (b) and (c) are the EDS graphs corresponding to the data given in Table 4.4

Table 4.4: Data of EDAX analysis at three randomly selected sites

Point	Elements	wt%	at%
1	C	1.78	8.17
	Cu	98.22	91.83
2	C	1.90	9.27
	Cu	98.10	90.73
3	C	1.83	8.48
	O	2.09	7.27
	Cu	96.08	84.24

4.5 Density and Volume percentage of MWCNT in the Composite

Density of MWCNT is about four times less compare to the pure copper, hence it is expected that there will be decrease in density of the composite in comparison to the pure copper. As the density of the composite decreases, there will be effect on the specific properties of the composite like specific resistivity. Density of the composite can be determined by measuring mass and volume of the composite sample or by Archimedes principal. In this experiment, the density of Cu and MWCNT/Cu composite is measured by the Archimedes principle. For measuring the density of the composites, samples in the pellet form were synthesized from MWCNT/Cu composite powder, prepared from electrolyte containing 25, 50, 75, 100 and 125 mg/l MWCNT. The mass of each sample was measured by precision weighing machine. Then the weighing of 50ml beaker containing 40 ml water was done by using precision weighing machine and keeping the beaker containing water in the pan the weighing machine was set to zero. Then the sample pellet was completely immersed in the beaker containing water, one by one and the weight was noted down. This reading corresponds to the buoyant force, which was equated to the product of density of water, volume of sample and gravitational constant (ρ_{water} V_{sample} g). Density of water was taken as 980 kg/m^3. Thus, the volume of sample was determined by the above method. The calculated volume was divided by the mass of the pellet measured by the precision weighing machine to determine the density of the composite.

Density of composite is determined by neglecting the voids. For determining the volume fraction of the MWCNT in the composite, we assumed density of MWCNT as

2.1 gm/cm^3 (as per the specification given by supplier) and density of pure copper compact is determined by Archimedes principle, which is found to be 8.142 gm/cm^3. For each sample of composite the mass of the copper and mass of MWCNT in the composite were determined by the following equation [2]

$$m_{Cu} = m_t \left[\frac{100 \times \rho_{MWCNT} + \rho_{composite}}{\rho_{MWCNT} \times \rho_{composite}} \times \frac{\rho_{MWCNT} \times \rho_{Cu}}{\rho_{MWCNT} + \rho_{Cu}} \right] \quad (4.11)$$

$$m_{MWCNT} = m_t - m_{Cu} \quad (4.12)$$

where, m_{Cu} the mass of the copper in the composite, m_{MWCNT} the mass of the MWCNT in the composite, m_t the total mass of the composite measured by precision weighing machine, ρ_{MWCNT}, ρ_{Cu} are the density of MWCNT and copper and $\rho_{composite}$ is the density of composite determined by Archimedes principle. The mass will be determined in gram. In order to determine the volume fraction of copper and MWCNT in the composite the volume of copper (m_{cu}/ρ_{Cu}) or the volume of MWCNT (m_{MWCNT}/ρ_{MWCNT}) was divided by the total volume of the composite determined by the Archimedes principle respectively. The corresponding volume fractions of MWCNT/Cu composite samples, prepared from electrolyte containing 25, 50, 75, 100 and 125 mg/l MWCNT were about 5.5, 10.14, 14.75, 14.78, and 16.53% respectively as given in Table 4.5. The variation in the density and the vol% of the MWCNT in the composite was plotted in Figure 4.19.

Density and the vol% of the MWCNT in the composite pellet are on the ordinate whereas the MWCNT concentration is on the abscissa. From Figure 4.19, it is observed that initially there is gradual increase in the vol% of MWCNT in composite powder (pellet form) but above 75 mg/l of MWCNT in electrolyte the curve moves asymptotically with abscissa. The variation in the vol% in the MWCNT/Cu composite with increase in mass of MWCNT in the electrolyte is attributed to the agglomeration of MWCNT. As the mass of MWCNT in the electrolyte increases, MWCNT starts agglomeration during deposition. The force due to ionic flow may not be sufficient to drive agglomerates towards cathode and due to gravity, agglomerate gets settle down at bottom of the flask. At the end, agglomerates are easily removed from the product during rinsing.

Table 4.5: Density and vol% of MWCNT/Cu composite

SN.	Concentration of MWNT in electrolyte mg/l	Density gm/cm^3	Vol% of MWCNT
1	0	8.14	0
2	25	7.8	5.5
3	50	7.53	10.14
4	75	7.25	14.75
5	100	7.24	14.78
6	125	7.14	16.53

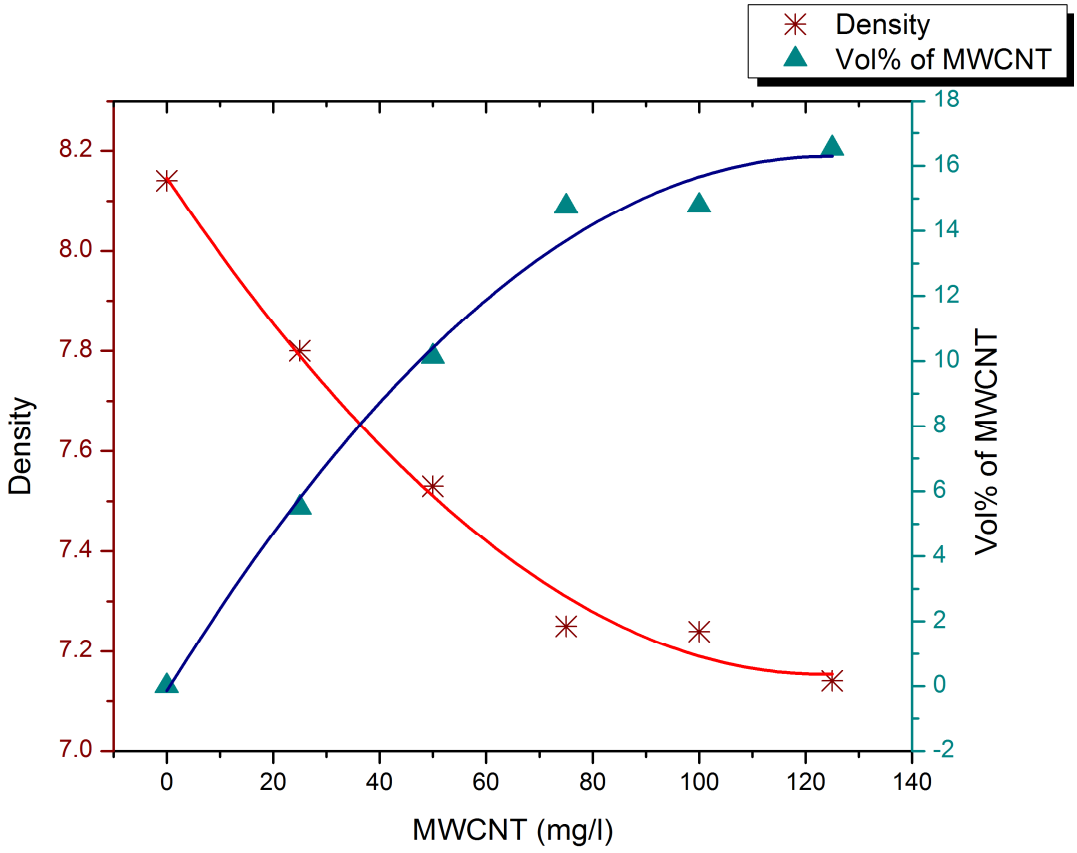

Figure 4.19: Graph shows the variation in density and vol% of MWCNT with respect to MWCNT concentration in electrolyte

4.6 Conclusion

1. Copper powder reinforced with MWCNTs was successfully produced by combining molecular mixing electro-co-deposition method and powder metallurgy. This composite powder comprised of pure copper extracted from 98% pure copper sulphate and MWCNTs.
2. From the XRD, EDS, FESEM and HRTEM analysis, it is observed that the MWCNTs are appropriately dispersed in the copper powder. In the newer method, the MWCNTs and copper particles interact at molecular level and hence dispersion takes place at the molecular level.
3. The nucleation of the copper took place at selective potential sites on the surface of MWCNT. These potential sites may be the possible defects on the surface of MWCNT and the open ends of MWCNT due to ultrasonication.
4. The electro-co-deposition method is similar to the electro refining process. The newer method therefore, is compatible with industrial process and suitable for bulk production. This electro refining process is used in the copper industry for copper refining purpose. Hence, this is one of the promising methods for uniform dispersion of CNTs in the copper matrix, which can be easily scaled up to the production level.
5. There was a gradual change in the Full Width at Half Maximum (FWHM) of the composite peak as well as it has been observed that the MWCNT reinforced composite peaks are shifted towards lower angle, which was sign of presence of impurity in the copper which causes strain in the composite.
6. In SEM image, it has been observed that the CNTs are reinforced in the copper composite, even, there is some unique triangular pyramid shape protrusion at the base, where the MWCNT is attached to the matrix is seen. This triangular pyramid is the copper coating on the surface of MWCNT, which confirms the proper bonding between copper and MWCNT.
7. In TEM analysis, it has been observed that the MWCNTs are reinforced throughout the matrix. The EDS analysis of MWCNT/Cu composite at three random sites shows that the MWCNT are distributed uniformly throughout the matrix. These observations confirm that the MWCNTs are successfully reinforced uniformly throughout the matrix by modified electro-co-deposition method.

In the next chapter, we discussed about the fabrication of the pellet and the wire from the MWCNT/Cu composite powder and mechanical characterisation of MWCNT/Cu composite.

References:

[1] Belgamwar SU, Sharma NN. Method of Producing Uniform Mixture of Copper and Carbon Nanotube in Bulk for Copper Metal Nanocomposite. 2454/DEL/2102A, 2012.

[2] Callister WD, Rethwisch DG. Fundamentals of Material Scienec and Engineering An Integrated Approach. 4 th. John wiley and Sons, Inc; 2012.

[3] Suryanarayana C, Grant Norton M. X-Ray Diffraction A Practical Approach. New York: Springer Science +Business Media, LLC; 1998.

[4] Cullity BD (University of ND. Elements of X-Ray Diffraction. Massachusetts, USA: ADDISON-WESLEY Publishing Company, INC.; 1956.

[5] Guazzone F, Payzant EA, Speakman SA, National OR, Ridge O. Microstrains and Stresses Analysis in Electroless Deposited Thin Pd Films. Ind Eng Chem Res 2006;45:8145–53.

[6] He J, Ye J, Lavernia EJ, Matejczyk D, Bampton C, Schoenung JM. Quantitative analysis of grain size in bimodal powders by x-ray diffraction and transmission electron microscopy. J Mater Sci 2004;39:6957–64.

[7] Bushroa a. R, Rahbari RG, Masjuki HH, Muhamad MR. Approximation of crystallite size and microstrain via XRD line broadening analysis in TiSiN thin films. Vacuum 2012;86:1107–12.

[8] Zhang J, Xu K, Ji V. Dependence of strain energy on the grain orientations in an FCC-polycrystalline ® lm on rigid substrate. Appl Surf Sci 2002;185:177–82.

[9] Walsht FC, Herront ME. Electrocrystallization and electrochemical control of crystal growth: fundamental considerations and electrodeposition of metals. J Phys D Appl Phys 1991;24:217–25.

[10] Pavlović LJ, Pavlović MG, Pavlović MM, Nikolić ND, Tomić M V. The Effect of Periodically Changing Regimes on the Electrodeposition of Silver Powder. Int J Electrochem Sci 2011;6:6741–50.

[11] Kim KT, Cha S Il, Hong SH, Hong SH. Microstructures and tensile behavior of carbon nanotube reinforced Cu matrix nanocomposites. Mater Sci Eng A 2006;430:27–33.

[12] Pavlović MG, Pavlović LJ, Maksimovi VM, Nikolić ND, Popov KI. Characterization and Morphology of Copper Powder Particles as a Function of Different Electrolytic Regimes. Int J Electrochem Sci 2010;5:1862–78.

[13] Belgamwar SU, Sharma NN. Synergistic electro-co-deposition and molecular mixing for reinforcement of multi-walled carbon nanotube in copper. Mater Sci Eng B 2013;178:1452–7.

[14] Dresselhaus MS, Dresselhaus G, Charlier JC, Hernández E. Electronic, thermal and mechanical properties of carbon nanotubes. Philos Trans A Math Phys Eng Sci 2004;362:2065–98.

[15] Miyamoto Y, Berber S, Yoon M, Rubio A, Tom D. Onset of nanotube decay under extreme thermal and electronic excitations $. Phys B Condens Matter 2002;323:78–85.

[16] Charlier J. Defects in Carbon Nanotubes. Acc Chem Res 2002;35:1063–9.

[17] Sung D, Park N, Kim G, Hong S. Enhanced binding strength between metal nanoclusters and carbon nanotubes with an atomic nickel defect. Nanotechnology 2012;23:205204.

[18] Wang F, Arai S, Endo M. Metallization of multi-walled carbon nanotubes with copper by an electroless deposition process. Electrochem Commun 2004;6:1042–4.

Chapter 5

Mechanical Characterization of MWCNT/Cu Composite Pellets and Wire

5.1 Introduction

In the previous chapter MWCNT/Cu composite powder was characterized by XRD, EDS, FESEM and HRTEM in order to confirm the proper reinforcement of MWCNT in the copper matrix. In this chapter, the mechanical properties of the formed composite pellet and wire are presented and compared properties with the standard copper wire available in the market and pure copper wire fabricated by the electro-co-deposition method. The potential application of the MWCNT/metal matrix composite is in the structural material in the form of pellet and wires and therefore the need is to investigate their properties, which is done in this chapter.

Several mechanical properties of MWCNT/Cu synthesized by modified electro-co-deposition method are discussed in this chapter, including yield strength, ultimate tensile strength, hardness, percentage elongation. It is well thought-out that the strengthening mechanism is associated with load transfer from the metal matrix to the nanotubes. In general, micromechanical models are widely adopted by materials scientists to predict the tensile behaviour of micro-composites reinforced with short fibres, whiskers and particulates. The micromechanical models for discontinuously fibre-reinforced composites are briefly discussed in the later part of the chapter.

5.2 Tensile Testing

MWCNT/Cu composite pellets and the pure copper pellet were hot rolled to the diameter of 1.5 mm. The rod of 1.5 mm diameter of the MWCNT/Cu composite was then cold drawn through a series of tungsten carbide dies to 0.813 mm (AWG No. 20) wire. Due to cold drawing process, there was the cold working stress, which needs to be relieved. Therefore, after cold working annealing of copper wire was carried out in order to relieve the cold working stress in the cold drawn MWCNT/Cu composite wire. Figure 5.1 shows the schematic of the wire drawing process.

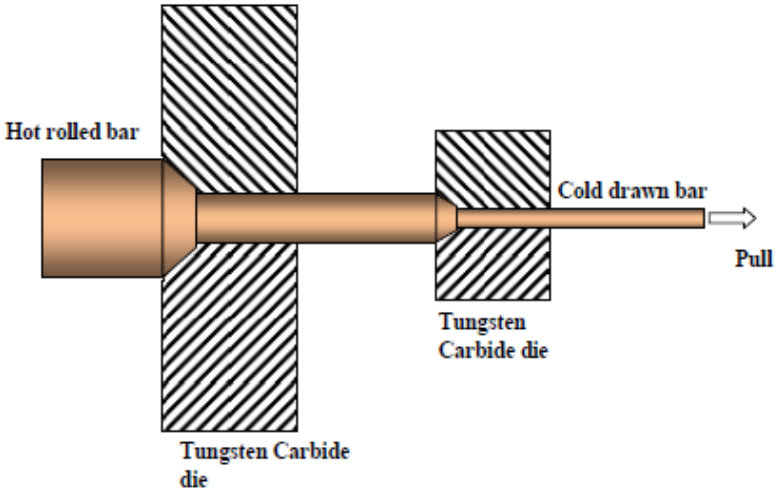

Figure 5.1: Schematic of the wire drawing process

In a tensile test, the ends of a test piece are fixed into grips, one of which is attached to the load-measuring device on the tensile machine and the other to the straining device. The strain is usually applied by means of a motor-driven crosshead and the elongation of the specimen is indicated by its relative movement [1]. The load necessary to cause this elongation may be obtained from the elastic deflection of either a beam or proving ring, which may be measured by using hydraulic, optical or electromechanical methods. A schematic of tensile test machine with a loaded sample is presented in Figure 5.2

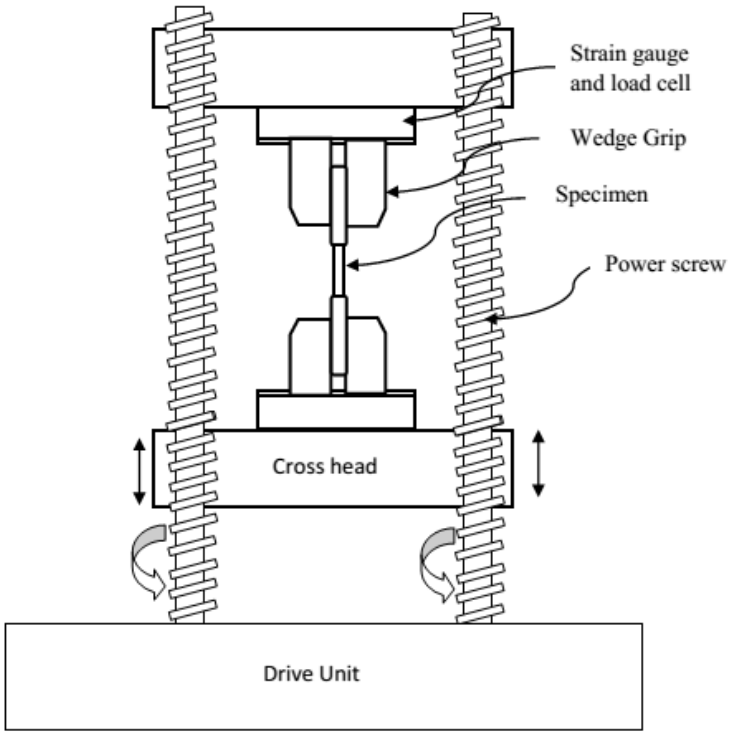

Figure 5.2: Schematic of the tensile testing of the sample

The specimens under tensile testing can also give information on the type of fracture exhibited. Usually in ductile materials, the 'cup-and-cone' type of fracture is extremely common. In this, the fracture starts at the centre of the necked portion of the test piece and at first grows roughly perpendicular to the tensile axis, so forming the 'cup', but then, as it nears the outer surface, it turns into a 'cone' by fracturing along a surface at about 45° to the tensile axis. In the present case, wire samples with 25 mg/l, 50 mg/l, 75 mg/l, 100 mg/l, 125 mg/l and pure copper undergone the tensile testing and all the samples exhibit the ductile failure by forming a neck at the centre and failing with 'cup-and- cone' formation.

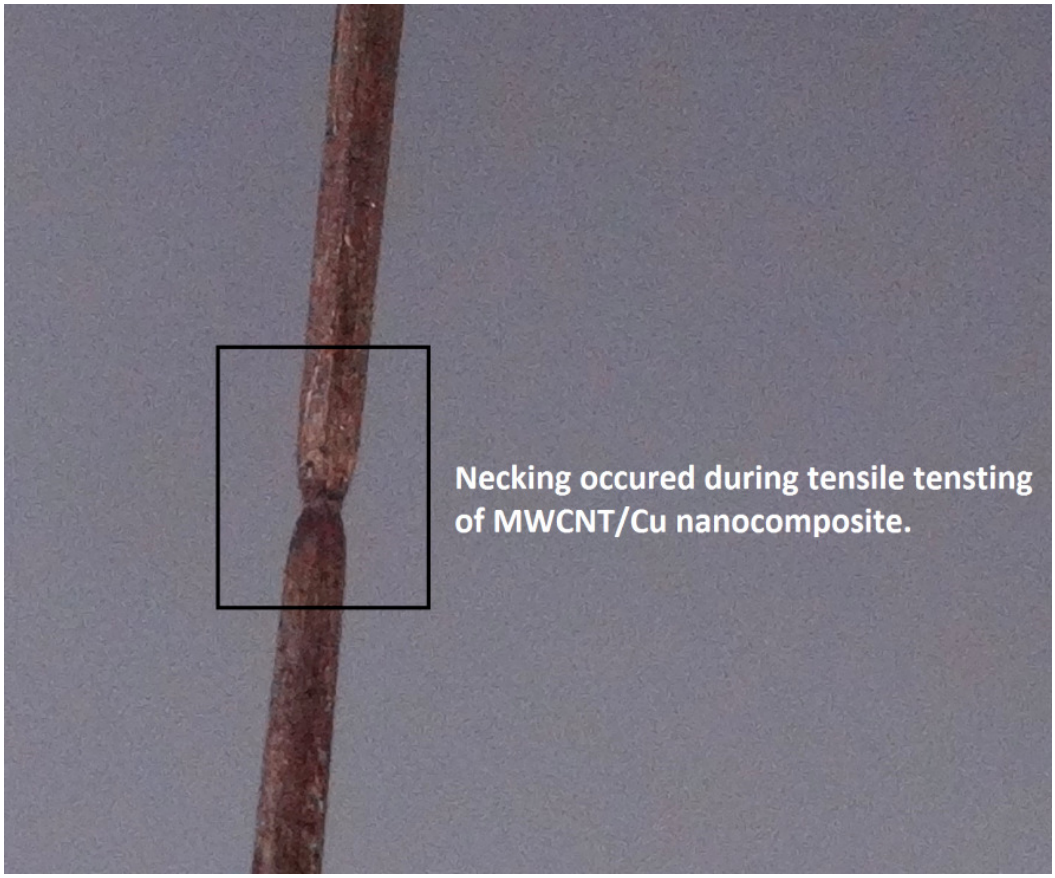

Figure 5.3: Neck formation during tensile testing of 100 mg/l concentration of MWCNT in electrolyte

For example, the neck formation at the centre of the specimen is shown in the Figure 5.3. Figure 5.3 shows the neck formation at the centre of the sample (100 mg/l concentration of MWCNT in electrolyte) during tensile testing, which was a sign of ductile failure. The

samples fail with the 'cup-and-cone' geometry as seen in Figure 5.4, in which the outer region fails due to shear whereas the inner region fails due to tensile force. Figure 5.4(a) and (b) shows the cone and cup formed after failure of pure copper wire fabricated by the modified electro-co-deposition method. Both, the cup and cone are almost smooth. There are no corrugation or fibrous structure at the edge of the cap and cone.

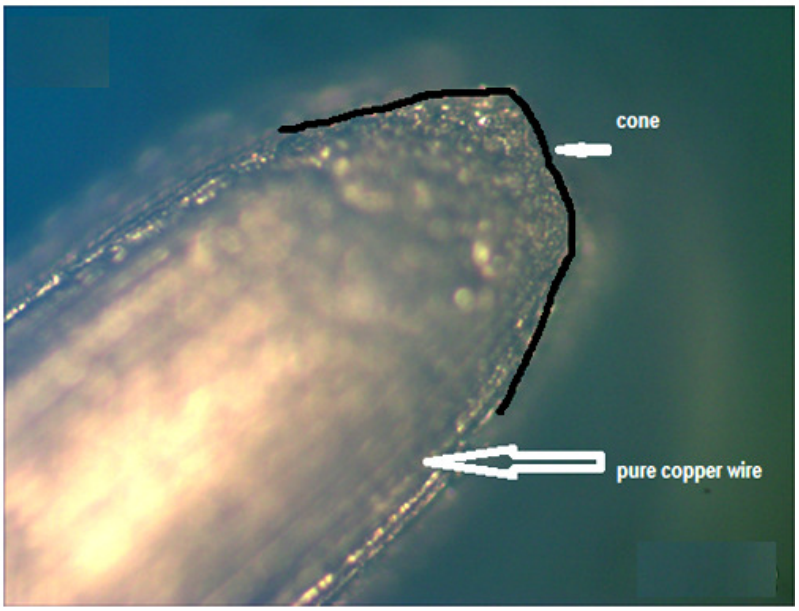

(a) Cone

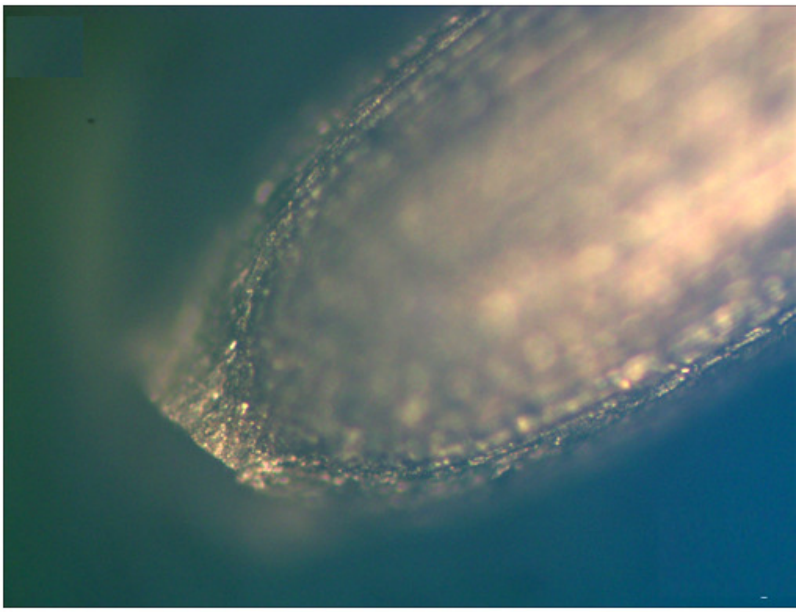

(b) Cup

Figure 5.4: (a) Optical image of the cone formed after ductile failure of the sample, (b) Formation of the cup after tensile failure of the sample

Figure 5.5 (a) and (b) are the optical image of cone and cup formed after failure of MWCNT/Cu composite. The cup as well as cone end looks corrugated, which is due to the presence of MWCNTs in the composite. The cup corrugations are highlighted by the black line.

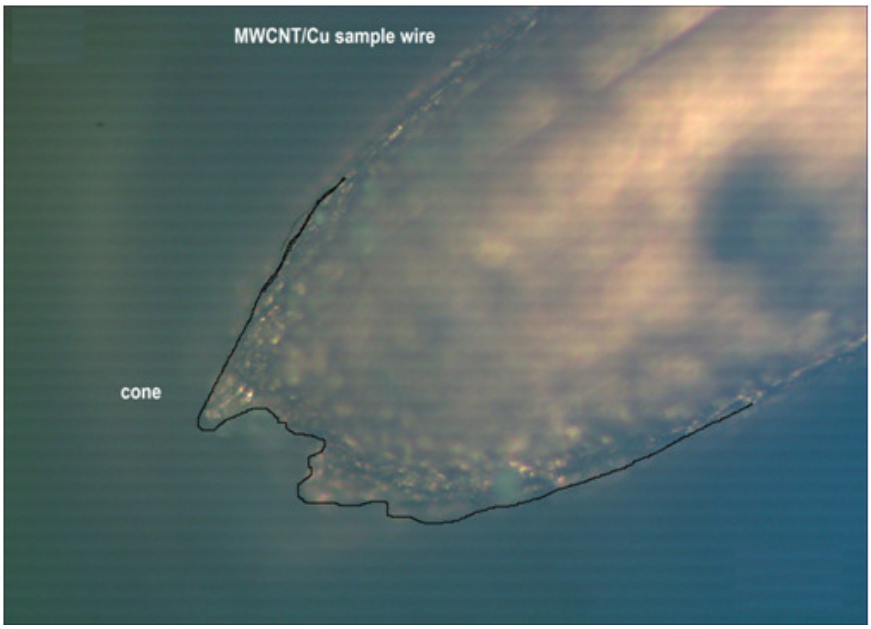

(a) Cone

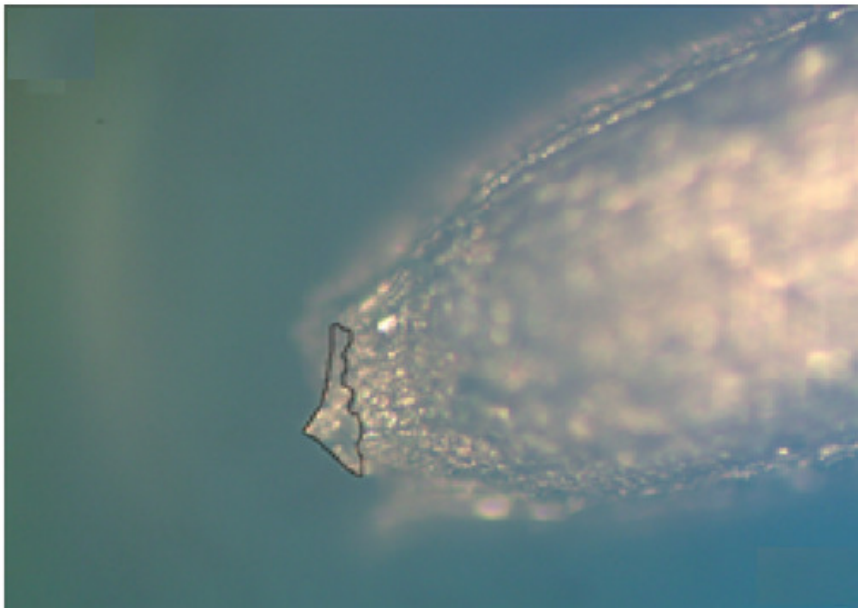

(b) Cup

Figure 5.5: (a) Cone after failure of sample having 100 mg/l concentration of MWCNT in electrolyte (b) Cup after failure of sample having 100 mg/l concentration of MWCNT in electrolyte (highlighted corrugated structure at the cup side all due to presence of MWCNT)

The stress-strain curves as shown in Figure 5.6 were obtained from the tensile test of MWCNT/Cu composites as well as the pure copper wire synthesized using newer method. In order to compare the tensile behaviour of the all the six samples, stress-strain curves are plotted on the same graph. From the Figure 5.6, it is can be observed that the ultimate tensile strength of the composite increases with increase in MWCNT concentration in the composite. The yield strength (stress corresponding to the 0.2% offset strain), Young's modulus (determined by calculating the slope of stress-strain curve in elastic limit) and ultimate tensile strength (maximum stress the sample can carry) were calculated from the stress–strain curves.

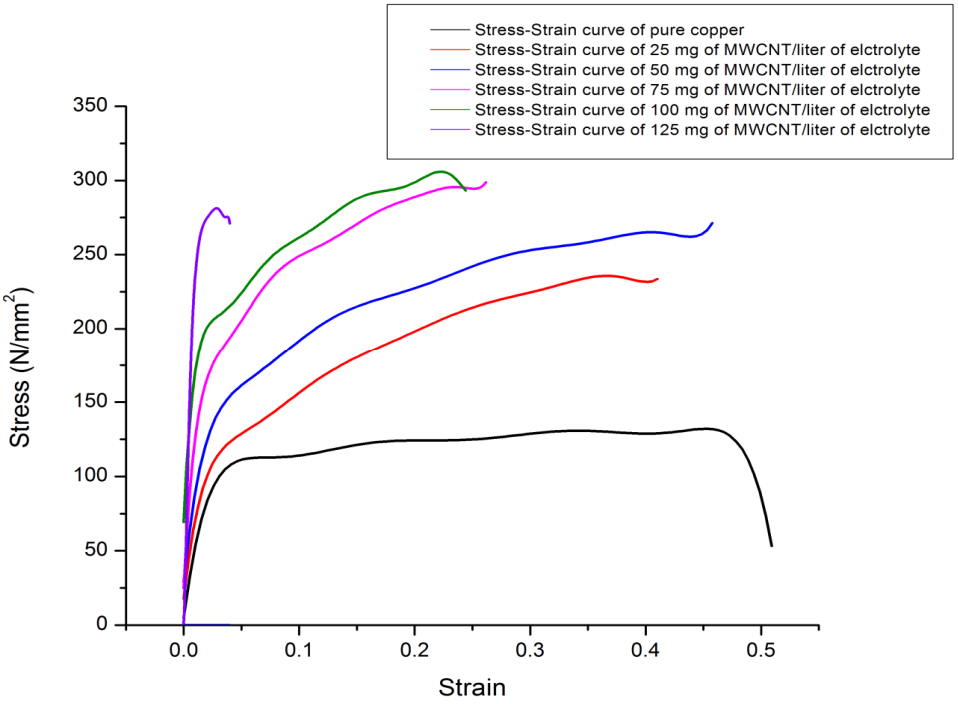

Figure 5.6: Stress and strain curve of MWCNT/Cu composite

5.2.1 Elastic modulus of MWCNT/Cu composite

All samples prepared and tested for tensile test were also characterised for elastic modulus. Metals are chosen for structural applications because they have desirable combinations of mechanical properties. Strength, stiffness and toughness are the desired properties of metal. However, the lower Young's modulus results in lower stiffness, which cause considerable elastic deformation under loading. If any metal is used for the transmission line which is having lower stiffness (elastic modulus), then due to lower

stiffness the self-weight of wire may cause deformation, which will result in the sagging of transmission line. Large elastic deformation of the wire is unacceptable. A large stiffness (elastic modulus) translates into smaller deformation due to self-weight and avoids the sagging of wire, and is thus desirable due to economic reasons.

All the six samples (MWCNT/Cu composite) were subjected to the tensile test for the elastic modulus. The gauge length of the sample was 20 mm whereas the diameter of the sample was 0.81 mm which was reduced to 0.6mm in test area forming a dog bone structure. The crosshead speed of universal testing machine used for tensile loading was 0.5 mm/min.

It has been observed that with increase in concentration of MWCNT in the electrolyte leading to increase in vol% of MWCNT in the copper matrix causes the Young's modulus of the composite to increase. On an atomic scale, elastic strain at macroscopic level is manifested as small changes in the inter-atomic spacing and the stretching of inter-atomic bond [2]. Therefore, the magnitude of the modulus of elasticity is a measure of the resistance to separation of adjacent atoms, that is, the inter-atomic bonding forces. Furthermore, this modulus is proportional to the slope of the inter-atomic force-separation curve. Figure 5.7 shows the force-separation curves for materials having inter-atomic bonds; the slope at r_0 is indicated.

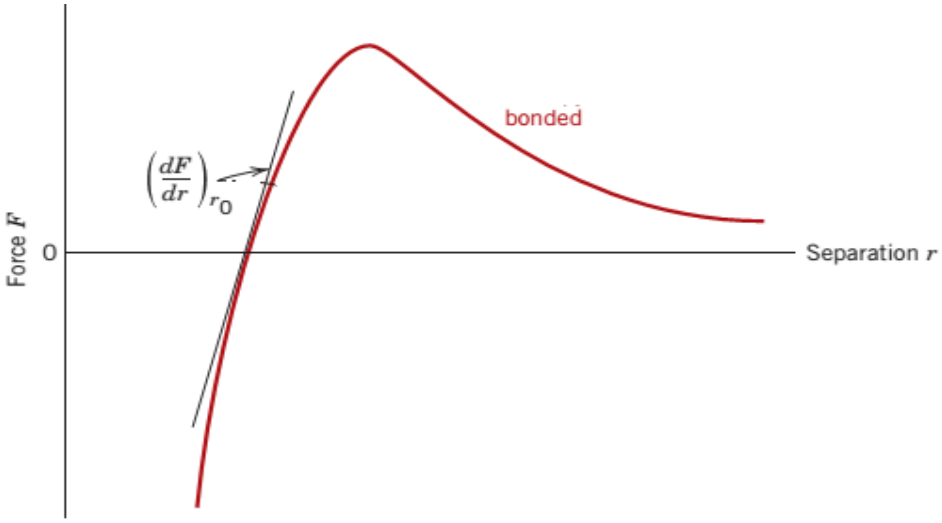

Figure 5.7: The graph is adopted from material science and engineering book by Callister [2]. Force versus inter-atomic separation of bonded atoms. The magnitude of the modulus of elasticity is proportional to the slope of each curve at the equilibrium inter-atomic separation r_0.

Furthermore, this modulus is proportional to the slope of the inter-atomic force-separation curve and is given by [2]:

$$E\alpha\left(\frac{dF}{dr}\right)_{r0} \tag{5.1}$$

In the present experiment the Young's modulus increases with addition of MWCNT in the copper matrix, this means the *(dF/dr)* slope increase with addition of MWCNT in the copper matrix. As the slope *(dF/dr)* is more means the inter-atomic force is more. This phenomenon shows that the there is proper bonding between carbon nanotube and metal matrix.

At the same time, the separation of the particles is avoided due to the strain developed around the reinforced MWCNT in the matrix. These strains also cause hindrance to the movement of the dislocation resulting in increase in Young's modulus. Table 5.1 shows the Young's modulus value for the six samples. The value of Young's modulus increases with addition of MWCNT in the composite. In the Table 5.1, 51.57 GPa is the Young's modulus corresponding to the pure copper synthesized by modified electro-co-deposition method. This value of Young' modulus is comparable to the Young's modulus of pure copper determined by W.M. Daoush [3] which was 51.6 GPa.

Table 5.1: Variation in Young's modulus values with increase of MWCNT concentration in composite

S.No.	Concentration of MWCNT in the electrolyte	Young's Modulus
	mg/l	GPa
1	0	51.57
2	25	60.18
3	50	74.55
4	75	90.57
5	100	91.935
6	125	110.73

As MWCNT is reinforced in the composite in the proportion of 25 mg/l, 50 mg/l, 75 mg/l, 100 mg/l and 125 mg/l the Young's modulus increases gradually to 60.18 to 110.73 as given in Table 5.1.

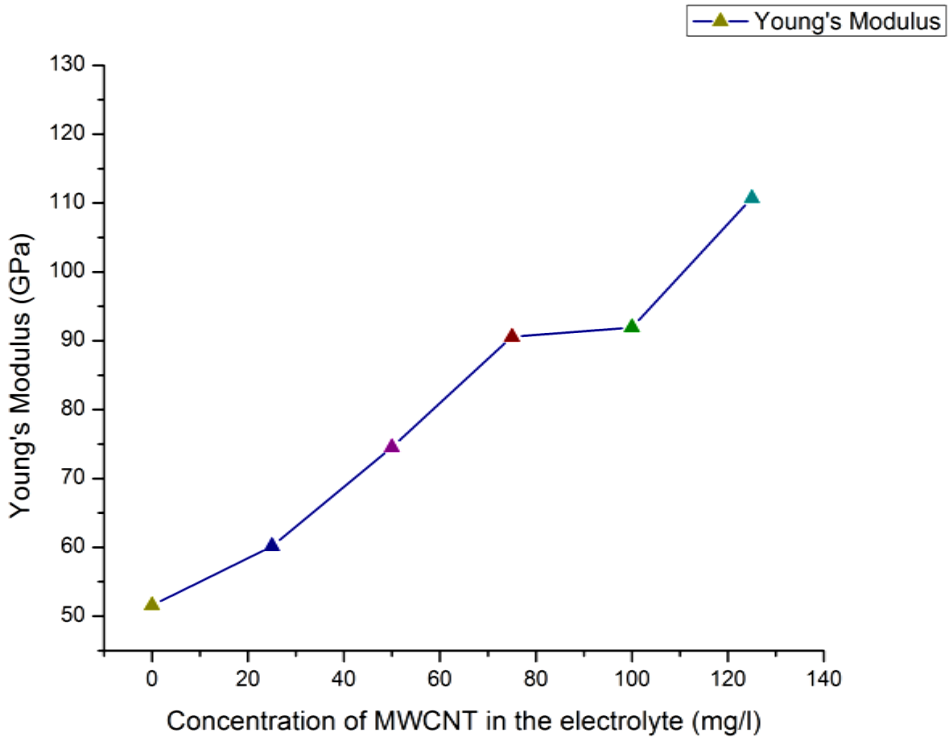

Figure 5.8: Change in Young's modulus (modulus of elasticity) with increase in concentration of MWCNT in the electrolyte

A plot is drawn for the change in Young's modulus with reinforcement of MWCNT in the copper composite and is shown in Figure 5.8. Young's modulus vs. concentration of MWCNT in the electrolyte is drawn in Figure 5.8 and the Young's modulus data corresponding to concentration of MWCNT in the electrolyte from Table 5.1 is plotted. It is observed from the plotted value in Figure 5.8 that the Young's modulus of MWCNT/Cu composite with 125 mg/l concentration of MWCNT in the electrolyte is determined as 110.73 GPa, which is about 2.15 times compared to that of pure Cu, which is measured as 51.57 GPa. The higher values of Young's modulus show that the MWCNT/Cu composites are successfully fabricated by electro-co-deposition.

From Figure 5.6, it has been observed that the percentage elongation of the sample in tensile testing decreases with increase in MWCNT concentration in the electrolyte. Percent elongation is determined by dividing the elongation at the moment of rupture by the initial gauge length and multiplying by 100. In case of pure copper, the percentage elongation is 38.4%, which was decreased to 32.9% with addition of 25 mg/l concentration of MWCNT in the electrolyte. Then it gradually comes down to 29%, 23.5%, 14.7% and 7% with addition of 50, 75, 100 and 125 mg/l concentration of

MWCNT in the electrolyte respectively. The data corresponding to decrease in elongation is given in Table 5.2. A Graph for Percent elongation vs. MWCNT concentration in the electrolyte is drawn and is shown in Figure 5.9. Form the Figure 5.9, it is observed that the percentage elongation also decreased by increasing the MWCNT concentration in the composite. This means the elastic properties of the copper were decreased by increasing the CNTs in the copper matrix.

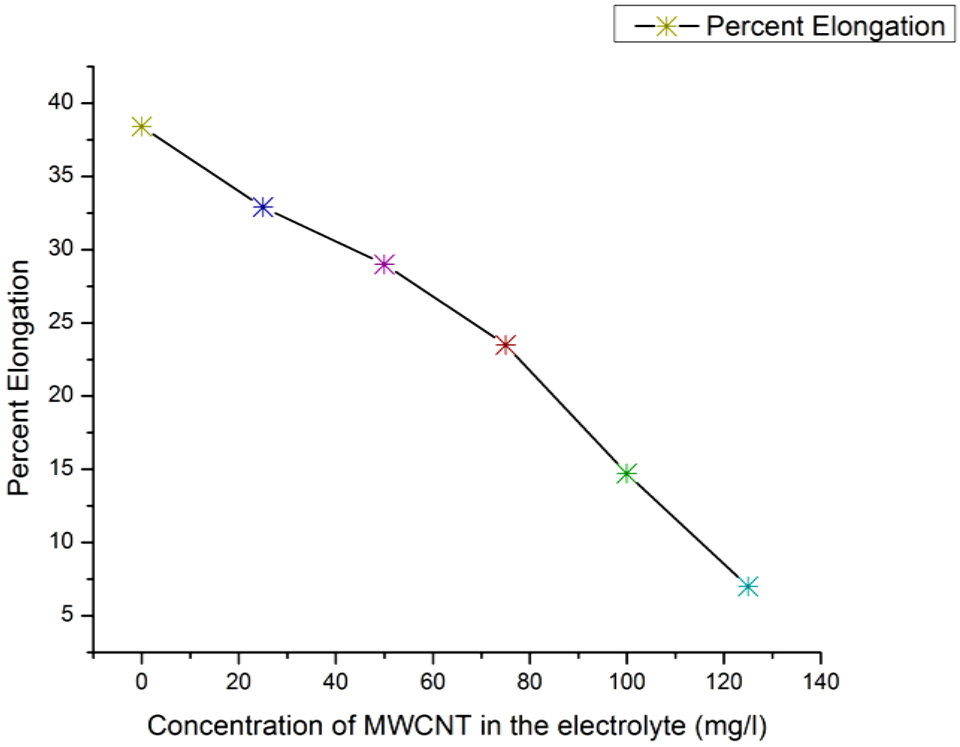

Figure 5.9 Graph showing the percentage elongation of MWCNT/Cu composite with respect to concentration of MWCNT in the electrolyte

Table 5.2: Data of variation in percentage elongation with increase in MWCNT concentration in electrolyte

S.No.	Concentration of MWCNT in the electrolyte(mg/l)	% elongation
1	Pure copper	38.4
2	25	32.9
3	50	29.0
4	75	23.5
5	100	14.7
6	125	7.0

5.2.2 Yield and ultimate tensile strength of MWCNT/Cu composite

A yield strength or yield point of a material is defined as the stress at which a material begins to deform plastically. Prior to the yield point the material will deform elastically and will return to its original shape when the applied stress is removed. When a yield point is not easily defined based on the shape of the stress-strain curve, an *offset yield point* is arbitrarily defined. The value for this is commonly set at 0.2% strain. A convention has been established, by which a straight line is constructed parallel to the elastic portion of the stress–strain curve at 0.2% strain offset. The stress corresponding to the intersection of this line and the stress–strain curve as it bends over in the plastic region is defined as the yield strength.

An image of stress vs strain taken from the Origin software is shown in Figure 5.10. In Figure 5.10, a line is indicated which is parallel to the elastic portion of the stress-strain curve. The line intersect with the stress-strain curve at A and the stress corresponding to that point is the yield strength which is 54 MPa for pure copper as seen from Figure 5.10. The coordinates of the parallel line are shown in object properties window in the Figure 5.10. Slope of that line can be determined by using these coordinates and it is the Young's modulus of the sample. A line is drawn parallel to the strain axis from the maximum stress value. This line intersects with the stress axis and the value corresponding to that intersects is the ultimate tensile strength.

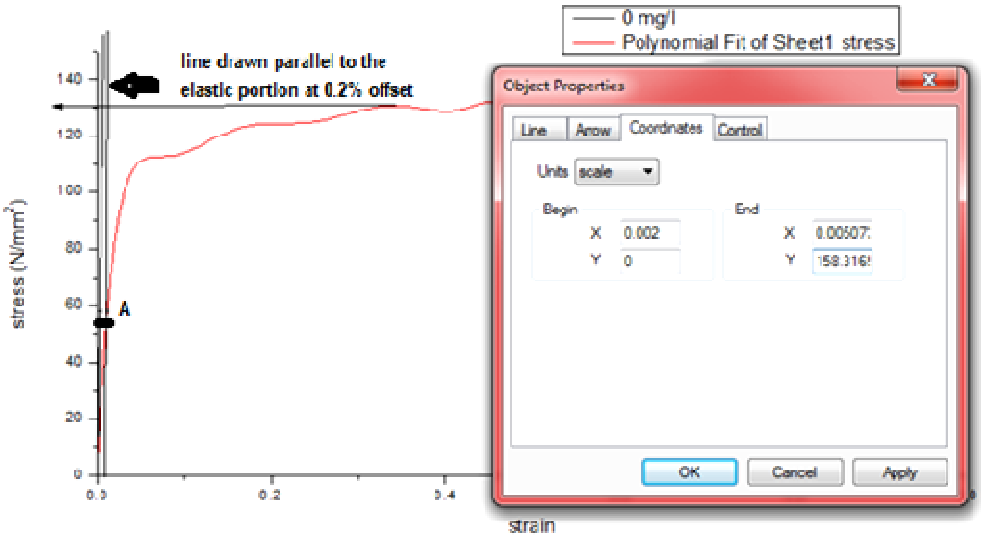

Figure 5.10: Stress-strain curve of pure copper and the object properties window shows the coordinate of line drawn parallel to the elastic region

Similarly, the yield strength and ultimate tensile strength of all six samples (25 mg/l, 50 mg/l, 75 mg/l, 100 mg/l and 125 mg/l) were determined. The values of yield strength corresponding to the MWCNT concentration in electrolyte are plotted in Figure 5.11. The wire produced from pure copper synthesized using electro-co-deposition method shows yield strength (0.2% offset strain) of 54 MPa and an ultimate tensile strength of 131 MPa. Then yield strength gradually increases to 62, 68.5, 85.18, 153.05 and 228 MPa with addition of 25, 50, 75, 100 and 125 mg/l concentration of MWCNT in the electrolyte respectively. According to Figure 5.11, the MWCNT/Cu composite produces yield strength of 228 MPa, which is about four times greater than that of pure copper. Moreover, as seen from Figure 5.12, the ultimate tensile strength of the MWCNT/Cu composite is about 306 MPa (for 100 mg/l concentration), which is more than two times greater than that of pure copper. The improvement observed in the MWCNT/Cu composite is comparable to the published articles [3,4].

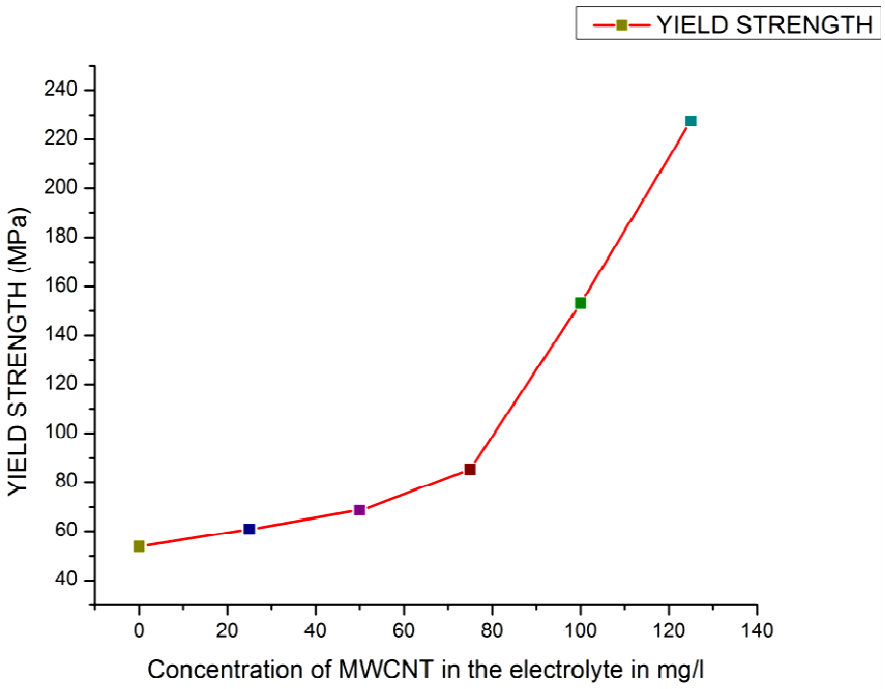

Figure 5.11: Yield strength versus concentration of MWCNT in the electrolyte in mg/l

The ultimate tensile strength increases to 235.5, 264.92, 295.41 and 306.11 MPa with addition of 25, 50, 75 and 100 mg/l concentration of MWCNT in the electrolyte. The improvement in the yield strength and ultimate tensile strength is attributed to homogeneous dispersion of MWCNT in the copper matrix at micro-level and strong

interfacial bonding, which improves the interfacial load-transfer ability. The increased strength is a sign of successful synthesis of MWCNT/Cu composite by electro-co-deposition process. However, the ultimate tensile strength of 125 mg/l concentration sample is 281.41 MPa, which is less than the 100 mg/l concentration sample. This is due to agglomeration of MWCNT on the grain boundaries. As discussed above the bond between the two MWCNT is very poor and which breaks easily and will not sustain higher load. As the sample subjected to tensile loading the agglomerated MWCNT get separated from each other which causes more strain at lower loading and results in low value ultimate tensile strength as seen in Figure 5.12.

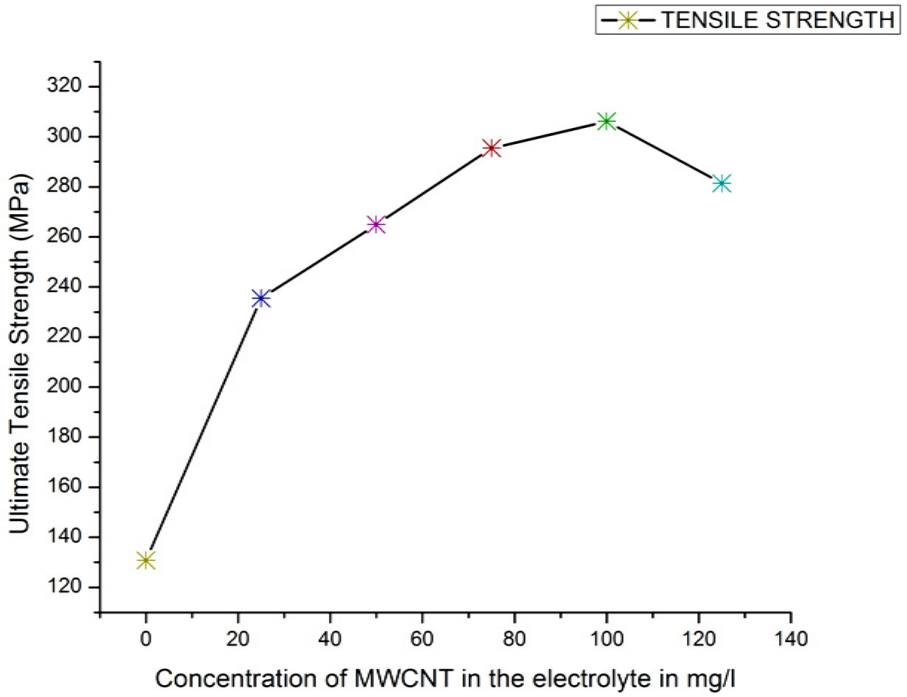

Figure 5.12: Ultimate tensile strength vs. concentration of MWCNT in the electrolyte

5.2.3 Micromechanical models of metal-carbon nanotube composite

In the previous section, it is considered that the strengthening mechanism is associated with load transfer from the metal matrix to the nanotubes. In general, micromechanical models are widely adopted by materials scientists to predict the tensile behaviour of micro-composites reinforced with fibres, whiskers and particulates. As CNTs exhibit large aspect ratios, we may ask whether the theories of composite mechanics and micromechanical models can be used to explain the mechanical properties of metal-CNT nanocomposites. Up till now, the principles of the mechanics of nano-materials (nano-

mechanics) are in the early stages of development [5–8]. The development of CNT-metal nanocomposites still faces obstacles due to the lack of basic understanding of the origins of strengthening, stiffening and toughening and the matrix-nanotube interfacial issues. The structure-property relationships of metal-matrix micro-composites are well recognized and reported. Several factors are known to contribute to the increments in yield strength and stiffness of metal-matrix micro-composites. These include effective load transfer from the matrix to the reinforcement, increasing dislocation density, homogenous dispersion of fillers and refined matrix grain size. Micromechanical models such as, Rule of mixtures (ROM), Cox and Halpin-Tsai are often used to predict the Young's modulus of discontinuously/continuously reinforced fibre composites. All these models are discussed in detail in Appendix-A.

The elastic modulus of the MWCNT/Cu composites was calculated using various models given in Appendix-A and the summary of calculated values are presented in Table 5.3. For the model calculations, the values of E_{Cu} =51.57 GPa, E_{CNT} =800 GPa, and aspect ratio l/d of CNT =400 have been assumed

Table 5.3: Summary of Young's modulus of the composite calculated using micromechanical models

Concentration of MWNT mg/L ⟹		**0**	**25**	**50**	**75**	**100**	**125**
Micromodels ⇩		Young's Modulus					
Rule of Mixture [5]	**Axial loading**	51.57	92.73	127.39	161.96	162.19	175.29
	Transverse loading	51.57	54.37	56.97	59.83	59.84	61
Voigt-Ruess model [15]		51.57	68.76	83.38	98.13	98.22	103.86
Halpin Tsai [18]		51.57	71.11	87.98	105.19	105.31	111.95
Cox Model [19]	$\chi_1 = 3/8$	51.57	65.01	76.37	87.73	87.81	92.11
	$\chi_2 = 1/5$	51.57	78.03	100.39	122.75	122.89	131.37
Experimental value		51.57	60.18	74.55	90.57	91.935	110.73

It is found that the predicted values from modified rule of mixture method (Voigt-Ruess Model) and Halpin-Tsai are close to the mean of the experimental value. Some of the

values calculated by Halpin-Tsai are larger than the measured values. This is attributed to the greater porosity compared to the standard parent material.

5.3 Effect of MWCNT content on the Hardness of Composites

The hardness of the MWCNT/Cu composites as well as the pure copper synthesized by electro-co-deposition method was measured by Vickers hardness test. Figures 5.13 shows that the Vickers hardness values of the composites increased from about 361 MPa (for pure copper fabricated by electro-co-deposition process) up to 412 MPa (at 125 mg/l concentration of MWCNT in electrolyte), equivalent to an increase of about 12.5%. From the Figure 5.13 it is clear that there is no considerable change in the hardness value of 100 mg/l and 125 mg/l concentration of MWCNT in the electrolyte. This means, when the MWCNT concentration in the electrolyte is less, the amount of MWCNT in the composite is less and which in turn helps in uniform distribution of MWCNT in the matrix and less agglomeration.

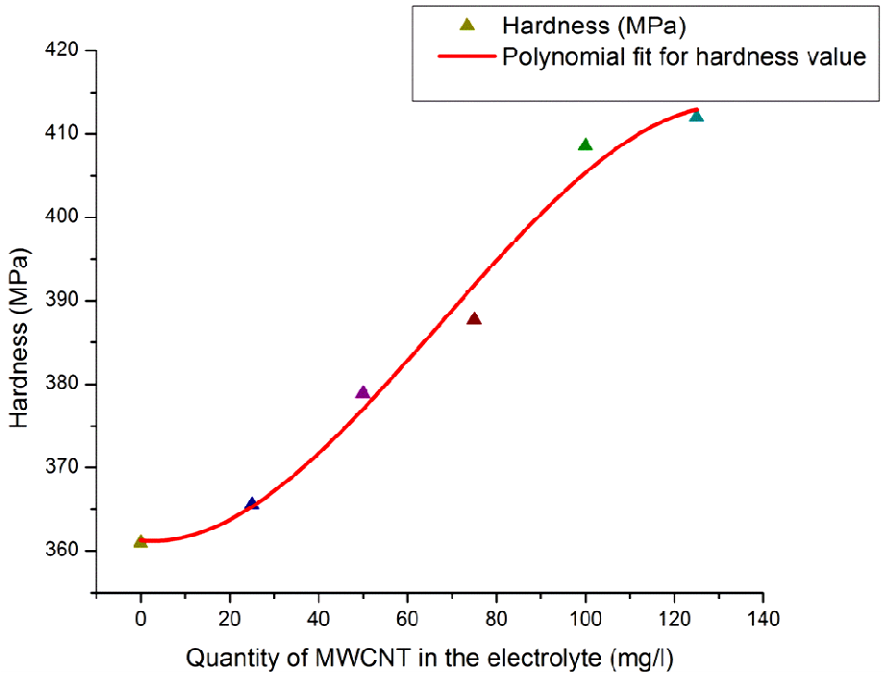

Figure 5.13: Hardness of MWCNT/Cu composite vs. concentration of MWCNT in the electrolyte

The efficient distribution of the MWCNT in the copper matrix results in enhancement in hardness and strength. The possible two reasons for this phenomenon are:

1. Close examination of Figure 5.14 shows that the copper particles are nucleated on the surface of the MWCNT. As the nucleation and the growth of copper took place on the surface of MWCNT, MWCNT occupies the grain boundary position and MWCNT will not cause an interstitial or subtitutional defect. In order to have the plastic deformation, dislocation must move across the grain boundary. However, the grain boundary acts as a barrier to dislocation movement because of the two grains are of different orientations and dislocation have to change the direction while passing into other grain. Now, in MWCNT/Cu composite, in addition to misorientation of grains, MWCNTs are present along the grain boundary and the crystal structure and chemical properties of MWCNT is altogether different than Cu crystal structure and therefore the boundaries between two different phases also cause impediments to movements of dislocations; this cause the hardening of MWCNT/Cu composite.

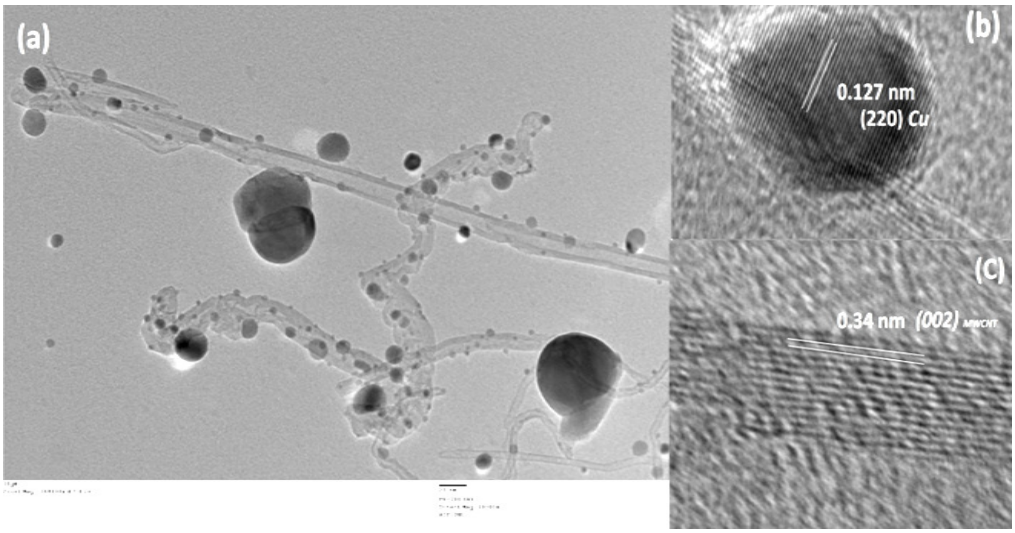

Figure 5.14: HRTEM images of MWCNT/Cu interface: (a) MWCNTs with copper particles nucleated on the surface; (b) lattice fringes of Cu, interplanar spacing d_{220}; (c) lattice fringes of MWCNT, interplanar spacing d_{002}

2. The size of MWCNT is much larger than the Cu atom and this is another reason for not creating an interstitial or subtitutional defect. The MWCNT instead will cause lattice strain in the copper matrix around the nanotubes. Hence, there will be repulsion between lattice strain caused due to MWCNT and dislocation strain

(depending on the type of strain), this will act as barriers for the movement of the dislocation, and the hardness of the composite enhances.

As the concentration of the MWCNT in the electrolyte increased from 100 mg/l to 125 mg/l, more MWCNTs were dispersed in the copper matrix. However, as the amount of MWCNT increases in the composite, agglomeration of the nanotube starts. The agglomeration was all due to the van der waals force, which was much weaker. Under applied load this agglomeration bond would have failed and therefore there was very less improvement in the hardness, (seen in the Figure 5.13) or may even cause decrease in hardness [9].

5.3.1 Effect of electrolysis parameters on hardness

We also investigated the influence of electrolysis parameters like current supplied, copper sulphate concentration in the electrolyte, multiwalled carbon nanotube content, pH and ultra-sonication time of electrolyte on hardness of the pellets formed from the composite powder. The Taguchi's statistical method was used to design the experiments and hierarchical levels are drawn to conclude a most significant parameter, which can alter electrical properties of the MWCNT/Cu composite. The available literature on CNT/copper composite lacks any statistical investigation to conclude on parameter, which may significantly influence mechanical property of the composite.

5.3.1.1 *Experimental design*

Experimental design has several advantages. It aids in identifying the vital process parameter, which will control and improves the process. It also helps in the development of the new methods for which historical data are not available. Conventional methods of design of experiments required a large number of experiments with increase in number of parameters and its levels. Alternatively, Taguchi has proposed more than 60 signal to noise (S/N) ratio functions [10]. In the present work we have investigated, as the maximum hardness as performance index and have chosen larger-the-better S/N ratio.

$$\frac{S}{N} = -10\log\frac{1}{N_i}\sum\frac{1}{y_i^2} \tag{5.10}$$

where, y_i denotes the N_i observations of response variables.

In modified electro-co-deposition method, major parameters, which influence the quality of formed powder, are 1) pH 2) current supplied 3) MWCNT concentration in

the electrolyte 4) ultra-sonication time of electrolyte and 5) copper sulphate concentration in the electrolyte. With the five parameters as variables and considering three levels of each variable, a fractional factorial design of 3^5 experiments is done with L_{18} orthogonal array. Table 5.4 shows the five control parameters and their levels. The five Parameters are arranged in 2-6 columns in the standard L_{18} orthogonal array as shown in Table 5.5.

Table 5.4: Control parameters and their levels

Parameters	**Level 1**	**Level 2**	**Level 3**
A: pH	1	2	3
B: Current (amp)	4	6	8
C: MWCNT (mg/l)	50	75	100
D: ultra-sonication time (hrs)	3	4	6
E: $CuSO_4.5H_2O$ concentration gm/l	75	100	125

Table 5.5: The basic Taguchi L_{18} orthogonal array

Expt	**A**	**B**	**C**	**D**	**E**	**Notation**		**Expt**	**A**	**B**	**C**	**D**	**E**	**Notation**
1	1	1	1	1	1	$A_1B_1C_1D_1E_1$		10	1	1	3	3	2	$A_1B_1C_3D_3E_2$
2	1	2	2	2	2	$A_1B_2C_2D_2E_2$		11	1	2	1	1	3	$A_1B_2C_1D_1E_3$
3	1	3	3	3	3	$A_1B_3C_3D_3E_3$		12	1	3	2	2	1	$A_1B_3C_2D_2E_1$
4	2	1	1	2	2	$A_2B_1C_1D_2E_2$		13	2	1	2	3	1	$A_2B_1C_2D_3E_1$
5	2	2	2	3	3	$A_2B_2C_2D_3E_3$		14	2	2	3	1	2	$A_2B_2C_3D_1E_2$
6	2	3	3	1	1	$A_2B_3C_3D_1E_1$		15	2	3	1	2	3	$A_2B_3C_1D_2E_3$
7	3	1	2	1	3	$A_3B_1C_2D_1E_3$		16	3	1	3	2	3	$A_3B_1C_3D_2E_3$
8	3	2	3	2	1	$A_3B_2C_3D_2E_1$		17	3	2	1	3	1	$A_3B_2C_1D_3E_1$
9	3	3	1	3	2	$A_3B_3C_1D_3E_2$		18	3	3	2	1	2	$A_3B_3C_2D_1E_2$

5.3.1.2 *Hardness measurements*

The Vickers test is reliable for measuring the hardness of metals. The Vickers machine uses a penetrator that is square, but tipped on one corner so it has the appearance of a playing card 'diamond' and an angle of 136 degrees between opposite faces. The impression left by the Vickers penetrator is a dark square on a light background. The Vickers impression is more easily "read" for area size than the circular impression of the Brinell method. Like the Brinell test, the Vickers number is determined by dividing the load by the surface area of the indentation (H = P/A). The load varies from 1 to 120 kilograms. To perform the Vickers test, the specimen is placed on an anvil that has a screw-threaded base. The anvil is turned raising it by the screw threads until it is close to the point of the indenter. With start lever activated, the load is slowly applied to the indenter. The full load is normally applied for 10 to 15 seconds. The load is released and the anvil with the specimen is lowered. The two diagonals of the indentation left in the surface of the material after removal of the load are measured using a microscope and their average calculated. The area of the sloping surface of the indentation is calculated. The Vickers hardness is the quotient obtained by dividing the kgf load by the square mm area of indentation.

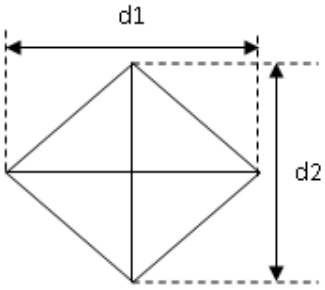

F = load in kgf

d = arithmetic mean of two diagonals d_1 and d_2

$$HV = \frac{(2F \sin\ (136^\circ/2))}{d^2} = \frac{1.8544\ F}{d^2}$$

WPM Leipzig Hardness testing machine was used for measuring the Vickers hardness for the pure copper sample and the MWCNT/Cu composites. The hardness was measured under a load of 5 kg [11].

5.3.1.3 *Statistical analysis of experimental results*

The hardness obtained for the product in all the two sets (each with four readings) of eighteen experiments, mentioned in Table B.1 in Appendix-B, have been subjected to statistical analysis.

A) Taguchi analysis

The experiments are performed to optimize the parameters in order to maximize the hardness hence larger the better characteristic S/N ratio had been used. In Appendix-B, Table B.1 shows the actual indentation data whereas; Table B.3 shows Experimental results for vicker hardness and their corresponding S/N ratio for L_{18} standard orthogonal array.

The average S/N ratios for all five parameters for all levels are plotted and are shown in Figure 5.15. From the Table 5.6 it is clear that the MWCNT concentration is one of the most significant parameter, which influences the hardness of the product. The product obtained by increasing MWCNT shows higher hardness. The other parameters namely concentration of $CuSO_4$, pH of the electrolyte, concentration of MWCNT, current and sonication follows in this order to influence the product hardness.

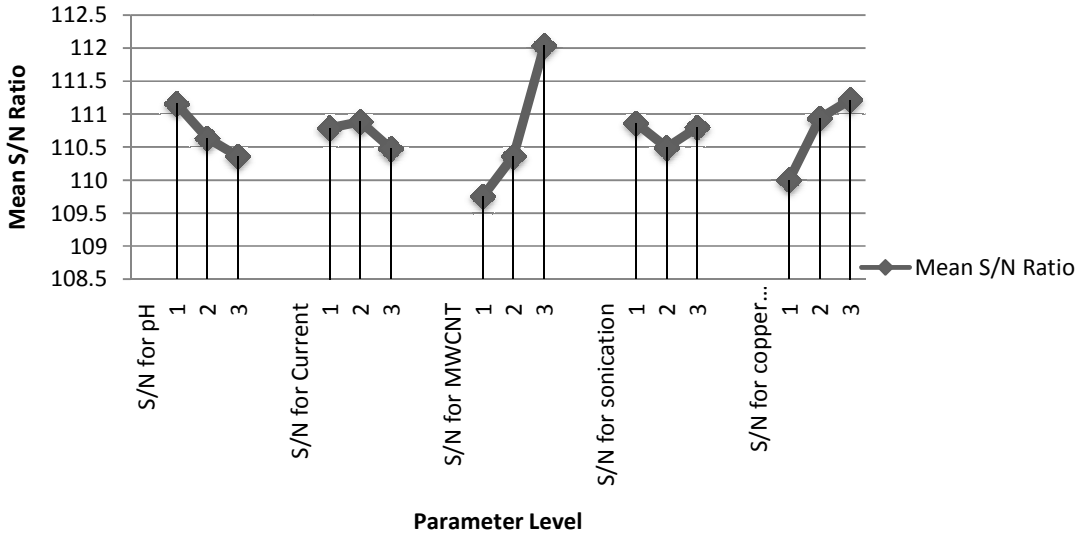

Figure 5.15: The larger the better S/N graph for resistivity

From Figure 5.15, it is clear that the level 3 of parameter C will cause the highest hardness value and hence highest MWCNT concentration will be the best choice to have higher hardness. Similarly, for the second more influencing parameter that is $CuSO_4$ concentration (parameter E) level 3 is more influencing. The pH of the solution, current and sonication time are the third, fourth and fifth parameters and their corresponding levels are 1, 2 and 1 are suitable. Therefore, the best combination of the process is $A_1B_2C_3D_1E_3$. As the experiment of this combination was not performed in the set of eighteen experiment, separate three experiments were conducted with this combination. The observed hardness

average values of three samples were 426 MPa, 437 MPa, and 442 MPa. The average hardness value is found to be 435 MPa. Further, we have done the Pareto ANOVA to confirm the observation.

Table 5.6: Effect calculation by determining the range between S/N ratio

	S/N for pH		S/N for current		S/N for MWCNT		S/N for sonication		S/N for copper sulphate
1	111.157551	1	110.789622	1	109.754	1	110.86	1	110.0015
2	110.63459	2	110.8877025	2	110.364	2	110.49	2	110.9354
3	110.362825	3	110.4776414	3	112.036	3	110.8	3	111.2181
	0.79472586		0.410061032		2.2818		0.3705		1.216609
	3		4		1		5		2

B) Pareto ANOVA analysis

Pareto ANOVA[12] is a simplified ANOVA method using 80/20 Pareto principle. This method is quick and easy to analyze the results of parametric variation in an experiment without requirement of detailed ANOVA and f-test. Pareto ANOVA also helps in identifying the most significant parameter among all the parameters as well as the relevant optimum. Table 5.7 shows the Pareto analysis of parameter's S/N ratio for hardness of the samples reported in the work.

From Pareto chart Figure 5.16, the contribution of parameter C is around 68.09% followed by parameter E, A, B and D. The conclusion corroborates with the analysis done using Taguchi method in previous section.

Table 5.7: Pareto ANOVA analysis of S/N ratio of parameters for the resistivity

	S/N for pH	S/N for current	S/N for MWCNT	S/N for sonication time	S/N for $CuSO_4$
1	111.158	110.790	109.754	110.862	110.001
2	110.635	110.888	110.364	110.492	110.935
3	110.363	110.478	112.036	110.801	111.218
	110.718	110.718	110.718	110.718	110.718
Sum of Squares of difference	0.979	0.275	8.374	0.236	2.432
contribution%	7.961	2.237	68.099	1.922	19.780

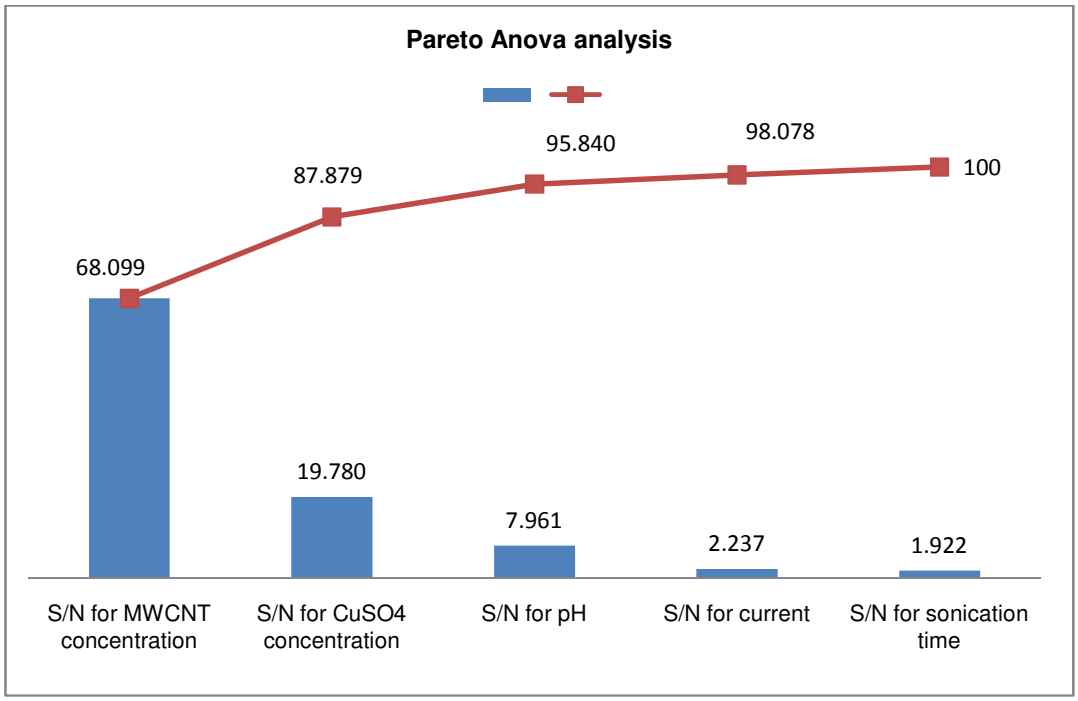

Figure 5.16: Pareto diagram for determining contribution of parameters

C) Discussion

Pure copper pellets and MWCNT/Cu composite copper pellets were fabricated by modified electro-co-deposition method and tested for hardness using WPM Leipzig Hardness testing machine. All the samples were tested under the identical conditions with the help of hardness tester.

From the results, it is observed that the hardness of the copper composite increases with addition of MWCNT in the copper matrix. By Taguchi and Pareto ANOVA analysis, it was concluded that the MWCNT concentration in the electrolyte is the most influencing parameter of the process for hardness of the composite. The presence of MWCNT on the grain boundary create hurdle for the movement of the dislocation and hence requires more power for penetration, which result in increase in hardness.

More concentration of the $CuSO_4$ in the electrolyte causes higher apparent density of the copper powder [13,14]. This increase in the apparent density helps in improving the density of composite, which will result in improvement in the hardness value. The pH value of the electrolyte is the third influencing parameter. Increase in concentration of H_2SO_4 results in decrease in pH value of the electrolyte, in turn the grain size decrease [15], which is one of the desirable characteristic. With higher concentration of electrolyte the conductivity of the electrolyte also increases. With the value of pH 1 or 2 the grain

size will be in the range of 8 nm [15]. Smaller the grain size, larger the force required for the deformation and hence its hardness improves with higher concentration of H_2SO_4.

Current density and the sonication time were the least significant parameters for the hardness value of the composite. However, smaller current density causes dendritic growth of copper which helps in the uniform dispersion as well as entrapment of the MWCNT in the copper matrix [16] and proper sonication also helps in the uniform dispersion of the MWCNT [17].

5.4 Conclusion

1. The formed wire have better mechanical properties in comparison to pure copper wire formed by the modified method and also in comparison to commercially available standard copper wire. The results of betterment of properties of form copper wire is attributed to homogeneous dispersion of MWCNTs in the Cu matrix which in turn is due to the modification of the electro-co-deposition method.
2. The wire produced from MWCNT/Cu composite powder shows four times yield strength (0.2% offset strain) than the pure copper fabricated by the same method. The ultimate tensile strength of the MWCNT/Cu composite is about 306 MPa (for 100 mg/l concentration), which is more than two times greater than that of pure copper. The hardness of MWCNT/Cu composite also shows improvement in comparison to that of the pure copper.
3. From the experiments and statistical analysis it has been observed that the hardness of the CNT reinforced copper composite synthesized by the modified electro-co-deposition is increased in all the products formed in all the experiments.
4. Characterization results show that the CNTs are well dispersed in the copper matrix and product formed is having uniform hardness.
5. The statistical study of effect on modified electro-co-deposition parameter on the hardness carried out by Taguchi statistical method showed that the concentration of MWCNT and $CuSO_4$ concentration in the electrolyte had the greatest influence on the synthesis of MWCNT reinforced copper composite. The bath composition like pH of the solution, sonication time and current supplied presented less significance on hardness of the composite.

In the next chapter, electrical characterization of the formed MWCNT/Cu composite is discussed.

References:

[1] Smallman RE, Ngan AHW. Physical Metallurgy and Advanced Materials. 7th ed. Burlington, MA 01803: Elsevier; 2007.

[2] Callister WD, Rethwisch DG. Fundamentals of Material Scienec and Engineering An Integrated Approach. 4 th. John wiley and Sons, Inc; 2012.

[3] Daoush WM, Lim BK, Mo CB, Nam DH, Hong SH. Electrical and mechanical properties of carbon nanotube reinforced copper nanocomposites fabricated by electroless deposition process. Mater Sci Eng A 2009;513-514:247–53.

[4] Chai G, Sun Y, Sun J "Jenny", Chen Q. Mechanical properties of carbon nanotube–copper nanocomposites. J Micromechanics Microengineering 2008;18:035013.

[5] Guz IA, Rodger AA, Guz AN, Rushchitsky JJ. Developing the mechanical models for nanomaterials. Compos Part A Appl Sci Manuf 2007;38:1234–50.

[6] Guz IA, Rushchitsii YY. Comparison of Mechanical Properties and Effects in Micro- and Nanocomposites with Carbon Fillers (Carbon Microfibers, Graphite Microwhiskers, and Carbon Nanotubes). Mech Compos Mater 2004;40:179–90.

[7] Liu WK, Park HS, Qian D, Karpov EG, Kadowaki H, Wagner GJ. Bridging scale methods for nanomechanics and materials. Comput Methods Appl Mech Eng 2006;195:1407–21.

[8] Bhushan B. Nanotribology and nanomechanics. Wear 2005;259:1507–31.

[9] Feng Y, Yuan HL, Zhang M. Fabrication and properties of silver-matrix composites reinforced by carbon nanotubes. Mater Charact 2005;55:211–8.

[10] Mitra A. Introduction to quality control and improvement fundamentals of quality control. 3 rd ed. Hoboken, New Jersey: John wiley and Sons, Inc.; 2008.

[11] Deng C, Zhang X, Wang D, Lin Q, Li A. Preparation and characterization of carbon nanotubes/aluminum matrix composites. Mater Lett 2007;61:1725–8.

[12] Ghani J., Choudhury I., Hassan H. Application of Taguchi method in the optimization of end milling parameters. J Mater Process Technol 2004;145:84–92.

[13] Orhan G, Gezgin G. Effect of electrolysis parameters on the morphologies of copper powder obtained at high current densities. J Serbian Chem Soc 2012;77:651–65.

[14] Maksimović V, Pavlović LJ, Pavlović M, Tomić M. Characterization of Copper Powder Particles obtained by Electrodeposition V. Assoc Metall Eng Serbia 2009;15:19–27.

[15] Natter H, Hempelmann R. Nanocrystalline Copper by Pulsed Electrodeposition: The Effects of Organic Additives, Bath Temperature, and pH. J Phys Chem 1996;3654:19525–32.

[16] Pavlović MG, Pavlović LJ, Maksimovi VM, Nikolić ND, Popov KI. Characterization and Morphology of Copper Powder Particles as a Function of Different Electrolytic Regimes. Int J Electrochem Sci 2010;5:1862–78.

[17] Belgamwar SU, Sharma NN. Synergistic electro-co-deposition and molecular mixing for reinforcement of multi-walled carbon nanotube in copper. Mater Sci Eng B 2013;178:1452–7.

Chapter 6

Electrical Characterization of MWCNT/Cu Composite

6.1 Introduction

As studied in the previous chapters, carbon nanotubes, possesses remarkable mechanical and physical properties [1–6], have become an ideal reinforcing filler element in composite materials for enhancing mechanical and functional properties. In recent years, great interest has developed in the fabrication and study of carbon nanotube (CNT) reinforced metals. However, the effective fabrication of CNT-reinforced metals depends on the homogenous and uniform dispersion of CNTs in the metal matrix and the interfacial adhesion between them. Indeed, the intrinsic van der Waals forces among CNTs always lead to agglomeration, which lowers the reinforcement between CNTs and matrix.

Due to its excellent electrical conductivity, pure Cu was widely used in the electronics industry, but its intrinsic softness often caused the failure of electronic components. Strengthening of pure copper through various ways usually leads to a considerable increase in electrical resistivity [7,8]. Hence, though there is improvement in the mechanical properties but it is at the cost of electrical property, which is unacceptable. However, MWCNT/Cu composite fabricated by modified electro-co-deposition method showed good interfacial bonding between the carbon nanotube and copper matrix. In the previous chapter, it is pointed out that CNT-reinforced Cu displays high tensile strength, modulus of elasticity, hardness and ultimate tensile strength. The experimentally observed electrical resistivity for 9 *nm* diameter CNT is 0.88 to $5.1\times10^{-8}\,\Omega$m [9–12] is comparable to copper, and the current carrying capacity (ampacity) is $1000\times10^{6}\,A/cm^{2}$ which is 1000 times higher than the copper [10]. We found that the electrical resistivity of the form composite was decreased by 8 to 10 % compare to that of pure Cu.

6.2 Resistivity Measurement

Micro-area's resistance is surface resistance of an object ignoring the thickness, and it is expressed with Rs (surface resistance) and the unit is ohm (Ω). The testing methods for finding resistance are classified into two kinds. One is non-contact measurement method,

and the other is contact measurement method. Comparing both of them, the former has many advantages, such as non-contact, non-damage, and non-stain with the tested sample. However, it has disadvantages such as the equipments are more complicated and the cost is too high. The testing area is more limited. But, the contact testing method is relatively more economic and more often used method. Among them, four-point probe [13–15] testing method is used widely.

6.3 Four Point Probe Method

A four-point method is a simple system for measuring the resistivity of materials with low resistance such as metals and semiconductors. By passing a current through two outer probes and measuring, the voltage through the inner probes allows the measurement of the resistivity (Figure 6.1). Non-ohmic contact resistance (resistance which does not obey ohm's law) at probes 1, 4 and metal is eliminated in this method.

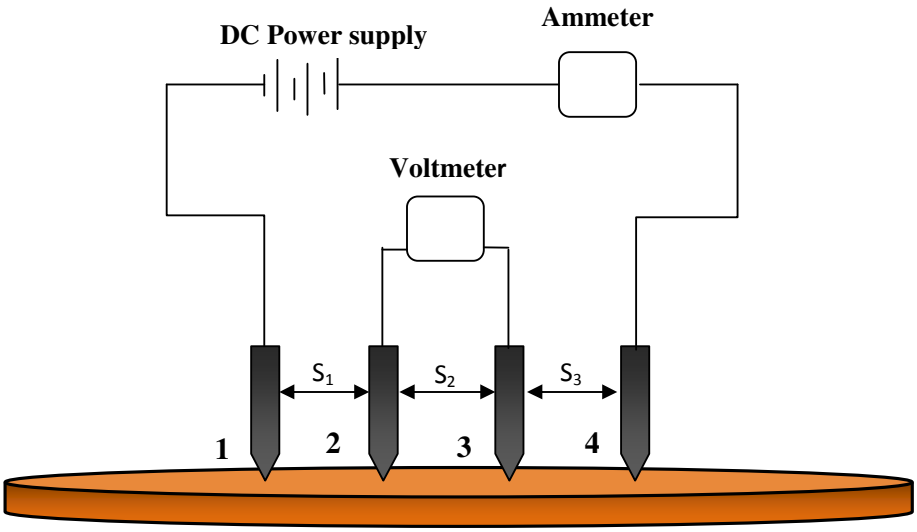

Figure 6.1: Schematic of four-point probe

If the sample has any resistance to the flow of electrical current, then there will be a drop of voltage as the current flows along the sample, for example between the two wires (or probes) labeled 2 and 3 in Figure 6.1. The voltage drop between probes 2 and 3 can be measured by a voltmeter. The resistance of the sample between probes 2 and 3 is the ratio of the voltage registering on the voltmeter to the value of the output current of the power supply. The high impedance of the voltmeter minimizes the current flow through the portion of the circuit comprising the voltmeter. Thus, since there is no

potential drop across the contact resistance associated with probes 2 and 3, only the resistance associated with the sample between probes 2 and 3 is measured.

In the four-point probe setup, the voltage potential V adjacent to a probe carrying current can be given by:

$$V = \frac{\rho I}{2\pi r} \tag{6.1}$$

where, ρ is the surface resistivity of a material of semi-infinite size, I is the current in the probe, and r is the distance between the voltage measurement and the current probe.

Using dimensions in Figure 6.1, the voltage at probe no.2 is,

$$V_2 = \frac{\rho I}{2\pi\left[\left(\frac{1}{S_1}\right)-\left(\frac{1}{S_2+S_3}\right)\right]} \tag{6.2}$$

The voltage at probe no.3 is,

$$V_3 = \frac{\rho I}{2\pi\left[\left(\frac{1}{S_1+S_2}\right)-\left(\frac{1}{S_3}\right)\right]} \tag{6.3}$$

To get total voltage, subtract the voltages $V_2 - V_3$,

$$V = \frac{\rho I}{2\pi\left[\left(\frac{1}{S_1}\right)+\left(\frac{1}{S_3}\right)-\left(\frac{1}{S_2+S_3}\right)-\left(\frac{1}{S_1+S_2}\right)\right]} \tag{6.4}$$

Rearranging to get the resistivity,

$$\rho = \frac{2\pi V\left[\left(\frac{1}{S_1}\right)+\left(\frac{1}{S_3}\right)-\left(\frac{1}{S_2+S_3}\right)-\left(\frac{1}{S_1+S_2}\right)\right]}{I} \tag{6.5}$$

However, if all probe spaces are equal sizes, then above equation is reduced to

$$\rho = 2\pi s\left(\frac{V}{I}\right)\rho \tag{6.6}$$

where, 'V' is the voltage drop between probes 2 and 3, the 'I' is current in the circuit (between probes 1 and 4), and 's' is the distance between probes 2 and 3.

Electrical resistivity measurements of MWCNT/Cu composite pellet sample

The electrical resistivity of six pellets samples were measured by the four-point probe method (Signatone: QuadMap-M80). With intension to minimize the resistance heating, 1 *A* current was supplied through the sample. The ambient was maintained at 23°C All samples were tested at five sites on pellets as shown in Figure 6.2. Correction factors according to the positioning of the four point probe on the sample are used [16] and the resistivity values are determined from the *V/I* (*V* is voltage and *I* is current) values. Figure 6.3 (a) and (b) shows images of mapped pure copper pellet, and one of the MWCNT reinforced copper pellet synthesized by modified electro-co-deposition method. The average resistivity of the pure copper pellet is found to be $5.403\times10^{-08}\,\Omega\,\mathrm{m}$ and that of the MWCNT reinforced copper pellet is $5.067\times10^{-08}\,\Omega\,\mathrm{m}$.

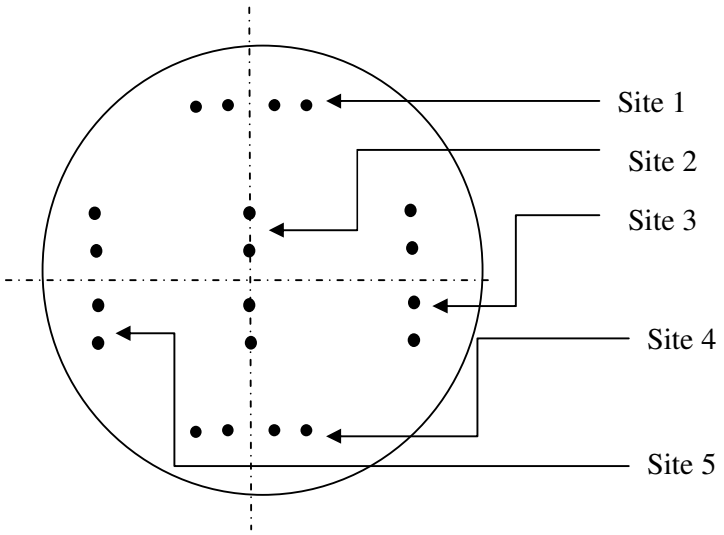

Figure 6.2: Five test sites on the sample

Data corresponding to each pellet is given below the respective figures in Figure 4.3. As seen in the image, the electrical resistivity of MWCNT reinforced copper composite is slightly on lower side compare to pure copper, which is also fabricated by the same method. However, this result contradicts with the several previous results [8,17–20]. From Figure 6.3(b), the maximum variation of resistance $\frac{V}{I}(\Omega/sq)$ is around 7.14 %, which is almost negligible. Small variation in resistance across the surface confirms uniform dispersion and proper reinforcement of MWCNT in the copper matrix.

Pure Copper

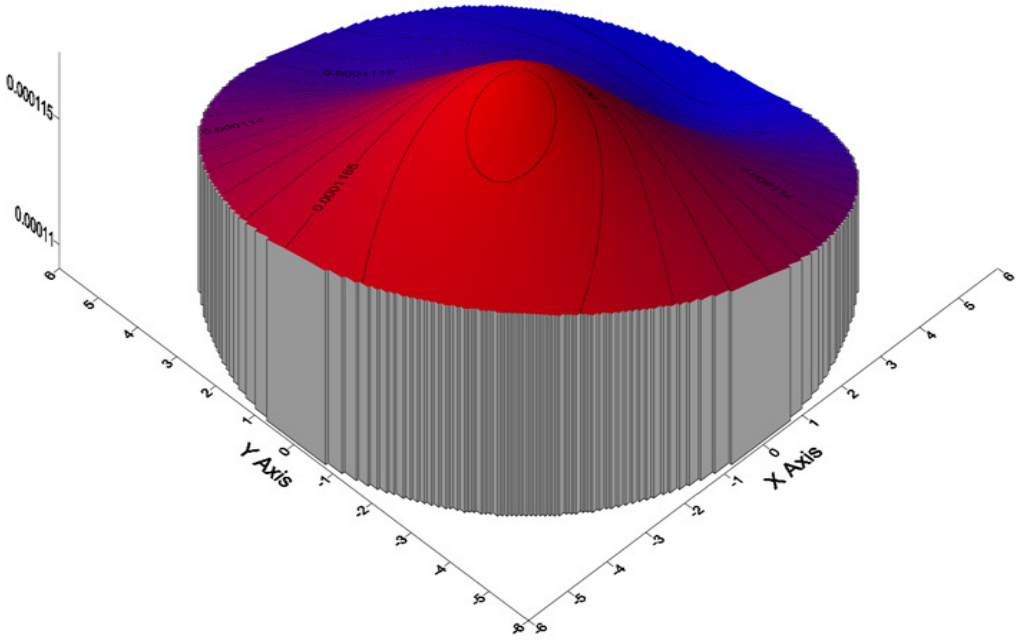

(a) Average resistivity $= 5.4031\times10^{-08}\,\Omega$ m

100 mg/l MWCNT concentration in the electrolyte

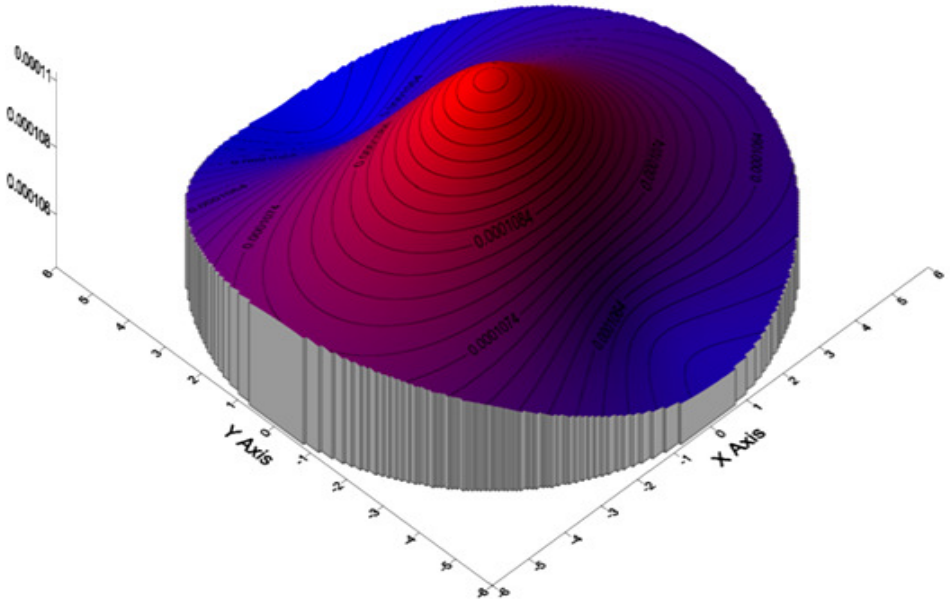

(b) Average resistivity $= 5.067\times10^{-08}\,\Omega$ m

Figure 6.3: Mapped image of pellet synthesized by the method of modified electro-co-deposition (a) pure copper (b) MWCNT reinforced copper

Table 6.1(a): Resistivity data for pure copper pellet

Pt	*V/I*	Thk((μm)	Res(Ω*m*)	Conductivity(Ω*m*)$^{-1}$
1	26×10^{-6}	600	6.23×10^{-8}	1.61×10^{7}
2	24×10^{-6}	600	4.94×10^{-8}	2.02×10^{7}
3	25×10^{-6}	600	5.14×10^{-8}	1.94×10^{7}
4	26×10^{-6}	600	5.35×10^{-8}	1.87×10^{7}
5	26×10^{-6}	600	5.35×10^{-8}	1.87×10^{7}

Table 6.1(b): Resistivity data for MWCNT/Cu composite pellet (100 mg/l MWCNT concentration in electrolyte)

Pt	*V/I*	Thk (μm)	Res(Ωm)	Conductivity(Ωm)$^{-1}$
1	25×10^{-6}	600	5.99×10^{-8}	1.67×10^{7}
2	24×10^{-6}	600	4.94×10^{-8}	2.02×10^{7}
3	23×10^{-6}	600	4.73×10^{-8}	2.11×10^{7}
4	24×10^{-6}	600	4.94×10^{-8}	2.02×10^{7}
5	23×10^{-6}	600	4.73×10^{-8}	2.11×10^{7}

Actual resistivity of the commercial copper is about 1.678 x10^{-8} Ωm [21]. The values of copper and MWCNT/Cu resistivity, which were observed during experimentation was about 3 to 4 time higher than the commercial copper. As seen in the previous chapter, the density of the copper pellet and MWCNT/Cu composite fabricated by modified electro-co-deposition method, have less density compare to the commercial copper. Decrease in density may be due to the porous nature of the pellets. The porous nature of the copper and MWCNT/Cu composite and random orientation of MWCNT in the MWCNT/Cu composite causes increase in resistivity. Density of MWCNT/Cu composite is much less than the pure copper pellet and this is due to the presence of MWCNT in the composite.

6.4 Specific Conductivity of MWCNT/Cu Composite Pellet

Specific conductivity is the ratio of conductivity to the density of the composite [22]. The resistivity of the MWCNT/Cu composite pellet is equal or less than the pure copper pellet as shown in Table 6.2, which is due to the presence of MWCNT in the composite as well as the voids present in the composite pellet. However, the density of the MWCNT/Cu composite decreases with increase in MWCNT concentration in the composite. Hence, the specific conductivity of the MWCNT/Cu composite will be greater than the pure copper fabricated in an identical protocol. For the following calculation, the volume of pellet is 7.6 cm^3.

Table 6.2: Data showing specific conductivity of the composite

Concentration of MWNT in electrolyte mg/l	Vol% of MWCNT	Resistivity Ωm	Conductivity $(\Omega m)^{-1}$	Density kg/m^3	Mass kg	Specific conductivity
0	0	5.40×10^{-8}	1.85×10^{-7}	8140	61.87×10^{-3}	2.27×10^{3}
25	5.5	5.28×10^{-8}	1.89×10^{-7}	7800	59.28×10^{-3}	2.43×10^{3}
50	10.13	5.32×10^{-8}	1.88×10^{-7}	7530	57.23×10^{-3}	2.49×10^{3}
75	14.75	5.19×10^{-8}	1.92×10^{-7}	7250	55.10×10^{-3}	2.66×10^{3}
100	14.78	5.06×10^{-8}	1.97×10^{-7}	7240	55.03×10^{-3}	2.73×10^{3}
125	16.53	5.18×10^{-8}	1.93×10^{-7}	7140	54.27×10^{-3}	2.70×10^{3}

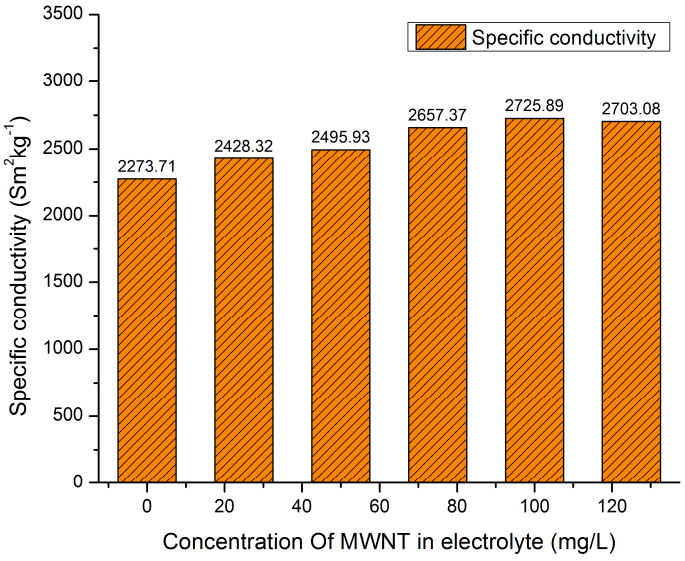

Figure 6.4: Specific conductivity of the MWCNT/Cu composite vs. concentration of MWCNT in the electrolyte

Therefore, the maximum increase in specific conductivity for above MWCNT/Cu composite was 19.88% higher than Cu with 100mg/l concentration of MWCNT in the electrolyte. Similar kind of results are observed by C. Subramanian et al. [22]. In some applications where the weight of an item is very important, specific conductivity is more important than absolute high conductivity – it is often possible to make the conductor thicker to make up for a lower conductivity; and then a high specific conductivity is desirable.

Electrical resistivity of copper and MWCNT/Cu composite wire

In the previous section, we observed that there was 3 to 4 times difference in resistivity of commercial copper and the copper and MWCNT/Cu composite fabricated by modified electro-co-deposition method. This variation is attributed to the porous structure of the copper and MWCNT/Cu composite and the random orientation of MWCNT in the copper matrix. In order to overcome above issues, the copper and MWCNT/Cu composite pellets were hot rolled and then cold drawn to 0.724 mm diameter wire. These wires then tested for electrical characterization. The electrical resistivity measurement of the MWCNT/Cu wire (diameter 0.724 (AWG No. 21) and length as 120 mm) was performed using Agilent 4284A precision LCR meter and Agilent 16047A test fixture at 20°C. An auto balancing bridge method was used for the measurement of resistance. Three specimens for each composite sample were tested, and the final electrical resistance value was obtained by averaging the three values. Resistivity was calculated by using diameter and the length of the specimen. Figure 6.5 shows that at the room temperature, electrical resistivity of the MWCNT/Cu composites decreases with increase in concentration of MWCNT in the electrolyte. Data given in Table 6.3 shows that the electrical resistivity of the MWCNT/Cu composite decreases by about 9% compare to the pure copper synthesized using same protocol.

Nevertheless, the performance of carbon nanotube reinforced composites depends on the interface between carbon nanotube and the copper matrix. The carbon nanotube wets poorly with metal matrix, and therefore the interface between the carbon nanotubes and the copper powders is weak. However, an adequate surface treatment of carbon nanotube minimizes the contact resistance. A rough surface on the MWCNT surface helps in better mechanical bonding between the MWCNT and copper matrix. In the present method,

appropriate ultrasonication time aids in detangling the MWCNT as well as create suitable active sites for reduction of copper ions on the surface of MWCNT.

Table 6.3: Data for variation in electrical resistivity with respect to concentration of MWCNT in the electrolyte is tabulated below

S.No.	Concentration of MWCNT in the electrolyte mg/l	Electrical resistivity Ω m
1	0 (Pure copper)	1.63×10^{-8}
2	25	1.59×10^{-8}
3	50	1.54×10^{-8}
4	75	1.53×10^{-8}
5	100	1.49×10^{-8}
6	125	1.48×10^{-8}

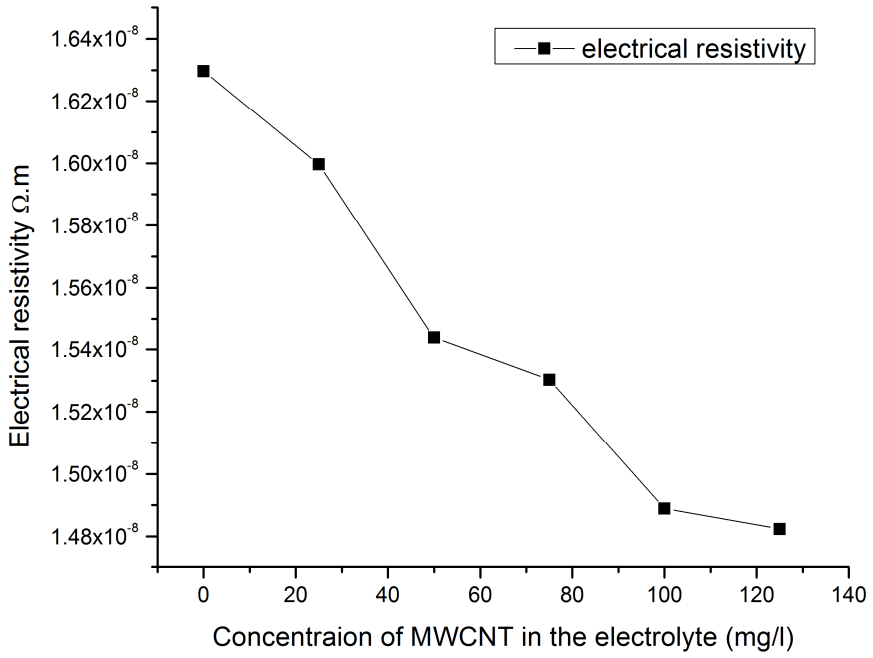

Figure 6.5: Electrical resistivity versus concentration of MWCNT in the electrolyte (mg/l)

Moreover, in the modified method, copper particles and MWCNTs are in suspended manner and there is no piling up of MWCNT and copper particles on the surface of cathode like in standard electro-co-deposition method. Hence, copper ions get enough time and opportunity to attach to the active sites on MWCNTs surface in comparison to standard electro-co-deposition method. This helps in good bonding between MWCNT and copper, foster reduction in interfacial electrical resistance. This approach offers an advantage of metallization of MWCNT. Metallization of MWCNT decreases the interface

resistance and hence plummet the contact resistance between MWCNT and copper matrix. Secondly, the MWCNT are all metallic in nature as the band gap decreases with the diameter of the CNT [23]. Hence, the metallic nature of the MWCNT also helps in decreasing the electrical resistivity of MWCNT/Cu composite. The majority of the metalized MWCNT occupies the grain boundaries, forms a network for electrical pathway across the grain boundary, and thereby decreases the resistivity of MWCNT/Cu composite. From Figure 6.5, it is seen that the decrease in resistivity with 125 mg/l MWCNT concentration in the electrolyte is almost same as that of 100 mg/l concentration. For 125 mg/l MWCNT concentration, similar results were observed for yield strength and tensile strength in the previous chapter and hence, that is the saturation point for reinforcement of MWCNT in the copper matrix of this method.

6.5 Temperature Dependence of Resistivity

Variation in electrical resistivity of copper wire and MWCNT/Cu wire with temperature was performed using XPLORE 1.1^{TM} Physical Quantity Measurement System (PQMS) (four point probe setup). The sample was pasted on the sample mount as shown in Figure 6.6(a). The position of the sample was as close to the thermocouple as possible, as seen in Figure 6.6(b), to avoid the temperature lag readout. Four thin wires were soldered to the contact pads *I*+, *I*-, *V*+ and *V*-.

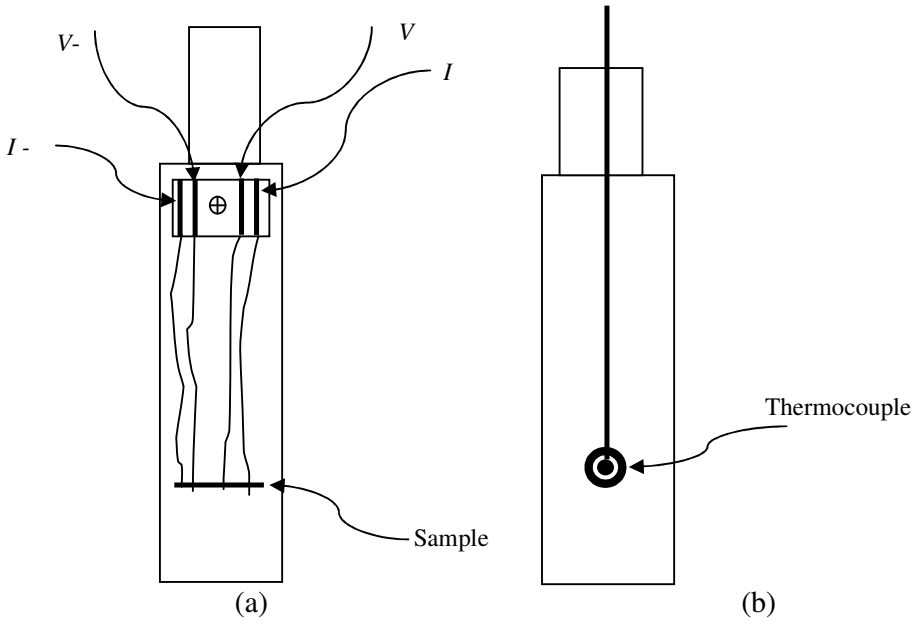

Figure 6.6: (a) Sample mount for I-V and (b) back side of the sample mount on which the thermocouple is attached for R-T measurement

These wires were then connected to the sample using silver epoxy, which ensured good electrical contact of the wire with the sample. The inserts were connected to the temperature controller module and the data for voltage and current at various temperatures were recorded.

In order to minimize the ohmic heating during experiment, the current was supplied in the range of 0 to 10 m*A* with an increment of 0.2 m*A*. Corresponding voltage data was recorded. Readings were taken for seven different temperatures per sample.

The first reading of all the samples, which was taken by using this apparatus at approximately 310 K is corroborates with the reading taken by the four-point probe method (Signatone: QuadMap - M80). These observations confirmed the reduction in electrical resistivity of MWCNT/Cu composite with increase in concentration of MWCNT. Data of each sample for the electrical resistivity at different temperatures is given in Table 6.4.

Consequently, the resistivity of MWCNT/Cu composite increases with increase in temperature as shown in Figure 6.7. As Seen from the Figure 6.7, at 310 K, the resistivity of the MWCNT/Cu composite is much less, than pure copper synthesized by an identical protocol. From the Figure 6.7, it has been observed that the increase in resistivity in MWCNT/Cu composite is faster than the pure copper. However, the resistivity of MWCNT/Cu is less than the pure copper up to 120°C. This feature is important for many applications where temperature is in between room temperature to 120°C.However the electrical resistivity of the MWCNT/Cu composite with 125 mg/l concentration in the electrolyte shows higher resistivity compare to 100 mg/l concentration in the electrolyte but less than the pure copper. This is attributed to the agglomeration of MWCNT in the MWCNT/Cu composite with 125 mg/l concentration of MWCNT in the electrolyte. From this behavior, it is concluded that the 125 mg/l is the saturation point for this process.

Table 6.4: Data for electrical resistivity of MWCNT/Cu composite at different temperatures

T K	Resistivity Ωm	T K	Resistivity Ωm	T K	Resistivity Ωm	T K	Resistivity Ωm	T K	Resistivity Ωm	T K	Resistivity Ωm
	Pure copper		**25 mg/l**		**50 mg/l**		**75 mg/l**		**100 mg/l**		**125 mg/l**
316.2	1.79×10^{-8}	310.6	1.65×10^{-8}	310.9	1.56×10^{-8}	312.9	1.55×10^{-8}	310.5	1.52×10^{-8}	312.1	1.60×10^{-8}
325.4	1.86×10^{-8}	325.8	1.66×10^{-8}	312	1.57×10^{-8}	325.6	1.55×10^{-8}	317.0	1.56×10^{-8}	315.3	1.57×10^{-8}
335	1.92×10^{-8}	340.1	1.69×10^{-8}	331	1.60×10^{-8}	340.0	1.61×10^{-8}	340.2	1.58×10^{-8}	341.4	1.62×10^{-8}
354.9	1.97×10^{-8}	355.2	1.79×10^{-8}	346	1.71×10^{-8}	355.0	1.74×10^{-8}	354.6	1.61×10^{-8}	354.3	1.80×10^{-8}
365.2	2.04×10^{-8}	370.0	1.83×10^{-8}	363.4	1.83×10^{-8}	369.6	1.81×10^{-8}	370.6	1.70×10^{-8}	369.4	1.74×10^{-8}
386.7	2.14×10^{-8}	384.8	2.00×10^{-8}	378.1	1.76×10^{-8}	385.1	1.81×10^{-8}	384.5	1.99×10^{-8}	385.2	2.10×10^{-8}

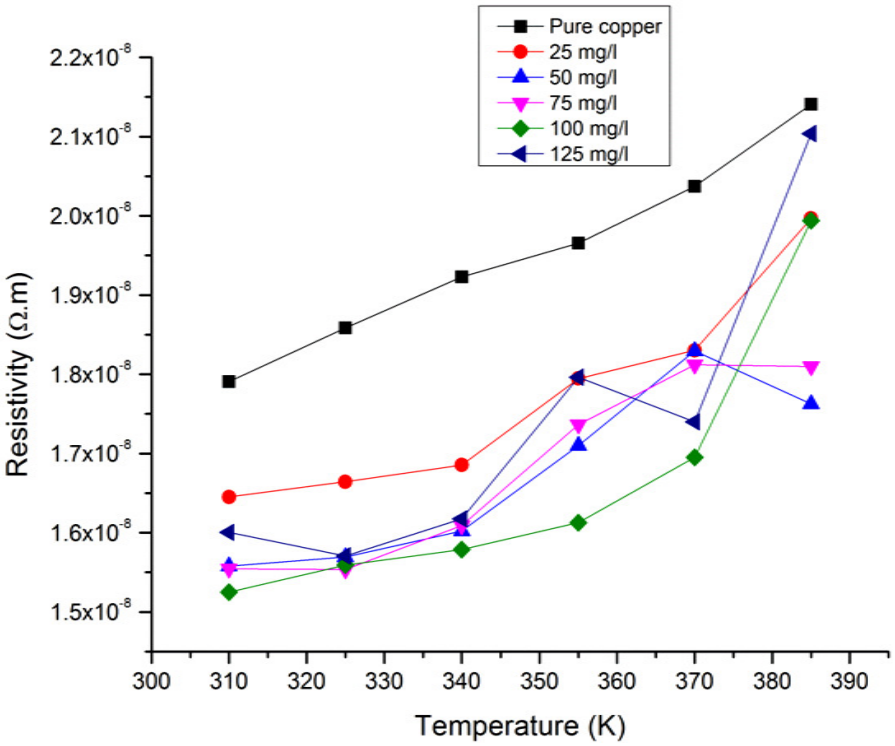

Figure 6.7: Variations in resistivity of MWCNT/Cu composite with temperature

6.6 Discussion

The electrical resistivity values for the MWCNT/Cu wire are summarized in Table 6.3. The electrical resistivity of MWCNT/Cu at room temperature ($\rho_{293\,K}$) is $1.52 \pm 0.05 \times 10^{-8}\,\Omega\,\mathrm{m}$ which is lower than that of commercial Cu ($1.6296 \times 10^{-8}\,\Omega\,\mathrm{m}$). The electrical resistivity of MWCNT/Cu approaching 400 K, is about $2 \pm 1.0 \times 10^{-8}\,\Omega\,\mathrm{m}$. This value is slightly lower than that of copper ($2.14 \times 10^{-8}\,\Omega\,\mathrm{m}$). However, in addition to lattice vibration of copper, lattice vibrations in MWCNT, which is present in the MWCNT/cu composite, will scatter the electrons that will result increase in resistivity at higher temperature. Furthermore, the increase of micro-strain in the Cu matrix also plays important role in the increase of electron scattering. The average value of temperature coefficient of resistivity for MWCNT/Cu, α, is $1.914 \pm 0.40 \times 10^{-1}\,\mathrm{K}^{-1}$ at 355 K, which is lower than that of Cu ($3.39 \times 10^{-1}\,\mathrm{K}^{-1}$). Thermal coefficient of resistivity value shows that the change in resistivity of MWCNT/Cu with respect to temperature. As the temperature, increase to around 400 K the average temperature coefficient of resistivity for MWCNT/Cu composite reach to $2.892 \times 10^{-1}\,\mathrm{K}^{-1}$. At 400 K, temperature coefficient

of resistivity value is slightly less than that of the Cu ($3.34\times10^{-1}\,\mathrm{K}^{-1}$) and still, the temperature coefficient of resistivity is less than the Cu matrix. This slight difference can be explained form by following three standpoints:

- First, the electrical conductivity of CNTs with diameter more than 9 nm is having same or even better electrical conductivity than that of pure Cu [10].
- Second, proper interface bonding between copper and MWCNT [11], reduces the interface resistance, leading to decrease in resistivity.
- Third, the majority of the SWNTs distributes along the grain boundary and forms a network leading to the continuity of the nanotube phase, which provides an interlinked electrical pathway for a reduction in resistivity [20,24].

Thus, electrical resistivity of MWCNT/Cu composites decreases with increase in concentration of MWCNT in the copper matrix.

In the next section, statistical investigation on MWCNT/Cu composite was carried out to conclude on parameter, which may significantly influence electrical property of the composite.

6.7 Effect of Electrolysis Parameters on Electrical Resistivity

6.7.1 Experimental design

In this section, the minimum resistivity as the performance index has been investigated. Therefore, out of 60 signal to noise ratio [25], smaller the better S/N ratio has been selected for the investigation.

$$\frac{S}{N} = -10\log_{10}\left[\frac{\sum_{i=1}^{n} y_i^2}{n}\right] \tag{6.7}$$

where, y_i denotes the n observations of response variables.

A modified electro-co deposition reported in [26,27] has been considered as the basic experiment and electrical resistivity is taken as investigated performance index of the experiment. The experiments were carried out at $50\pm2^{\circ}\mathrm{C}$.

In the modified electro-co-deposition method, major parameters, which influence the quality of formed powder are (1) pH, (2) current supplied, (3) MWCNT concentration in

the electrolyte, (4) ultra-sonication time of electrolyte, and (5) copper sulphate concentration in the electrolyte. With the five parameters as variables and considering three levels of each variable, a fractional factorial design of 3^5 experiments were done with L_{18} orthogonal array. Table 6.5 shows the five control parameters and their levels. The five parameters were arranged in 2-6 columns in the standard L_{18} orthogonal array as shown in Table 6.6.

Table 6.5: Control parameters and their levels

Parameters	**Level 1**	**Level 2**	**Level 3**
A: pH	1	2	3
B: Ultra-sonication time (hrs)	3	4	5
C: MWCNT (mg/l)	50	75	100
D: Current (amp)	4	6	8
E: $CuSO_4.5H_2O$ concentration (gm/l)	75	100	125

6.7.2 Electrical resistivity measurements

The electrical resistivity measurement of the MWCNT/Cu wire (diameter 0.46 mm) was performed using Agilent 4284A precision LCR meter and Agilent 16047A test fixture at 20°C. An auto balancing bridge method was used for the measurement of resistance. Three specimens for each composite sample were tested, and the final electrical resistance value was obtained by averaging the three values. Resistivity was calculated by using values of diameter and the length of the specimen.

6.7.3 Statistical analysis of experimental results

The electrical resistivity obtained for the product in all the three sets of eighteen experiments have been subjected to statistical analysis.

Table 6.6: The basic Taguchi L_{18} orthogonal array

Expt	A	B	C	D	E	Notation	Resistivity1 (Ω m)	Resistivity2 (Ω m)	Resistivity 3 (Ω m)	Resistivity (Ω m)	S/N ratio STB
1	1	1	1	1	1	$A_1B_1C_1D_1E_1$	1.58×10^{-8}	1.58×10^{-8}	1.57×10^{-8}	1.58×10^{-8}	96.02
2	1	2	2	2	2	$A_1B_2C_2D_2E_2$	1.52×10^{-8}	1.52×10^{-8}	1.53×10^{-8}	1.53×10^{-8}	96.33
3	1	3	3	3	3	$A_1B_3C_3D_3E_3$	1.50×10^{-8}	1.51×10^{-8}	1.53×10^{-8}	1.52×10^{-8}	96.37
4	2	1	1	2	2	$A_2B_1C_1D_2E_2$	1.55×10^{-8}	1.56×10^{-8}	1.51×10^{-8}	1.54×10^{-8}	96.25
5	2	2	2	3	3	$A_2B_2C_2D_3E_3$	1.53×10^{-8}	1.54×10^{-8}	1.54×10^{-8}	1.54×10^{-8}	96.27
6	2	3	3	1	1	$A_2B_3C_3D_1E_1$	1.48×10^{-8}	1.48×10^{-8}	1.50×10^{-8}	1.49×10^{-8}	96.53
7	3	1	2	1	3	$A_3B_1C_2D_1E_3$	1.52×10^{-8}	1.52×10^{-8}	1.54×10^{-8}	1.52×10^{-8}	96.31
8	3	2	3	2	1	$A_3B_2C_3D_2E_1$	1.48×10^{-8}	1.48×10^{-8}	1.46×10^{-8}	1.47×10^{-8}	96.61
9	3	3	1	3	2	$A_3B_3C_1D_3E_2$	1.56×10^{-8}	1.57×10^{-8}	1.57×10^{-8}	1.56×10^{-8}	96.09
10	1	1	3	3	2	$A_1B_1C_3D_3E_2$	1.49×10^{-8}	1.49×10^{-8}	1.47×10^{-8}	1.49×10^{-8}	96.53
11	1	2	1	1	3	$A_1B_2C_1D_1E_3$	1.58×10^{-8}	1.57×10^{-8}	1.59×10^{-8}	1.58×10^{-8}	96.00
12	1	3	2	2	1	$A_1B_3C_2D_2E_1$	1.52×10^{-8}	1.53×10^{-8}	1.50×10^{-8}	1.52×10^{-8}	96.36
13	2	1	2	3	1	$A_2B_1C_2D_3E_1$	1.48×10^{-8}	1.50×10^{-8}	1.47×10^{-8}	1.48×10^{-8}	96.56
14	2	2	3	1	2	$A_2B_2C_3D_1E_2$	1.59×10^{-8}	1.59×10^{-8}	1.59×10^{-8}	1.59×10^{-8}	95.97
15	2	3	1	2	3	$A_2B_3C_1D_2E_3$	1.57×10^{-8}	1.58×10^{-8}	1.59×10^{-8}	1.58×10^{-8}	96.01
16	3	1	3	2	3	$A_3B_1C_3D_2E_3$	1.48×10^{-8}	1.50×10^{-8}	1.50×10^{-8}	1.49×10^{-8}	96.50
17	3	2	1	3	1	$A_3B_2C_1D_3E_1$	1.54×10^{-8}	1.54×10^{-8}	1.50×10^{-8}	1.53×10^{-8}	96.29
18	3	3	2	1	2	$A_3B_3C_2D_1E_2$	1.56×10^{-8}	1.57×10^{-8}	1.56×10^{-8}	1.56×10^{-8}	96.09

6.7.4 Taguchi analysis

The experiments were performed to optimize the parameters in order to minimize the electrical resistivity hence smaller the better characteristic S/N ratio was used. The response for average S/N ratio for electrical resistivity is given in the Table 6.7.

Table 6.7: Response table for average S/N ratio for electrical resistivity factors

Level	Mean S/N for pH	Level	Mean S/N for current	Level	Mean S/N for MWCNT	Level	Mean S/N for sonication time	Level	Mean S/N for $CuSO_4$ concentration
A1	96.27	B1	96.36	C1	96.11	D1	96.16	E1	96.40
A2	96.26	B 2	96.25	C 2	96.32	D 2	96.35	E 2	96.21
A3	96.31	B 3	96.24	C 3	96.42	D 3	96.35	E 3	96.25
Max-Min	0.052		0.12		0.31		0.20		0.19
Ranking	5		4		1		2		3

The average S/N ratios for all five parameters for all levels are plotted and are shown in Figure 6.8. From the Table 6.7 it is clear that the MWCNT is the most significant parameter, which influences the resistivity of the product. The product obtained by higher MWCNT concentration depicts less resistivity. Even from Figure 6.8, it is clear that as the concentration of the MWCNT increase the resistivity decreases. Level 3 of parameter C results in smaller resistivity and hence the highest concentration of MWCNT in the electrolyte is the best choice for lower resistivity. The other parameters namely ultra-sonication time, concentration of $CuSO_4$, current supplied and pH of the electrolyte follows in this order to influence the product resistivity. From Figure 6.8, it is clear that the level 3 of parameter D will cause the smallest variability and hence highest ultra-sonication time will be the best choice to have lower resistivity. Similarly, for the third more influencing parameter that is $CuSO_4$ (parameter E) the level 1 is suitable. For current (parameter B) and pH (parameter A) are the fourth and fifth parameters and their corresponding levels are 1, and 3 suitable. Further, Pareto ANOVA also confirms the observation. The best combination is found to be $A_3B_1C_3D_3E_1$. Three experiments are conducted with this combination and observed that the resistivity of the composite is $1.49\ (\pm 0.2) \times 10^{-8}\ \Omega$ m.

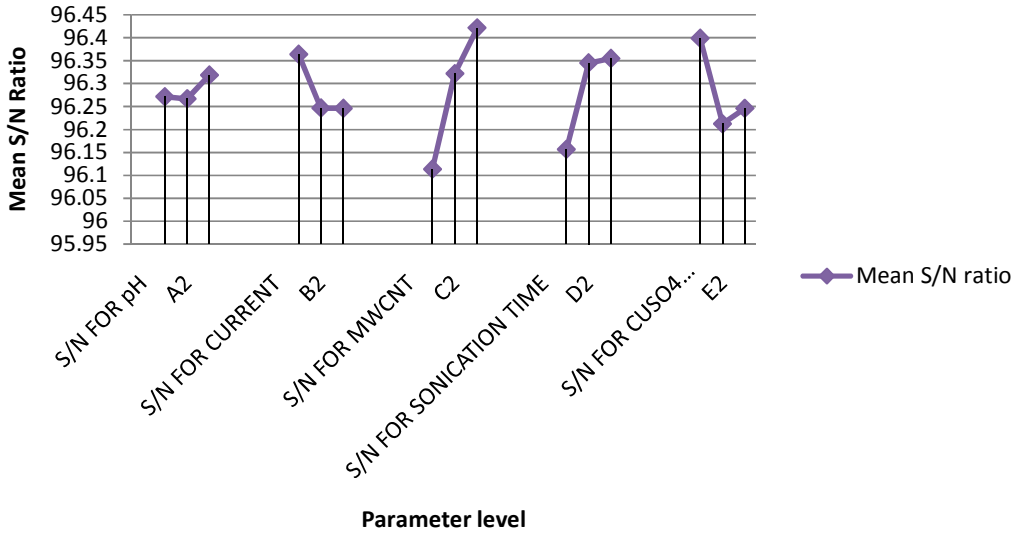

Figure 6.8: The smaller the better S/N graph for electrical resistivity

6.7.5 Pareto ANOVA analysis

Pareto ANOVA [25,28] is a simplified ANOVA method using 80/20 Pareto principle. This method is quick and easy to analyze the results of parametric variation in an experiment without requirement of detailed ANOVA and f-test. Pareto ANOVA also helps in identifying the most significant parameter among all the parameters as well as the relevant optimum. Table 6.8 shows the Pareto analysis of parameter's S/N ratio for resistivity for the experiments reported in the work.

From Pareto chart Figure 6.9, the contribution of parameter D is around 47.69% followed by parameter A, E, C and B. The conclusion corroborates with the analysis done using Taguchi method in previous section.

Table 6.8: Pareto ANOVA analysis of S/N ratio of parameters for the resistivity

Parameter Level	S/N For pH	S/N For Current	S/N For MWCNT	S/N For Sonication Time	S/N For $CuSO_4$ Concentration
1	96.27	96.36	96.11	96.15	96.39
2	96.26	96.25	96.32	96.34	96.21
3	96.32	96.25	96.42	96.35	96.24
Average	96.28	96.28	96.28	96.28	96.28
SSD	0.0049	0.027	0.15	0.075	0.060
% Contribution Ratio	1.56	8.76	47.00	23.80	18.87

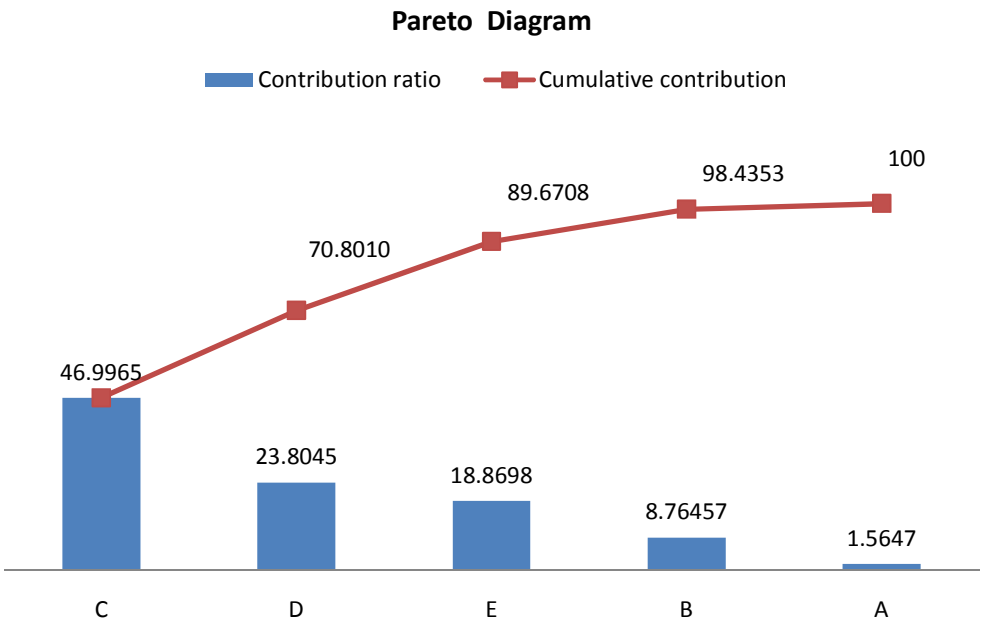

Figure 6.9: Pareto diagram for determining contribution of parameters

6.7.6 Discussion

Pure copper wire and MWCNT/Cu composite wire were fabricated by combination of modified electro-co-deposition and powder metallurgy method. All samples of pure copper and MWCNT/Cu composite were tested under the identical conditions with the help of Agilent 4284A precision LCR meter and Agilent 16047A test fixture at 20°C. Mean resistivity value of pure copper wire determined by Agilent 4284 precision LCR method is $1.63\times10^{-8}\,\Omega\,\mathrm{m}$, which is higher than any other resistivity value tabulated in Table 6.3. From the results it is observed that the resistivity of the copper decreases with addition of MWCNT in the copper matrix when modified electro-co-deposition and powder metallurgy method is used.

Analysis by Taguchi and Pareto ANOVA concluded that MWCNT concentration is the most influencing parameter of the process reported in this work. According to X.J. Zhou et al. [23], the band gap decreases with an increase in diameter of the CNT. MWCNT is a set of concentric SWCNTs with different diameter and chirality [29]. The MWCNT used in the experiment are of 10 to 15 nm in diameter, which is much higher than the reported [10] diameter for conducting CNT. Hence, as the band gap decreases with increase in diameter of the tube and therefore the MWCNT will be of

a metallic nature. Metallic nature of MWCNT will cause reduction in resistivity of the MWCNT/Cu composite decreases. The second, most influencing parameter on the resistivity of the MWCNT/Cu composite was the ultra-sonication time. A probe ultra-sonicator (Sonics VCX 500) was used to treat the electrolyte at settings of 500 W and at 20 kHz. Based on the known volume of the electrolyte (400 ml), the specific ultra-sonication energy per minute per unit volume (e_v) is calculated as $7.4\times10^4 kJ/m^3$. The specific ultra-sonication energy per unit volume can be determined by multiplying e_v with duration of ultra-sonication. The average agglomeration size of carbon nanotube (CNT) decreases to 5 μm from 7 μm [30] respectively by ultra-sonicating the electrolyte solution for level 3 of parameter D. Lowering of agglomeration size results in uniform dispersion of MWCNT in the copper matrix. This uniform dispersion of MWCNT in the copper matrix helps in reduction of resistivity and isotropic property of the material.

Concentration of $CuSO_4.5H_2O$ in the electrolyte is the third most influencing parameter. It has been observed by Grujicic [31] that the nuclei population density decreases with increase in $CuSO_4.5H_2O$ concentration. However, the combination of high pH value (parameter A) and low concentration of $CuSO_4.5H_2O$ results in coarser grain structure [31]. Low pH value of the electrolyte means the conductivity of the solution is less and less concentration of the $CuSO_4.5H_2O$ means the concentration of Cu^{2+} is less. Therefore, the rate of deposition of copper ions decreases and copper ions get sufficient time to rearrange them on the cathode surface, which results in the coarser grain structure of the copper. Due to larger size of the grain, the length of grain boundary will also decrease and MWCNT will occupy along the grain boundary. This aids in decreasing the electrical resistivity of the matrix. Taguchi and Pareto ANOVA suggest that for the best result the concentration of the $CuSO_4$ should be of level 1 i.e. 75 gm/l and pH should be of level 3 (parameter A) which will facilitate larger size of grain. This will also help more nuclei formation on the surface of cathode as well as MWCNT surface. Exactly similar observations are made using as shown in High resolution Transmission Electron Microscope (HRTEM) and are Figure 6.10.

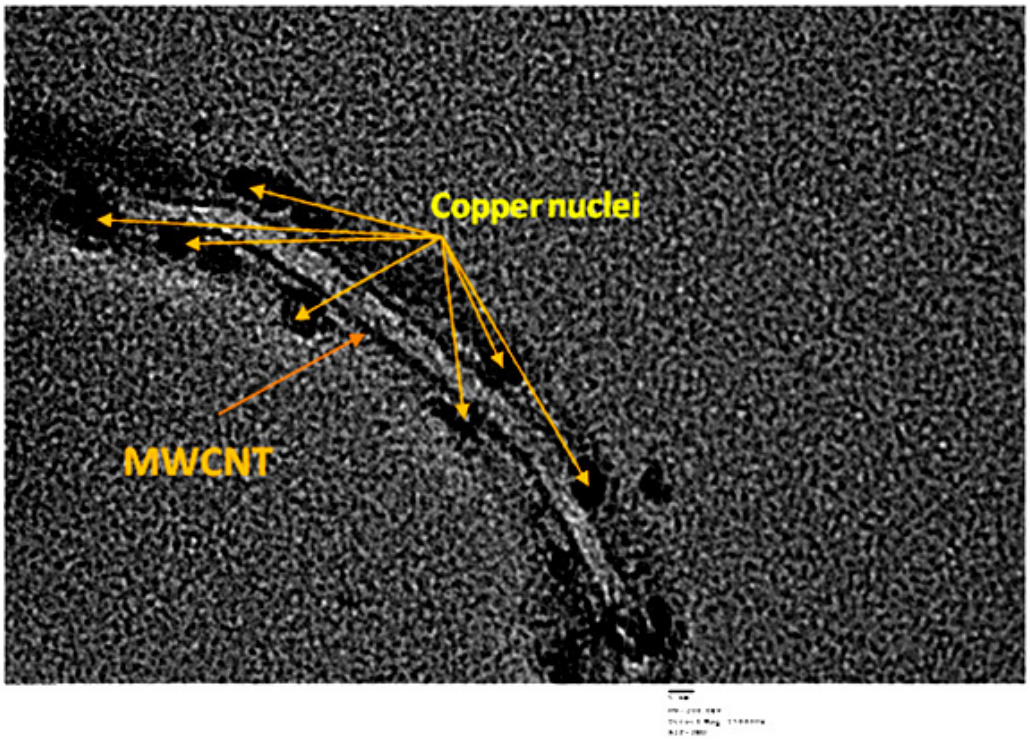

Figure 6.10: High resolution transmission electron microscope (HRTEM) image showing growth copper nuclei on the surface of the MWCNT

From the Taguchi analysis, it is observed that the resistivity decreases with increase in MWCNT concentration. Mazaheri et al. [32] also observed improvement in electrical conductivity by reinforcement of MWCNT in the zirconia matrix and it is attributed to wt% and the uniform dispersion of CNT in the matrix. Taguchi analysis also suggests the higher wt% of MWCNT (level 3) for improvement in electrical conductivity. Current supplied is the second last least influencing parameter among all considered parameters but important point to note is that at level 1 that is smaller current density causes dendritic growth of copper, which helps in the uniform dispersion, as well as entrapment of the MWCNT in the copper matrix [26,33].

6.8 Conclusion

Experiments using modified electro-co-deposition for reinforcement of MWCNT in copper were carried out to study the electrical properties of MWCNT/Cu composite. The experiments are performed on pelletized composite and the wire drawn from pellet.

1. There is small decrease in electrical resistivity with addition of MWCNT in the copper matrix. This small change in resistivity results in 16.6% improvement in the specific conductivity of the copper.
2. The electrical resistivity of the wire, which was drawn from above six samples by hot rolling and cold drawing process, was checked by using Agilent 4284A precision LCR meter and it was observed that the maximum reduction in electrical resistivity is about 9%.
3. It was also observed that the electrical resistivity of the MWCNT/Cu composite increase with temperature similar to the pure copper. However, it remains below the resistivity of the copper up to 125°C, which is the operating temperature of several electrical devices.
4. From statistical investigation on MWCNT/Cu composite, it has been observed that the resistivity of the MWCNT reinforced copper composite synthesized by the modified electro-co-deposition is decreased in all the products formed in all the experiments.
5. The statistical study showed that the MWCNT concentration in the composite and ultra-sonication time of electrolyte had the greatest influence on the synthesis of MWCNT reinforced copper composite. The bath composition like concentration of $CuSO_4$, current supplied and pH of the electrolyte presented less significance effect on electrical resistivity of the composite.

References:

[1] Dai H. Carbon Nanotubes: Synthesis , Integration , and Properties. Acc Chem Res 2002;35:1035–44.

[2] Yao N, Lordi V, Introduction I. Young's modulus of single-walled carbon nanotubes. J Appl Phys 1998;84:1939–43.

[3] Xie H. Thermal and electrical transport properties of a self-organized carbon nanotube pellet. J Mater Sci 2007;42:3695–8.

[4] Dergan A. Electronic and transport properties of carbon nanotubes. 2010.

[5] Dresselhaus MS, Dresselhaus G, Charlier JC, Hernández E. Electronic, thermal and mechanical properties of carbon nanotubes. Philos Trans A Math Phys Eng Sci 2004;362:2065–98.

[6] Iijima S. Helical microtubules of graphitic carbon. Nature 1991;354:56–8.

[7] Praveen BM, Venkatesha TV. Electrodeposition and properties of Zn–Ni–CNT composite coatings. J Alloys Compd 2009;482:53–7.

[8] Xu CL, Wei BQ, Ma RZ, Liang J, Ma XK, Wu DH. Fabrication of aluminum – carbon nanotube composites and their electrical properties. Carbon N Y 1999;37:855–8.

[9] Hong S, Myung S. NANOTUBE ELECTRONICS A fl exible approach to mobility. Nat Nanotechnol 2007;2:207–8.

[10] Ebbesen TW, Lezec HJ, Hiura H, Bennett JW, Ghaemi H., Thio T. Electrical conductivity of individual carbon nanotube. Nature 1996;382:54–6.

[11] Dai H. Carbon nanotubes: opportunities and challenges. Surf Sci 2002;500:218–41.

[12] Hjortstam O, Isberg P, Soderholm S, Dai H. Can we achieve ultra-low resistivity in carbon nanotube-based metal composites? Appl Phys A Mater Sci Process 2004;78:1175–9.

[13] Yang K, He J, Puneet P, Su Z, Skove MJ, Gaillard J, et al. Tuning electrical and thermal connectivity in multiwalled carbon nanotube buckypaper. J Phys Condens Matter 2010;22:334215.

[14] Rosa JL, Robin a., Silva MB, Baldan C a., Peres MP. Electrodeposition of copper on titanium wires: Taguchi experimental design approach. J Mater Process Technol 2009;209:1181–8.

[15] Zhu HW, Xu CL, Wu DH, Wei BQ, Vajtai R, Ajayan PM. Direct synthesis of long single-walled carbon nanotube strands. Science 2002;296:884–6.

[16] Swartzendruber LJ. Correction factor table for four point probe resistivity measurement on thin, circular semiconductor samples,National Bureau of Standards Technical Note 199. 1964.

[17] Kim C, Lim B, Kim B, Shim U, Oh S, Sung B, et al. Strengthening of copper matrix composites by nickel-coated single-walled carbon nanotube reinforcements. Synth Met 2009;159:424–9.

[18] Daoush WM, Lim BK, Mo CB, Nam DH, Hong SH. Electrical and mechanical properties of carbon nanotube reinforced copper nanocomposites fabricated by electroless deposition process. Mater Sci Eng A 2009;513-514:247–53.

[19] Daoush WM. Processing and characterization of CNT/Cu nanocomposites by powder technology. Powder Metall Met Ceram 2009;47:531–7.

[20] Yang YL, Wang YD, Ren Y, He CS, Deng JN, Nan J, et al. Single-walled carbon nanotube-reinforced copper composite coatings prepared by electrodeposition under ultrasonic field. Mater Lett 2008;62:47–50.

[21] World T, Factbook C. The world copper factbook 2012. Internatioanl Copp Study Gr 2012.

[22] Subramaniam C, Yamada T, Kobashi K, Sekiguchi A, Futaba DN, Yumura M, et al. One hundred fold increase in current carrying capacity in a carbon nanotube-copper composite. Nat Commun 2013;4:2202.

[23] Zhou X, Park J-Y, Huang S, Liu J, McEuen P. Band Structure, Phonon Scattering, and the Performance Limit of Single-Walled Carbon Nanotube Transistors. Phys Rev Lett 2005;95:146805.

[24] Zhan G-D, Kuntz JD, Garay JE, Mukherjee AK. Electrical properties of nanoceramics reinforced with ropes of single-walled carbon nanotubes. Appl Phys Lett 2003;83:1228.

[25] Mitra A. Introduction to quality control and improvement fundamentals of quality control. 3 rd ed. Hoboken, New Jersey: John wiley and Sons, Inc.; 2008.

[26] Belgamwar SU, Sharma NN. Synergistic electro-co-deposition and molecular mixing for reinforcement of multi-walled carbon nanotube in copper. Mater Sci Eng B 2013;178:1452–7.

[27] Belgamwar SU, Sharma NN. Method of Producing Uniform Mixture of Copper and Carbon Nanotube in Bulk for Copper Metal Nanocomposite. 2454/DEL/2102A, 2012.

[28] Ghani J., Choudhury I., Hassan H. Application of Taguchi method in the optimization of end milling parameters. J Mater Process Technol 2004;145:84–92.

[29] Takesue I, Haruyama J, Kobayashi N, Chiashi S, Maruyama S, Sugai T, et al. Superconductivity in Entirely End-Bonded Multiwalled Carbon Nanotubes. Phys Rev Lett 2006;96:057001.

[30] Ruan B, Jacobi AM. Ultrasonication effects on thermal and rheological properties of carbon nanotube suspensions. Nanoscale Res Lett 2012;7:127.

[31] Grujicic D, Pesic B. Electrodeposition of copper: the nucleation mechanisms. Electrochim Acta 2002;47:2901–12.

[32] Mazaheri M, Mari D, Razavi Z, Schaller R, Fantozzi G. Multi-walled carbon nanotube / nanostructured zirconia composites: Outstanding mechanical properties in a wide range of temperature. Compos Sci Technol 2011.

[33] Pavlović MG, Pavlović LJ, Maksimovi VM, Nikolić ND, Popov KI. Characterization and Morphology of Copper Powder Particles as a Function of Different Electrolytic Regimes. Int J Electrochem Sci 2010;5:1862–78.

Chapter 7

Overall Conclusions and Future Scope

7.1 Overall Conclusions

MWCNT reinforced Cu composite was successfully synthesized by a novel method of modified electro-co-deposition method. A systematic study on mechanical and electrical properties of MWCNT/Cu composite was carried out. This chapter goes over the main points of the research on MWCNT/Cu composites and provides future research direction and possible guideline in the area of MWCNT/Cu composite.

Due to high melting point (1083° *C*) of the copper, it becomes very difficult to fabricate a composite by melting and stirring method. Therefore, it is commonly preferred to fabricate the MWCNT/Cu composite by electro-chemical or powder metallurgy method. Both methods are widely used to fabricate the MWCNT/Cu composite. However, powder metallurgy is a method, where the production of bulk MWCNT/Cu composite is possible whereas, uniform dispersion of MWCNT can be achieved by electrochemical method but the production will be in the form of thin film. Fabrication of freestanding structure is difficult by the electro-co-deposition method.

1] The innovative modified electro-co-deposition method suggested in chapter 3 is a combination of molecular level mixing, electro-co-deposition method and powder metallurgy. The method is capable of producing MWCNT/Cu composite powder in bulk at atmospheric pressure and at around $50 \pm 2^{\circ}C$ with particle less than $63\mu m$ in diameter, with high purity of copper (100%) and MWCNT (99%). As the operating temperature is so low there is very less possibility of damage to the MWCNT like powder metallurgy.

2] Field emission scanning electron microscopy and high-resolution transmission electron microscopy confirmed the MWCNT are uniformly dispersed in the copper matrix. In support to this, the EDS also confirm the uniform dispersion of carbon nanotube in the copper matrix by showing almost uniform composition at different sites. This result corroborates with result achieved by the other research group for electro-co-deposition method.

3] From HRTEM and FESEM analysis in chapter 4, it was clearly observed that the molecular interaction occurs between the MWCNT and copper matrix. The nucleation of the copper took place at some selective potential sites on the surface of MWCNT. This molecular level interaction between MWCNT and copper helps in proper bonding between copper and MWCNT matrix as well as it helps in the uniform dispersion of MWCNT in the copper matrix.

4] The modified electro-co-deposition method resembles with the electro refining process. This electro refining process is used in the copper industry for copper refining purpose. Hence, this is one of the promising methods for uniform dispersion of MWCNTs in the copper matrix, which can be easily scaled up to the production level.

5] Physical characterization, in Chapter 5, of the pellets form from the powder shows that the density of the MWCNT/Cu composite decreases with addition of MWCNT in the copper matrix. This helps in improving the specific properties of the material.

6] MWCNT/Cu composite powder formed by modified electro-co-deposition method was converted to wire by hot rolling and the cold drawing process. The formed wire was tested for the mechanical properties. It was observed that the tensile testing the failure of MWCNT/Cu composite was ductile in nature. MWCNT/Cu composite showed the “cup-and-cone” formation at the point of failure.

7] The Young’s modulus of MWCNT/Cu composite with 125 mg/l concentration of MWCNT in the electrolyte is determined as 110.73 GPa, which is about 2.15 times compared to that of pure Cu, which is measured as 51.57 GPa. The higher values of Young’s modulus show that the MWCNT/Cu composites are successfully fabricated by electro-co-deposition. However, the percentage elongation of the MWCNT/Cu composite decreases, with increase in concentration of MWCNT in the composite. In case of pure copper, the percentage elongation is 38.4%, which was decreased to 32.9% with addition of 25 mg/l concentration of MWCNT in the electrolyte. Then it gradually comes down to 7% with addition of 125 mg/l concentration of MWCNT in the electrolyte. This means the ductility of the MWCNT/Cu was decreased by increasing the MWCNTs in the copper matrix.

8] The wire produced from pure copper synthesized using electro-co-deposition method shows yield strength (0.2% offset strain) of 54 MPa and an ultimate tensile

strength of 131 MPa. Whereas, the MWCNT/Cu composite produces yield strength of 228 MPa, which is about four times greater than that of pure copper. Moreover, the ultimate tensile strength of the MWCNT/Cu composite is about 306 MPa (for 100 mg/l concentration in the electrolyte), which is two times greater than that of pure copper. The improvement in the yield strength and ultimate tensile strength is attributed to homogeneous dispersion of MWCNT in the copper matrix at micro-level and strong interfacial bonding between MWCNT and Cu matrix.

9] Modulus of elasticity the composite was calculated using micromechanical models like rule of mixture, Voigt-Ruess model, Halpin Tsai and Cox model. For the model calculations, the values of E_{Cu} =51.57 GPa, E_{CNT} =800 GPa, ν_{Cu} =0.36, and aspect ratio l/d of CNT =400 have been assumed. The values of modulus of elasticity determined by the Cox model (for $\chi_1 = 3/8$, for random in plane orientation) are more close to the experimental values. The maximum variation, which was observed between experimental values and the Cox model result, is 16.81%. Cox model underestimated the value for the highest concentration of the MWCNT in the electrolyte.

10] In Chapter 5, the hardness testing was also carried out. The hardness of the MWCNT/Cu composites as well as the pure copper synthesized by identical protocol was measured by Vickers hardness test. The maximum increment in the Vickers hardness values of the composites is from about 361 MPa for pure copper to 412 MPa. The increase in hardness of the composite is about 12.5%.

11] In Chapter 5, the effect of electrolysis parameters on hardness was studied by statistical method using Taguchi and Pareto ANOVA. This study shows that the concentration of MWCNT and $CuSO_4$ concentration in the electrolyte had the greatest influence on the hardness value of MWCNT reinforced copper composite. The bath composition like pH of the solution, sonication time, and current supplied presented less significant effect on hardness of the composite.

12] In Chapter 6, electrical characterization of MWCNT/Cu composite was carried out. Electrical characterization of the MWCNT/Cu composite pellet shows, slight decrease in resistivity of the composite with addition of MWCNT in the copper matrix. The average resistivity of the pure copper pellet is found to be $5.4031\times10^{-08}\,\Omega\,\mathrm{m}$ whereas, for the MWCNT/Cu composite copper pellet (100 mg/l concentration of MWCNT in the copper matrix) is $5.067\times10^{-08}\,\Omega\,\mathrm{m}$.

This shows 6.22% decrease in resistivity of the composite pellet. The resistivity was checked at five different on the surface of the pellet by using four-point probe system. The maximum variation, which was observed in the resistivity, is about 7.14%, which is almost negligible. This confirms the uniform dispersion of the MWCNT in the copper metal matrix. However, there is very small decrement in the resistivity, its specific conductivity increases noticeably. The maximum increase in specific conductivity for above MWCNT/Cu composite was 16.58% higher than Cu, which is very useful where the weight of an item is very important.

13] Electrical resistivity of the wire drawn from the pellet was measured by using Agilent 4284A precision LCR meter. It was observed that the maximum reduction in electrical resistivity is about 9%. It was also observed that the electrical resistivity of the MWCNT/Cu increase with temperature similar to the copper. But, it remains below the resistivity of the copper up to $125^{\circ}C$, which is the operating temperature of several electrical devices.

14] Statistical investigation on MWCNT/Cu composite was carried out to conclude on parameter, which may significantly influence electrical property of the composite. The statistical study showed that the MWCNT concentration in the composite and ultra-sonication time of electrolyte had the greatest influence on the synthesis of MWCNT reinforced copper composite. The bath composition like concentration of $CuSO_4$, current supplied and pH of the electrolyte presented less significant effect on electrical resistivity of the composite.

7.2 Future Scope of the Work

No research concludes with an absolute end. There is enough room for innovation in the various stages of MWCNT/Cu composite processing. Several areas of MWCNT/Cu composite need better understanding so design strategies can be improved further. The research in this area will find a milestone when the MWCNT/Cu wire will be used in the real life. From the perspective of present work, the following aspects can be studied and investigated further.

1] Thermal characterization

The improvement in mechanical and electrical properties due to addition of MWCNTs has been discussed in detail in Chapter 5 and 6. Apart from structural

applications, CNT/MM composites have great potential as thermal management materials. Addition of CNTs has been shown to improve the thermal conductivity and decrease in the coefficient of thermal expansion, which is useful for the electronic packaging industry. However, increase in the thermal conductivity is subject to the presence of uniformly distributed CNTs in the matrix.

2] Alignment

Alignment of MWCNT in the copper matrix is one of the important areas in the MWCNT/Cu composite. It is well known that the best properties of CNTs are directional. Best thermal as well as mechanical properties of carbon nanotube are in the axial direction. Therefore, the composites with aligned MWCNTs are anticipated to have better mechanical and thermal properties in the direction of alignment. Parallel and orthogonal alignment of metallic and semiconductor Carbon nanotube is possible by dielectrophoresis [1] as well as use of magnetic fields [2-4] in processing MWCNT/Cu composites needs to be explored for the alignment. Such alignment can be brought about by using aligned preform or through processing. For such type of alignment, provision for in situ monitoring is required.

3] Interface MWCNT and copper matrix

Study of thermodynamics and kinetic factors is important to know the bonding between the metal matrix and MWCNT. Good bonding between MWCNTs and the metal matrix will help in more enhancements in the mechanical strengthening and will result in decrease of contact resistance between MWCNT and metal matrix.

4] Computational work

Study on computational techniques in MWCNT/Cu composites is very less and very few studies have been reported. Computational techniques will help in predicting the properties of the composite. Computation technique will also help in maneuvering the composition of the composite according to the application.

5] Exploring Novel applications

Application of the composite should not be restricted up to structural application only. Study must be carried out to explore the new areas of application for MWCNT/Cu composite. It is possible to use the composite in the area of micro-electro-mechanical

systems, nano-electro-mechanical systems, for energy harnessing and so on. Some composites shown very interesting results in MEMS device which need to explore more [5,6]. There is a wide scope of application of composite in day-to-day life. However, in order to realize these scopes, more research is required to find solutions to the challenges. With the application-oriented research, it is expected that the presence of composite will be realised in many application in near future.

References:

[1] Padmaraj D, Zagozdzon-Wosik W, Xie L-M, Hadjiev VG, Cherukuri P, Wosik J. Parallel and orthogonal E-field alignment of single-walled carbon nanotubes by ac dielectrophoresis. Nanotechnology 2009;20:035201.

[2] Camponeschi E, Vance R, Al-Haik M, Garmestani H, Tannenbaum R. Properties of carbon nanotube-polymer composites aligned in a magnetic field. Carbon N Y 2007;45:2037-46.

[3] Choi ES, Brooks JS, Eaton DL, Al-Haik MS, Hussaini MY, Garmestani H, et al. Enhancement of thermal and electrical properties of carbon nanotube polymer composites by magnetic field processing. J Appl Phys 2003;94:6034.

[4] Jiang W, Ding G, Peng H. Measurement and model on thermal conductivities of carbon nanotube nanorefrigerants. Int J Therm Sci 2009;48:1108-15.

[5] Teh K-S, Lin L. MEMS sensor material based on polypyrrole-carbon nanotube nanocomposite: film deposition and characterization. J Micromechanics Microengineering 2005;15:2019-27.

[6] Shen G, Cheng Y, Tsai L. Synthesis and Characterization of Ni – P-CNT ' s Nanocomposite Film for MEMS Applications. IEEE Trans Nanotechnol 2005;4:5-10.

Table A.1: Broadening due to combined size and strain in Guassian and Lorentzian Fit

				Gaussian Fit (degree)	Lorentzian Fit (degree)
Material	Plane	2θ	θ	β	β
Pure copper	111	43.46	21.73	0.253	0.21
	200	50.6	25.3	0.272	0.24
	220	74.27	37.13	0.343	0.31
25 mg/l	111	43.27	21.63	0.255	0.21
	200	50.39	25.19	0.292	0.26
	220	74.07	37.03	0.349	0.32
50 mg/l	111	43.28	21.64	0.265	0.23
	200	50.41	25.2	0.286	0.24
	220	74.07	37.03	0.363	0.33
75 mg/l	111	43.25	21.63	0.267	0.23
	200	50.38	25.19	0.315	0.28
	220	74.06	37.03	0.375	0.35
100 mg/l	111	43.25	21.62	0.273	0.23
	200	50.38	25.19	0.318	0.29
	220	74.04	37.02	0.41	0.38
125 mg/l	111	43.3	21.65	0.246	0.22
	200	50.43	25.21	0.309	0.28
	220	74.1	37.05	0.373	0.34

Micromechanical Models of Metal-Carbon Nanotube Composite

In general, micromechanical models are widely adopted by materials scientists to predict the tensile behaviour of micro-composites reinforced with fibres, whiskers and particulates. As CNTs exhibit large aspect ratios, we may ask whether the theories of composite mechanics and micromechanical models can be used to explain the mechanical properties of metal-CNT nanocomposites. Up till now, the principles of the mechanics of nano-materials (nano-mechanics) are in the early stages of development [1–4]. The development of CNT-metal nanocomposites still faces obstacles due to the lack of basic understanding of the origins of

strengthening, stiffening and toughening and the matrix-nanotube interfacial issues. The structure-property relationships of metal-matrix micro-composites are well recognized and reported. Several factors are known to contribute to the increments in yield strength and stiffness of metal-matrix micro-composites. These include effective load transfer from the matrix to the reinforcement, increasing dislocation density, homogenous dispersion of fillers and refined matrix grain size. Micromechanical models such as, Rule of mixtures (ROM), Cox and Halpin-Tsai are often used to predict the stiffness and strength of discontinuously/continuously reinforced fibre composites.

A Rule of mixture

Rule of mixture (ROM) is one of the simplest models for determining elastic modulus of the composite. The arrangement or orientation of the fibers relative to one another, the fiber concentration, and the distribution all have a significant influence on the strength and other properties of fiber-reinforced composites. With respect to orientation, two extremes are possible: (1) a parallel alignment of the longitudinal axis of the fibers in a single direction, and (2) a very random alignment. In this model, at first, we consider longitudinal and transverse alignment of CNT with respect to the direction of applied load. In longitudinal loading, the applied load is parallel to the length of fiber (an iso strain[1] situation) is known as a Voigt condition. In transverse loading, the applied load is perpendicular to the length of fiber, is known as a Reuss condition.

An expression for the modulus of elasticity of a continuous and aligned fibrous composite in the direction of alignment (or longitudinal direction) [5] is

$$E_{cl} = E_m(1-V_f) + E_f V_f \tag{A.1}$$

An expression for the modulus of elasticity of a continuous and aligned fibrous composite in the perpendicular direction fibre [5] is

$$E_{ct} = \frac{E_f E_m}{E_f(1-V_f) + E_m V_f} \tag{A.2}$$

where, E_{cl} is modulus of elasticity of composite in longitudinal direction, E_{ct} is modulus of elasticity of composite in perpendicular direction, E_m is modulus of elasticity of matrix, E_f is modulus of elasticity of fibre, $(1-V_f)$ volume fraction of matrix and V_f is volume fraction of fibre.

[1] Iso strain situation means strain in composite, matrix and fiber is same $\varepsilon_c = \varepsilon_m = \varepsilon_f$

However, in actual case the fibres are orientated randomly and the load transfer is not efficient. Under these circumstances, a 'rule-of-mixtures' expression for the elastic modulus similar to Equation (A.1) may be used, as follows:

$$E_{ct} = KE_f V_f + E_m(1 - V_f) \quad \text{(A.3)}$$

In this expression, K is a fiber efficiency parameter that depends on V_f and the E_f/E_m ratio. If we consider two limiting cases i.e. 1) Parallel to fibers and 2) Fibers randomly and uniformly distributed within three dimensions in space then the magnitude of K will be in the range of 1 to 0.2 [5,6].

In the present case, elastic modulus of MWCNT/Cu composite has been determined by ROM. For the model calculations, the values of E_{Cu} = 51, 57 GPa, and E_{CNT} = 800 GPa, have been assumed. Data for the vol% and density is taken from the previous chapter and given in A.4. The data for longitudinal and transverse loading is calculated by using equation (A.1) and equation (A.2). Calculated data is tabulated in A.3.

Table A.2: Density and vol% of MWCNT/Cu nanocomposite

S.No.	Concentration of MWNT in electrolyte mg/l	Density g/cm^3	Vol% of MWCNT
1	0	8.14	0
2	25	7.8	5.5
3	50	7.53	10.13
4	75	7.25	14.75
5	100	7.24	14.78
6	125	7.14	16.53

Table A.3: Data for Young's modulus for longitudinal equation (A.1) and transverse loading equation (A.2)

Longitudinal	Transverse
Upper bound of Young's Modulus of Composite	Lower bound of Young's Modulus of Composite
GPa	GPa
51.57	51.57
92.73	54.37
127.39	56.97
161.96	59.83
162.19	59.84
175.29	61.00

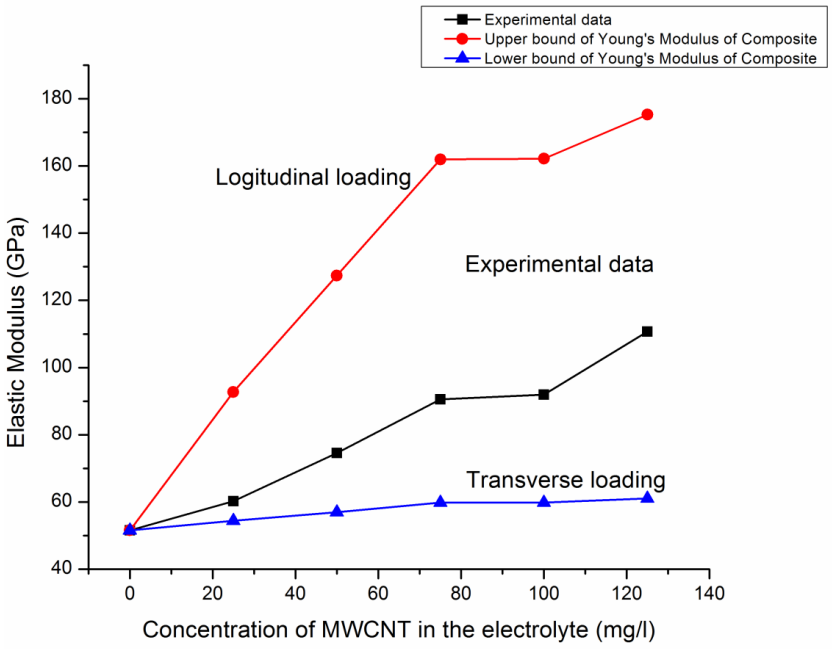

Figure A.1: Graphs showing the comparison between elastic modulus of nanocomposite by longitudinal equation (A.1) and transverse equation (A.2) loading and experimental value of elastic modulus of MWCNT/Cu nanocomposite prepared by modified electro-co-deposition. The ROM is observed to fit the data well

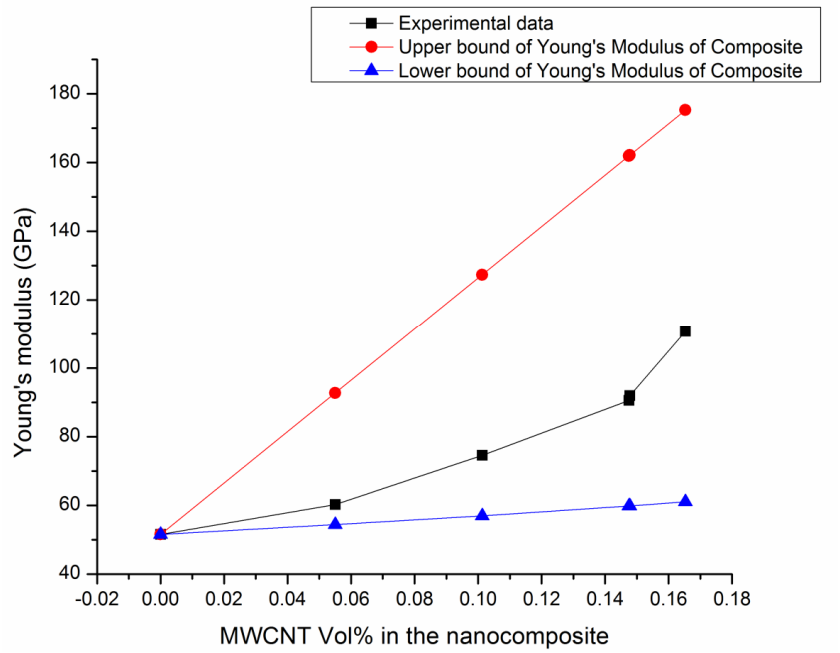

Figure A.2: Graphs showing the comparison between elastic modulus (Young's modulus) of nanocomposite by longitudinal equation (A.1) and transverse equation (A.2) loading vs. MWCNT Vol% in the MWCNT/Cu nanocomposite prepared by modified electro-co-deposition

However, a simple ROM has been found to fit experimentally obtained data, as shown in Figure A.1 and A.2, in the case of MWCNT/Cu nanocomposites synthesized by electro-co-deposition method. As the concentration of the MWCNT in the composite increases, the graph moves towards upper bound. This shows that, the load transfer efficiency improves with increase in concentration of MWCNT in the nanocomposite. In case of new ROM equation (A.3), two limiting cases were taken in to consideration i.e. 1) Parallel to fibers and 2) Fibers randomly and uniformly distributed within three dimensions in space and the magnitude of K is in the range of 1 to 0.2

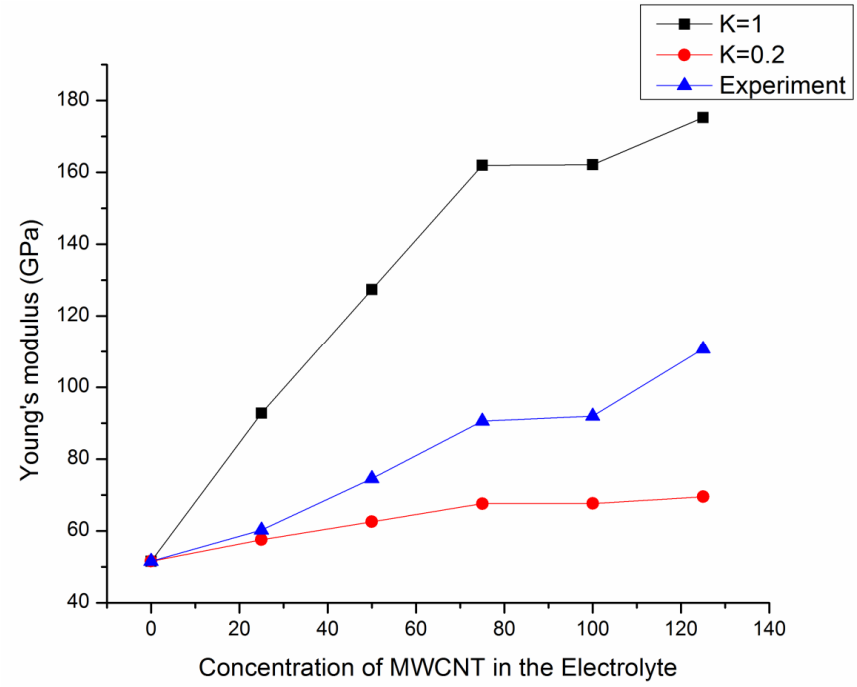

Figure A.3: Graphs showing the comparison between two limiting conditions of corrected ROM equation (A.3) and experimental value of elastic modulus (Young's modulus) vs. MWCNT concentration in the electrolyte.

For the Figure A.3, it is observed that, at low concentration of MWCNT in the electrolyte, the experimental values are close to the curve drawn with K = 0.2. This implies that, with the low concentration of the MWCNT in the electrolyte, MWCNTs are uniformly distributed in three-dimensional space. However, as the concentration of the MWCNT increases the load transfer efficiency also improves and the Experimental values tends towards the curve drawn with K = 1.

However, in actual composites, where the fibers randomly and uniformly distributed within a specific plane, for the laminated composite combined, Voigt-Reuss model is

used. The elastic modulus for the randomly oriented CNT composites can be given by the combined Reuss-Voigt Model [7,8], which is given as follows:

$$E = 0.375E_{cl} + 0.625E_{ct} \tag{A.4}$$

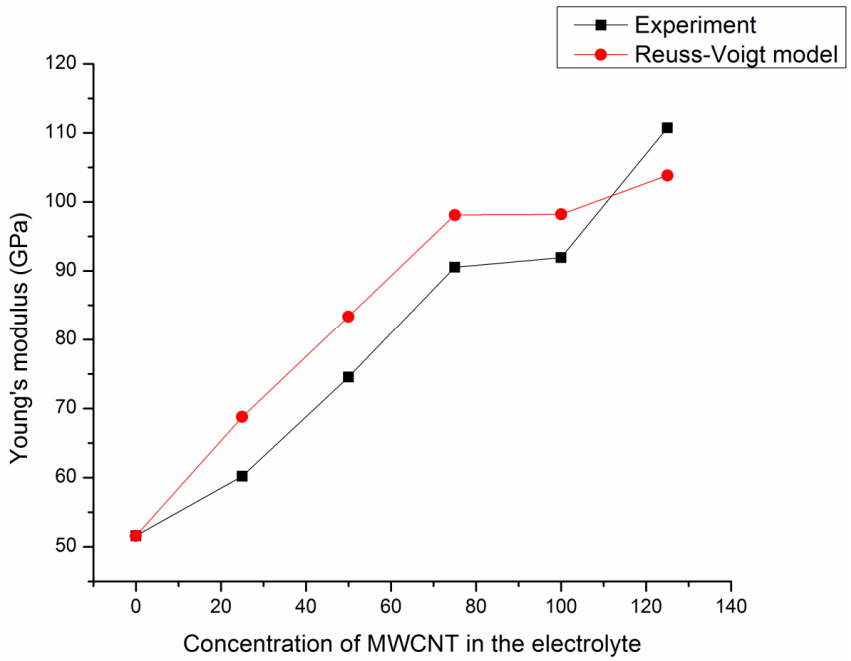

Figure A.4: The Graph is for Reuss-Voigt model and experimental value of elastic modulus (Young's modulus) vs MWCNT concentration in the electrolyte

From Figure A.4 supports the claim in the previous figure. The experimental values with low concentration of MWCNT in the electrolyte are not in one plane and reinforced throughout the matrix uniformly. As the concentration of the MWCNT increases, there is a possibility of having more MWCNT in a plane after cold drawing. Hence, the experimental value approaches the model graph.

B COX model

While modelling the Rule of Mixtures formula for nano-composites, many assumptions are made. We assume that fibres are uniformly distributed throughout the matrix and that there is perfect bonding between fibres and matrix. The matrix is assumed free of voids. For convenience, applied loads are taken either parallel or normal to the fibre direction. The lamina is initially assumed to be in a stress-free state (no residual stresses), and equal stress and equal strain assumptions are made. However, transverse strain mismatch exists at the boundary of fibres and matrix. Fibre and matrix are taken to behave as

linearly elastic materials. Moreover, their different poisson ratios means there could be a shear stress between the fibre and matrix. Also, the rule of mixtures does not work for random fibre composites since it does not take into account the fibre orientation and fibre-matrix interaction effects. Based on these considerations, the elastic modulus is given by the following form [9,10]:

$$E_c = \chi_1 \chi_2 E_f V_f + E_m V_m \tag{A.5}$$

where, all variables have same meaning as before χ_1 represents the effect of fibre orientation. The effect of fibre length or effective length of fibre that carries load is represented by χ_2.χ_1 takes the value of 3/8 for random-in-plane fibre orientation. For three-dimensional random fibre orientation, the value is taken to be 1/5. χ_2 is described as

$$\chi_2 = 1 - \frac{\tanh(ns)}{ns} \tag{A.6}$$

where, 's' is the fiber aspect ratio (l/D) and n is defined as

$$n^2 = \frac{2E_m}{E_f(1+vm)\ln\left(\frac{P_f}{V_f}\right)} \tag{A.7}$$

where, ν_m is the Poisson's ratio of the matrix and P_f is the fiber packing factor. Packing fraction comes out to vary between 0.85 and 0.91. For the model calculations, the values of E_{Cu} = 51.57 GPa, E_{CNT} = 800 GPa, ν_{Cu} = 0.36, and aspect ratio l/d of CNT = 400 have been assumed.

Table A.4: Values determined for Young's modulus by Cox model for $\chi_1 = 3/8$ and $\chi_1 = 1/5$

S.N.	Concentration of MWCNT in electrolyte	Vol% of MWCNT	Cox mode ($\chi_1 = 3/8$)	Cox mode ($\chi_1 = 1/5$)	Experimental results
1	0	0	51.57	51.57	51.57
2	25	0.055	65.01	78.03	60.18
3	50	0.1013	76.37	100.39	74.55
4	75	0.1475	87.73	122.75	90.57
5	100	0.1478	87.81	122.89	91.935
6	125	0.1653	92.11	131.37	110.73

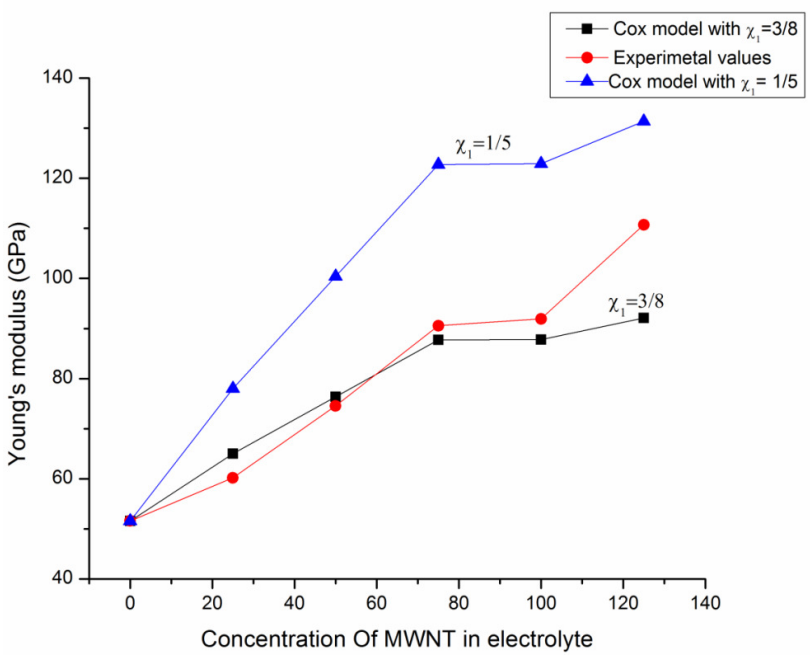

Figure A.5: Graphs for comparison of Young's modulus by Cox model for $\chi_1 = 3/8$ and $\chi_1 = 1/5$ and Experimental data.

This model takes into account the orientation as well as the aspect ratio of the reinforced fibers. The model has been applied to MWCNT/Cu composites prepared by modified electro-co-deposition method. It was observed that the predicted and experimentally measured values were very close to each other for $\chi_1 = 3/8$ compare to $\chi_1 = 1/5$. However, at higher concentration of MWCNT in the metal matrix the experimental values deviates from the $\chi_1 = 3/8$ curve this may be due to agglomeration of MWCNT at higher concentration.

C Halpin-Tsai (HT) equations

The HT equations correlate experimentally, the property of composite material with specific characteristics of matrix and reinforcing phases along with their proportions and geometries. The Halpin Tsai composite model predicts the increase in storage modulus with increasing CNT concentrations for oriented fibres. Halpin-Tsai equations have also been found to predict mechanical property with high accuracy in the case of small CNT concentrations in polymer [11–13] and metal matrix CNT [14] composites. The Halpin-Tsai equations use the mechanical properties of the fibre and the matrix to calculate the properties of the composite [15]. The equation can be expressed in a general form as

$$\frac{P}{P_m} = \left(\frac{1 + \eta \delta V_f}{1 - \eta \delta V_f} \right) \tag{A.8}$$

where,

$$\eta = \frac{\frac{P_f}{P_m} - 1}{\frac{P_f}{P_m} + \delta} \tag{A.9}$$

Here, P represents any one of the composite moduli listed in Table A.3. P_f and P_m are the corresponding moduli of the fibre and matrix respectively, δ is a parameter that depends on the particular elastic property being considered. V_f is the volume fraction of fibre in the metal matrix composite.

Table A.5: Traditional Halpin-Tsai parameters for composites

P	P_f	P_m	δ	**Comments**
E_{Cl}	E_f	E_m	$2(l/D)$	Longitudinal modulus
E_{ct}	E_f	E_m	2	Transverse modulus
G_{12}	G_f	G_m	1	Longitudinal shear
(Note: l/D – fibre aspect ratio)				

Qian et al. [16] have used the Halpin-Tsai equations to derive the modulus of a randomly oriented fibre composite as a function of the longitudinal and composite moduli, as stated below

$$E_c = \frac{3}{8}\left(\frac{1 + (2l/D)\eta_L V_f}{1 - \eta_L V_f} \right) + \frac{5}{8}\left(\frac{1 + 2\eta_T V_f}{1 - \eta_T V_f} \right) \tag{A.10}$$

(Note: Subscripts, L and T denote longitudinal and transverse components, respectively.)

The above formula is valid for a continuous fibre reinforced composite. Mechanical properties calculated from these formulae have been found to be quite accurate for specimens with small CNT concentrations in polymer and metal. For the model calculations, the values of E_{Cu} = 51.57 GPa, E_{CNT} = 800 GPa, and aspect ratio l/d of CNT = 400 have been assumed.

Table A.6: Young's modulus by Halpin-Tsai model

$\eta = \frac{\frac{E_f}{E_m} - 1}{\frac{E_f}{E_m} + \delta}$	$E_L = \left(\frac{1 + (2l/D)\eta_L V_f}{1 - \eta_L V_f}\right) = 0.03493$	$\eta = \frac{\frac{E_f}{E_m} - 1}{\frac{E_f}{E_m} + \delta}$	$E_T = \left(\frac{1 + 2\eta_T V_f}{1 - \eta_T V_f}\right) = 0.8286977$	$E_c = \frac{3}{8}\left(\frac{1 + (2l/D)\eta_L V_f}{1 - \eta_L V_f}\right) + \frac{5}{8}\left(\frac{1 + 2\eta_T V_f}{1 - \eta_T V_f}\right)$
Longitudinal		Transverse		Halpin-Tsai
Fractional Change of Parameter	Composite Parameter	Fractional Change of Parameter	Composite Parameter	
1	51.57	1	51.57	51.57
1.78	91.37	1.14	58.96	71.11
2.43	125.03	1.28	65.75	87.98
3.08	158.66	1.42	73.11	105.19
3.08	158.88	1.42	73.16	105.31
3.33	171.66	1.48	76.13	111.95

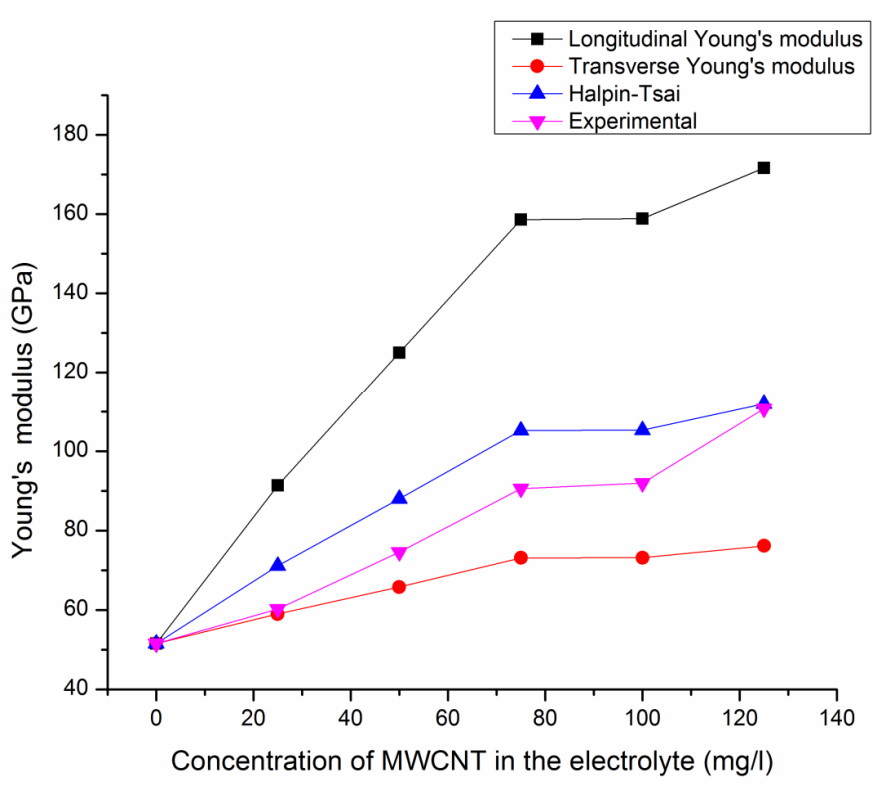

Figure A.6: Graphs for comparison of Young's modulus by Halpin-Tsai mode and Experimental data

The Halpin-Tsai equations shows us the importance of fibre geometry alone on the stiffness properties at both constant volume fraction and packing geometry and changing from a sphere (aspect ratio of one in the principal material direction) to a long fibre (aspect ratio approaching infinity). Furthermore, the equations predict the elastic modulus of the composite, in agreement with experimental results.

As seen in the previous section, the elastic modulus of the MWCNT/Cu composites was calculated using various models as presented in Table A.7. The elastic modulus value for MWCNT has been assumed as 800 GPa [17].

Table A.7: Summary of Young's modulus of the composite calculated using micromechanical models

Concentration of MWNT mg/l ⟹		**0**	**25**	**50**	**75**	**100**	**125**
Micromodels ⇩		Young's Modulus					
Rule of Mixture [5]	**Axial loading**	51.57	92.73	127.39	161.96	162.19	175.29
	Transverse loading	51.57	54.37	56.97	59.83	59.84	61
Voigt-Ruess model [15]		51.57	68.76	83.38	98.13	98.22	103.86
Halpin Tsai [18]		51.57	71.11	87.98	105.19	105.31	111.95
Cox Model [19]	$\chi_1 = 3/8$	51.57	65.01	76.37	87.73	87.81	92.11
	$\chi_2 = 1/5$	51.57	78.03	100.39	122.75	122.89	131.37
Experimental value		51.57	60.18	74.55	90.57	91.935	110.73

It is found that the predicted values from modified rule of mixture method (Voigt-Ruess Model) and Halpin-Tsai are close to the mean of the experimental value. Some of the values calculated by Halpin-Tsai are larger than the measured values. This is attributed to the porosity compared to the standard parent material.

References:

[1] Guz IA, Rodger AA, Guz AN, Rushchitsky JJ. Developing the mechanical models for nanomaterials. Compos Part A Appl Sci Manuf 2007;38:1234–50.

[2] Guz IA, Rushchitsii YY. Comparison of Mechanical Properties and Effects in Micro- and Nanocomposites with Carbon Fillers (Carbon Microfibers, Graphite Microwhiskers, and Carbon Nanotubes). Mech Compos Mater 2004;40:179–90.

[3] Liu WK, Park HS, Qian D, Karpov EG, Kadowaki H, Wagner GJ. Bridging scale methods for nanomechanics and materials. Comput Methods Appl Mech Eng 2006;195:1407–21.

[4] Bhushan B. Nanotribology and nanomechanics. Wear 2005;259:1507–31.

[5] William D. Callister DGR. Fundamentls of Material Science and Engineering An Integrated approach. 4th ed. John wiley and Sons, Inc; 2012.

[6] Agarwal A, Bakshi SR, Lahiri D. Carbon Nanotubes Reinforecd Metal Matrix Composite. Boca Raton, Florida: CRC Press, Taylor and Francis Group; 2011.

[7] Bakshi SR, Lahiri D, Agarwal a. Carbon nanotube reinforced metal matrix composites – a review. Int Mater Rev 2010;55:41–64.

[8] Callister WD, Rethwisch DG. Fundamentals of Material Scienec and Engineering An Integrated Approach. 4 th. John wiley and Sons, Inc; 2012.

[9] Cox HL. The elasticity and strength of paper and other fibrous materials. Br J Appl Phys 1952;3:72–9.

[10] Curtis PT, Bader MG, Bailey JE. The stiffness and strength of a polyamide thermoplastic reinforced with glass and carbon fibres. J Mater Sci 1978;13:377–90.

[11] Guthy C, Du F, Brand S, Winey KI, Fischer JE. Thermal Conductivity of Single-Walled Carbon Nanotube/PMMA Nanocomposites. J Heat Transfer 2007;129:1096.

[12] Song YS, Youn JR. Evaluation of effective thermal conductivity for carbon nanotube/polymer composites using control volume finite element method. Carbon N Y 2006;44:710–7.

[13] Yeh M-K, Tai N-H, Liu J-H. Mechanical behavior of phenolic-based composites reinforced with multi-walled carbon nanotubes. Carbon N Y 2006;44:1–9.

[14] Bakshi SR, Singh V, Balani K, McCartney DG, Seal S, Agarwal A. Carbon nanotube reinforced aluminum composite coating via cold spraying. Surf Coatings Technol 2008;202:5162–9.

[15] Bakshi SR, Agarwal A. An analysis of the factors affecting strengthening in carbon nanotube reinforced aluminum composites. Carbon N Y 2011;49:533–44.

[16] Qian D, Dickey EC, Andrews R, Rantell T. Load transfer and deformation mechanisms in carbon nanotube-polystyrene composites. Appl Phys Lett 2000;76:2868.

[17] Yu M, Lourie O, Dyer MJ, Moloni K, Kelly TF, Ruoff RS. Strength and Breaking Mechanism of Multiwalled Carbon Nanotubes Under Tensile Load. Science (80-) 2000;287:637–40.

[18] Lusti HR, Gusev A a. Finite element predictions for the thermoelastic properties of nanotube reinforced polymers. Model Simul Mater Sci Eng 2004;12:S107–S119.

[19] Raabe D, Hangen U. Introduction of a modified linear rule of mixtures for the modelling of the yield strength of heavily wire drawn in situ composites. Compos Sci Technol 1995;55:57–61.

Vicker Hardness testing Data for Statistical Analysis

Table B.1: Vicker hardness testing data with 5 kg of loading

Sample No	Horizontal diagonal of diamond	Vertical diagonal of diamond	Average	Hardness (MPa)	Sample No	Horizontal diagonal of diamond	Vertical diagonal of diamond	Average	Hardness (MPa)
No. 1	0.528	0.563	0.545	305.98	No. 1	0.563	0.576	0.569	280.41
	0.569	0.572	0.571	279.06		0.58	0.564	0.572	278.04
	0.583	0.576	0.58	270.43		0.576	0.597	0.587	264.07
	0.583	0.573	0.578	272.06		0.564	0.571	0.567	282.48
No. 2	0.528	0.521	0.524	330.78	No. 2	0.531	0.497	0.514	344.33
	0.514	0.507	0.51	349.03		0.528	0.515	0.522	334.31
	0.514	0.493	0.503	358.72		0.5	0.507	0.503	358.72
	0.493	0.494	0.494	372.99		0.483	0.49	0.486	384.80
No.3	0.458	0.468	0.463	423.82	No.3	0.452	0.477	0.465	421.29
	0.46	0.469	0.465	421.29		0.476	0.45	0.463	423.82
	0.46	0.458	0.459	430.90		0.46	0.465	0.463	425.09
	0.456	0.458	0.457	435.50		0.463	0.463	0.463	424.46
No. 4	0.542	0.556	0.549	302.12	No. 4	0.545	0.552	0.549	301.97
	0.54	0.546	0.543	308.33		0.552	0.551	0.551	298.97
	0.544	0.545	0.545	306.37		0.545	0.559	0.552	298.48
	0.538	0.538	0.538	313.93		0.524	0.533	0.529	325.46
No. 5	0.514	0.528	0.521	335.20	No. 5	0.521	0.521	0.521	335.21
	0.503	0.521	0.512	346.67		0.508	0.51	0.509	350.46
	0.524	0.532	0.528	326.01		0.527	0.531	0.529	324.73
	0.529	0.53	0.53	324.31		0.539	0.511	0.525	329.91
No. 6	0.5	0.486	0.493	374.04	No. 6	0.493	0.497	0.495	371.42
	0.479	0.493	0.486	384.80		0.507	0.503	0.505	356.26
	0.503	0.493	0.498	366.26		0.486	0.507	0.497	368.83
	0.497	0.5	0.498	366.26		0.486	0.5	0.493	374.04
No. 7	0.539	0.538	0.538	313.93	No. 7	0.528	0.528	0.528	326.44
	0.5	0.507	0.503	358.72		0.521	0.514	0.517	339.72
	0.528	0.521	0.524	330.78		0.521	0.514	0.517	339.72
	0.531	0.532	0.531	322.19		0.538	0.531	0.535	318.02
No.8	0.552	0.549	0.55	300.28	No.8	0.545	0.535	0.54	311.91
	0.521	0.535	0.528	326.44		0.514	0.521	0.517	339.72
	0.529	0.538	0.534	319.26		0.507	0.521	0.514	344.33
	0.528	0.528	0.528	326.44		0.522	0.515	0.518	338.36
No.9	0.556	0.55	0.553	297.58	No.9	0.558	0.542	0.55	300.60

Sample No	Horizontal diagonal of diamond	Vertical diagonal of diamond	Average	Hardness (MPa)	Sample No	Horizontal diagonal of diamond	Vertical diagonal of diamond	Average	Hardness (MPa)
	0.535	0.542	0.538	313.93		0.542	0.549	0.545	305.98
	0.547	0.556	0.551	299.46		0.535	0.542	0.538	313.93
	0.538	0.553	0.546	305.20		0.549	0.559	0.554	296.46
No.10	0.458	0.465	0.462	426.37	No.10	0.472	0.458	0.465	420.03
	0.472	0.469	0.47	410.79		0.47	0.467	0.468	414.45
	0.458	0.454	0.456	436.82		0.453	0.446	0.45	449.73
	0.458	0.462	0.46	429.60		0.465	0.451	0.458	432.86
No.11	0.479	0.493	0.486	384.80	No. 11	0.486	0.482	0.484	388.12
	0.458	0.472	0.465	420.03		0.486	0.493	0.49	379.36
	0.472	0.465	0.469	413.83		0.483	0.479	0.481	393.18
	0.486	0.483	0.484	387.56		0.486	0.493	0.49	379.36
No.12	0.535	0.542	0.538	313.93	No. 12	0.528	0.538	0.533	320.09
	0.528	0.532	0.53	323.88		0.536	0.533	0.535	318.02
	0.542	0.538	0.54	311.91		0.524	0.538	0.531	322.61
	0.521	0.549	0.535	318.02		0.538	0.544	0.541	310.31
No.13	0.535	0.521	0.528	326.44	No. 13	0.521	0.528	0.525	330.34
	0.521	0.514	0.517	339.72		0.535	0.538	0.536	315.96
	0.532	0.517	0.525	330.34		0.529	0.524	0.526	328.17
	0.525	0.521	0.523	332.54		0.521	0.524	0.523	332.98
No.14	0.451	0.444	0.448	453.23	No. 14	0.431	0.445	0.438	474.31
	0.465	0.458	0.462	426.37		0.465	0.476	0.471	410.18
	0.472	0.469	0.47	410.79		0.467	0.458	0.463	425.09
	0.465	0.462	0.464	423.19		0.462	0.465	0.464	423.19
No.15	0.556	0.549	0.552	298.33	No.15	0.542	0.549	0.545	305.98
	0.57	0.576	0.573	276.69		0.556	0.566	0.561	289.17
	0.568	0.568	0.568	281.79		0.564	0.556	0.56	290.24
	0.562	0.563	0.562	287.74		0.569	0.552	0.561	289.17
No.16	0.458	0.465	0.462	426.37	No. 16	0.457	0.456	0.456	436.82
	0.451	0.448	0.45	449.73		0.458	0.461	0.46	430.25
	0.458	0.456	0.457	435.49		0.456	0.462	0.459	432.20
	0.455	0.462	0.458	432.86		0.454	0.458	0.456	436.82
No.17	0.569	0.563	0.566	283.87	No.17	0.563	0.563	0.563	287.38
	0.556	0.549	0.552	298.33		0.553	0.549	0.551	299.46
	0.566	0.569	0.568	282.14		0.576	0.573	0.575	275.35
	0.569	0.568	0.569	281.10		0.563	0.567	0.565	284.91
No.18	0.528	0.531	0.53	324.30	No. 18	0.535	0.537	0.536	316.78
	0.545	0.549	0.547	304.04		0.551	0.538	0.544	306.76
	0.535	0.531	0.533	320.09		0.531	0.521	0.526	328.60
	0.541	0.542	0.541	310.31		0.528	0.535	0.531	322.19

Table B.2: Three test samples for verification

Sample No	Horizontal Diameter of diamond	Vertical Diameter of diamond	Average	Hardness (MPa)
1	0.4615	0.4766	0.469	413.31
	0.4498	0.4539	0.452	445.31
	0.4664	0.4617	0.464	422.25
	0.4639	0.4628	0.463	423.50
				426.09
2	0.4569	0.4555	0.456	436.82
	0.4583	0.4511	0.455	439.80
	0.4546	0.4618	0.458	433.10
	0.4542	0.4573	0.456	437.81
				436.88
3	0.4469	0.4547	0.450	447.41
	0.4493	0.4609	0.455	439.02
	0.4546	0.4517	0.453	442.82
	0.4642	0.4463	0.455	438.74
				441.99

$$HV = \frac{(2F \sin\ (136^\circ/2))}{d^2} = \frac{1.8544 \times 9.807 \times F}{d^2}$$

Table A.3: Experimental results for Vicker hardness and their corresponding S/N ratio for L_{18} standard orthogonal array

Sample No.	pH	Current (AMP)	MW-CNT (mg)	Sonication Time (hr)	Copper Sulfate (gm)	H1	H2	H3	H4	H5	H6	H7	H8	hardness	$\left(\sum_{i=1}^{5} y_i\right)^2$	$\sum_{i=1}^{5} y_i^2$		Variance	$\sum_{i=1}^{5} \frac{1}{y_i^2}$		$S/N = -10\log\frac{1}{N_i}\sum\frac{1}{y_i^2}$
1	1	4	20	3	30	305.98	279.05	270.43	272.06	280.41	278.04	264.07	282.48	279.06	623031.68	624119.1	1087.41	271.85	10.32×10^{-5}	1.03×10^{-10}	108.892
2	1	6	30	4	40	330.78	349.02	358.72	372.98	344.32	334.31	358.72	384.80	354.21	1003722.31	1006121	2398.57	599.64	6.42×10^{-5}	6.42×10^{-11}	110.95
3	1	8	40	5	50	423.82	421.29	430.89	435.49	421.29	423.82	425.09	424.45	425.77	1450250.02	1450421	170.76	42.69	4.41×10^{-5}	4.41×10^{-11}	112.58
4	2	4	20	4	40	302.12	308.33	306.37	313.92	301.96	298.97	298.48	325.45	306.95	753767.17	754344.2	576.97	144.24	8.51×10^{-5}	8.51×10^{-11}	109.73
5	2	6	30	5	50	335.20	346.66	326.01	324.30	335.20	350.45	324.73	329.90	334.06	892777.11	893471.6	694.52	173.63	7.19×10^{-5}	7.19×10^{-11}	110.46
6	2	8	40	3	30	374.03	384.80	366.26	366.26	371.41	356.26	368.82	374.03	370.23	1096615.79	1097087	471.41	117.85	5.84×10^{-5}	5.84×10^{-11}	111.36
7	3	4	30	3	50	313.92	358.72	330.78	322.18	326.44	339.72	339.72	318.01	331.19	877498.25	878977	1478.71	369.67	7.33×10^{-5}	7.33×10^{-11}	110.38
8	3	6	40	4	30	300.21	326.44	319.26	326.44	311.91	339.72	344.32	338.35	325.83	849349.61	850935.2	1585.58	396.39	7.58×10^{-5}	7.58×10^{-11}	110.2
9	3	8	20	5	40	297.58	313.92	299.46	305.20	300.59	305.98	313.92	296.46	304.14	740026.61	740359.1	332.50	83.12	8.66×10^{-5}	8.66×10^{-11}	109.65
10	1	4	40	5	40	426.37	410.78	436.82	429.59	420.03	414.44	449.73	432.85	427.58	1462611.32	1463732	1120.96	280.24	4.39×10^{-5}	4.39×10^{-11}	112.61
11	1	6	20	3	50	384.80	420.03	413.83	387.56	388.12	379.36	393.18	379.36	393.28	1237379.36	1239036	1656.71	414.17	5.19×10^{-5}	5.19×10^{-11}	111.87
12	1	8	30	4	30	313.92	323.88	311.91	318.01	320.09	318.01	322.61	310.31	317.34	805676.36	805845.9	169.52	42.38	7.95×10^{-5}	7.95×10^{-11}	110.02
13	2	4	30	5	30	326.44	339.72	330.34	332.54	330.34	315.96	328.16	332.98	329.56	868895.29	869216.9	321.57	80.39	7.37×10^{-5}	7.37×10^{-11}	110.35
14	2	6	40	3	40	453.22	426.37	410.78	423.18	474.31	410.18	425.09	423.18	430.79	1484665.02	1488055	3390.02	847.503	4.33×10^{-5}	4.34×10^{-11}	112.65
15	2	8	20	4	50	298.33	276.69	281.79	287.74	305.98	289.16	290.24	289.16	289.89	672289.81	672865.5	575.70	143.92	9.54×10^{-5}	9.54×10^{-11}	109.23
16	3	4	40	4	50	426.37	449.73	435.49	432.85	436.82	430.24	432.20	436.82	435.06	1514284.03	1514617	333.29	83.32	4.23×10^{-5}	4.23×10^{-11}	112.76
17	3	6	20	5	30	283.86	298.33	282.13	281.10	287.38	299.46	275.35	284.91	286.57	656981.97	657472.4	490.45	122.61	9.76×10^{-5}	9.76×10^{-11}	109.13
18	3	8	30	3	40	324.30	304.04	320.09	310.31	316.78	306.76	328.60	322.18	316.63	802070.69	802611.6	540.87	135.21	7.99×10^{-5}	8×10^{-11}	110.00

PATENT

- "Method of producing uniform mixture of copper and carbon nanotube in bulk for copper metal nanocomposite" Indian Patent, Application No.: 2454/DEL/2012A, Publication Date: 07/12/2012, ISSUE NO. 49/2012

RESEARCH PUBLICATIONS

A International Journals (*Peer-reviewed*)

1) **Belgamwar SU,** Sharma NN. Synergistic electro-co-deposition and molecular mixing for reinforcement of multi-walled carbon nanotube in copper, Mater. Sci. Eng. B (2013), Volume 178, Issue 20, 1 December 2013, Pages 1452−1457.
2) **Belgamwar SU,** Sharma NN. Enhancement of electrical and mechanical properties of multiwalled carbon nanotube copper composite wire, (*communicated in Material Science and Engineering B)*

B Conferences

1) Sharma, NN, **Belgamwar SU.** Ultraconductive copper using carbon nanotubes, Proc. of "ALIGARH NANO-4 International 2014" an International Conference on Nanoscience and Nanotechnology, March 8-10, 2014.
2) Sharma, NN, **Belgamwar SU.** Copper Nanocomposites: A Solution to Depleting Copper Reserves, Proc. of International Conference on Materials for the Future, 2013, Thrissur, Kerala.
3) **Belgamwar SU,** Avadhani GS, Sharma NN. Functionalisation of MWCNT in order to improve bonding in Cu/MWCNT composite, Proc. of International conference on emerging Technologies- Micro to Nano 2013, K.K. Birla, BITS-Pilani, Goa Campus, Goa , India.
4) **Belgamwar SU,** Sharma NN. DISADVANTAGED copper ore to rich copper metal by carbon nanotube reinforcement, Proc. of national Seminar on Emerging trends in base metal mining in india, The Indian Institute of Metals, Khetri Nagar Chapter, Jan. 19, 2012, Hindustan Copper Limited, Khetri Nagar, India.
5) **Belgamwar SU,** Sharma NN. Cu/Metals Reinforced with Carbon Nanotubes: Value Addition, Technology and Developments, Proc. of International conference on Opportunities and Challenges for Mineral Industries, The Indian Institute of Metals, Khetri Nagar Chapter, Jan. 17, 2011, Hindustan Copper Limited, Khetri Nagar, India.

Brief biography of the Candidate

Sachin U Belgamwar received the B.E. degree in Mechanical Engineering from Anuradha Engineering College, Chikhli, Amaravati University, India in 1999, and the M.E. degree in Mechanical Engineering from Birla Institute of Technology and Science, Pilani India, in 2001. After working for six years in different engineering colleges, he joined the Mechanical Engineering Department, Birla Institute of Technology and Science, BITS-Pilani, Pilani Campus, PILANI, INDIA in January 2007, as a faculty member, where he is presently working as a Lecturer. His research interests include electrochemical synthesis of carbon nanotube reinforced metal-matrix composites, quantification of carbon nanotube distribution in composites, and microstructure-property correlations, characterization of the composite and MEMS.

Brief biography of the Supervisor

Prof. (Dr.) Niti Nipun Sharma completed his B.E. (Mechanical) from REC, Srinagar (now NIT, Srinagar) and M.E. (Mechanical) and Ph.D. both from BITS, Pilani. He is a faculty in Mechanical Engineering Department for over 18 years now currently serving as full Professor in Mechanical Engineering Department. Prof. Sharma served as visiting professor in EPFL, Switzerland during May-August 2014. He is first recipient of Kris Ramachandran best faculty award in 2010 at BITS, Pilani.

Prof. Sharma specialized in Robotics and was a part of team which developed 'ACYUT', the humanoid from BITS. He later during his Ph.D. worked on dynamics of nanorobots proposed a simple method to include modelling of Brownian motion attributable to thermal agitation to predict the dynamics of Nanorobots. His methodology of analyzing synergism in local and global motion of non-rigid kind of nanoparticles due to thermal agitation from surrounding medium has recently been shown to model radiation of nanoparticle validating with Planck's Radiation Law.

Three patents, over 70 technical papers in high impact factor journals and peer reviewed National and International conferences, around two dozen invited/keynote talks in India and abroad and with ten funded projects from nodal agencies like DBT, UGC, CSIR-CEERI, NPMASS and Industries, currently Prof. Sharma is working in Interdisciplinary areas of MEMS and Nanotechnology.

He is Guest Editor, Journal of Bionanoscience (Springer), Associate Editor of International Journal of Smart Sensors and Intelligent Systems, has reviewed many articles for IEEE Tr. Systems, Man and Cybernetics, IEEE Tr. Education, has been on-board of many Technical Committees of reputed National and International Conference. He was co-chair for International Conference on Emerging Technologies: Micro to Nano 2013 (ETMN-2013) jointly organised by BITS-Pilani and CSIR - Central Electronics Engineering Research Institute, Pilani, International Conference on Emerging Mechanical Technology Macro to Nano (EMTM2N-2007). He also co-organized 2nd ISSS-MEMS-2007 conference with CEERI, Pilani

Prof. Sharma also holds the post of Dean, Academic Registration & Counselling Division at BITS-Pilani, Pilani Campus since 2010.